

Working together
toward
sustainable
sand mining
and management.



Supported by:

Federal Ministry
for the Environment, Nature Conservation,
Nuclear Safety and Consumer Protection

based on a decision of
the German Bundestag



Deltares



Sand Budget Mekong Delta

Final Report



Deltares (The Netherlands)
Centre for Environmental Fluid Dynamics (Vietnam)

Subcontractors
IHE-Delft Institute for Water Education
Southern Regional Hydrometeorological Centre
Thien Nam

Sand Budget Mekong Delta

Final Report

Client	WWF-Vietnam
Contact	Mr. A. Ha Huy
Reference	
Keywords	Mekong Delta, Sand budget, Sand mining, Delft3D-FM

Document control

Version	1.0
Date	30-08-2023
Project nr.	11206927-000
Document ID	11206927-000-ZKS-0009
Pages	139
Classification	
Status	final

Author(s)	Organization	Reviewer	Approver
Sepehr Eslami	Deltares	Kees Sloff (Deltares)	Bart Grasmeijer (Deltares)
Trang Dinh	Deltares		
Mick van der Wegen	IHE-Delft, Deltares		
Floortje Roelvink	Deltares		
Roeland Nieboer	Deltares		
Antonio Moreno Rodenas	Deltares		
Ruben White	Deltares		
Thanh Quoc Vo	IHE-Delft		
Dano Roelvink	IHE-Delft, Deltares		
Johan Reynolds	IHE-Delft, Deltares		
Tran Ngoc Anh	CEFD		
Pham Thi Tuyet May	CEFD		
Hoang Thai Binh	CEFD		
Tran Vinh Quang	CEFD		
Pham Duy Huy Binh	CEFD		
Ly Tuan Minh	CEFD		

The allowed use of this table is limited to check the correct order-performance by Deltares. Any other client-internal-use and any external distribution is not allowed.

Doc. Version	Author	Reviewer	Approver
1.0	Sepehr Eslami	Kees Sloff (Deltares)	Bart Grasmeijer (Deltares)

Summary

In the context of the International Climate Initiative (IKI) project, the current study aims to derive the first account of the sand budget in the Vietnamese Mekong Delta (VMD). The rapidly urbanizing Mekong Delta, as one of the lowest-lying delta's worldwide, is under stress from various climatic and anthropogenic drivers and, consequently, disproportionately vulnerable to various environmental forces. Salt intrusion, land subsidence, flooding, coastal erosion, deteriorating water quality, and biodiversity depletion are among processes that threaten Vietnam's food security and the strategic development of the delta. Recent scientific findings demonstrate that riverbed-, riverbank- and coastal erosion, tidal amplification and salt intrusion are mainly driven by anthropogenic sediment starvation of the delta. Sediment starvation can be classified under two categories: A) Fine sediment shortage due to hydropower developments in the upper Mekong Basin, and B) coarse sediment decline due to sand mining within (and beyond) the VMD.

This study, in a nearly a decade-long trajectory of sand extraction estimation, shows that sand mining in the order of $35\text{-}55\text{ M m}^3/\text{yr}$ is amongst the main drivers of riverbed incision and morphological instability of the VMD. The total sand flux entering the Mekong delta ($2\text{-}4\text{ M m}^3/\text{yr}$) is far less than current sand extraction rates. Despite limited departure of sand from the delta ($0\text{-}0.6\text{ M m}^3/\text{yr}$) and with foreseen sand demand in the coming decades, the existing mobile sand stock ($367\text{-}550\text{ M m}^3$) cannot last longer than a decade (see Figure 1).

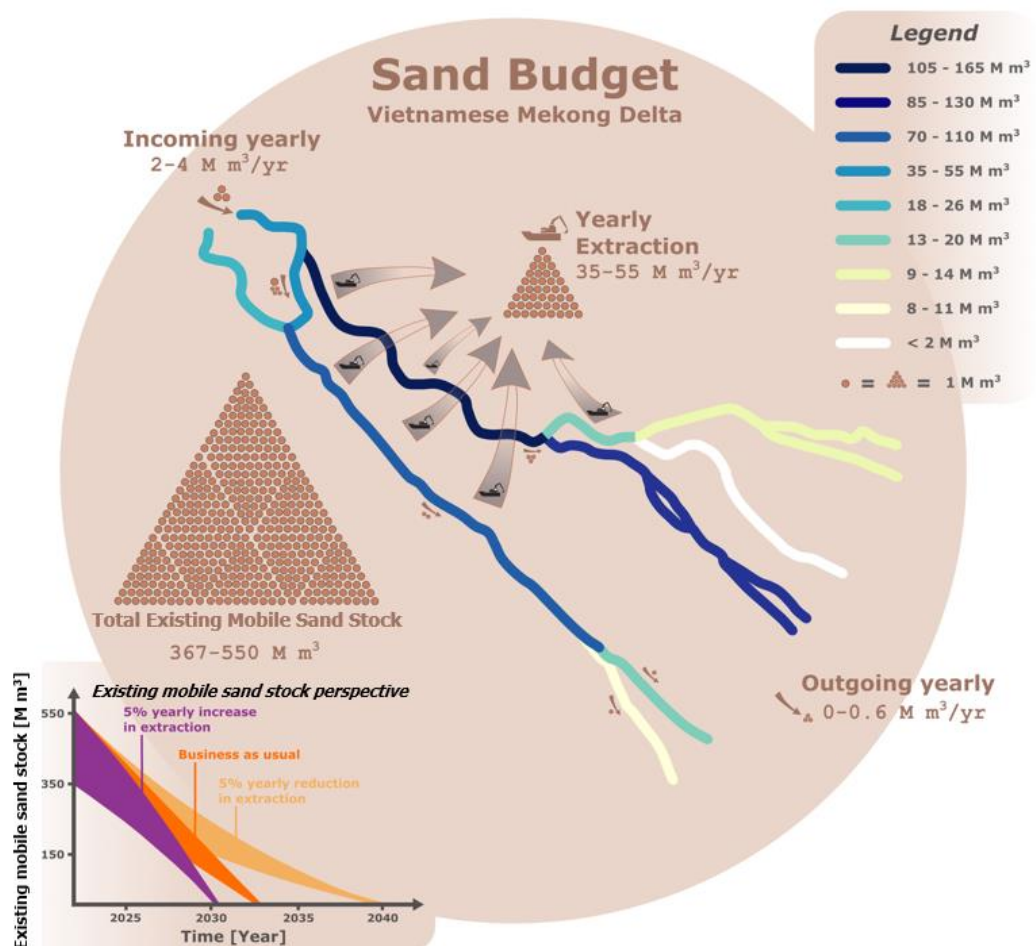


Figure 1: Sand budget of the Mekong Delta with a perspective of sand availability towards mid-century.

The results of this study have significant implication for managing resources of the VMD. Figure 1 shows the upper and lower estimates of the existing mobile sand stock decline under three different scenarios of extraction: a) 5% increase in current extraction rates, b) business as usual, and c) gradual reduction of extraction rates at a 5% rate. Under a mitigating regime of controlled reduction to river sand dependency, the existing mobile sand stock may last until 2040. However, this project does not study the morphological and environmental impacts of total extraction of the existing sand. While this will likely lead to further riverbank instability (bank erosion) as well as coastal erosion, based on the existing salinity projections, a loss of half Billion m³ of sediment from the VMD riverine system can lead to 10-15% increase in areas affected by salt intrusion within the VMD. Note that the existing sand budget is a snapshot in 2022. For example, the sand supply from upstream can decline because of further extraction in Cambodia. Furthermore, the erosion from sand mining upstream also travels downstream. Therefore, it is advised to consider the transboundary nature of sediment management beyond the VMD in multi-lateral cooperations. The results can serve as an important basis for a sustainable governance of the Mekong's natural resources, and to reduce the VMD's vulnerability to climate change and anthropogenic impact.

The adopted approach

The study approach combines collection of a unique delta-wide field campaign comprising of hydrodynamic data, seismic survey over 550 km of the deltaic river system, detailed multibeam bathymetric survey to monitor sand movement, and suspended and bedload sediment sampling (Work Package, WP1). The project collected additional existing data from MRC and provincial authorities. Furthermore, a state-of-the art numerical modelling (WP2) provided a powerful framework to integrate various elements of the sand budget. This and a series of national and provincial VMD stakeholders' consultation resulted in the current report that marks the completion of the IKI Mekong sand budget project. Figure 2 provides an overview of how activities contributed to the determination of the delta-wide sand budget.

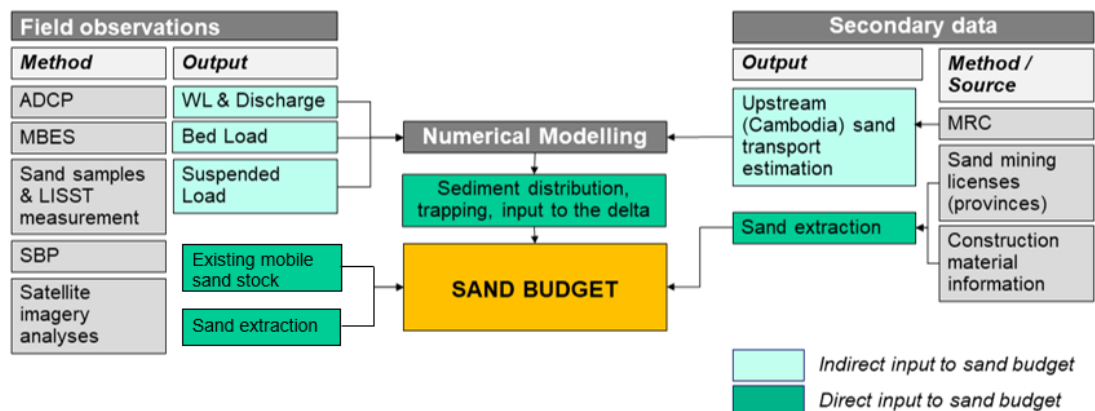


Figure 2: Overview of how project components contribute to the development of the Mekong Sand Budget.

Central to the development of the sand budget was a Delft3D-Flexible Mesh numerical model, with which sediment dynamics of the VMD were simulated (sediment and water distribution, sediment input to the delta, sediment trapping). Field observations such as discharge measurements, multibeam surveys, riverbed and suspended sediment samples were input to the numerical model for qualitative and/or quantitative calibration and validation of the model and to further inform expert judgement to integrate the developed knowledge. In addition to the numerical model, field observations and secondary data on sand extraction, existing mobile sand stock, and upstream (Cambodia) sand input were essential to the outcome.

Existing mobile sand stock (WP1)

The existing mobile sand stock along the Mekong River was derived based on a 550 km sub-bottom profiling campaign. The collected signal was post-processed using borehole data, surface grab samples, and the collected bathymetric data (See Figure 1 for results, and Figure 3 for extent). The upper Tien and the Co Chien Rivers have the highest mobile sand stock, followed by Bassac River. Mobile sand stock is significantly lower in the lower Mekong and the Ham Luong River. The total existing mobile sand stock of the VMD is estimated at 367-550 M m³. This estimate is perhaps on the conservative side as it is based on the mobile sand layer. This leaves the possibility that additional buried sources of sand (not detected in this study) are available underneath the mobile sand layer. This does not mean that these resources are easily accessible for extraction.

Bed load transport estimation for the dry and wet season surveys (WP1)

Bedload transport estimates were derived from dune tracking analysis (see Figure 3). Bed load during the wet season was 10 to 60 times higher than during the dry season. Highest bed loads were observed at Tan Chau, with a total bed load of approximately $2000 \cdot 10^{-5}$ m³/s during the wet season. At Long Xuyen and Cao Lanh, high bed loads of $1000 \cdot 10^{-5}$ m³/s and $1200 \cdot 10^{-5}$ m³/s were observed.

The estimation of sand extraction across the delta using satellite imagery (WP1)

Sand extraction rates were estimated by 1) detecting vessels in satellite images (Sentinel-2), 2) converting the number of vessels to an extracted sand volume estimate based on production rates, and 3) correcting for cloud coverage. Between 2017 and 2022, the annual sand extraction was estimated to vary between 35 and 55 Mt/yr. Note that the resolution of the existing satellite images imposes limitations on the accuracy of the estimates, and further scrutiny is required.

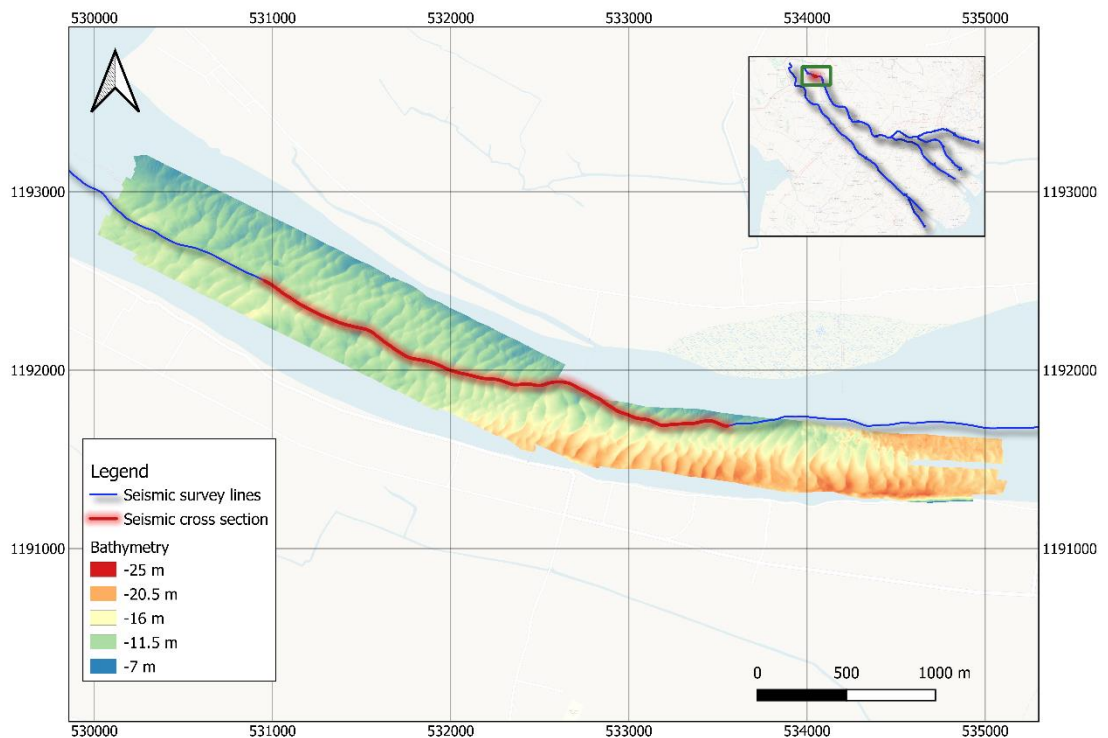


Figure 3: An overview of the seismic survey over the Mekong Delta for existing mobile sand stock estimate (top right panel) and an example of detailed multi-beam bathymetric survey (the main panel) demonstrating the dune fields, in this case, near Tan Chau (Tien River), close to the Cambodian border.

Delft3D-Flexible Mesh numerical modelling results (WP2)

The 2D Delft3D-FM model describes the Mekong River from Kratie including the Ton Le Sap Lake in Cambodia, river flood plains in Cambodia and Vietnam, the 9 river branches through the VMD and a 70km stretch over the continental shelf offshore. Successful hydrodynamic model calibration by roughness variation was carried out against measured data in terms of water levels (16 stations) and flow discharges (5 stations) for the 2021-2022 period. Scarce data from literature at locations in Cambodia show that suspended sand transport is an order of magnitude larger than sand bed load, whereas the transport of fines (silt/mud) is an order of magnitude larger than suspended sand transport. In the current study, sand transport validation was carried out based on unique, MBES-derived bed load estimates that were of the same order of magnitude as the modelled bed load.

Model results showed that total 2022 sand transport volumes hardly exceed 7Mt/yr (generally much smaller) and remain much smaller in large parts of the VMD compared to yearly estimated sand mining volumes of ~50 Mt/yr. Sand transport volume predictions remain uncertain depending on scarce model input data. However, sensitivity analyses showed that yearly sand transport volumes remain low for a range of best estimate model input parameter variations. Important factors influencing sand transports include the presence of mud and the availability of sand in the bed (bed composition). Modelled sand transports estimate towards the sea at the estuarine mouths of the different branches show that sand supply towards the mouth area remains much smaller than sand supply volumes into the VMD. These estimates at the estuarine mouth could potentially improve with a 3D model that accounts for salt-fresh water dynamics, but as salinity is mainly a dry season phenomenon, we expect this to be of smaller importance compared to other factors.

Contents

	Summary	4
	List of Abbreviations	11
	List of Figures	12
	List of Tables	19
1	Introduction	21
1.1	Background	21
1.2	Study objective	22
1.3	Overall project approach	22
1.4	Objectives of the current report	23
1.5	Structure of the current report	23
1.6	Synthesis of the existing literature	24
2	Field observations and data collection (WP1)	26
2.1	Monitoring sites and methods	26
2.1.1	Main measurement stations	27
2.1.2	Dune tracking using Multi-Beam Echo Sounder (MBES)	28
2.1.3	Sub-Bottom Profiling (SBP)	28
2.2	Monitoring results	29
2.2.1	Water Level	29
2.2.1.1	Regular measurement	29
2.2.1.2	Dry season campaign	30
2.2.1.3	Wet season	32
2.2.2	Discharge	35
2.2.2.1	Regular measurement	35
2.2.2.2	Dry season	36
2.2.2.3	Wet season	39
2.2.3	Suspended sediment concentration	41
2.2.3.1	Regular measurement	41
2.2.3.2	Dry season	42
2.2.3.3	Wet season	44
2.2.4	Riverbed sample	47
2.2.4.1	Dry season	47
2.2.4.2	Wet season	48
2.2.5	SBP data collection	48
2.2.6	MBES survey summary	49
2.2.6.1	Dry season	50
2.2.6.2	Wet season	50
2.3	Secondary data collection	51
3	Data analysis (WP1)	53

3.1	Bed load transport	53
3.1.1	Introduction	53
3.1.2	Approach	53
3.1.3	Description of sand wave characteristics from visual inspection	56
3.1.3.1	Dry Season	56
3.1.3.2	Wet Season	57
3.1.4	Bed load transport from 2D correlation analysis	59
3.1.4.1	Dry Season	59
3.1.4.2	Wet Season	62
3.1.5	Bedload transport compared to other studies	71
3.2	Existing mobile sand stock	71
3.2.1	Sub-bottom profiling as the main approach	71
3.2.2	Sub-bottom data	71
3.2.3	In-river boreholes and grab samples	71
3.2.4	Multi-beam data	74
3.2.5	Interpretation method	75
3.2.6	Existing mobile sand stock calculation method	76
3.2.7	Results	76
3.2.8	Total existing mobile sand stock	79
3.2.9	Discussion	79
3.3	Sand extraction estimates	79
3.3.1	Background	79
3.3.2	Methodology	82
3.3.3	Results	85
3.3.4	Discussions	88
4	Sand transport modelling (WP2)	89
4.1	Introduction	89
4.1.1	Area description and flow dynamics	89
4.1.2	Hydrodynamic modelling	90
4.1.3	Observation based sediment properties.	91
4.2	Model setup	94
4.2.1	Software requirements	94
4.2.2	Software description	94
4.2.3	Hydrodynamic model setup	95
4.2.4	Grid generation and improvement	95
4.2.5	Bathymetry	97
4.2.6	Boundary conditions	98
4.2.7	Initial conditions	98
4.2.8	Sediment transport model setup	98
4.3	Hydrodynamic model validation	100
4.4	Sediment transport scenario simulations	104
4.5	Sand transport calibration	104
4.5.1	Bed load	104
4.5.2	Suspended load	107
4.6	Comparison to fine sediment transport modelling	112
4.7	Sand transport modelling discussion	113
5	Stakeholder engagement	115

5.1	Consultations	115
5.2	Workshops	116
5.2.1	Inception workshop	116
5.2.2	1 st Progress workshop	117
5.2.3	2 nd Progress workshop (Validation Workshop)	118
5.3	Trainings	119
5.3.1	Training on monitoring	119
5.3.2	Training on modelling	120
6	Sand Budget Mekong Delta (WP2)	124
7	References	126
A	Appendix-A	131
A.1	Dry season riverbed sampling results	132
A.2	Wet season riverbed sampling results	135
B	Appendix B	138

List of Abbreviations

Abbreviation	Description
ADCP	Acoustic Doppler Current Profilers
CEFD	Centre for Environmental Fluid Dynamics
DARD	Department of Agriculture and Rural Development
DONRE	Department of Natural Resources and Environment
IKI	International Climate Initiative
LISST	Laser In-Situ Scattering and Transmissometry
MARD	Ministry of Agriculture and Rural Development
MBES	Multi-beam echosounder survey
MoC	Ministry of Construction
MoNRE	Ministry of Natural Resources and Environment
MPI	Ministry of Planning and Investment
MRC	Mekong River Commission
NSE	Nash-Sutcliffe efficiency
RGSPan	River Geomorphology Stability Plan (parallel project)
SBP	Sub-bottom Profiling
SSC	Suspended Sediment Concentration
VMD	Vietnamese Mekong Delta
VNDDMA	Viet Nam Dike and Disaster Management Authority
WL	Water Level
WP	Work Package

List of Figures

Figure 1: Sand budget of the Mekong Delta with a perspective of sand availability towards mid-century.	4
Figure 2: Overview of how project components contribute to the development of the Mekong Sand Budget.	5
Figure 3: An overview of the seismic survey over the Mekong Delta for existing mobile sand stock estimate (top right panel) and an example of detailed multi-beam bathymetric survey (the main panel) demonstrating the dune fields, in this case, near Tan Chau (Tien River), close to the Cambodian border.	6
Figure 1-1: An overview of the Mekong River and its catchment area across six countries, draining through the Vietnamese Mekong Delta in red dashed line (from Eslami, 2022).	21
Figure 1-2: An imaginary cross-profile of the VMD through an estuarine system, the observed rates of trends (red) and the primary anthropogenic (black) drivers along with climate change (purple) (from Eslami, 2022).	22
Figure 1-3: The project timeline against the seasonal variability of the Mekong River discharge.	23
Figure 1-4: Sand mining and sand barges in An Giang (a) and Tien Giang (b) provinces, Vietnam (Pictures: Courtesy of Huynh Buu Dau/Tuoi Tre News)	24
Figure 2-1: Overview of monitoring locations. Hydrodynamic and sediment observations were collected at five Category 1 stations (WL, discharge, SSC, sediment samples) and four Category 2 stations (WL, discharge, SSC, sediment samples). Stations no.1 to no.4 are MBES in dry season, while in wet season MBES survey was carried out at all 12 stations.	26
Figure 2-2: Overview of the sediment sampling locations	29
Figure 2-3: Daily average water level data from regular measurement at stations on Tien River.	29
Figure 2-4: Daily average water level data from regular measurement at stations on Hau River.	30
Figure 2-5: Dry season water level observations in Tien River (black boxes: discharge measurement period).	31
Figure 2-6: A zoomed in on water level measurements on 31 st March in Tien River.	31
Figure 2-7: Dry season water level observations in Hau River (black boxes: discharge measurement period)	31
Figure 2-8: A zoomed in on water level measurements on 31 st March in Hau River.	32
Figure 2-9: Wet season water level observations in Tien River (black boxes: discharge measurement period).	33
Figure 2-10: A zoomed in on water level measurements on 24 th of September in Tien River.	34
Figure 2-11: Wet season water level observations in Hau River (black boxes: discharge measurement period).	34

Figure 2-12: A zoomed in on water level measurements on 24 th of September in Hau River.	34
Figure 2-13: Daily average discharge data from regular measurement at stations on Tien river.	35
Figure 2-14: Observed daily average discharge of regular measurement at stations on Hau River.	35
Figure 2-15: Dry season discharge and water level data at stations on Tien River during daytime measurements: (a) Tan Chau, (b) Cho Lach, (c) Vam Nao, (d) My Tho, (e) My Thuan, (f) Binh Dai.	38
Figure 2-16: Dry season discharge and water level data at stations on Hau River during daytime measurements: (a) Chau Doc, (b) Can Tho, (c) Dai Ngai	39
Figure 2-17: Wet season discharge and WL data at stations on Tien River during daytime measurements: (a) My Tho, (b) My Thuan, (c) Binh Dai, (d) Cho Lach.	40
Figure 2-18: Wet season discharge and water level data at stations on Hau River during daytime measurements: (a) Can Tho, (b) Dai Ngai.	41
Figure 2-19: Daily average SSC data from regular measurement at stations on Tien River.	42
Figure 2-20: Daily average SSC data from regular measurement at stations on Hau River.	42
Figure 2-21: SSC data in dry season at stations on Tien River with two different measurement techniques.	43
Figure 2-22: SSC data in dry season at stations on Hau River with two different measurement techniques.	44
Figure 2-23: SSC data in wet season at stations on Tien River with two different measurement techniques	46
Figure 2-24: SSC data in dry season at stations on Hau River with two different measurement techniques.	47
Figure 2-25: A summary of dry season riverbed sampling results.	48
Figure 2-26: A summary of the wet season riverbed sampling results.	48
Figure 2-27: Riverbed sampling results from SBP survey campaign	49
Figure 2-28: Example of upstream sub-bottom profile (upper: Chau Doc, lower: My Tho)	49
Figure 2-29: Example of a dune field near Can Tho and the movement between 2 MBES phases	50
Figure 2-30: Example of a dune field near Tan Chau and the movement between 2 MBES phase.	51
Figure 3-1: Flow chart of how bed load transport is obtained from multi-beam survey results.	54
Figure 3-2: An example of cross correlation analysis, depicting the sand waves (coloured bathymetry), the contours of sand waves for the first (black line) and second (blue line) bathymetric survey and the observed migration distance and direction for a single transect point (red line). The example points are extracted from the 2D cross-correlation analysis for Can Tho.	54

Figure 3-3: Sand wave field gradients, showing slope magnitudes for the Can Tho sand wave field during the dry season.	55
Figure 3-4: Overview of MBES data acquired during the dry season monitoring. Polygons denote overlapping MBES data for successive measurements to be used for the dune tracking. Transects are drawn in the dominant sand wave migration direction for validation of the automated dune tracking.	56
Figure 3-5: Bed elevation profiles for transects across sand wave fields during the dry season campaign. The distance is defined in the downstream direction.	57
Figure 3-6: Overview of MBES data acquired during the wet season monitoring for which we can track dunes. Transects are drawn in the dominant sand wave migration direction for validation of the automated dune tracking.	58
Figure 3-7: Bed elevation profiles for transects across sand wave fields during the wet season campaign (see Figure 3-6). The distance is defined in the downstream direction.	59
Figure 3-8: Upper panel: Sand wave fields and bed load transport vectors for Tan Chau during the dry season . Lower panels: Distributions for the sand wave height, sand wavelength, migration rate, and bed load transport.	60
Figure 3-9: Upper panel: Sand wave fields and bed load transport vectors for Chau Doc, field 1 , during the dry season . Lower panels: Distributions for the sand wave height, sand wavelength, migration rate, and bed load transport.	61
Figure 3-10: Upper panel: Sand wave fields and bed load transport vectors for Chau Doc, field 2 , during the dry season . Lower panels: Distributions for the sand wave height, sand wavelength, migration rate, and bed load transport.	61
<i>Figure 3-11: Upper panel: Sand wave fields and bed load transport vectors for Can Tho during the dry season. Lower panels: Distributions for the sand wave height, sand wave</i>	62
Figure 3-12: Upper panel: Sand wave fields and bed load transport vectors for Tan Chau during the wet season . Lower panels: Distributions for the sand wave height, sand wavelength, migration rate, and bed load transport.	64
Figure 3-13: Upper panel: Sand wave fields and bed load transport vectors for Chau Doc during the wet season . Lower panels: Distributions for the sand wave height, sand wavelength, migration rate, and bed load transport.	64
Figure 3-14: Upper panel: Sand wave fields and bed load transport vectors for Can Tho during the wet season . Lower panels: Distributions for the sand wave height, sand wavelength, migration rate, and bed load transport.	65
Figure 3-15: Upper panel: Sand wave fields and bed load transport vectors for Vam Nao during the wet season . Lower panels: Distributions for the sand wave height, sand wavelength, migration rate, and bed load transport.	66
Figure 3-16: Upper panel: Sand wave fields and bed load transport vectors for Cho Lach 2 during the wet season . Lower panels: Distributions for the sand wave height, sand wavelength, migration rate, and bed load transport.	67

- Figure 3-17: Upper panel: Sand wave fields and bed load transport vectors for **Long Xuyen** during the **wet season**. Lower panels: Distributions for the sand wave height, sand wavelength, migration rate, and bed load transport. 68
- Figure 3-18: Upper panel: Sand wave fields and bed load transport vectors for **Cao Lanh** during the **wet season**. Lower panels: Distributions for the sand wave height, sand wavelength, migration rate, and bed load transport. 68
- Figure 3-19: Estimation of the effective river width (arrows) for total bed load estimation, showing cross-sections (red lines) and dune field regions (dashed squares) observed in the MBES results, for the five stations where cross-sections were available 69
- Figure 3-20: Overview of all the SBP coverage (purple line) and the grab samples. The numbers are the sample IDs. The symbol shape represents the different sediment classes, and colours indicate the subclasses based on grain size (D50). 72
- Figure 3-21: In-river boreholes to aid the seismic interpretation available at three provinces (The red points in the map), mostly situated in the lower delta. 73
- Figure 3-22: A location near Tan Chau where both MBES and SBP data were recorded. From the bathymetric data we can see the extent of the sand waves whereas the sub-bottom data can image the base of the mobile layer and therefore its thickness. 73
- Figure 3-23: Three examples of the width of the section with sand versus the river cross-section. 74
- Figure 3-24: SBP section near Tan Chau. The sand dunes are clearly visible, and the base and thickness of the mobile sand layer is mapped. Below the base of the mobile layer there are sedimentary structures visible to which no sediment class can be assigned without any additional ground truthing (e.g., boreholes). 75
- Figure 3-25: Example of a SBP with two boreholes (SH25 and SH27) and one grab sample (indicating fine sand) helping to outline the top sand layer even if there are no clear sand ripples or dunes present. 75
- Figure 3-26: Thickness of the top (existing mobile) sand layer along every 1 m of the Mekong River. At river sections where no thickness is shown in the map, no sand layer was observed. 77*
- Figure 3-27: Lower estimate of the existing mobile sand stock along sections of 3 kilometres. These are calculated with (Equation 3-1, using the sand thickness from and assuming a lateral extent of the sand layer spanning 50% of the river width. 78*
- Figure 3-28: Upper estimate of the existing mobile sand stock along sections of 3 kilometres. These are calculated with Equation 3-1, using the sand thickness and assuming a lateral extent of the sand layer spanning 75% of the river width. 78*
- Figure 3-29: A: PlanetScope image of Area of Interest, B: Zoomed in on A, C: definition of vessel dimensions, D: Vessel dimensions as found by Hackney et al., (2021). 81
- Figure 3-30: Scheme of active dredging barge geometries and sizes from high-resolution imagery (Google earth basemap, Airbus, 2023) 83
- Figure 3-31: Blobs detected as potential vessels (brown blobs) and filtered barges with cranes (orange blobs) for a section of the Mekong during 2021. 84

Figure 3-32: Production chart of a 10 m ³ grab dredgers based on hoisting time and dredging depth (Central Dredging Association, 2023).	84
Figure 3-33: Percentage of cloud cover in a tile area next to Vinh Long (2017-2022), for (above) the full Sentinel 2 series, and (below) the filtered cloudless conditions.	85
Figure 3-34: Filtered barges with vessels (blobs) detected between 2022-01-01 and 2022-12-31 for a section of the Mekong River.	86
Figure 3-35: Number of active barges with cranes (BC) detected between 2017-01-01 and 2023-01-01 in the Vietnam Mekong Delta (daily sum of all tiles)..	86
Figure 3-36, Manually classified active barges with cranes vs. double moored transport vessels (which show the same geometrical characteristics in S2 imagery), zone-example.	87
Figure 3-37: Annual extracted sand volume estimated in this study between 2017 and 2023-01-01 in black (min) and grey (max) bar charts compared to those determined by other studies previously.	88
Figure 4-1: Temporal variation of daily water discharge at Kratie (data from Darby et al., 2016).	89
Figure 4-2: The annual flood peaks and volumes at Kratie from 1961 to 2022. The green and black boxes indicate significant (mean \pm SD) and extreme (mean \pm 2 SD) drought or flood years respectively (SD refers to standard deviation).	90
Figure 4-3: Kratie mass percentage of sediment fractions in suspended load 2019 and SSC at 4 vertical positions in water column (upper panels) and bed load (middle panel, mind that up to 10 samples are presented per date); Prek Kdam mass percentage of sediment fractions in suspended load 2019 and SSC at 4 vertical positions in water column.	92
Figure 4-4: Mass percentage of sediment fractions in sediment suspension 2018 and 2019 (1 st and 2 nd rows), suspended sediment concentration (3 rd row) and river discharge (4 th row) for Chau Doc (left panels) and Tan Chau (right panels).	93
Figure 4-5: Bed sediment composition distribution over VMD based on grab samples.	94
Figure 4-6: Numerical grid consisting of 1D elements and 2D cells.	96
Figure 4-7: Numerical grid and river topography and shelf topography of the VMD.	97
Figure 4-8: Bathymetry collected in the Mekong Delta	98
Figure 4-9: Calibrated manning's roughness.	100
Figure 4-10: Model performance of water levels at Cambodia stations in 2021-2022.	102
Figure 4-11: Model performance of water levels at Vietnamese stations in 2021-2022.	102
Figure 4-12: Model performance of discharges at Cambodian stations.	103
Figure 4-13: Discharge validation for Vietnamese stations.	103
Figure 4-14: Dry season bed load transport at Tan Chau (upper panel), Chau Doc (middle panel) and Can Tho (lower panel). Model results are given in red lines (D=100 μ m, runfsD100), blue	

lines (D=200µm, runfs) and yellow lines (D=300µm, runfsD300). Grey area reflects bed load estimate ranges (mean+/- standard deviation including flow width uncertainty) averaged over 18 days based on MBES analysis.	105
Figure 4-15: Wet season bed load transport at, from top to down, Tan Chau, Chau Doc, Can Tho, Vam Nao, Co Lach, Long Xuyen, Cao Lanh. Model results are given in red lines (D=100µm, runfsD100), blue lines (D=200µm, runfs) and yellow lines (D=300µm, runfsD300). Grey area reflects bed load estimate ranges (mean+/- standard deviation including flow width uncertainty) averaged over 12 days based on MBES analysis.	106
Figure 4-16: Dry season cumulative bed load transport through Tan Chau (upper panel), Chau Doc (middle panel) and Can Tho (lower panel) cross sections. Model results are given in red lines (D=100µm, runfsD100), blue lines (D=200µm, runfs) and yellow lines (D=300µm, runfsD300). Grey area reflects bed load estimate ranges (mean+/- standard deviation including flow width uncertainty) averaged over 18 days based on MBES analysis and extrapolated over cross-section.	106
Figure 4-17: Wet season cumulative bed load transport through (from top to down) Tan Chau, Chau Doc, Can Tho, Vam Nao, Co Lach, Long Xuyen, Cao Lanh cross-sections. Model results are given in red lines (D=100µm, runfsD100), blue lines (D=200µm, runfs) and yellow lines (D=300µm, runfsD300). Grey area reflects bed load estimate ranges (mean+/- standard deviation including flow width uncertainty) averaged over 12 days based on MBES analysis and extrapolated over cross-section.	107
Figure 4-18: Comparison of modelled (sand and mud, runfsm) and observed SSC levels.	108
Figure 4-19: Colour definition of VMD river branches. Provincial borders in white lines.	108
Figure 4-20: 2022 Cumulative river flow distribution over VMD river branches	109
Figure 4-21: Runfs cumulative sand transport over year 2022 for various stations spread over the VMD that have MBES data.	109
Figure 4-22: 2022 cumulative bed load (left column) and suspended load (right column) sand transport for runfs (upper row) and runfssdb (lower row)	110
Figure 4-23: 2022 cumulative sand transport along Co Chien and Bassac branches. Solid line reflects runfs whereas thin lines reflect runfsD100 and thick lines runfsD300.	111
Figure 4-24: 2022 cumulative mud transport for runfsm	112
Figure 4-25: 2022 cumulative total (bed load + suspended load) sand transport for runfsm.	112
Figure 4-26: 2022 cumulative sand transport along two main Mekong branches for different model runs, where runfsm may be considered as the most adequate.	114
Figure 5-1: Inception workshop in Can Tho	117
Figure 5-2: Consortium team members answered participant's questions during 1 st Progress workshop.	118
Figure 5-3: Consortium team members presenting draft sand budget results in the 2 nd progress workshop.	119

Figure 5-4: Demonstration / testing EdgeTech 6205s (Multi-beam Echo Sounder, MBES) components	120
Figure 5-5: Modelling training in Can Tho.	123
Figure 5-6: Training to use sand budget model.	123
Figure 6-1: An overview of contribution from different activities leading to the VMD sand budget.	124
Figure 6-2: Estimates of various components of the sand budget.	125
Figure 6-3: An outlook towards mid-century given the upper and lower estimates of incoming, outgoing, extraction and existing mobile sand stock.	125

List of Tables

Table 2-1: Overview of the field measurements supporting the sand budget.	27
Table 2-2: Observed water level at 4 Cat-2 stations and 5 Cat-1 stations in dry season campaign.	31
Table 2-3: Water level features at 4 Cat-2 stations and 5 Cat-1 stations in wet season campaign.	33
Table 2-4: Observed discharge at 4 Cat-2 stations and 5 Cat-1 stations in dry season campaign.	36
Table 2-5: Observed discharge features at 4 Cat-2 stations and 2 Cat-1 stations in wet season campaign.	39
Table 2-6: Suspended sediment concentration (LISST) at 4 Cat-2 stations and 5 Cat-1 stations in dry season.	42
Table 2-7: Suspended sediment concentration (Bottle) at 4 Cat-2 stations and 5 Cat-1 stations in dry season.	43
Table 2-8: Suspended sediment concentration (LISST) at 4 Cat-2 stations and 5 Cat-1 stations in wet season.	45
Table 2-9: Suspended sediment concentration (Bottle) at 4 Cat-2 stations and 5 Cat-1 stations in wet season.	45
Table 2-10: MBES overall results in dry season	50
Table 2-11: MBES overall results in wet season	51
Table 3-1: Overview of bed load transport estimates for the VMD. Note that total bed loads (Jordan et al., 2019) are converted to 10^{-5} m ³ /s, and bed load per unit river width (Stephens et al., 2017) to 10^{-8} m ³ /s/m, according to the units in the following sections.	56
Table 3-2: Overview of the approximate measurement area that is suitable for dune tracking analysis, the approximate sand wavelength, height, and migration distance during the dry season survey period based on visual inspection of multibeam measurements .	57
Table 3-3: Overview of the approximate measurement area suitable for dune tracking analysis, the approximate sand wavelength, height, and migration distance during the wet season survey period based on visual inspection of multibeam measurements . Sand wave characteristics for My Thuan are mentioned in brackets since this sand wave was only observed for a single survey. For this reason, we cannot track the dune migration. For Binh Dai and Dai Ngai, sand wave characteristics are mentioned in brackets since they are too small in height and length for dune tracking analysis. For Cho Lach 1, no correlation can be observed between the phase 1 and 2 measurements since migration distances and sand wave shape change were too large.	58
Table 3-4: Summary of the dry season results from the 2D correlation and Fourier analyses; sand wave field characteristics, migration direction and rates and the resulting bed load for Can Tho, Tan Chau, and Chau Doc. Both mean results and the standard deviation are given.	60

Table 3-5: Summary of the wet season results from the 2D correlation and Fourier analyses; sand wave field characteristics, migration direction and rates and the resulting bed load for Tan Chau, Chau Doc, and Can Tho. Both mean results and the standard deviation are given.	62
Table 3-6: Summary of the wet season results from the 2D correlation and Fourier analyses; sand wave field characteristics, migration direction and rates and the resulting bed load for Vam Nao, Cho Lach, Long Xuyen, and Cao Lanh. Both mean results and the standard deviation are given.	63
Table 3-7: Estimation of the total bed load transport in $10^{-8} \text{ m}^3/\text{S}$ during the wet season based on the bed load estimate per unit river width and the estimated effective river width.	70
Table 3-8: Estimation of the total bed load transport in $10^{-8} \text{ m}^3/\text{S}$ during the wet season based on the bed load estimate per unit river width and the estimated effective river width.	70
Table 3-9: Lower and upper estimates of total existing mobile sand stock for the Mekong River	79
Table 3-10: Overview of satellite imagery datasets	80
Table 3-11: Overview of the difference between the methodology applied in this study, Hackney et al. (2021) and Gruel et al. (2022).	85
Table 4-1: Sediment classification (Wentworth scale)	91
Table 4-2: Describes how data were used for model validation and calibration.	99
Table 4-3: Location of stations.	101
Table 4-4: Definitions of various simulation ID's (run-names).	104
Table 4-5: Sediment load through cross-sections. * Indicates mouth cross-section.	113
Table 5-1: List of Consultation Meetings	115
Table 5-2: Survey statistics of participants before the training course on using the model.	121
Table 5-3: Survey statistics of participants after the training course on using the model.	122
Table 5-4: Evaluation of the quality of the training course.	122

1 Introduction

1.1 Background

The Vietnamese Mekong Delta (hereafter, VMD, see Figure 1-1) is existential to the livelihood, jobs, and food security of more than 17 M people in Vietnam and beyond. By producing 50% of the national staple food and 40% of the nation's fisheries, the VMD accounts for 18% of Vietnam's GDP. The rapidly urbanizing VMD, as one of the lowest-lying delta's worldwide, is under stress from various climatic and anthropogenic drivers and disproportionately vulnerable to various environmental forces. Salt intrusion, land subsidence, flooding, coastal erosion, deteriorating water quality, and biodiversity depletion are among processes that threaten Vietnam's food security and the strategic development of the delta (see Figure 1-2). Recent scientific findings demonstrate that riverbed-, riverbank- and coastal erosion, tidal amplification and salt intrusion are mainly driven by anthropogenic sediment starvation of the delta (Bravard et al., 2013; Brunier et al., 2014; Anthony, 2015; Eslami et al., 2019b). For example, (Eslami et al., 2019b, 2021a, b) showed that salt intrusion in the VMD has only been marginally influenced by climate change, but mostly driven by riverbed erosion due to sediment starvation. In the context of global climate change, and the increasing threats of *relative* sea level rise (Eslami et al., 2021b; Minderhoud et al., 2020), preserving the riverbed levels of the VMD becomes an existential priority as a mitigating strategy towards a changing climate.



Figure 1-1: An overview of the Mekong River and its catchment area across six countries, draining through the Vietnamese Mekong Delta in red dashed line (from Eslami, 2022).

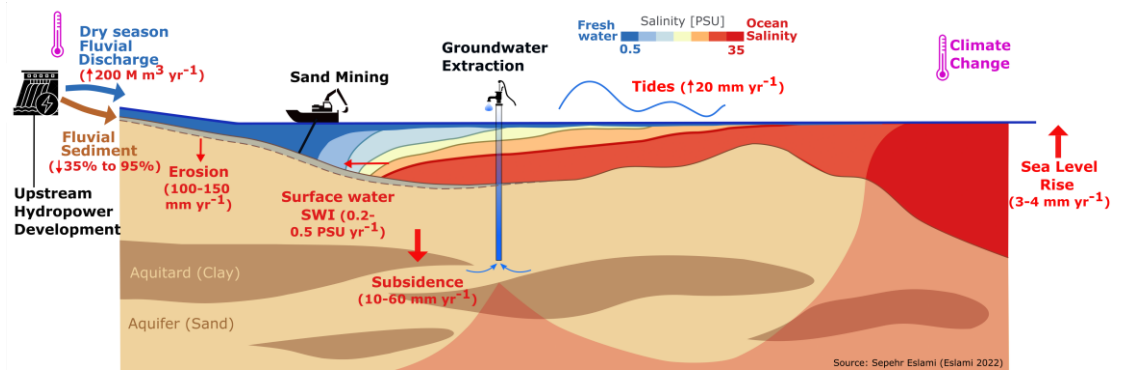


Figure 1-2: An imaginary cross-profile of the VMD through an estuarine system, the observed **rates of trends** (red) and the primary anthropogenic (black) drivers along with **climate change** (purple) (from Eslami, 2022).

Sediment starvation can be classified under two categories: A) Fine sediment shortage due to hydropower developments in the upper Mekong Basin, and B) coarse sediment decline due to sand mining within (and beyond) the VMD. Considering the hydropower development in Mekong tributaries, the aggregate sediment trapping of the dams are predicted to reduce sediment supply by 36% (moderate)-95% (worst case) (Manh et al., 2015), and a recent study measured 75% reduction in suspended sediment supply to the VMD (Thi Ha et al., 2018). Estimates of sand mining within the VMD have increased in time from 10-12 Mt Yr⁻¹ (Bravard et al., 2013; Brunier et al., 2014) based on morphological changes and surveying the miners, to 25-30 Mt Yr⁻¹ (Jordan et al., 2019) based on local observations of sand extraction and its extrapolation, and 40-50 Mt Yr⁻¹ (Eslami et al., 2019b) based on the 2015 issued sand mining licenses. While bedload ($0.18 \pm 0.07 \text{ Mt yr}^{-1}$) is a small (1%) fraction of the total annual sediment load of the lower Mekong River (Koehnken, 2014; Hackney et al., 2020), even when considering suspended sand ($6 \pm 2 \text{ Mt yr}^{-1}$), the total sand flux entering the Mekong delta ($6.18 \pm 2.01 \text{ Mt yr}^{-1}$) is far less than current sand extraction rates (50 Mt yr^{-1}). With foreseen 1 billion m³ sand demand until 2040 (SIWRP, 2015) and continuous erosion due to upstream sediment trapping, a systematic derivation of VMD sand budget is a crucial step towards sustainable management of the deltaic natural resources.

1.2 Study objective

In the context of the International Climate Initiative (IKI) project, the current study aims to derive an accurate account of the VMD sand budget. The study approach combines available and new data (Work Package WP1), state-of-the art numerical modelling (WP2) and national and provincial VMD stakeholders' consultation (WP1 and WP2). The analyses will include an estimation of the incoming sediment from Cambodia, an updated estimate of sand extraction within the delta, the distribution of sediments within the (major) multi-channel estuarine system and an estimation of the existing sand reserves in the delta. The results from this project will serve as basis for a sustainable governance and mitigation of the VMD's vulnerability to climate change and anthropogenic influence.

1.3 Overall project approach

To derive a robust sand budget, four factors need to be determined; 1) the sand entering the lower Mekong Delta, 2) sand leaving the delta, 3) extracted sand in the delta and 4) local existing mobile sand stock of the VMD. In the current study, this is realized by combining existing literature, new and existing measurements (WP1) and numerical modelling (WP2), in close and continuous exchange with the local stakeholders. More specifically, the sand budget is derived measuring the fluvial sand supply to the VMD, obtaining realistic estimates of the sand mining volumes by satellite imagery analyses, together with determining the existing mobile sand stock of the VMD through sub-bottom profiling (WP1) and evaluating the sediment

exchange with the sea (using model and data). The existing numerical models were calibrated and validated by secondary data and new observations (WP2). Figure 1-3 presents the realized timeline of the project and the various activities carried out throughout 2022 and 2023. These findings are integrated and used to establish the existing and future (2030-2050) sand budget, in close cooperation with the client and key stakeholders. In addition to the existing measurements, we measured the following additional parameters within the VMD at several locations (also see Chapter 2):

- Water level (hereafter, WL)
- Discharge
- Suspended Sediment Concentration (hereafter, SSC)
- Bedload transport by dune tracking; Multi-Beam Echo-Sounder survey (hereafter, MBES)
- Existing mobile sand stock by means of Sub-Bottom Profiling (SBP)
- Riverbed composition from bottom-sediment grabs (sieving curves)

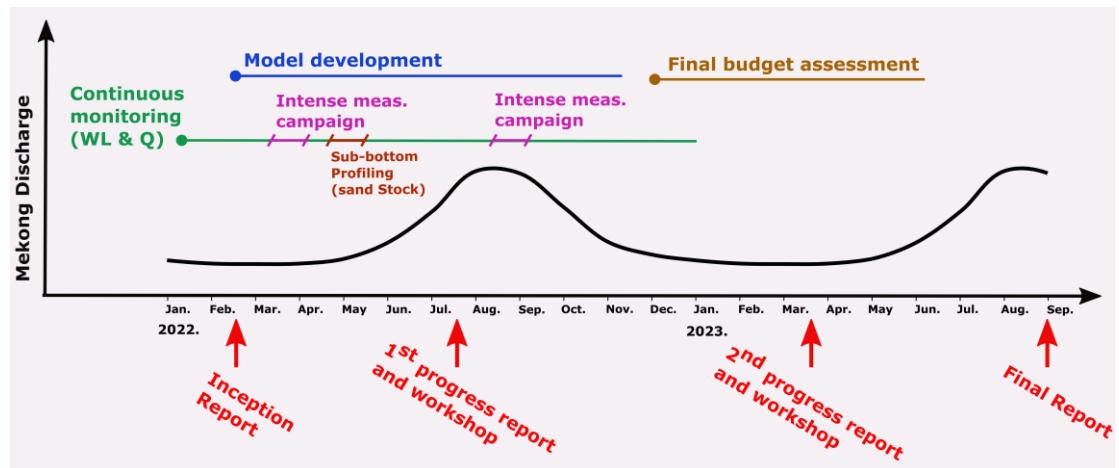


Figure 1-3: The project timeline against the seasonal variability of the Mekong River discharge.

1.4 Objectives of the current report

In compliance with the project agreement number FY22-VN-MDL-0029, the present document is the final report to convey definitive results of the 18-month project “Consultancy services to develop a delta-wide sand budget for the Vietnamese Mekong Delta Region” to WWF-Vietnam, MARD-VNDDMA and WWF-Germany and other stakeholders. The current project is part of the larger project “Drifting Sands: Mitigating the impacts of climate change in the Mekong Delta through public and private sector engagement in the sand industry”.

1.5 Structure of the current report

The current project “Consultancy services to develop a delta-wide sand budget for the Vietnamese Mekong Delta Region” has been divided into two work packages:

- - Work package 1: Field Observations
- - Work Package 2: Numerical modelling and derivation of the *sand budget*

Chapter 1 expands on the background and provides an introduction; Chapter 2 summarizes all the field measurements carried out continuously over the year 2022 or during the two intense field campaigns; Chapter 3 presents the results of the modelling work; Chapter 4 assembles the stakeholder consultation and engagement activities, and Chapter 5 includes the conclusions and the final results of the sand budget.

1.6 Synthesis of the existing literature

Sediment in the Mekong Delta can be distinguished as fine (silt and mud) mainly transported as suspended load, and coarse (sand) transported as bed or suspended load. With sediment starvation key to different destructive trends in the delta (e.g., tidal amplification, erosion, salt intrusion, elevation loss), most of the work done previously has been focused on suspended sediment (~99%), more than 95% of which is fine sediment. The earlier estimates of sediment transport by the Mekong River were ~160 Mt Yr⁻¹ (Milliman and Fransworth, 2011), which is expected to have reduced by 36% (moderate)-95% (worst case) (Manh et al., 2015; Darby et al., 2016; Thanh et al., 2017; Thi Ha et al., 2018; Dunn et al., 2019).



Figure 1-4: Sand mining and sand barges in An Giang (a) and Tien Giang (b) provinces, Vietnam (Pictures: Courtesy of Huynh Buu Dau/Tuoi Tre News)

While the coarse sediment (sand) **transport**, mainly in form of **bedload**, only accounts for ~1% of total sediment transport (Koehnken, 2014; Hackney et al., 2020), yet, the sheer volumes of sand extraction within the delta (Bravard et al., 2013; Brunier et al., 2014; Jordan et al., 2019; Eslami et al., 2019b), estimated ~50 Mt Yr⁻¹, makes the relevance of sand and its transport on par with fine sediment. These amounts are responsible for a large part of the observed riverbed

and bank erosion within the delta. As the effect of sand deficit travels very slowly downstream, apart from some impact from Cambodian sand mining, this is a domestic issue with potential domestic solutions. Furthermore, due to very slow movement of sand in the fluvial system, replenishment of the mined mobile sand stock is out of any policy or management timeline perspective. Therefore, the present study will play a crucial role in providing a holistic view of sand budget within the VMD as input for developing strategic policy development.

While there is plenty of scattered information contributing to understanding of the VMD sand budget, there is still no clear account of that for the delta. Gugliotta et al., (2017) carried out an extensive survey of bed material sampling over the entire fluvial/estuarine part of the VMD and showed a clear distribution of sand and mud over the delta. Various survey campaigns (e.g., Allison et al., 2017; Jordan et al., 2019) have shown sand dunes and their movement as well as footprints of sand extraction. As the pioneers in raising the issue of sand mining along the Mekong, (Bravard et al., 2013; Brunier et al., 2014) estimated nearly 10-12 Mt Yr⁻¹ of sand extraction based on survey of the sand mining companies and morphological changes within the tidal river system of the VMD. (Jordan et al., 2019) carried out a multi-beam survey along ~20km of the Tien River, just North of My Thuan, and spotted nearly ~8 M m³ of sand mining per year in the study area. This, if extrapolated to the entire delta, translates to ~25-30 Mt Yr⁻¹. Eslami et al., (2019b) published the issued sand mining licenses over the entire delta summing up ~40-50 Mt Yr⁻¹ of legal sand extraction fields.

Given limitations in the field observations and potential illegal sand mining, the numbers can be even higher than 50 Mt Yr⁻¹. At the same time, incoming bedload to the delta is estimated to be only about 0.18 ± 0.07 Mt yr⁻¹, being ~1% of total fluvial sediment supply to the delta and an additional 6 ± 2 Mt yr⁻¹ in form of suspended sand (Koehnken, 2014; Hackney et al., 2020). (Stephens et al., 2017) carried out multibeam survey along the lower Hau distributary channels (downstream of Can Tho) and measured suspended (90%) and bed load (10%) sand transport. Then by applying a numerical model estimated 6.5 ± 1.6 Mt Yr⁻¹ of sand transport to the ocean, which mainly takes place during the wet season. Currently there is no estimate of existing mobile sand stock within the delta.

The above existing estimates, with their limitations, imply that most probably incoming and outgoing sand, within the natural system is in balance, or at least in the same order of magnitude. However, there is a huge deficit driven by sand mining from the river with grave consequences for riverbed/bank stability as well as salinity and tidal dynamics. With foreseen 1 billion m³ sand demand until 2040 (SIWRP, 2015), continuous erosion due to upstream sediment trapping and limited insight in existing mobile sand stock, a systematic derivation of VMD sand budget is a crucial step towards sustainable management of the deltaic natural resources.

2 Field observations and data collection (WP1)

2.1 Monitoring sites and methods

Field observations for the delta-wide sand budget of the VMD were carried out in three different field measurement timelines:

- **Dry season campaign:** 30th March to 23rd April 2022.
- **Wet season campaign:** 23rd September to 17th October 2022.
- **Regular measurement:** 365 days in 2022 (1st Jan to 31st Dec).

In both the dry and wet season monitoring campaigns, the following data were collected:

- 1 Water level (hereafter, WL).
- 2 Discharge.
- 3 Suspended Sediment Concentration (hereafter, SSC) by LISST and bottle samples.
- 4 Sub-Bottom Profiling (SBP, seismic geological survey for existing mobile sand stock estimation) and riverbed sampling (only in dry season).
- 5 Dune tracking for bedload estimation, using Multi-Beam Echo-Sounder (MBES).
- 6 Bed composition from bottom-sediment grab samples (sieving curves).

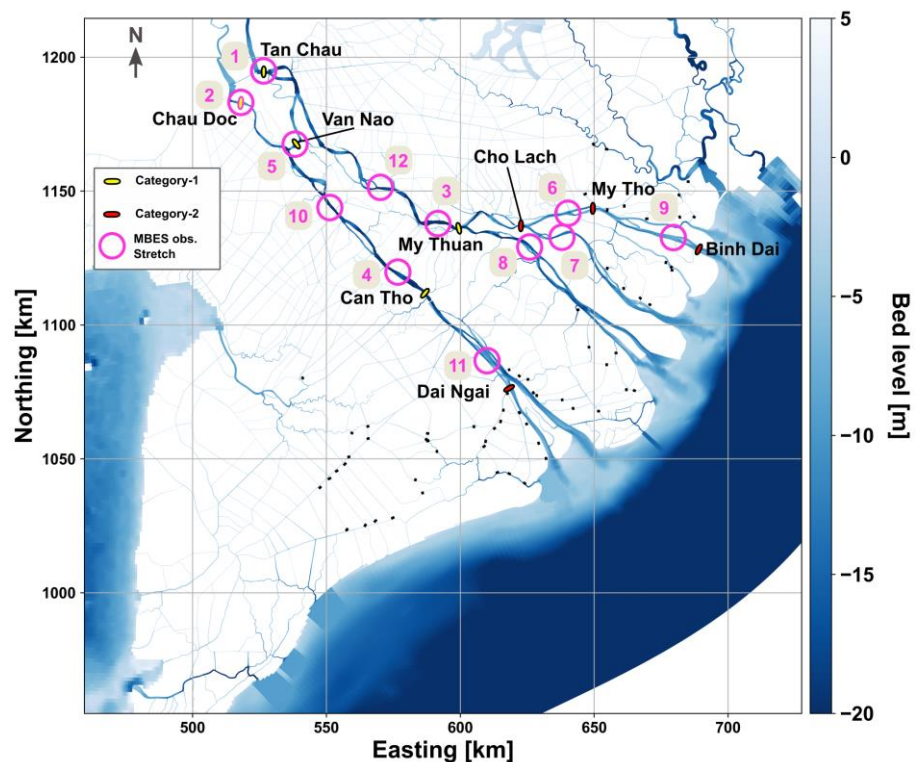


Figure 2-1: Overview of monitoring locations. Hydrodynamic and sediment observations were collected at five Category 1 stations (WL, discharge, SSC, sediment samples) and four Category 2 stations (WL, discharge, SSC, sediment samples). Stations no.1 to no.4 are MBES in dry season, while in wet season MBES survey was carried out at all 12 stations.

Figure 2-1 shows an overview of the monitoring sites and Figure 2-1 provides a detailed account of all the monitoring activities. Monitoring sites are initially defined by utilizing existing SRHMC's hydrological monitoring stations. The existing measurement stations are categorized as **Cat.1**: standard measurement stations of SRHMC with regular water level, discharge and SSC measurements and **Cat.2** that require additional mobilization for water discharge measurements, and **Cat.3** with only water level measurements.

Table 2-1: Overview of the field measurements supporting the sand budget.

	Duration	Location	Equipment
Regular Discharge	365 days (2022)	5 Cat – 1 stations: Tan Chau, Chau Doc, Vam Nao, Can Tho, My Thuan	Current meter (manual) ADCP (semi-auto) Rating curve (indirect)
Regular Water Level	365 days (2022)	5 Cat – 1 stations: Tan Chau, Chau Doc, Vam Nao, Can Tho, My Thuan 4 Cat – 2 stations: Binh Dai, Dai Ngai, Cho Lach, My Tho	Water poles (manual) Recorder (auto)
Regular SSC	365 days (2022)	5 Cat – 1 stations: Tan Chau, Chau Doc, Vam Nao, Can Tho, My Thuan	Sample + filter paper (manual)
ADCP Discharge	Dry: 10 obs / day for 6 days (30 March to 04 April 2022)	4 Cat – 2 stations: Binh Dai, Dai Ngai, Cho Lach, My Tho 5 Cat – 1 stations: Tan Chau, Chau Doc, Vam Nao, Can Tho, My Thuan	ADCP (semi-auto)
	Wet: 4 obs / day for 7 days (23 to 29 Sep 2022)	4 Cat – 2 stations: Binh Dai, Dai Ngai, Cho Lach, My Tho 2 Cat – 1 stations: Can Tho, My Thuan	
	Wet: 1 obs / day for 3 days (7, 10, 13 Oct 2022)	3 Cat – 1 stations: Tan Chau, Chau Doc, Vam Nao	
SSC	Dry: 7 obs / day in 2 days (31 March and 04 April 2022)	4 Cat – 2 stations: Binh Dai, Dai Ngai, Cho Lach, My Tho 5 Cat – 1 stations: Tan Chau, Chau Doc, Vam Nao, Can Tho, My Thuan	Sample + filter paper (manual) LISST (auto)
	Wet: 4 obs / day in 3 days (23, 26, 29 Sep 2022)		
Riverbed sample	Dry: 21 samples/station (30 March to 04 April 2022)	5 Cat – 1 stations: Tan Chau, Chau Doc, Vam Nao, Can Tho, My Thuan	Sample + lab analysis (manual)
	Wet: 21 samples/station (23 Sep to 13 Oct 2022)	4 Cat – 2 stations: Binh Dai, Dai Ngai, Cho Lach, My Tho	
SBP	Dry: 15 days (30th March – 13th April)	~550 km river route 35 crosslines 43 riverbed samples	Innomar SES-2000 compact
MBES	Dry: 15 days for both phases Phase 1: 7 days (30th March – 5th April) Phase 2: 8 days (15th April – 22nd April)	4 locations: Tan Chau, Chau Doc, My Thuan, Can Tho	Edgetech 6205s + side scan sonar system

2.1.1 Main measurement stations

From the range of stations operated by Southern Regional Hydro-meteorological Centre, two types of monitoring stations were utilized in this project for the purpose of hydrodynamic (*water level* and *discharge*) and *suspended sediment concentration* (SSC) observations:

- **Cat.1** stations: Tan Chau, Chau Doc, Vam Nao, Can Tho, My Thuan.
- **Cat.2** stations: Cho Lach, My Tho, Binh Dai, Dai Ngai.

A summary of these field observations (frequency, duration, etc.) is provided under Table 2-1. The survey activities for hydrodynamic monitoring and SSC were all conducted according to the Circulars, Decisions, and National Standards listed below, and:

- Circular No 30/2018/TT-BTNMT of MONRE on Technical regulations on monitoring and provision of information and data for specialized hydro-meteorological stations.
- Water Level: National Standard for Hydromet monitoring TCVN 12636-02:2019.
- Discharge: National Standard for Hydromet monitoring TCVN 12636-09:2020.
- Suspended Sediment Concentration: National Standard for Hydromet monitoring TCVN 12636-11:2021.
- Decision No. 1660/QD-TTg dated October 26, 2020 of the Prime Minister on the issuance of the list of state secrets in the resources and environment field.

2.1.2 Dune tracking using Multi-Beam Echo Sounder (MBES)

Dune tracking was adopted as a proxy for estimating bedload sand transport. This method was tested during the dry season for four survey locations (locations 1 to 4 in Figure 2-1), during which, except at My Thuan (station 3) at other three locations dune fields were identified and surveyed. During the flood season, MBES data were collected at twelve locations (locations 1 to 12 In Figure 2-1). The exact survey locations for the four Cat 1 stations (Station 1 - 4) were chosen following the dry season campaign and the important position of these stations close to the Cambodian border and before the two main rivers (Hau and Tien) split into estuarine distribution channels. For the other stations, we followed the SBP results and riverbed samples collected during that campaign, in close collaboration with the stakeholder to predict where the sand dunes are most likely present and suitable for dune tracking. Initial surveying tracks were outlined to optimize the dune exploration procedure. The chosen sites were located near hydrological stations, which helped the logistics and provided accurate water level measurements to be used for reference correction. Here we summarize the rationale for the choices of locations/stations bullet wise:

- Stations 1, 2, 3, and 4 are near the Tan Chau, Chau Doc, Can Tho, and My Thuan Hydrological Stations (Cat.1 Stations). These stations are essential to estimate sediment transport in the main channels.
- Station 5 at Vam Nao provides insights into the sand diversion from the Tien River to the Hau River.
- Stations 6, 7, and 8 represent sand transport within the different distributary channels.
- Station 9 indicates the sand exchange with the ocean.
- Station 11, just upstream of the estuarine junction, is supposed to represent the lower Hau sand transport regime (also see Stephens et al., 2017), where we expect less sand in the system (Allison et al., 2017).
- Stations 10 and 12 are near the Cao Lanh and Long Xuyen Hydrological Stations, located between Stations 1, 2, 3, and 4. These results give further insight into the main channel transport patterns.

2.1.3 Sub-Bottom Profiling (SBP)

The sub-bottom profiling procedure aims at acquiring information about the very shallow geology. By sending low-frequency sound waves that penetrate the riverbed, the sub-bottom profiler can record soil properties of layers up to 10-20m below the riverbed. By sailing along the river, we collected this information for approximately 550 km, providing an indication of the available existing mobile sand stock in the VMD (See Figure 2-2). Additional 35 cross-sectional SBP measurements were executed to estimate the distribution of sediment along the river width. Forty-three sediment samples were collected to help interpret the SBP results.

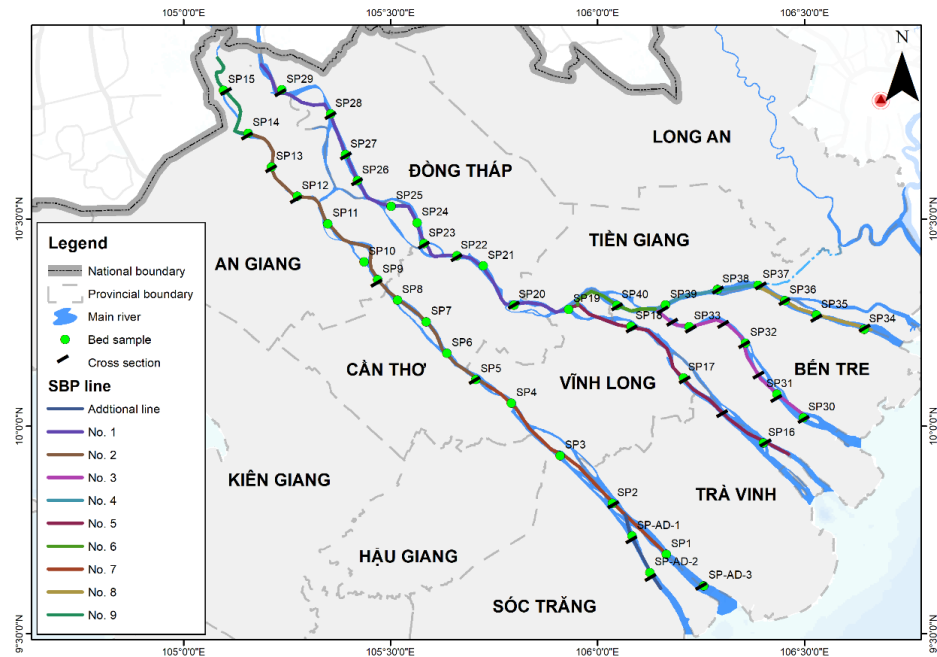


Figure 2-2: Overview of the sediment sampling locations

2.2 Monitoring results

2.2.1 Water Level

2.2.1.1 Regular measurement

Hourly water level data for 365 days in 2022 was retrieved from SRHMC regular measurement campaign. For visualization purpose, daily average data was presented in Figure 2-3 and Figure 2-4. During the dry season, due to weaker discharge tidal penetration is much larger in the system (Eslami et al., 2019a), while in the wet season the high discharge heavily dissipates tidal energy. Between January to July, all stations all affected by tide and this is evident in the semi-diurnal nature of the tides. As the flood season prevails between August to mid-November, tidal effects were more limited at downstream stations and we do not observe much of the semi-diurnal characteristics of tide in the upstream stations of Tan Chau, Chau Doc and Vam Nao. The average water level in these upstream stations is more regulated with the river stage, while average water level in the more downstream estuarine stations is more regulated with the sea water levels.

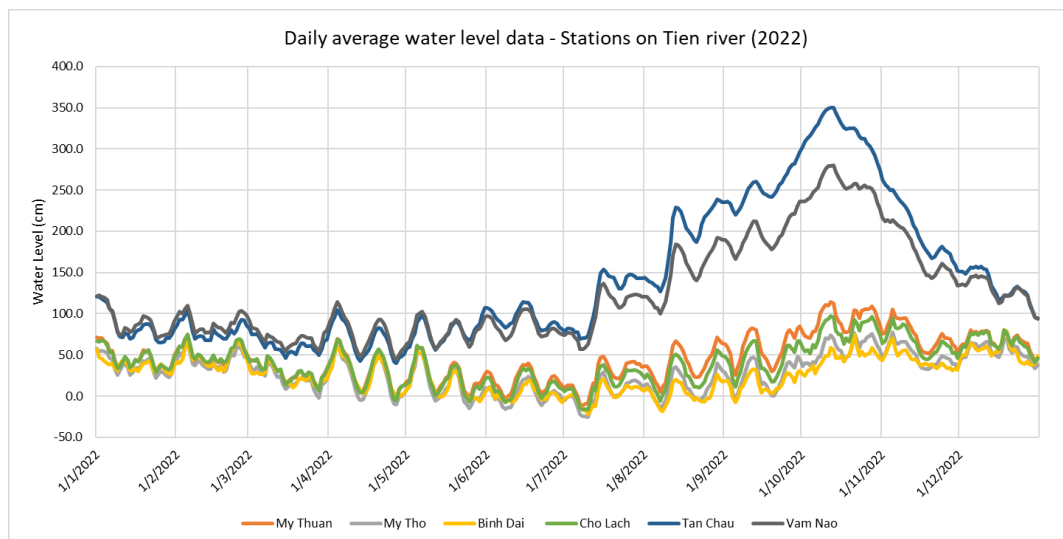


Figure 2-3: Daily average water level data from regular measurement at stations on Tien River.

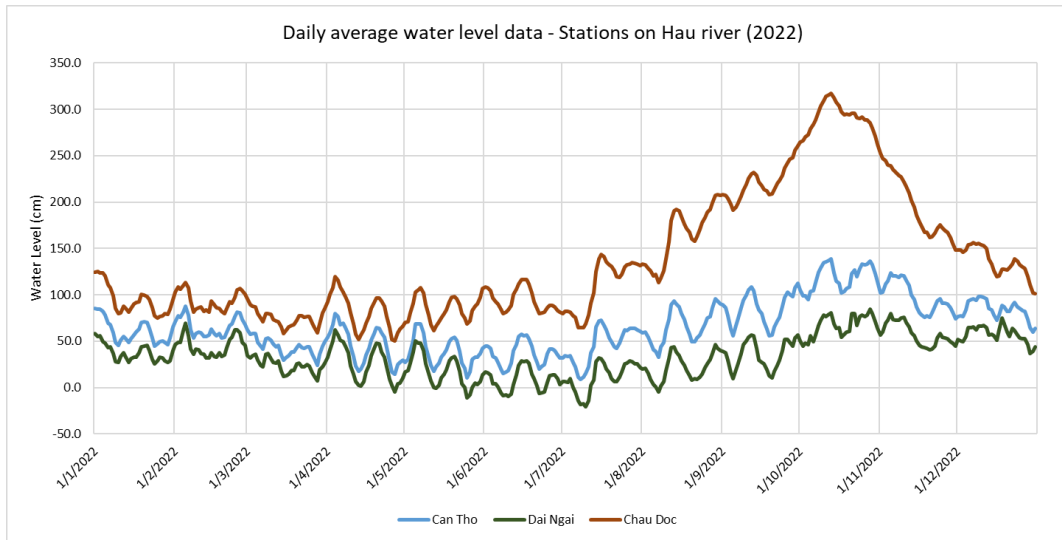


Figure 2-4: Daily average water level data from regular measurement at stations on Hau River.

2.2.1.2 Dry season campaign

Tien River: Water level in the dry season is affected mainly by East Sea semi-diurnal tide and ocean surge levels. Tidal propagation time from Binh Dai station (Dai estuarine channel) to Tan Chau station is about 6 - 7 hours (see also Eslami et al., 2019a). Minimum water level at downstream stations ranged from -150 – -20 cm [w.r.t. MSL], and from -10 – 50 cm at upstream stations. Meanwhile maximum water level is normally ~150cm for all stations (see.

Hau River: Water level in the dry season is affected purely by East Sea semi-diurnal tide and ocean surge levels. Tide transmission time from Dai Ngai station to Chau Doc station is about 5 - 6 hours (see also Eslami et al., 2019a). Minimum water level at downstream stations (Can Tho, Dai Ngai) ranged from -140 – 10 cm [w.r.t. MSL], and from 0 – 20 cm at upstream station (Chau Doc). Meanwhile maximum water level is normally ~150 – 170 cm for all stations.

Table 2-2: Observed water level at 4 Cat-2 stations and 5 Cat-1 stations in dry season campaign.

Stations	Mean	Median	Max		Min	
			Value	Date	Value	Date
Tan Chau	84.1	82.5	164.0	04/04/2022 22:00	-17.0	30/03/2022 15:00
Vam Nao	93.4	95.5	177.0	03/04/2022 21:00	-21.0	30/03/2022 14:00
My Thuan	45.4	49.5	160.0	04/04/2022 07:00	-117.0	30/03/2022 11:00
Cho Lach	44.8	52.0	169.0	04/04/2022 18:00	-136.0	30/03/2022 11:00
My Tho	35.5	48.0	162.0	03/04/2022 17:00	-143.0	30/03/2022 10:00
Binh Dai	35.6	40.0	162.0	03/04/2022 16:00	-146.0	30/03/2022 08:00
Chau Doc	97.6	95.0	184.0	04/04/2022 22:00	-12.0	30/03/2022 15:00
Can Tho	59.3	60.0	168.0	03/04/2022 19:00	-81.0	30/03/2022 12:00
Dai Ngai	39.2	46.0	187.0	03/04/2022 17:00	-138.0	30/03/2022 10:00

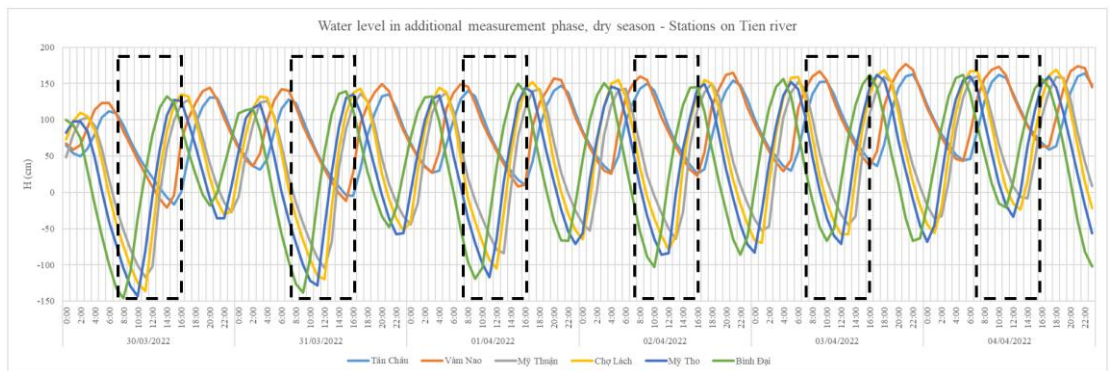


Figure 2-5: Dry season water level observations in Tien River (black boxes: discharge measurement period).

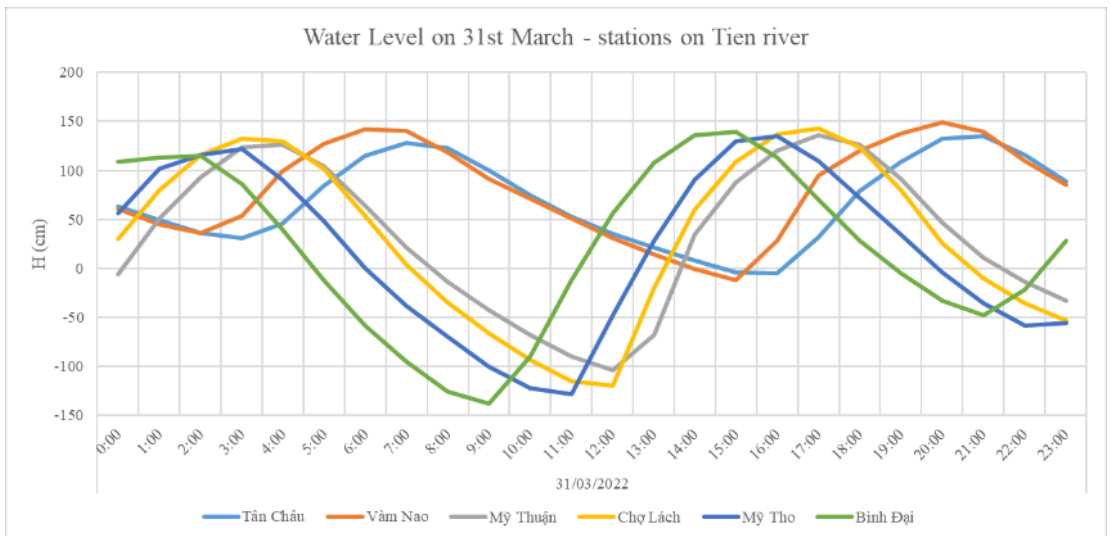


Figure 2-6: A zoomed in on water level measurements on 31st March in Tien River.

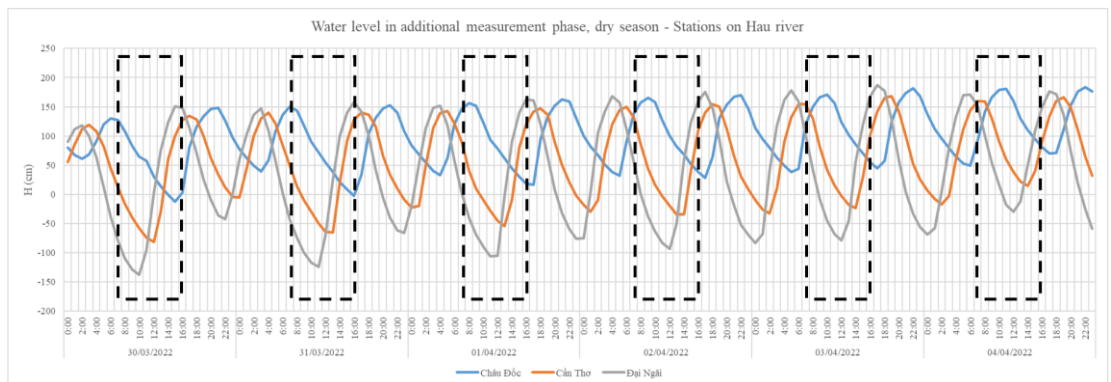


Figure 2-7: Dry season water level observations in Hau River (black boxes: discharge measurement period)

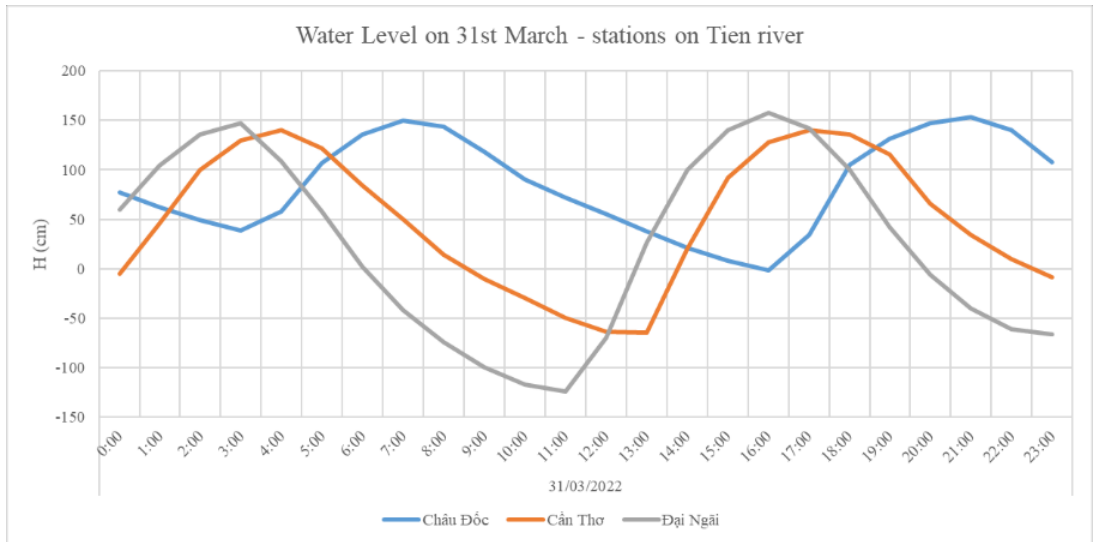


Figure 2-8: A zoomed in on water level measurements on 31st March in Hau River.

2.2.1.3 Wet season

Tien River: Water levels in the wet season are affected by East Sea semi-diurnal tide and flood flow from upstream. Water level in the more downstream stations is more determined by sea water level while the upstream water levels are more regulated with the river stage and the flood pulse. Tide transmission time from Binh Dai station (Dai estuary) to Tan Chau station is about 7 hours. Minimum water level at downstream stations ranged from -150 – -50 cm, and from 170 – 230 cm at upstream stations. Meanwhile maximum water level is around 120 – 150 cm at downstream stations and around 250 – 300 cm at upstream stations.

Hau River: Water levels in the wet season are affected by East Sea semi-diurnal tide and flood flow from upstream. Water level in the more downstream stations is more determined by sea water level while the upstream water levels are more regulated with the river stage and the flood pulse. Tide transmission time from Dai Ngai to Chau Doc station is about 6 hours. Minimum water level at downstream stations ranged from -100 cm (Dai Ngai) to 20 cm (Can Tho), and from 200 – 240 cm at Chau Doc. Meanwhile maximum water level is around 140 cm (Dai Ngai) and 170 cm (Can Tho) and around 250 – 270 cm at Tan Chau.

Table 2-3: Water level features at 4 Cat-2 stations and 5 Cat-1 stations in wet season campaign.

Stations	Mean	Median	Max		Min	
			Value (cm)	Date	Value (cm)	Date
Cat.1						
Tan Chau	274.83	274.5	311	29/09/2022 23:00	237	23/09/2022 02:00
Vam Nao	214.24	212	266	29/09/2022 22:00	157	23/09/2022 01:00
My Thuan	71.67	71.5	191	29/09/2022 19:00	-63	23/09/2022 23:00
Chau Doc	240.20	239	281	29/09/2022 23:00	198	23/09/2022 02:00
Can Tho	95.83	90	194	29/09/2022 19:00	-9	23/09/2022 23:00
Cat.2						
Cho Lach	55.45	60	180	29/09/2022 06:00	-99	23/09/2022 22:00
My Tho	36.01	44	163	28/09/2022 17:00	-120	23/09/2022 22:00
Binh Dai	22.79	32	160	26/09/2022 03:00	-151	29/09/2022 11:00
Dai Ngai	45.55	45	178	29/09/2022 18:00	-100	23/09/2022 22:00

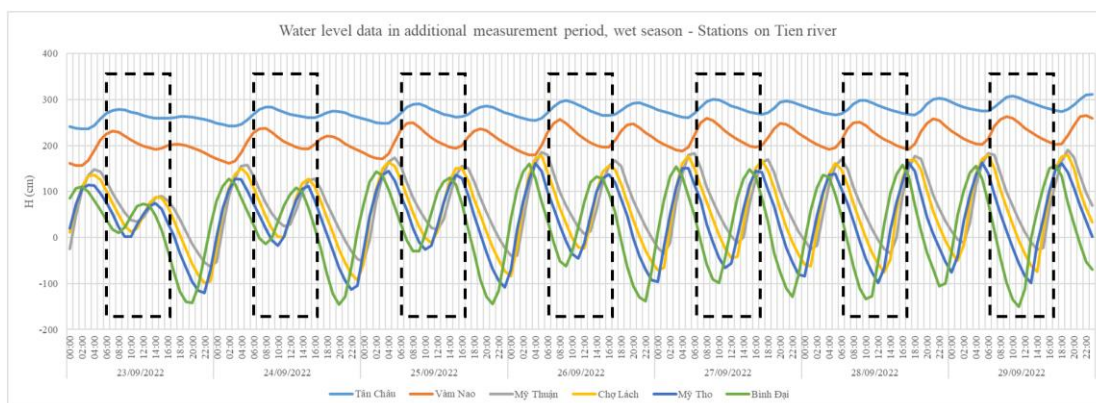


Figure 2-9: Wet season water level observations in Tien River (black boxes: discharge measurement period).

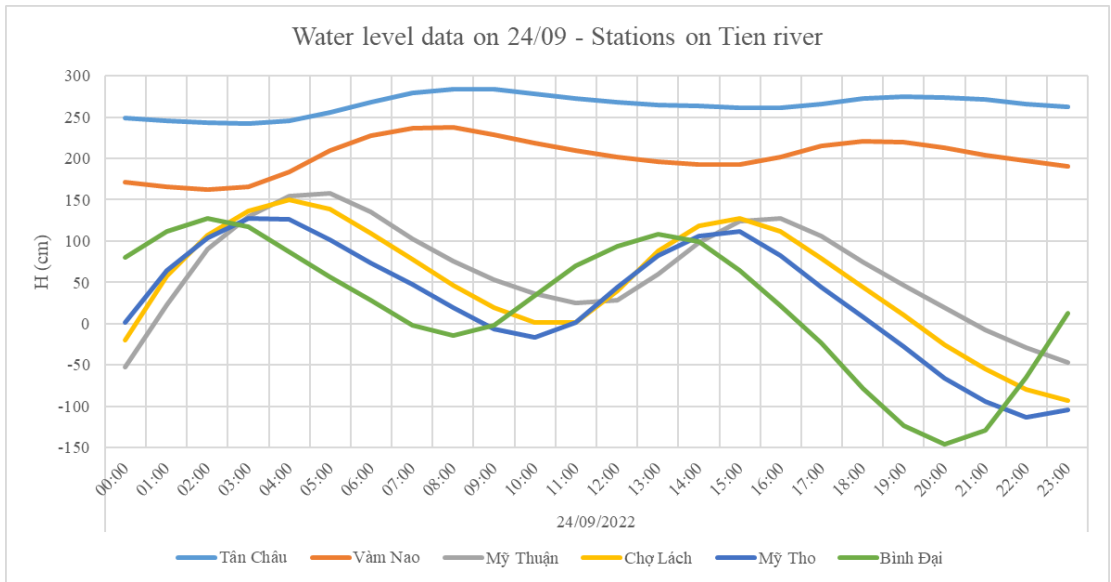


Figure 2-10: A zoomed in on water level measurements on 24th of September in Tien River.

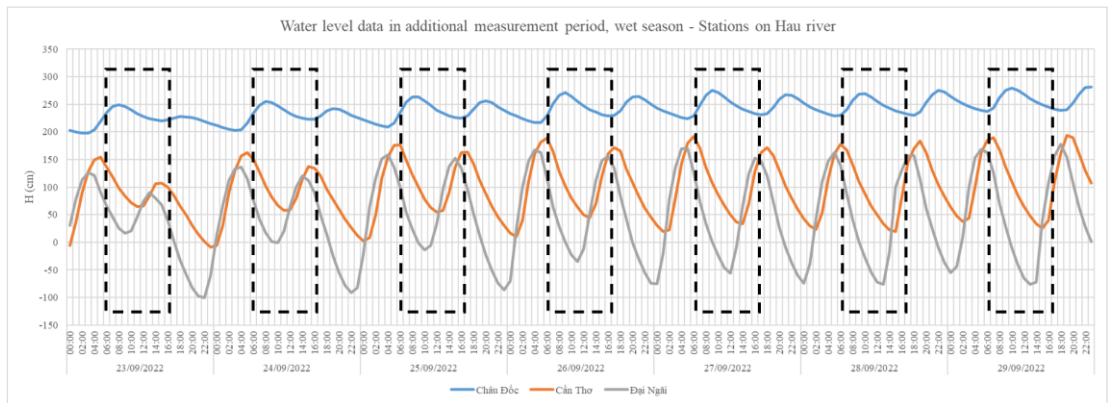


Figure 2-11: Wet season water level observations in Hau River (black boxes: discharge measurement period).

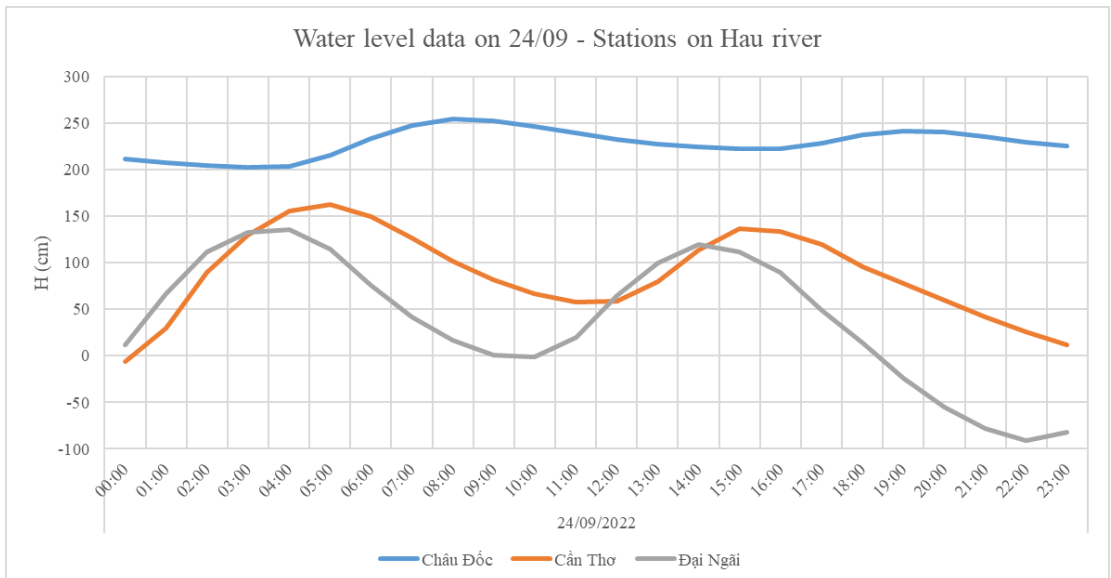


Figure 2-12: A zoomed in on water level measurements on 24th of September in Hau River.

2.2.2 Discharge

2.2.2.1 Regular measurement

Hourly discharge data for 365 days in 2022 was retrieved from SRHMC regular measurement campaign. For visualization purpose, daily average data was derived (see Figure 2-13 and Figure 2-14). Discharge value was quite small in dry season but gradually increase towards the wet season. Discharge data is in line with water level data, where it peaked around mid-October at all stations. Note that in the downstream stations (Can Tho and My Thuan), the tidal signal is observed throughout the year (*i.e.*, tidal river), but near Cambodian border the tidal signal in the discharge data significantly weakens in the wet season (also see Eslami et al., 2019a).

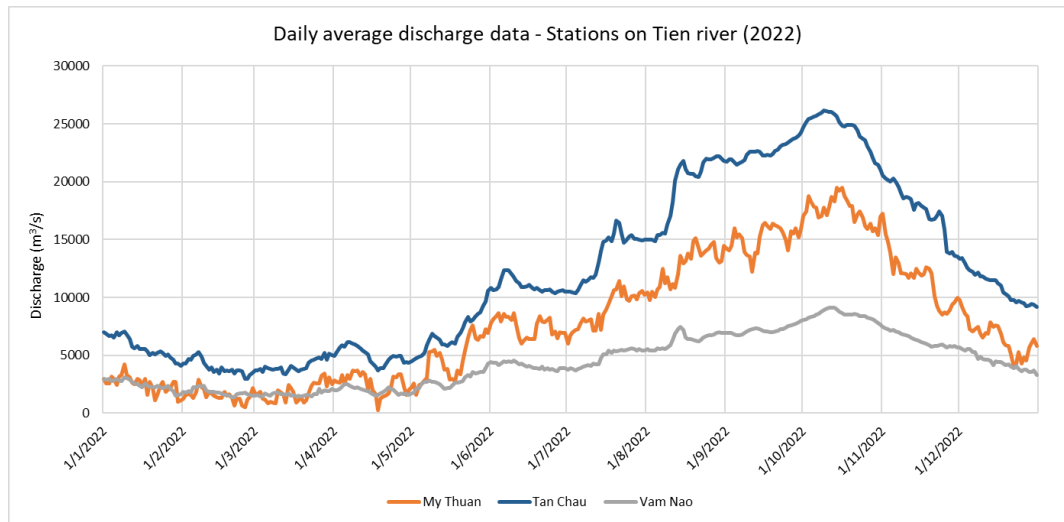


Figure 2-13: Daily average discharge data from regular measurement at stations on Tien river.

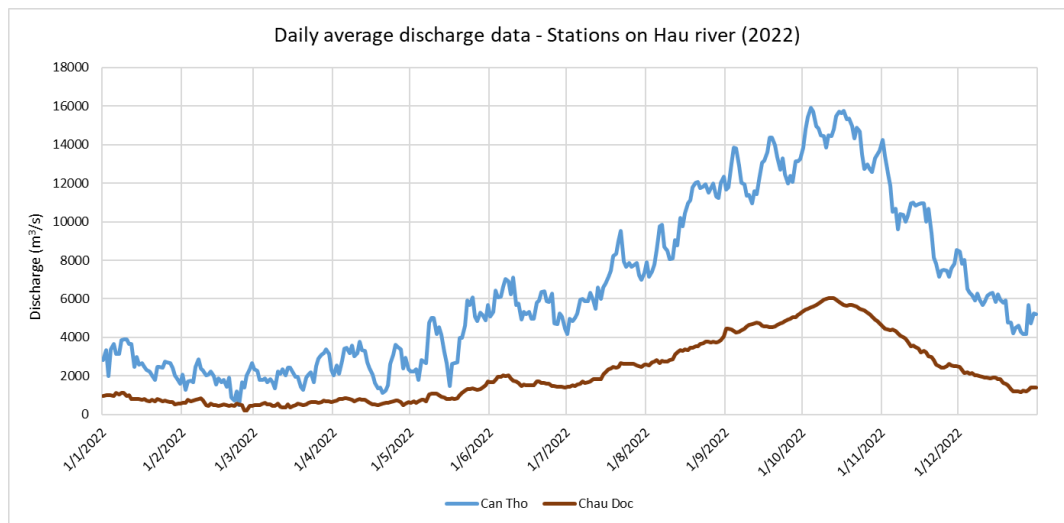


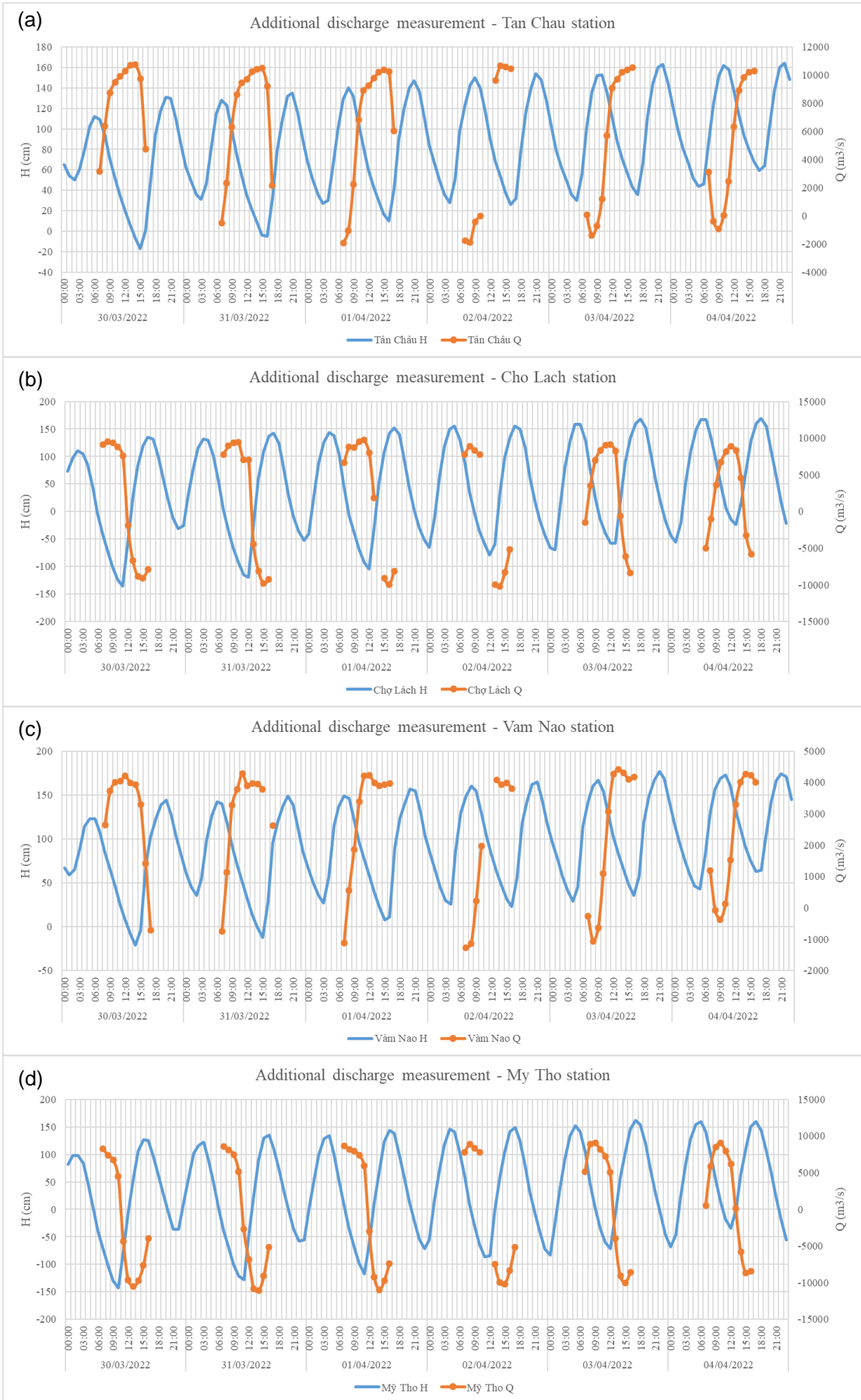
Figure 2-14: Observed daily average discharge of regular measurement at stations on Hau River.

2.2.2.2 Dry season

At upstream stations, discharge usually peaks around noon with downstream direction (positive value), in the low tide phase. Meanwhile, at downstream stations, discharge has 2 peaks, one in the morning during the low tide phase with downstream flow direction, and one in the afternoon during the high tide phase in the upstream direction (negative value). Table 2-4 below summarizes the observations and Figure 2-15 and Figure 2-16 show the observed values in both Tien and Hau River stations.

Table 2-4: Observed discharge at 4 Cat-2 stations and 5 Cat-1 stations in dry season campaign.

Station s	Mean	Median	Max (+)		Max (-)	
			Value	Date	Value	Date
Can Tho	4972	11328.8	16965.4	30/03/2022 09:00	-	-
My Thuan	5761.3	9813.7	18459.1	31/03/2022 10:00	-	-
My Tho	-315.5	88	9076	04/04/2022 10:00	-11094.8	31/03/2022 14:00
Binh Dai	-1678.1	-6028.4	16591.4	03/04/2022 08:00	-17731.7	01/04/2022 14:00
Dai Ngai	752.3	4327.6	8582.2	03/04/2022 10:00	-11782.8	31/03/2022 15:00
Cho Lach	1851.3	6693.2	9746.4	01/04/2022 11:00	-10183	02/04/2022 14:00
Tan Chau	6252	8905.7	10764.4	30/03/2022 14:00	-	-
Chau Doc	990.4	1791.7	2222.4	03/04/2022 15:00	-	-
Vam Nao	2598.4	3786	4421.4	03/04/2022 13:00	-	-



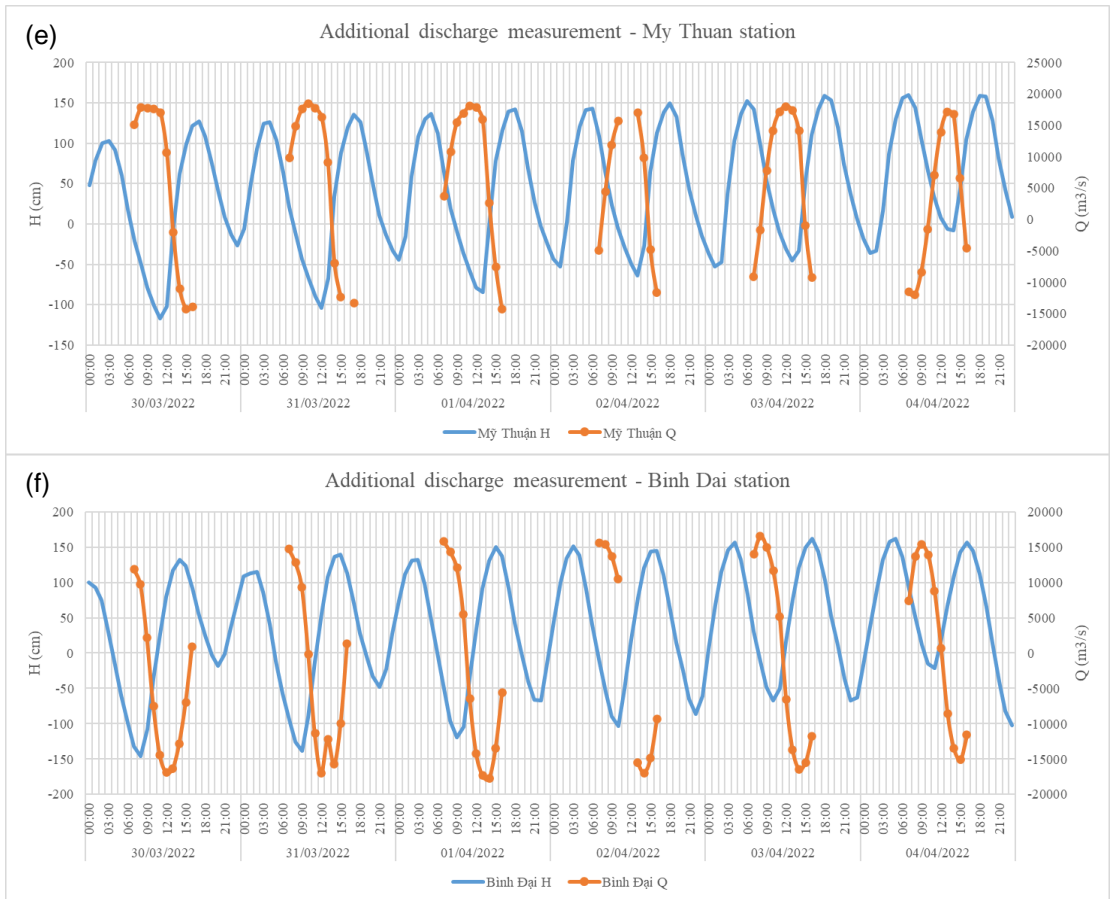
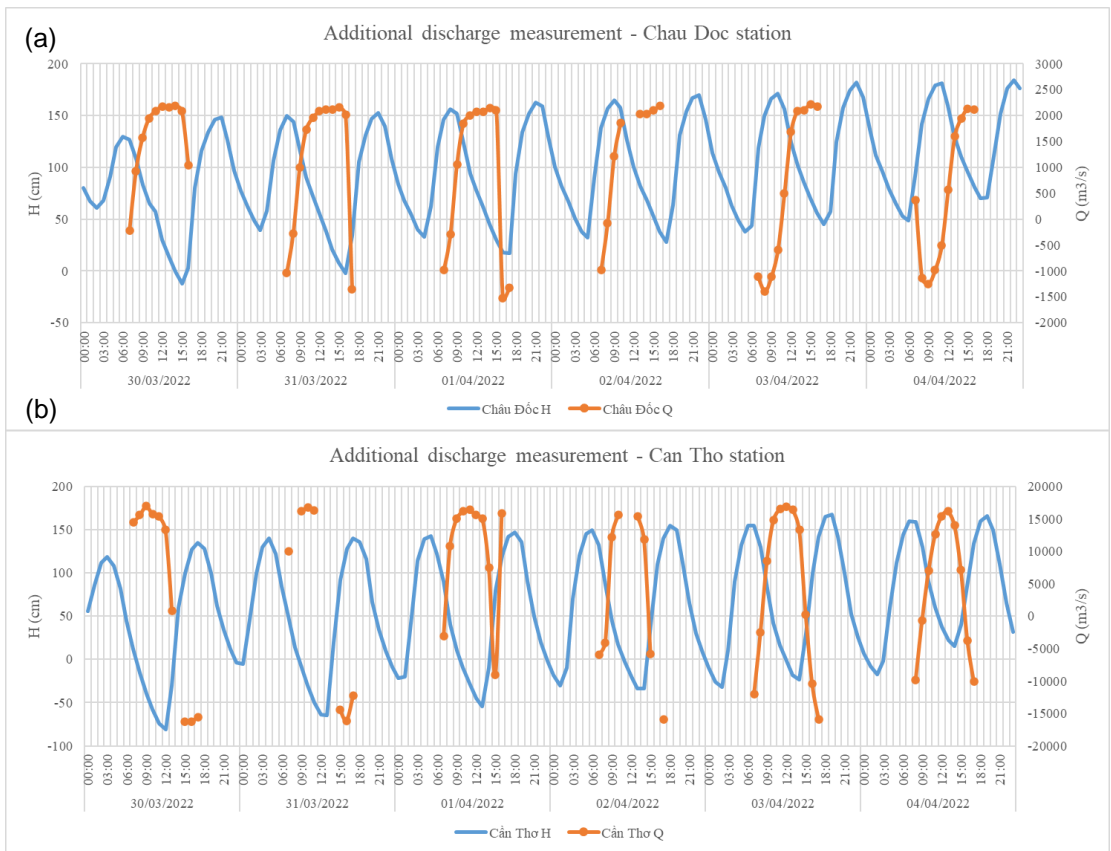


Figure 2-15: Dry season discharge and water level data at stations on Tien River during daytime measurements: (a) Tan Chau, (b) Cho Lach, (c) Vam Nao, (d) My Tho, (e) My Thuan, (f) Binh Dai.



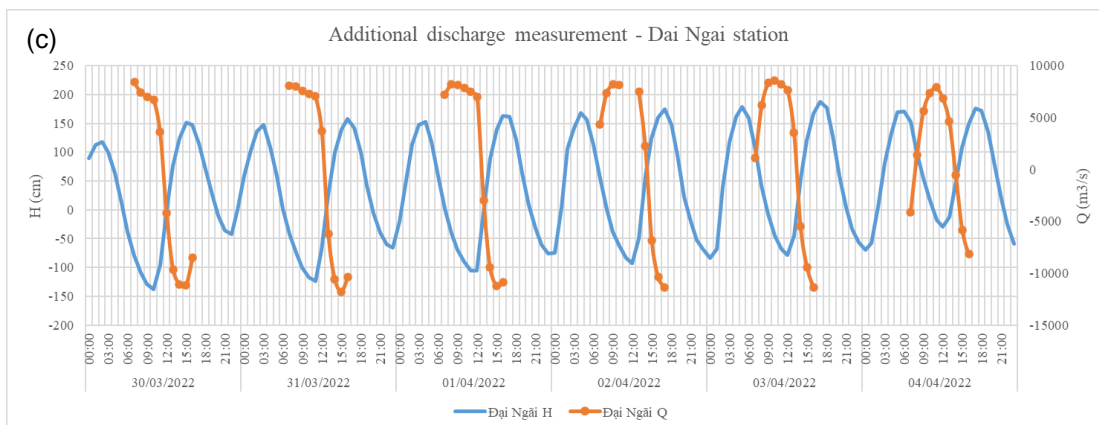


Figure 2-16: Dry season discharge and water level data at stations on Hau River during daytime measurements: (a) Chau Doc, (b) Can Tho, (c) Dai Ngai

2.2.2.3 Wet season

From the discharge data, we can see the increasing trend of the flood from 26th September. Before this date, discharge tends to peak at around 10 a.m. then have a sharp decline until it hit its lowest value at around 4 p.m. However, starting from 26th, discharge peaks from 10 a.m. and reaches its maximum value at 1 p.m. The tidal signal is clearly stronger in the more downstream stations (e.g., Binh Dai & Dai Ngai) leading to negative (upstream) tidal discharge, whereas in My Thuan and Can Tho, discharge is fully positive (downstream) though it reaches near zero before high water level. Table 2-5 Table 2-4 below summarizes the observations and Figure 2-17 and Figure 2-18 show the observed values in both Tien and Hau River stations.

Table 2-5: Observed discharge features at 4 Cat-2 stations and 2 Cat-1 stations in wet season campaign.

Station	No. of measure	Mean	Median	Max (+)		Max (-)	
				Value (m ³ /s)	Date-Time	Value (m ³ /s)	Date-Time
Cat.1							
Can Tho	28	12972.7	14104.8	21693	29/09/2022 13:00	-	-
My Thuan	28	15869.9	16574.0	24630	28/09/2022 13:00	-	-
Cat.2							
My Tho	28	6299.9	7691.1	10706	29/09/2022 10:00	-8018	29/09/2022 16:00
Binh Dai	28	10684.5	11598.1	17766	26/09/2022 07:00	-16557	29/09/2022 16:00
Dai Ngai	28	5810.9	5899.9	10542	29/09/2022 10:00	-5806	29/09/2022 16:00
Cho Lach	28	7600.4	8777.2	12795	28/09/2022 10:00	-3229	28/09/2022 16:00

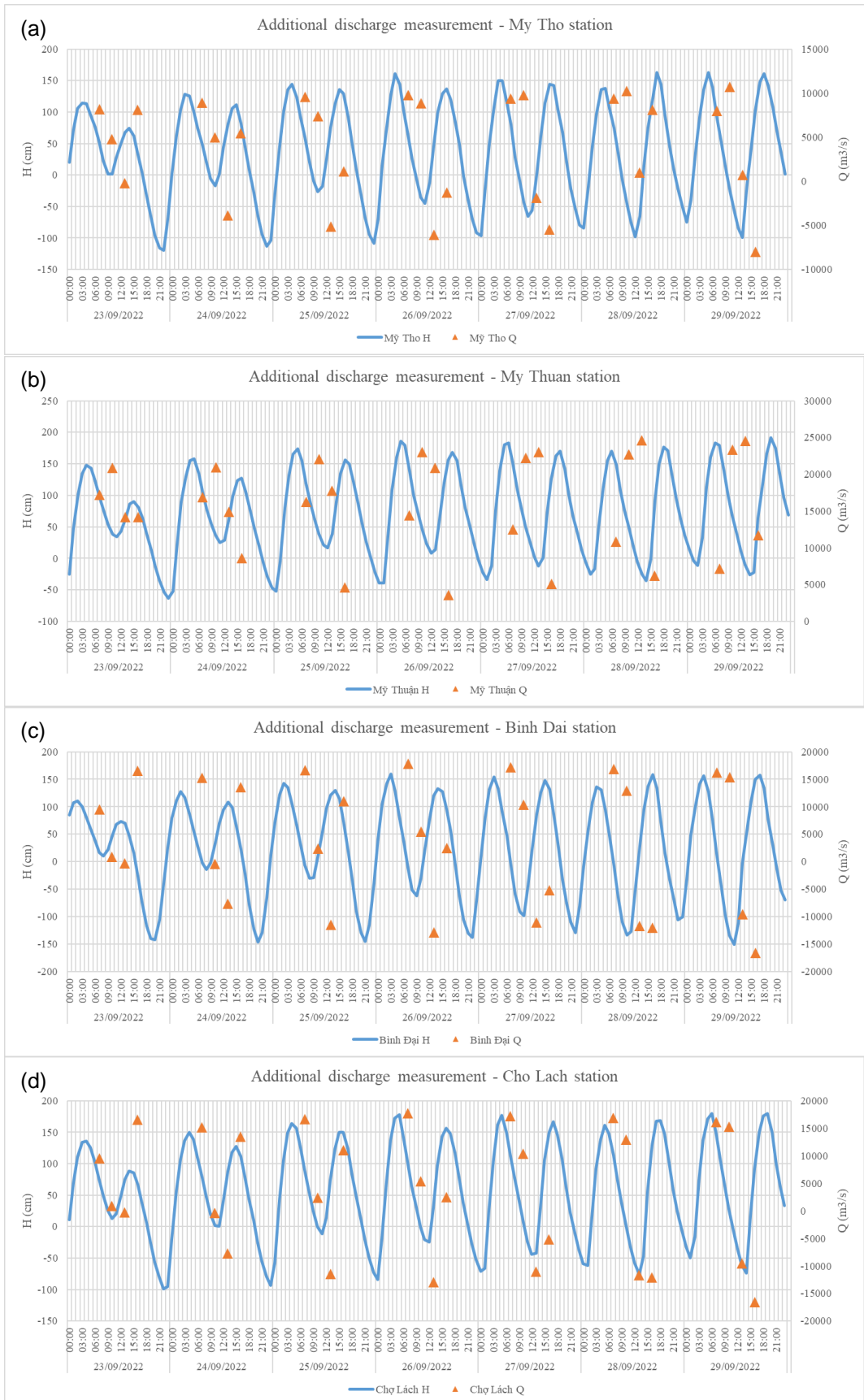


Figure 2-17: Wet season discharge and WL data at stations on Tien River during daytime measurements: (a) My Tho, (b) My Thuan, (c) Binh Dai, (d) Cho Lach.

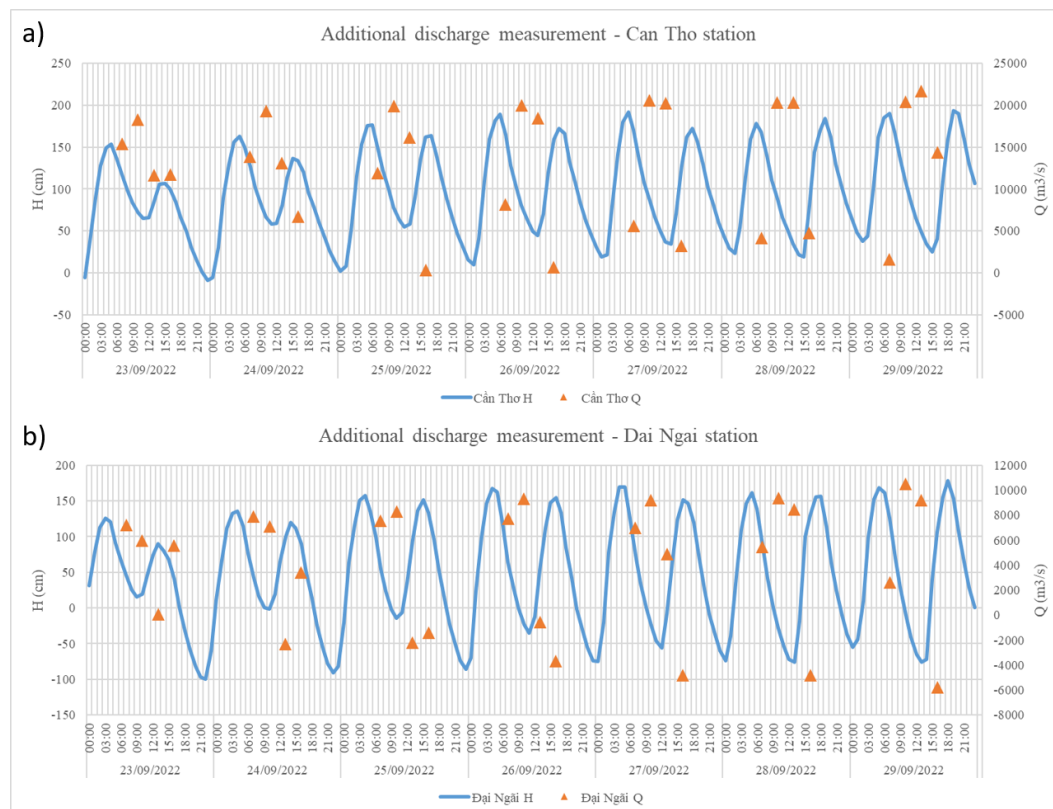


Figure 2-18: Wet season discharge and water level data at stations on Hau River during daytime measurements: (a) Can Tho, (b) Dai Ngai.

2.2.3 Suspended sediment concentration

To measure SSC during the measurement campaigns, two methods of LISST and water samples (bottle machinery) were employed. Normally, LISST data cannot directly be used as it needs calibration with water samples. The aim is to derive good correlation between LISST and water samples to retrieve a linear formula for LISST translation to SSC. The observed correlations in our case were not satisfactory as can happen during field operations. This even happens more in a very dynamic system such as the Mekong. Therefore, here we mainly rely on the water samples measurements that are the most reliable source of measurement.

2.2.3.1 Regular measurement

Suspended sediment samples were collected twice per day in the dry season and 3-4 times per day in the wet season. For visualization purpose, daily average data was derived (see Figure 2-19 and Figure 2-20). SSC signal has strong correlation to the discharge signal, with rather smaller values in the dry season that starting from mid-July fluctuates more dramatically and rise to occasionally very high values. This is partially a function of local flow velocities (dry season), and the upstream supply (in the wet season). Most of the fine and suspended sediment reaches the delta during the flood pulse. While the dry season SSC in both Tien and Hau Rivers have similar ranges of ~15-30 mg/L, the episodes of peak SSC in the Tien River are slightly higher than in Hau River. Nevertheless, the differences are not very significant.

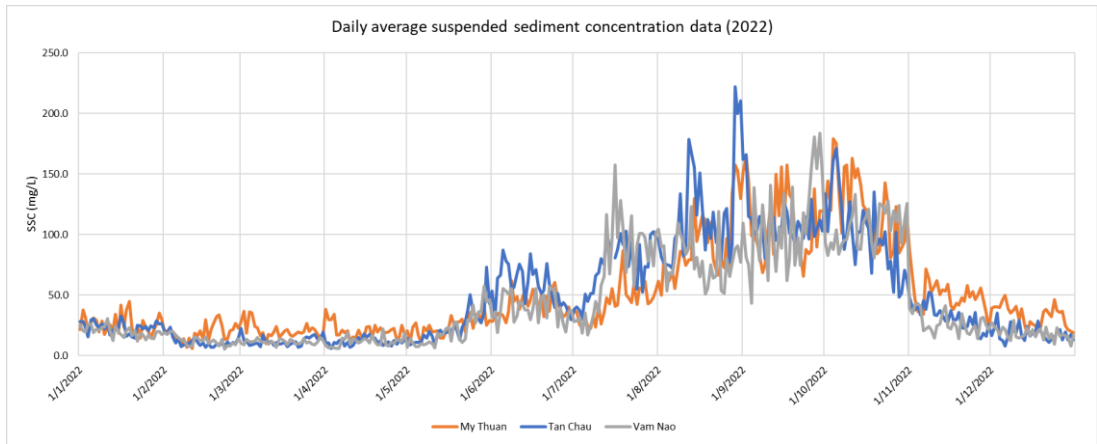


Figure 2-19: Daily average SSC data from regular measurement at stations on Tien River.

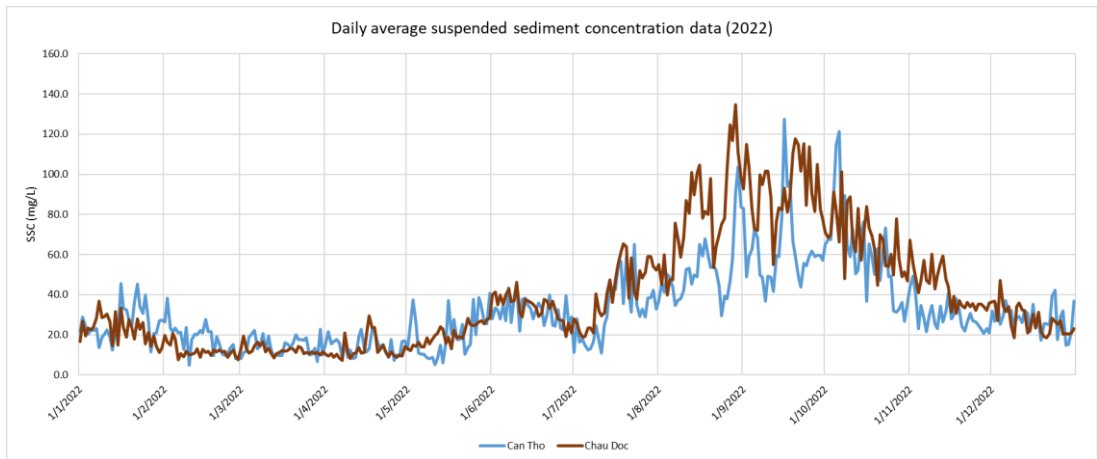


Figure 2-20: Daily average SSC data from regular measurement at stations on Hau River.

2.2.3.2 Dry season

Although LISST and Bottle machinery provide different data, but the overall trends with both equipment were similar, with upstream stations having 1 data peak around afternoon and downstream stations mostly with 2 peaks (except for Can Tho and My Thuan, with only 1 peak around morning – noon). Data at Tan Chau, Binh Dai and Dai Ngai stand out for their higher values for different reasons. The more downstream stations are influenced by estuarine mud, especially in the dry season and upstream stations are more influenced by upstream supply.

Table 2-6: Suspended sediment concentration (LISST) at 4 Cat-2 stations and 5 Cat-1 stations in dry season.

Stations	Mean	Median	Max		Min	
			Value	Date	Value	Date
Can Tho	7.8	7.4	19.5	31/03/2022 08:00	1.6	31/03/2022 12:00
My Thuan	9.6	8.6	23.6	31/03/2022 12:00	2.6	03/04/2022 09:00
My Tho	13.7	12.2	31.1	31/03/2022 14:00	4.2	03/04/2022 13:00
Binh Dai	29.2	27.3	67.8	31/03/2022 08:00	4.3	31/03/2022 16:00
Dai Ngai	71.8	66.2	179.6	31/03/2022 16:00	5.9	03/04/2022 07:00
Cho Lach	9.1	7.7	22.5	31/03/2022 16:00	1.4	03/04/2022 08:00
Tan Chau	1.8	1.5	5.0	31/03/2022 15:00	0.0	03/04/2022 11:00
Chau Doc	2.3	2.3	3.1	31/03/2022 14:00	1.1	03/04/2022 11:00
Vam Nao	6.2	9.3	12.9	31/03/2022 12:00	0.1	31/03/2022 07:00

Table 2-7: Suspended sediment concentration (Bottle) at 4 Cat-2 stations and 5 Cat-1 stations in dry season.

Stations	Mean	Median	Max		Min	
			Value	Date	Value	Date
Can Tho	40.7	40.5	62.0	03/04/2022 12:00	21.0	03/04/2022 08:00
My Thuan	40.0	41.0	57.0	31/03/2022 13:00	25.0	03/04/2022 08:00
My Tho	284.9	275.5	657.0	31/03/2022 15:00	73.0	03/04/2022 08:00
Binh Dai	306.2	326.5	494.0	03/04/2022 15:00	110.0	31/03/2022 16:00
Dai Ngai	367.9	417.5	637.0	31/03/2022 15:00	108.0	03/04/2022 14:00
Cho Lach	49.4	45.5	84.0	03/04/2022 13:00	17.0	03/04/2022 16:00
Tan Chau	25.1	21.0	56.0	03/04/2022 12:00	8.0	31/03/2022 08:00
Chau Doc	18.6	19.5	27.0	31/03/2022 14:00	7.0	31/03/2022 10:00
Vam Nao	20.6	19.5	41.0	03/04/2022 16:00	6.0	31/03/2022 09:00

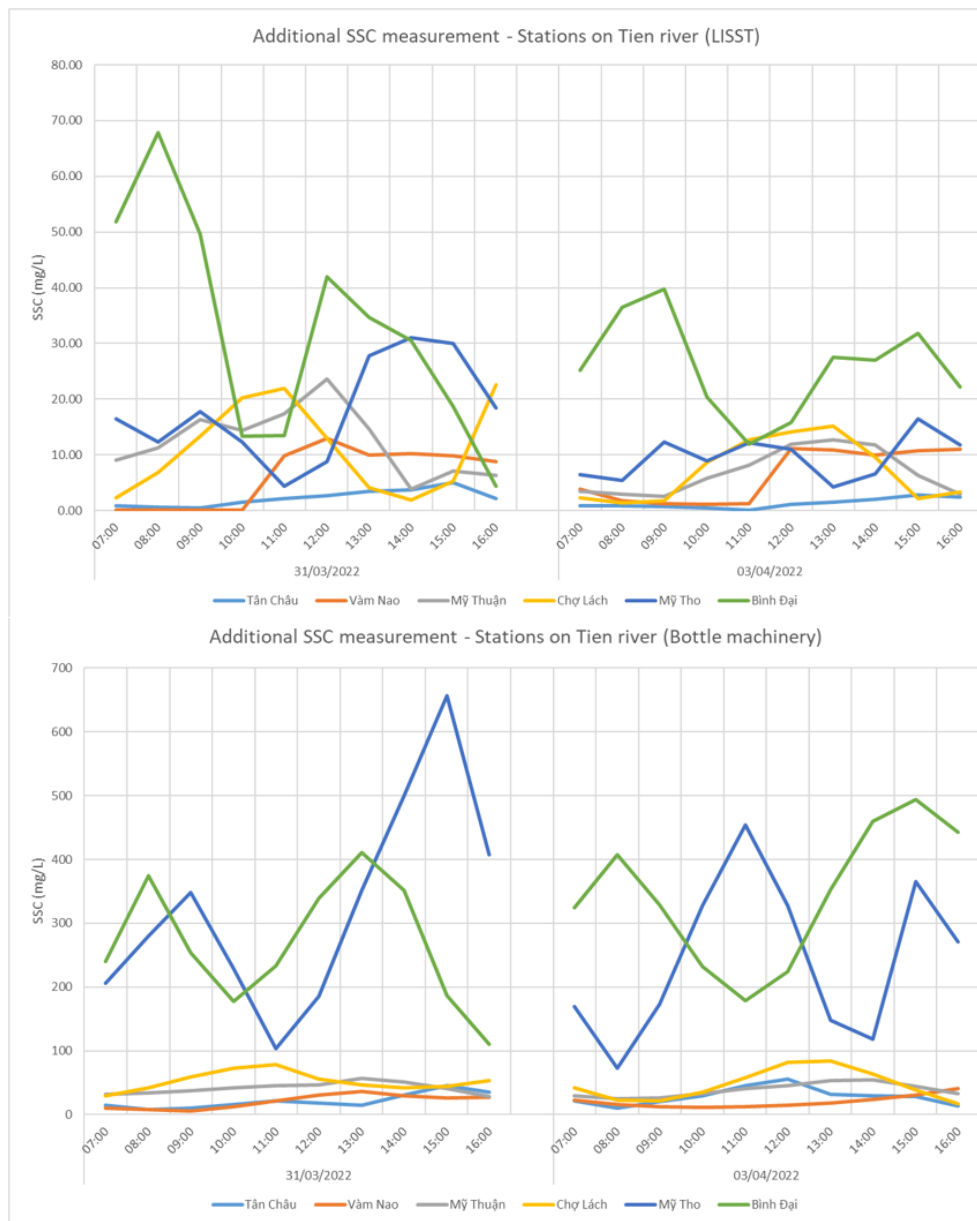


Figure 2-21: SSC data in dry season at stations on Tien River with two different measurement techniques.

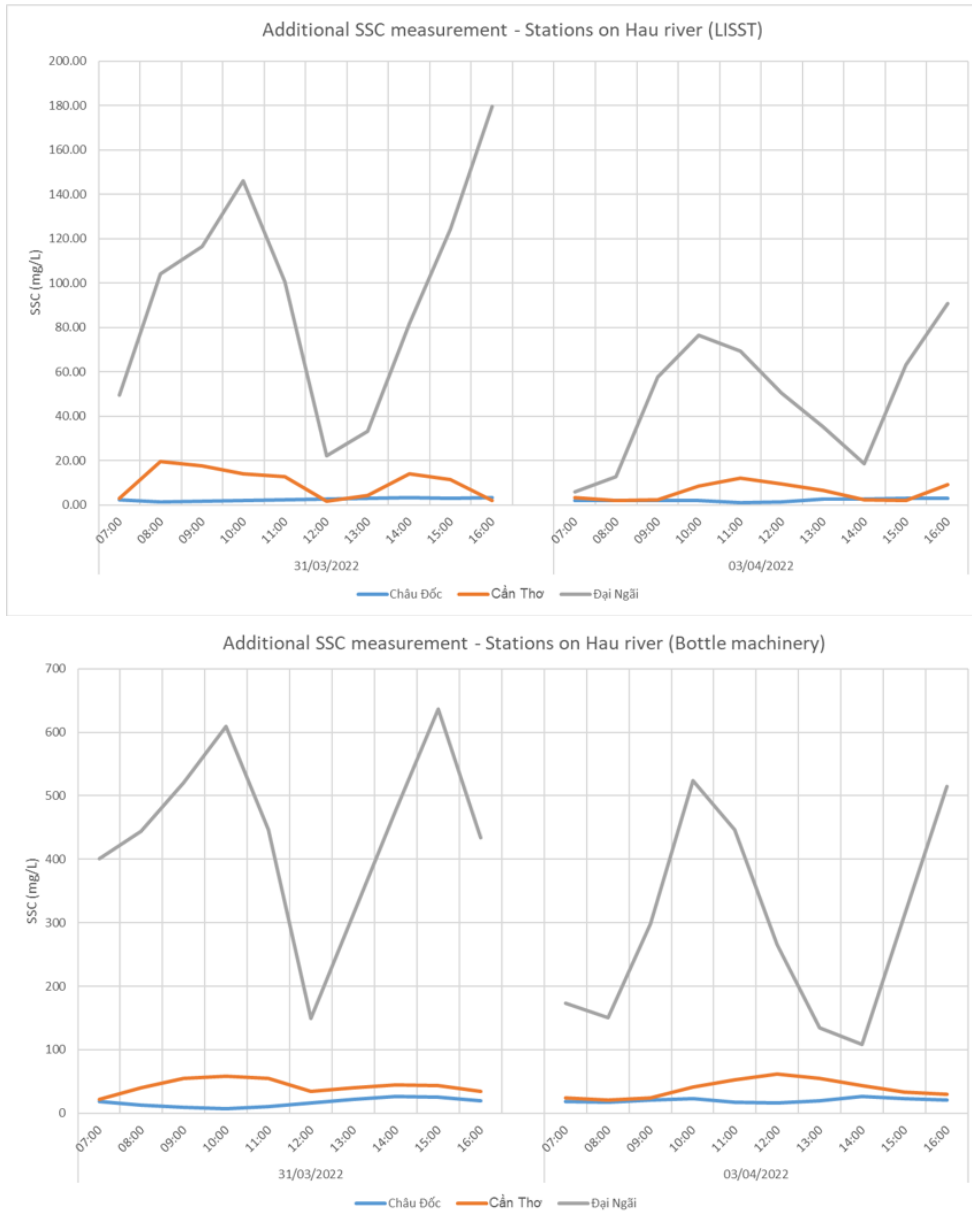


Figure 2-22: SSC data in dry season at stations on Hau River with two different measurement techniques.

2.2.3.3 Wet season

To measure SSC during the measurement campaigns, two methods of LISST and water samples (bottle machinery) were employed. LISST data cannot directly be used as it needs calibration with water samples. So, the general approach is that we aim to measure good correlation between LISST and water samples to be able to retrieve a linear formula for LISST signal to be translated to SSC. The observed correlations were not satisfactory as can happen during field operations. Therefore, in this report we mainly rely on the water samples measurements that are the most reliable source of measurement. Observed SSC curves (see Figure 2-23 and Figure 2-24) follow a similar trend to the discharge curve, as before the flood event, peaking at around 10 a.m and then gradually declining. Especially after the September 26th, SSC value is notably higher in more tidally dominated stations such as Binh Dai and Dai Ngai. The tidal velocities and the riverbed mud content, along with the delivered fluvial sediment of the flood pulse is perhaps mostly responsible for the higher sediment concentrations.

Table 2-8: Suspended sediment concentration (LISST) at 4 Cat-2 stations and 5 Cat-1 stations in wet season.

Station	No. of measure	Mean	Median	Max		Min	
				Value	Date-Time	Value	Date-Time
Can Tho	12	9.71	10.10	20.38	29/09/2022 13:00	1.35	29/09/2022 07:00
My Thuan	12	24.66	27.47	42.36	29/09/2022 13:00	3.37	29/09/2022 07:00
My Tho	12	12.83	10.14	29.77	29/09/2022 10:00	2.35	23/09/2022 13:00
Binh Dai	12	58.56	38.44	159.8 3	29/09/2022 10:00	5.12	23/09/2022 13:00
Dai Ngai	12	32.37	19.19	110.4 5	26/09/2022 10:00	1.96	29/09/2022 07:00
Cho Lach	12	23.08	19.50	61.61	29/09/2022 13:00	1.60	29/09/2022 07:00
Tan Chau	12	27.87	27.88	32.85	13/10/2022 07:00	20.68	10/10/2022 10:00
Chau Doc	12	33.16	31.86	39.16	13/10/2022 13:00	27.22	10/10/2022 07:00
Vam Nao	12	47.05	46.22	66.23	10/10/2022 16:00	31.24	13/10/2022 07:00

Table 2-9: Suspended sediment concentration (Bottle) at 4 Cat-2 stations and 5 Cat-1 stations in wet season.

Station	No. of measure	Mean	Median	Max		Min	
				Value	Date-Time	Value	Date-Time
Can Tho	12	52.00	53	97	29/9/2022 10:00	20	26/9/2022 7:00
My Thuan	12	109.25	105.5	165	26/9/2022 13:00	78	29/9/2022 7:00
My Tho	12	189.33	170	308	29/9/2022 10:00	86	23/9/2022 13:00
Binh Dai	12	217.42	196	475	29/9/2022 10:00	63	26/9/2022 16:00
Dai Ngai	12	113.75	112	208	29/9/2022 13:00	40	29/9/2022 7:00
Cho Lach	12	130.17	109	233	29/9/2022 13:00	60	26/9/2022 16:00
Tan Chau	12	166.75	154.5	271	7/10/2022 7:00	120	13/10/2022 7:00
Chau Doc	12	96.58	99.5	125	7/10/2022 7:00	71	13/10/2022 13:00
Vam Nao	12	130.58	123	169	7/10/2022 10:00	85	13/10/2022 10:00

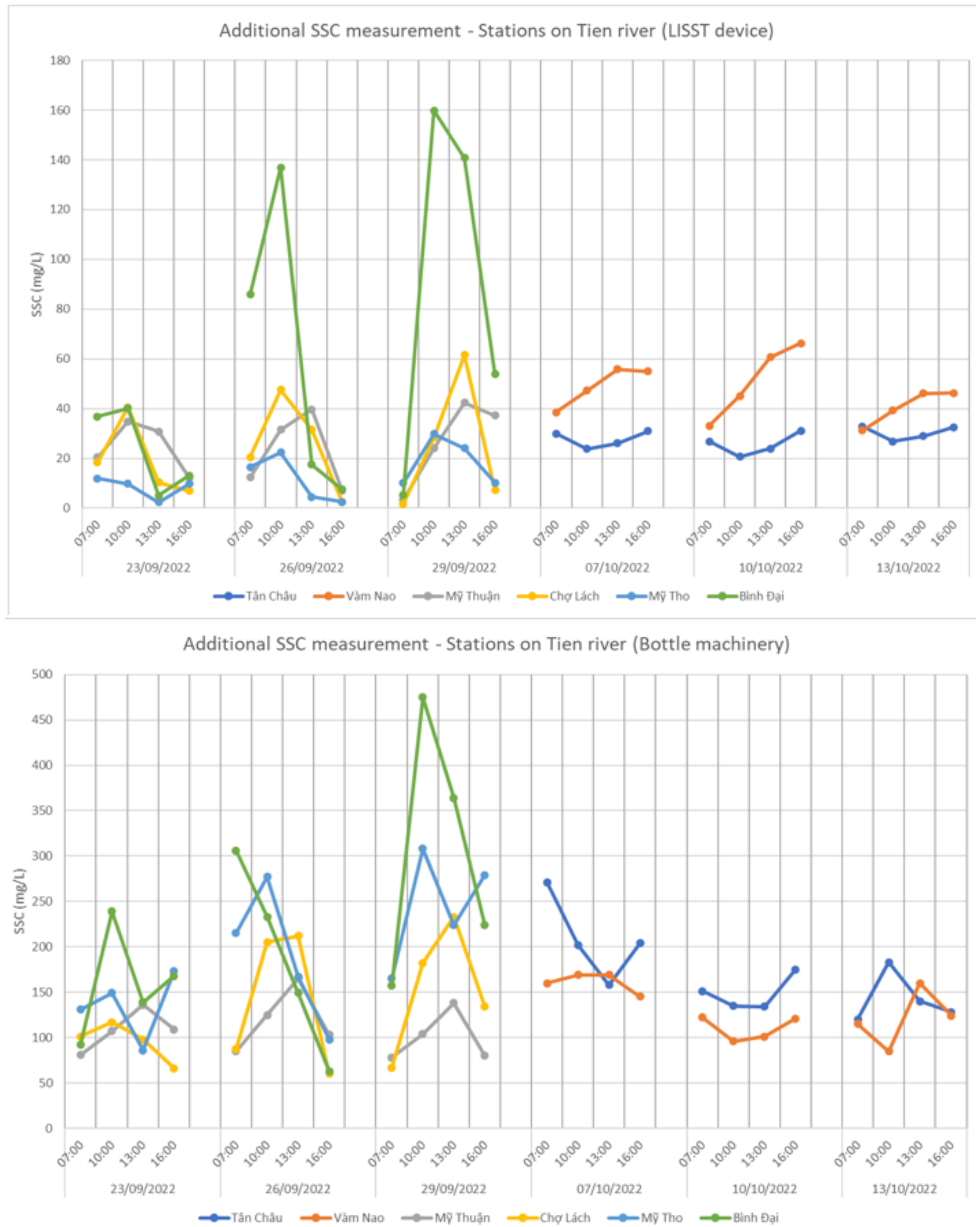


Figure 2-23: SSC data in wet season at stations on Tien River with two different measurement techniques

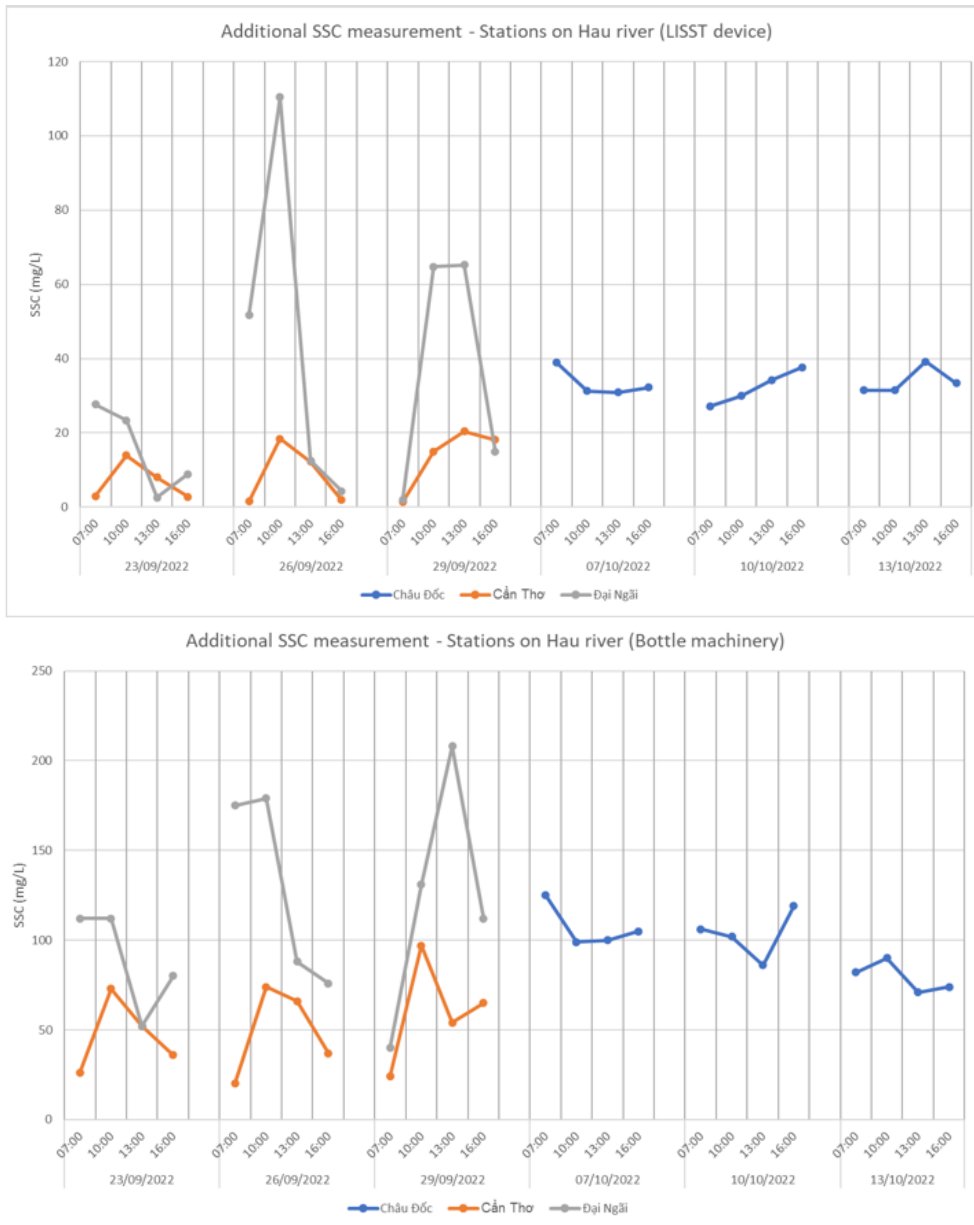


Figure 2-24: SSC data in dry season at stations on Hau River with two different measurement techniques.

2.2.4 Riverbed sample

2.2.4.1 Dry season

Bed samples vary between stations, with upstream stations having a larger grain component and Fine and Medium Sand. The more toward the East Sea, samples in the stations have a clear dominance component of Clay (also see Appendix A-1 for further details).

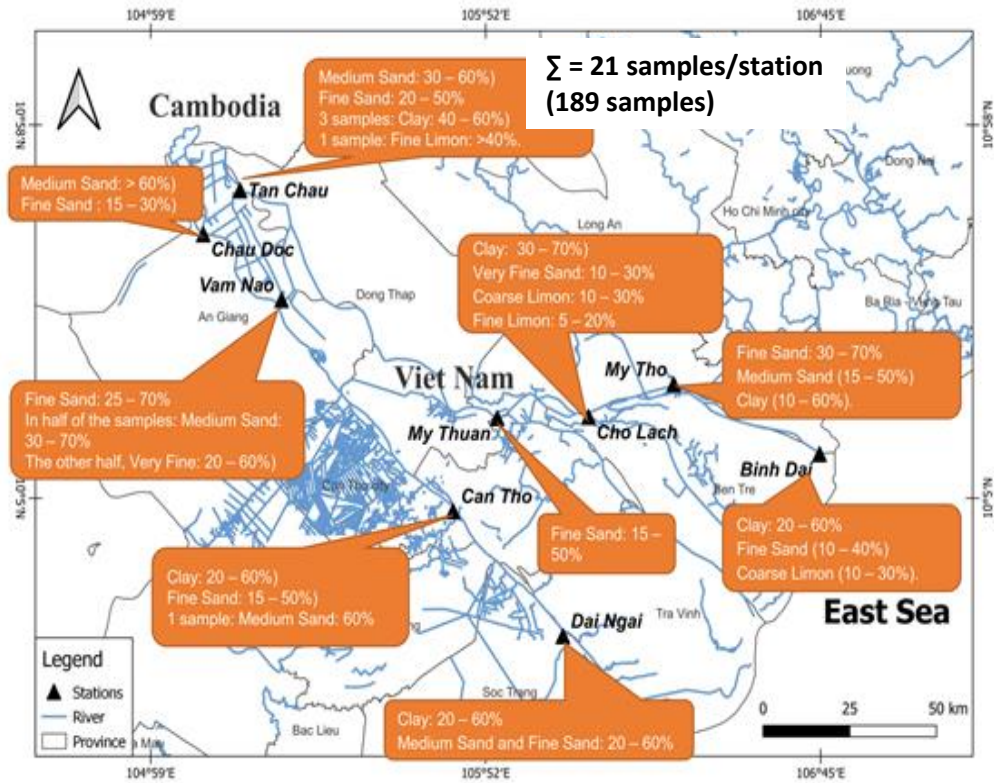


Figure 2-25: A summary of dry season riverbed sampling results.

2.2.4.2 Wet season

In upstream and midstream stations, the sample contain mostly of Fine sand (0.25 – 0.125mm). In downstream stations, the sample component consisted of more Clay (<0,002mm). At Vam Nao station, there was Clay at Vertical Profile I (also see Appendix A-2 for further details).

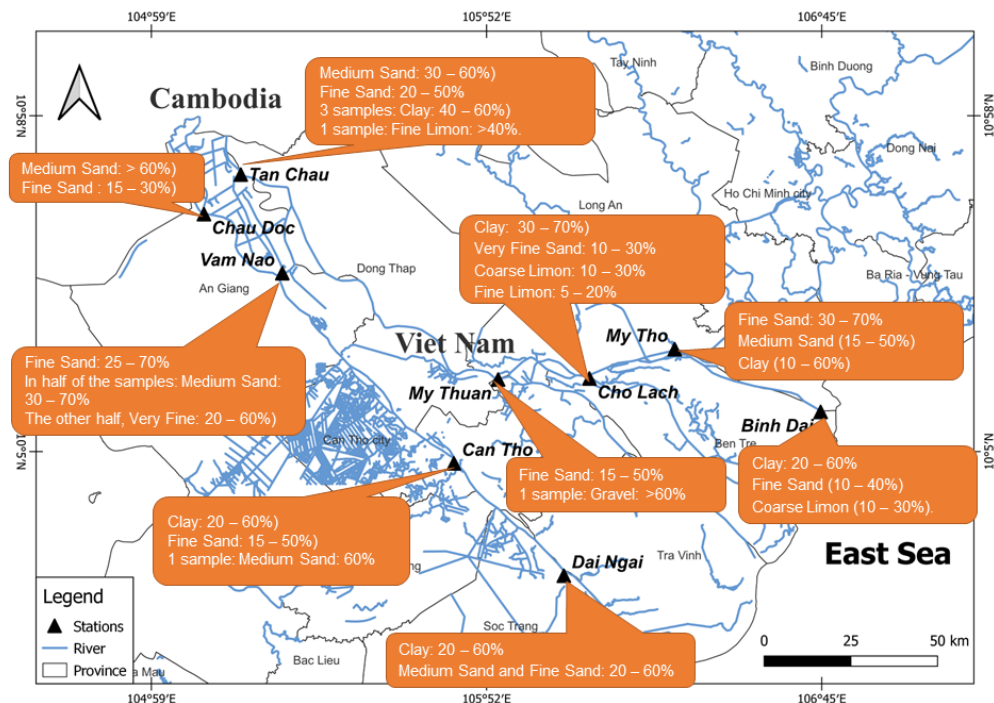


Figure 2-26: A summary of the wet season riverbed sampling results.

2.2.5 SBP data collection

Overall, ~550 km of SBP data were collected along all river branches of the VMD from the Cambodian border to within the estuarine distributary channels near the sea. The collected

data had good quality without any loss, interruption, or corruption. In addition, we collected 44 riverbed samples that showed a distribution of larger sediment upstream and a fining pattern downstream. Towards the lower estuarine channels, the fine-grained sediments gradually become mainly alluvial mud and muddy sand. Figure 2-27 shows an overview of the collected sediment samples along the SBP sailing tracks. Figure 2-28 provides examples of the collected seismic signal, where sandy and muddy areas can be distinguished from the sand waves versus the flat muddy riverbed areas.

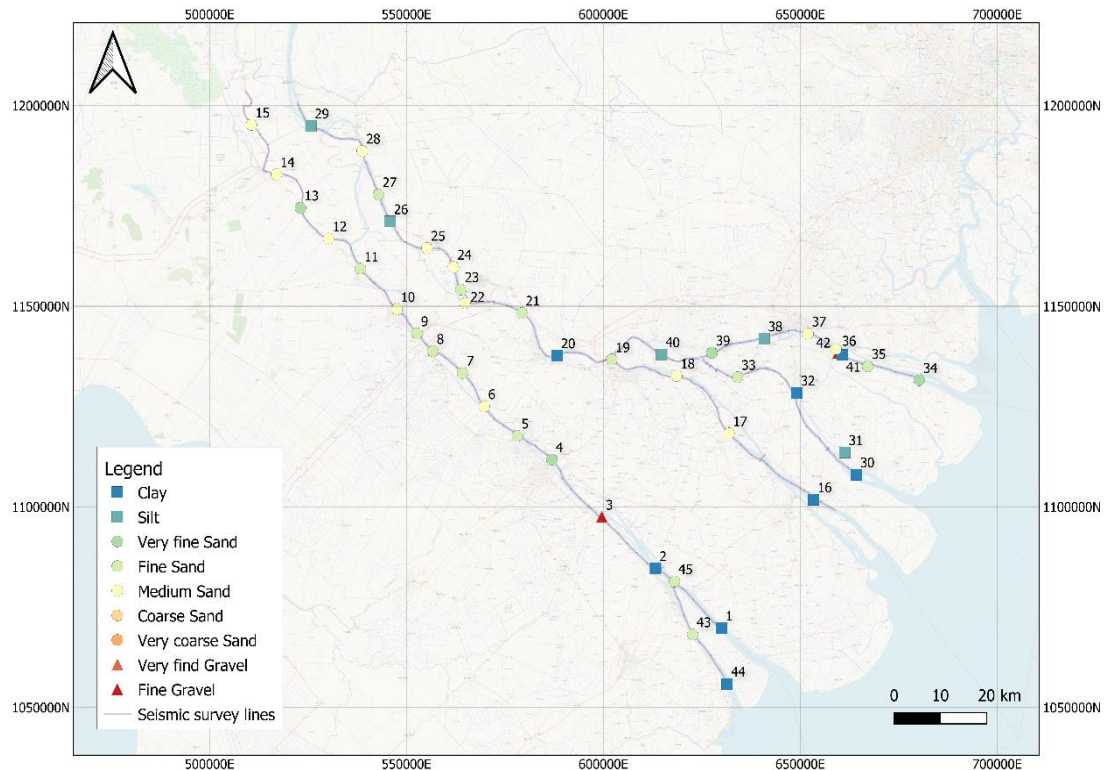


Figure 2-27: Riverbed sampling results from SBP survey campaign

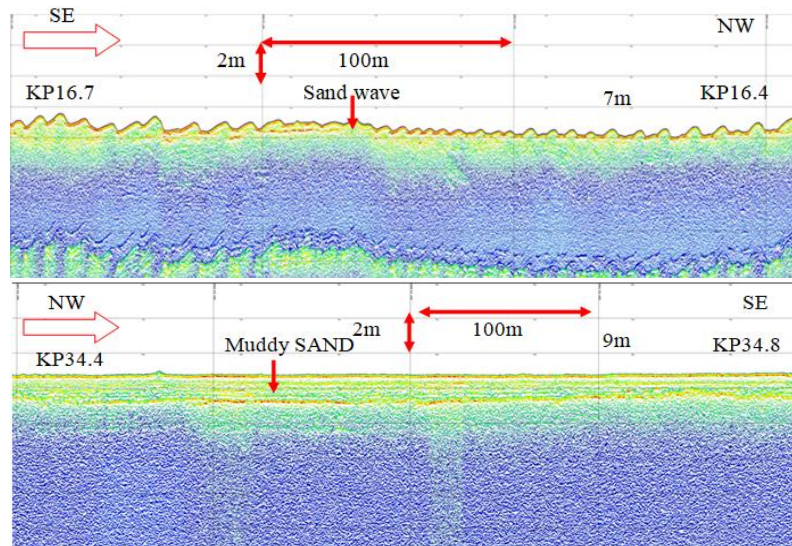


Figure 2-28: Example of upstream sub-bottom profile (upper: Chau Doc, lower: My Tho)

2.2.6 MBES survey summary

The MBES survey was to serve the bedload transportation estimates at different locations across the delta. The method relies on tracking individual dunes in a dune field in two consecutive MBES surveys (~12-15 days apart) within a spring-neap tidal cycle to arrive at a bedload transport. The migration of dunes is mostly driven by bed-load transport, and hence the migration speed of a dune can be translated to a bed-load transport rate. When the dune

lengths are smaller than 15-20m (very much depending on the actual data), it becomes very difficult or impossible to reliably identify the individual dunes in two different surveys as the small dunes or ripples tend to be deformed beyond the computation capacity. Therefore, when referring to *small dunes* in this report, we refer to areas where the sand wave lengths on the bed were too short to be used for dune-tracking and bedload transport estimation. When we refer to *ripples*, we refer to sand waves that were too small to even estimate their wavelength. The following sections summarize the quality of collected data during the MBES survey in the wet and dry seasons.

2.2.6.1 Dry season

During the dry season, MBES survey was conducted at 4 locations: My Thuan, Can Tho, Tan Chau, Chau Doc. Sand dunes of significant length (approximately 15-20m or longer) were found at Can Tho, Tan Chau and Chau Doc while at My Thuan, the dune sizes were too small and unsuitable for bed load transport estimation. Table 2-10 summarizes the observed dune fields and Figure 2-29 shows the example of surveyed dune field upstream of Can Tho City along the Hau River.

Table 2-10: MBES overall results in dry season

Location	Dune height	Dune length	Note
My Thuan	-	3 – 7 m	Small dune
Can Tho	1.0 - 1.2 m	23 - 31 m	
Tan Chau	1.0 - 3.5 m	50 - 100 m	
Chau Doc	0.6 -1.2 m	14 - 30 m	

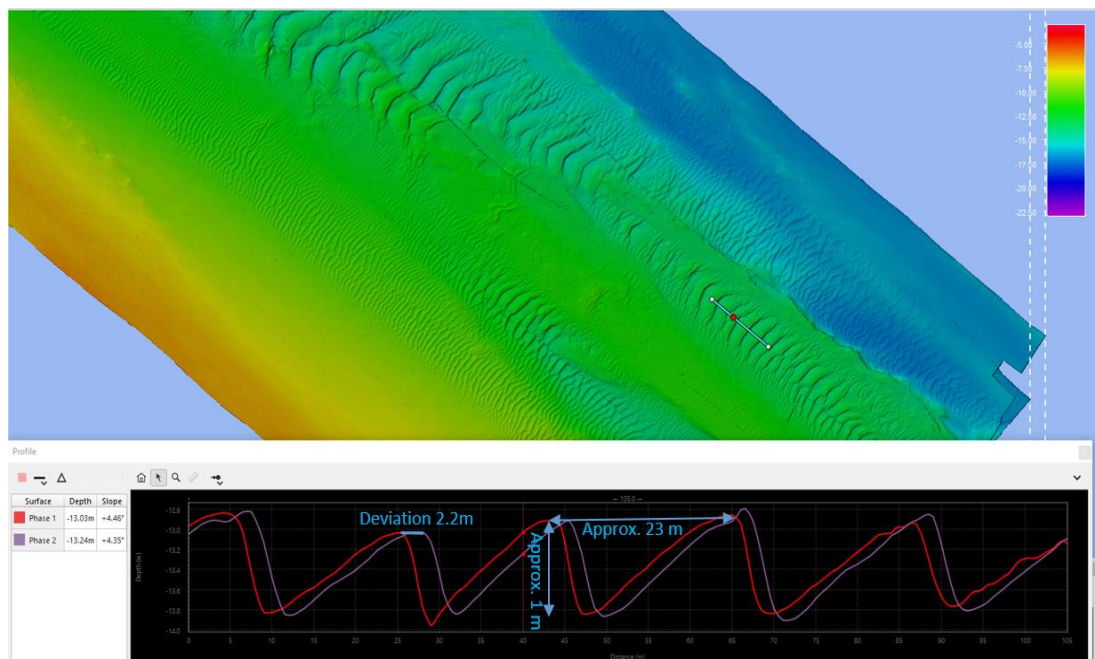


Figure 2-29: Example of a dune field near Can Tho and the movement between 2 MBES phases

2.2.6.2 Wet season

During the wet season, MBES survey was conducted at 12 locations. Sand dunes were found at 7 of them. In others, the sand waves were either too small (e.g., ripples) inappropriate to estimate sand transport or we only observed muddy riverbeds without dunes. Table 2-11 summarizes the observed dune fields and Figure 2-30 shows the example of surveyed dune field near Tan Chau along the Tien River.

Table 2-11: MBES overall results in wet season

Location	Dune height	Dune length	Note
Dai Ngai	0.1 - 0.5 m	4 - 10 m	small dune
Long Xuyen	1.0 - 2.5 m	30 - 70 m	
Can Tho	0.5 - 1.5 m	10 - 70 m	
Vam Nao	0.3 - 2 m	25 - 80 m	
Chau Doc	0.3 - 2 m	10 - 50 m	
Tan Chau	1.0 - 2.3 m	50 - 100 m	
Cao Lanh	1.0 - 3.6 m	15 - 22 m	
My Thuan	0.1 - 0.5 m	-	ripples
Cho Lach 2	0.3 - 1.0 m	40 - 50 m	
Cho Lach 1	0.1 - 0.5 m	-	ripples
Binh Dai	0.1 - 0.5 m	-	ripples
My Tho	0.1 - 0.5 m	-	ripples

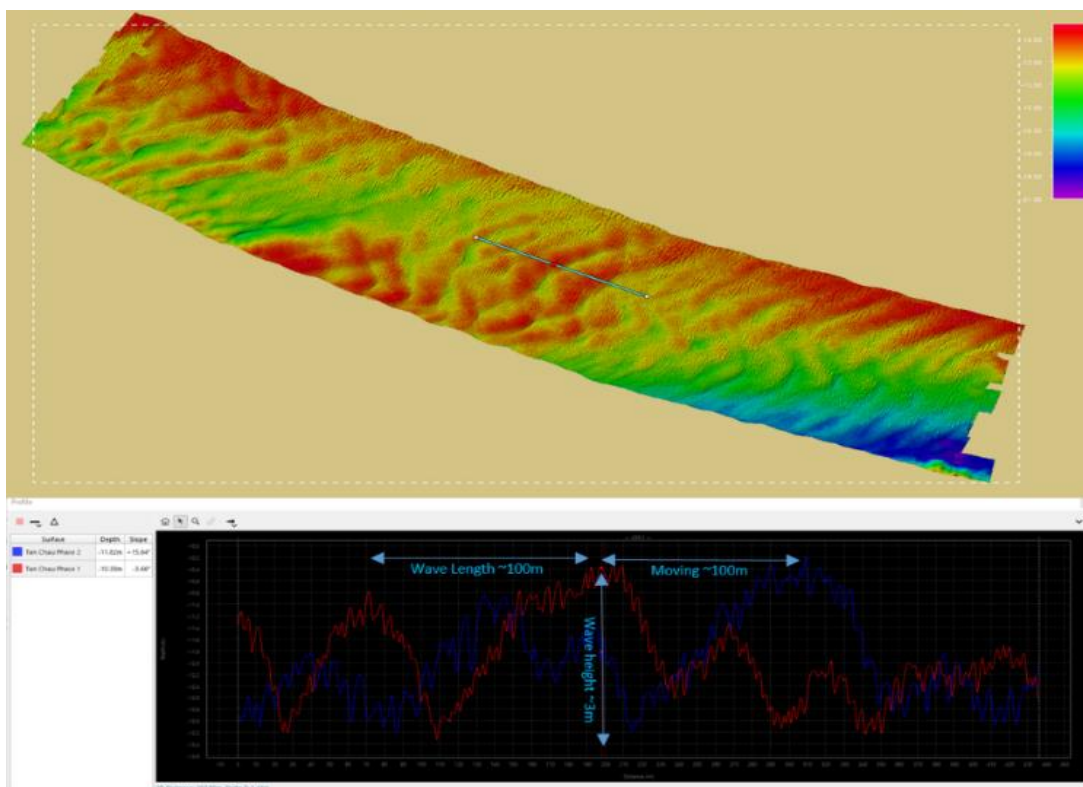


Figure 2-30: Example of a dune field near Tan Chau and the movement between 2 MBES phase.

2.3 Secondary data collection

Apart from the field observations, we also collected secondary data from various sources for a) the calibration and validation of the numerical model, b) improve interpretation of sub-bottom profiling results, and c) and for more insight into sand extraction volumes. This section summarizes these data as they are used in further data interpretation.

MRC water and sediment data

Data obtained from the Mekong River Commission (MRC) contained:

- At Tan Chau and Chau Doc:
 - Surveyed river cross-section profiles of 2018 (Vasilopoulos et al., 2021a)
 - *Hourly* water level and discharge between April and Dec 2019
 - *Daily* suspended sediment concentrations (SSC) between April and Dec 2019.
 - Grain size analysis on *bimonthly* sediment samples
- At **Kratie, Chaktomuk, Prek Dam**:
 - Daily water level measurement
 - Three to four-monthly discharge measurements
 - Three to four-monthly SSC between June and December
 - Bi-monthly grain size analysis of suspended sediment samples (Kratie and Prek Dam)
 - Bi-monthly grain size analysis of bed load sediment samples (Kratie only)

Borehole data

A total of 195 borehole data were collected from DONRE of three provinces (Hau Giang, Tra Vinh, Vinh Long) to support interpretation of the SBP signal for existing mobile sand stock estimation (see also chapter 3). Other provinces could not share this data without official letters from the ministry.

3 Data analysis (WP1)

3.1 Bed load transport

3.1.1 Introduction

By tracking migrating river bedforms in successive bathymetric surveys, a proxy for *bedload sediment transport* can be identified. Bedforms are topographic features at the interface of a moving flow and mobile matter, with sizes ranging from cm-scale ripples to sand waves over 1 km in length (Ashley, 1990). These features develop primarily on sand beds by the motion of sand particles, and therefore useful to assess transport of sand rather than silt and clay. The size and shape of bedforms depend on the water depth, current strength and direction, and grain size (Ashley, 1990). As they migrate, bedforms move large amounts of sediment as agents of bed-material transport (Bernard and Stéphane, 2011). Dune formation is often connected to 'bedload' transport, i.e., the movement of particles by rolling and jumping close to the bed and responding directly to spatial variations in bed-shear stress. Formally, turbulence (bursts) generated by the dunes will also cause bed-material to be temporarily transported in 'suspension'. But on the scale of the length of dunes it is still possible to treat the overall transport of sand as 'bed load', as the suspended sand particles settle out rapidly over these length scales. A common and reliable practice for deriving bed load transport from bed-level changes is the application of the two-dimensional *Exner equation* (Simons et al., 1965) to *time series of bed elevation profiles* obtained with echo sounders (Leary and Buscombe, 2020). This method assumes a bed profile in equilibrium with the prevailing flow conditions. This assumption is not always valid for natural rivers which show an inherent variability in sediment and water discharge conditions over the period of the dune-track recording. Still, the dune tracking method is one of the most accurate bedload prediction techniques (Leary and Buscombe, 2020).

3.1.2 Approach

Bedform dynamics were analysed in three steps. First, bedform regions were identified from the multibeam survey results and visually inspected to extract main bedform features. Hand-drawn transects across the sand wave regions give information on migration distances and directions and serve as check on the automatic detection and analysis of sand wave characteristics. A flow chart of the approach is depicted in Figure 3-1.

For each monitoring station, the MBES data was inspected to define regions where clear **overlapping dune fields** are present. A **coarse spatial filtering** is then applied to the bathymetry measurements to expose mobile bedforms. This essential filtering step involves an iterative procedure of varying the filter size and orientation to extract the bedforms of interest fluctuating around a zero mean. The filtering produces maps of the *static bathymetry* (the immobile bed), the *sand wave* field (dunes of approximately 10-50 m spacing), and potentially the *mega-ripple* field (m-scale spacing) based on the multibeam surveys.

Sand wave crests (transect locations) need to be defined for which sand wave characteristics and migration rates and directions are determined. First, the sand wave grid is rotated such that the main direction of sand waves is aligned with the columns of the grid. Transect points are then extracted by Fourier transformation on the columns of the sand wave grid. Wave crests and troughs are automatically detected and filtered to remove local minima / maxima. Crest points are used as transect points. If necessary, transect points can be added or deleted manually. Note that this method of Fourier transformation on a rotated grid requires a predefined migration direction. This predefined migration direction is only used to define the initial transect points. The 2D correlation method allows for a free transformation of wave crests in multiple directions.

The **migration distance and direction of sand waves** was identified with a two-dimensional cross-correlation analysis. A 2D cross-correlation analysis is a mathematical technique that is used to study changes in measured signals. In this case, it is used to determine the degree of similarity between the sand wave fields at different points in time (see Figure 3-2). Result of the analysis are the migration distance and migration direction, from which a migration rate can be inferred by including the date of measurement. Migration distances obtained from 2D correlation analysis are compared to visually identified migration distances (see Table 3-3) for validation.

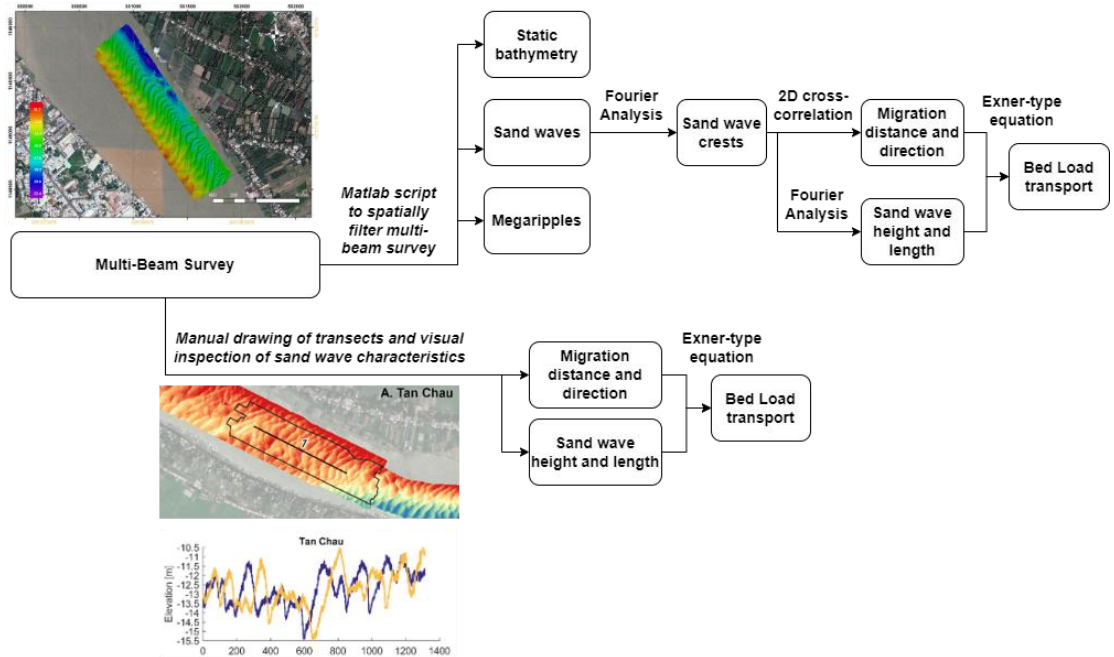


Figure 3-1: Flow chart of how bed load transport is obtained from multi-beam survey results.

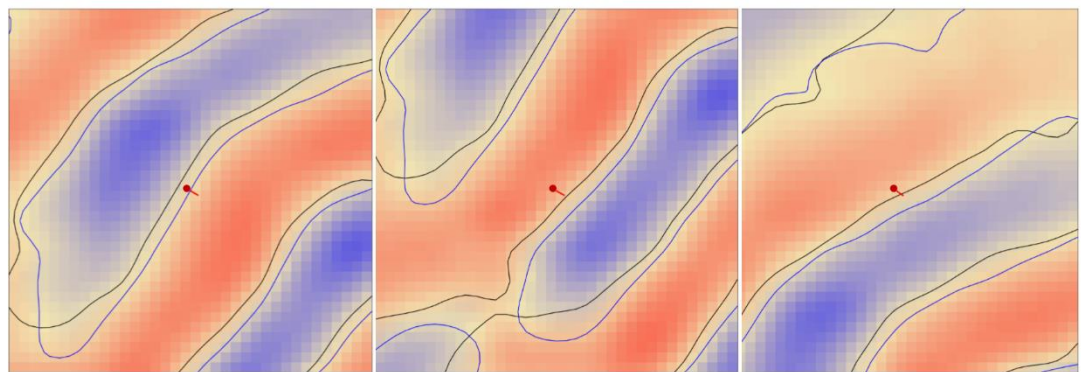


Figure 3-2: An example of cross correlation analysis, depicting the sand waves (coloured bathymetry), the contours of sand waves for the first (black line) and second (blue line) bathymetric survey and the observed migration distance and direction for a single transect point (red line). The example points are extracted from the 2D cross-correlation analysis for Can Tho.

A second proxy for the migration direction of sand waves, and hence net direction of sediment transport, is the bedform asymmetry (Barnard et al., 2013). For each transect location and for each bathymetric dataset, the migration direction is derived from bedform asymmetry by analysing the sand wave gradients. For each transect point, sand wave field slope magnitudes (see Figure 3-3) in a ~100 m radius are sorted in ascending order. The transect direction is then defined as the dominant slope direction for the 8% highest slope magnitudes.

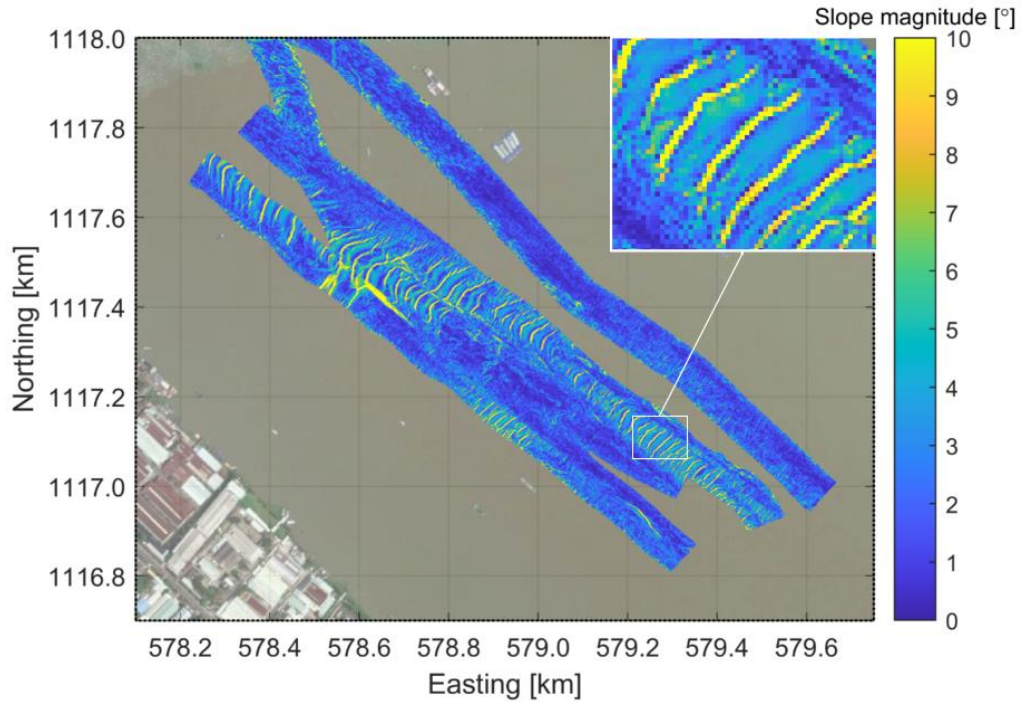


Figure 3-3: Sand wave field gradients, showing slope magnitudes for the Can Tho sand wave field during the dry season.

Sand wave characteristics are extracted for each transect point. The migration directions as derived from the 2D cross-correlation results are used to draw new transects across the initial transect points. Crest and trough locations are again identified using a Fourier transformation. For the analysis of sand wave characteristics, the first crest from the initial transect point in the direction of migration is chosen. The sand wavelength is then defined as the distance between the two adjacent troughs. The sand wave height is defined as the difference between the average trough depth compared to the crest height.

Bed load transport can be estimated from calculated migration rates and sand wave characteristics, using a continuity equation for sand of the Exner type. As concluded by Leary and Buscombe, (2020), reliable estimates of bed load transport can be obtained from the application of the Exner equation. The Exner equation for bed load transport q_b ($m^3/s/m$) assumes triangular dunes and requires the mean dune height H_D and the median dune celerity (migration rate) V_c as input:

$$q_b = (1 - p)V_c \frac{H_D}{2} - q_0$$

here p is the porosity of the sand and q_0 is a constant of integration (set to zero, see Leary and Buscombe, 2020).

Bed load estimates obtained following the procedure above are calculated per unit meter river width ($m^3/s/m$). To compare these estimates with Delft3D-FM simulated bed-material transports, they were converted to **total bed load transport (m^3/s)** for a given river cross-section through multiplication by the effective river width (part of the river carrying most of the flow and hence sediment). The effective width was determined by inspecting measured river profiles to identify the flow area. The lower bound of the effective width was the width of the sand wave field and the upper bound was the full river width.

Bed load transport calculations have been compared to **bed load transport estimates from literature for validation**. Only sparse data is available on bed load transport in the VMD. Most recent bed load estimates have been derived by Jordan et al., (2019) and Stephens et al., (2017) (see Table 3-1).

Table 3-1: Overview of bed load transport estimates for the VMD. Note that total bed loads (Jordan et al., 2019) are converted to $10^{-5} \text{ m}^3/\text{s}$, and bed load per unit river width (Stephens et al., 2017) to $10^{-8} \text{ m}^3/\text{s}/\text{m}$, according to the units in the following sections.

	Method	Season	Date	Location	Bed load transport	Converted bed load transport
Jordan et al., 2019	Bed load translation method (Nittrouer et al., 2008) on MBES surveys	Dry season	May 3 to 18, 2018	My Thuan	0.42 kg/s	$21 \cdot 10^{-5} \text{ m}^3/\text{s}$
		Wet season	October 2 to 10, 2018	My Thuan	2.81 kg/s	$141 \cdot 10^{-5} \text{ m}^3/\text{s}$
Stephens et al., 2017	Bed load translation method (Nittrouer et al., 2008) on MBES surveys	Wet season	September 22 to October 4, 2014	Can Tho	0.023 kg/s/m	$1150 \cdot 10^{-8} \text{ m}^3/\text{s}/\text{m}$
				Dai Ngai	0.028 kg/s/m during downstream flow 0.072 kg/s/m during upstream flow	$1400 \cdot 10^{-8} \text{ m}^3/\text{s}/\text{m}$ $3600 \cdot 10^{-8} \text{ m}^3/\text{s}/\text{m}$
				Cau Quan	0.19 kg/s/m	$9000 \cdot 10^{-8} \text{ m}^3/\text{s}/\text{m}$

3.1.3 Description of sand wave characteristics from visual inspection

3.1.3.1 Dry Season

During the dry season, MBES data were collected at four monitoring stations; Can Tho, Tan Chau, Chau Doc, and My Thuan. Figure 3-4 depicts an overview of the monitoring data and outlines the sand wave fields. Bed elevation profiles for transects across the sand wave fields are plotted in Figure 3-5, which give a first indication of the sand wave characteristics. For Can Tho, Tan Chau, and Chau Doc clear sand wave fields were observed. Longest and highest sand waves were found at Tan Chau, with large migration distances. At Chau Doc, only marginal migration was observed during the eighteen-day interval between successive measurements. Note that due to errors in the survey, bedload transport could not be computed at My Thuan station. Table 3-2 lists main observations from **visual inspection** of MBES results and **hand calculations** to check the 2D correlation results. In hand calculation, by manually drawing transects across the dune fields (e.g., Figure 3-4) we can have an early indication of sand wave characteristics and migration distance. This helps us verify the automated sand wave identification and avoid errors deriving the sand wave characteristics.

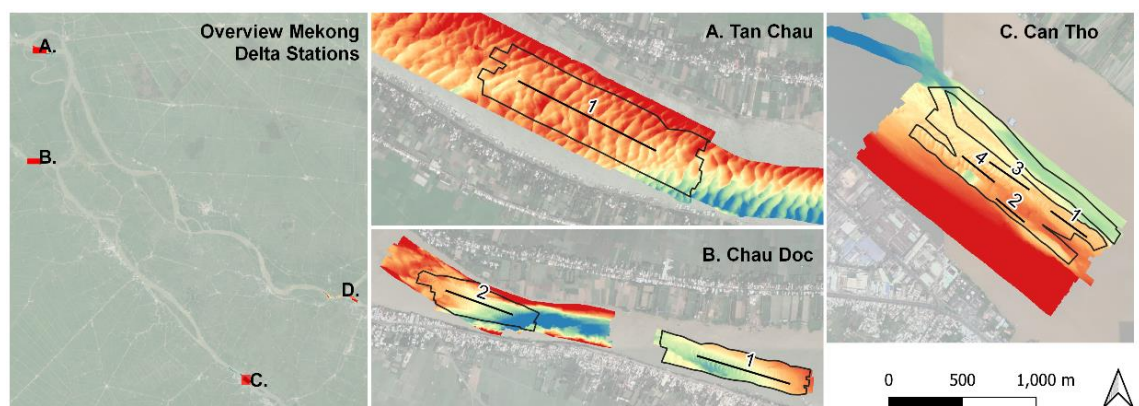


Figure 3-4: Overview of MBES data acquired during the dry season monitoring. Polygons denote overlapping MBES data for successive measurements to be used for the dune tracking. Transects are drawn in the dominant sand wave migration direction for validation of the automated dune tracking.

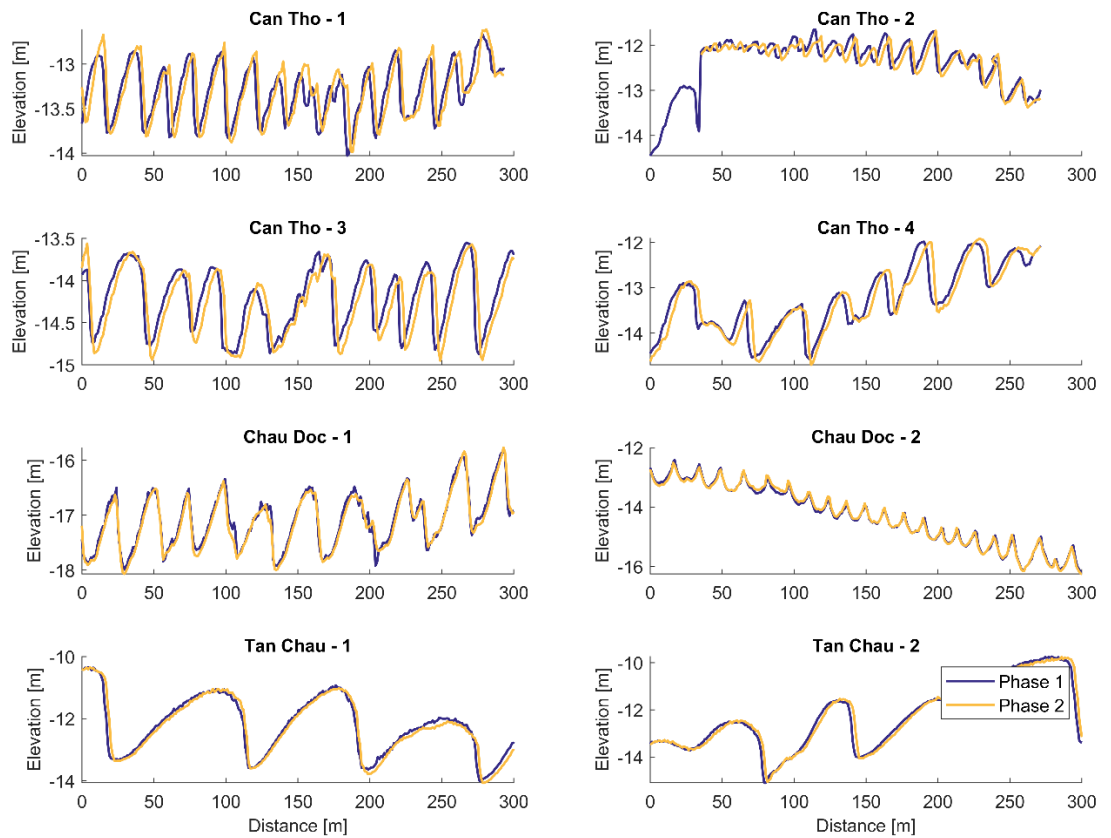


Figure 3-5: Bed elevation profiles for transects across sand wave fields during the dry season campaign. The distance is defined in the downstream direction.

Table 3-2: Overview of the approximate measurement area that is suitable for dune tracking analysis, the approximate sand wavelength, height, and migration distance during the dry season survey period based on visual inspection of multibeam measurements.

Site	Area [km ²]	Sand wavelength [m]	Sand wave height [m]	Migration distance [m]	Migration rate [10 ⁻⁸ m/s]	Bedload estimate [10 ⁻⁸ m ³ /s/m]
Tan Chau	0.6	50-100	1-3	2-6	125-400	50-300
Chau Doc 1	0.2	15-30	0.5-1.5	1	70	10-35
Chau Doc 2	0.2	15-20	0.5-1	0	0	0
Can Tho	0.5	15 - 40	0.5-1.5	2-4	125-250	20-100

3.1.3.2 Wet Season

During the wet season, MBES data were collected at twelve monitoring stations, as listed in Table 3-3. At seven stations, clear sand waves with wave lengths over 20 m were observed that can be tracked for a bed load estimate.

Figure 3-6 depicts an overview of the monitoring data and outlines the sand wave fields. Figure 3-7 gives an overview of bed elevation profiles for the seven stations where we can identify dunes. Table 3-3 lists main observations from visual inspection of MBES results and hand calculations to check the 2D correlation results (see Table 3-5 and Table 3-6).

Table 3-3: Overview of the approximate measurement area suitable for dune tracking analysis, the approximate sand wavelength, height, and migration distance during the wet season survey period based on **visual inspection of multibeam measurements**. Sand wave characteristics for My Thuan are mentioned in brackets since this sand wave was only observed for a single survey. For this reason, we cannot track the dune migration. For Binh Dai and Dai Ngai, sand wave characteristics are mentioned in brackets since they are too small in height and length for dune tracking analysis. For Cho Lach 1, no correlation can be observed between the phase 1 and 2 measurements since migration distances and sand wave shape change were too large.

Site	Area [km ²]	Sand wavelength [m]	Sand wave height [m]	Migration distance [m]	Migration rate [10 ⁻⁸ m/s]	Bedload estimate [10 ⁻⁸ m ³ /s/m]
1 – Tan Chau	1.1	80-120	1-2	50-100	5000-10000	2000-5000
2 – Chau Doc	1.0	20-50	0.5-1.5	15-20	1500-2000	250-1000
3 – My Thuan		[150-300]	[1-1.5]	[40]		
4 – Can Tho	0.8	10-70	0.5-1	15-30	1500-3000	250-1000
5 – Vam Nao	0.9	60-100	0.5-1.5	40 - 60	4000-6000	1000-2000
6 – My Tho		-	-	-		
7 – Cho Lach 1		15-20	0.5-1	-		
8 – Co Lach 2	1.1	20-60	0.5-1	20-30	2000-3000	500-1000
9 – Binh Dai	[0.2-0.6]	[5-10]	-	-		
10 – Long Xuyen	0.7	30-80	1-2.5	30-40	3000-4000	1000-2000
11 – Dai Ngai	[0.1-0.5]	[4-10]	-	-		
12 – Cao Lanh	1.8	50-200	1.5-4	40-60	4000-6000	3000-8000

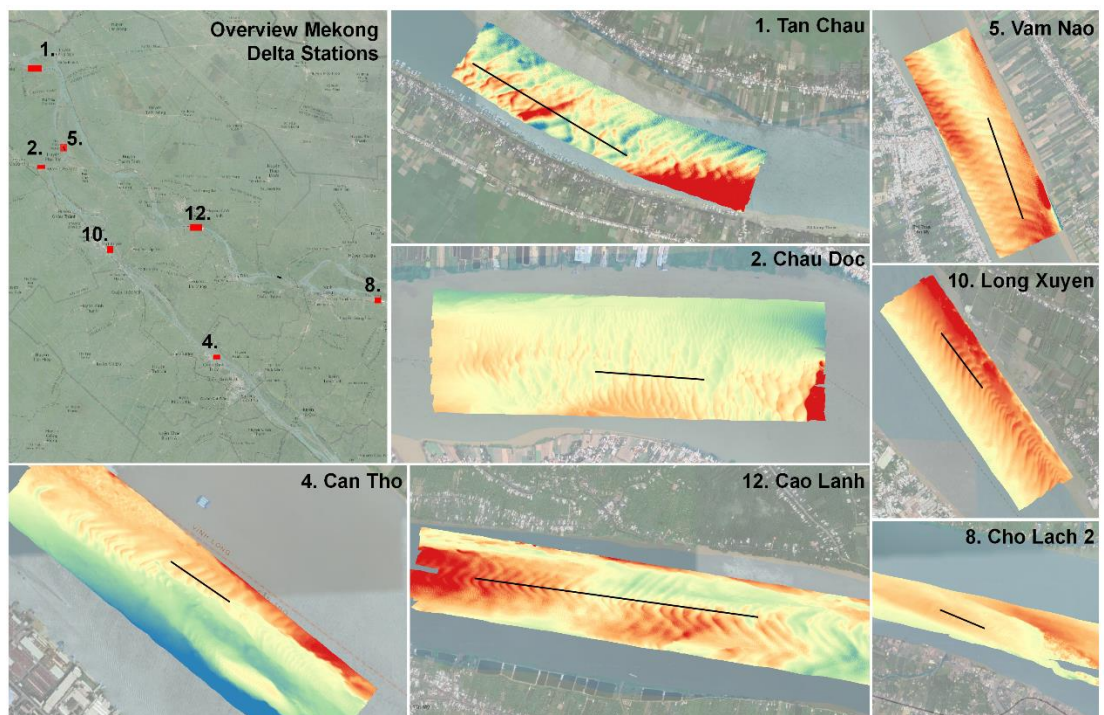


Figure 3-6: Overview of MBES data acquired during the wet season monitoring for which we can track dunes. Transects are drawn in the dominant sand wave migration direction for validation of the automated dune tracking.

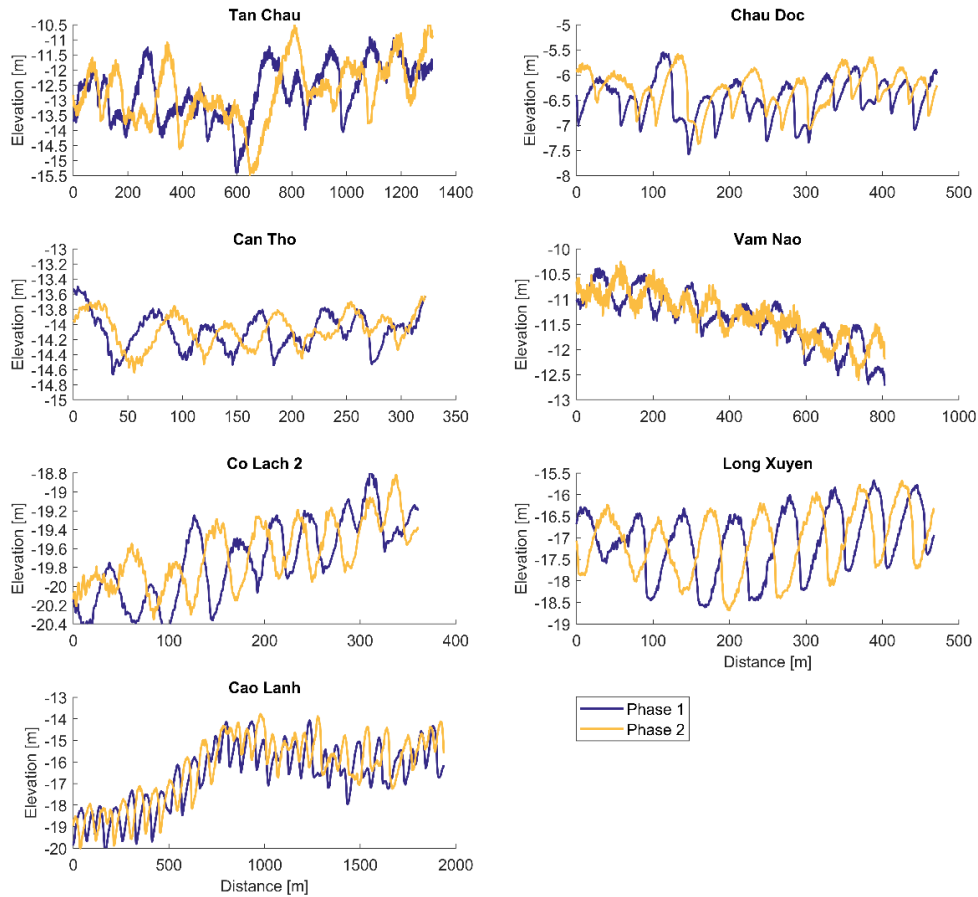


Figure 3-7: Bed elevation profiles for transects across sand wave fields during the wet season campaign (see Figure 3-6). The distance is defined in the downstream direction.

3.1.4 Bed load transport from 2D correlation analysis

3.1.4.1 Dry Season

Results from 2D correlation analysis on successive multibeam surveys for the dry season are summarized in Table 3-4 and displayed in Figure 3-8 to Figure 3-11. The results of 2D correlation align well with those from visual examination and manually drawn transects (Table 3-2), providing high confidence in the accuracy of the results.

Sand wave heights and lengths are largest for Tan Chau, with mean wave heights of 2 m and wave lengths of 83 m, in contrast to the 0.5-0.7 m mean wave heights and 19-27 m wave lengths for Can Tho and Chau Doc (see Table 3-4). Mean *migration distances* are much longer for Can Tho (2.7 m) and Tan Chau (2.5 m) than for Chau Doc. At Chau Doc, waves at the downstream field (nr 1) migrated 1.1 m downstream, whereas waves at the upstream field (nr 2) in the river bend even showed minor (0.2 m) upstream migration. Sand wave characteristics and migration distances obtained with 2D-correlation and Fourier analyses are in good agreement with visual observations summarized in Table 3-3.

Bed load is a function of the migration rate, sand wave height and length. Since all three components are highest for Tan Chau, mean bed load at Tan Chau reaches up to $100 \cdot 10^{-8}$ m³/m/s, compared to $37 \cdot 10^{-8}$, $14 \cdot 10^{-8}$, and $1 \cdot 10^{-8}$ m³/m/s for Can Tho, Chau Doc 1, and Chau Doc 2, respectively (see Table 3-4).

Table 3-4: Summary of the dry season results from the 2D correlation and Fourier analyses; sand wave field characteristics, migration direction and rates and the resulting bed load for Can Tho, Tan Chau, and Chau Doc. Both mean results and the standard deviation are given.

	Station							
	Tan Chau		Chau Doc 1		Chau Doc 2		Can Tho	
	Mean	Std	Mean	Std	Mean	Std	Mean	Std
Sand wave height [m]	2.0	0.7	0.6	0.3	0.5	0.2	0.7	0.3
Sand wavelength [m]	83	30	23	9	19	9	27	13
Migration Direction [°]	95	4	94	4	270	0	125	16
Migration Distance [m]	2.5	0.7	1.1	0.4	0.2	0.1	2.7	0.8
Migration Rate [10^{-8} m/s]	160	48	69	27	10	6	174	48
Bed load [10^{-8} m³/m/s]	101	46	14	5	1	1	37	17

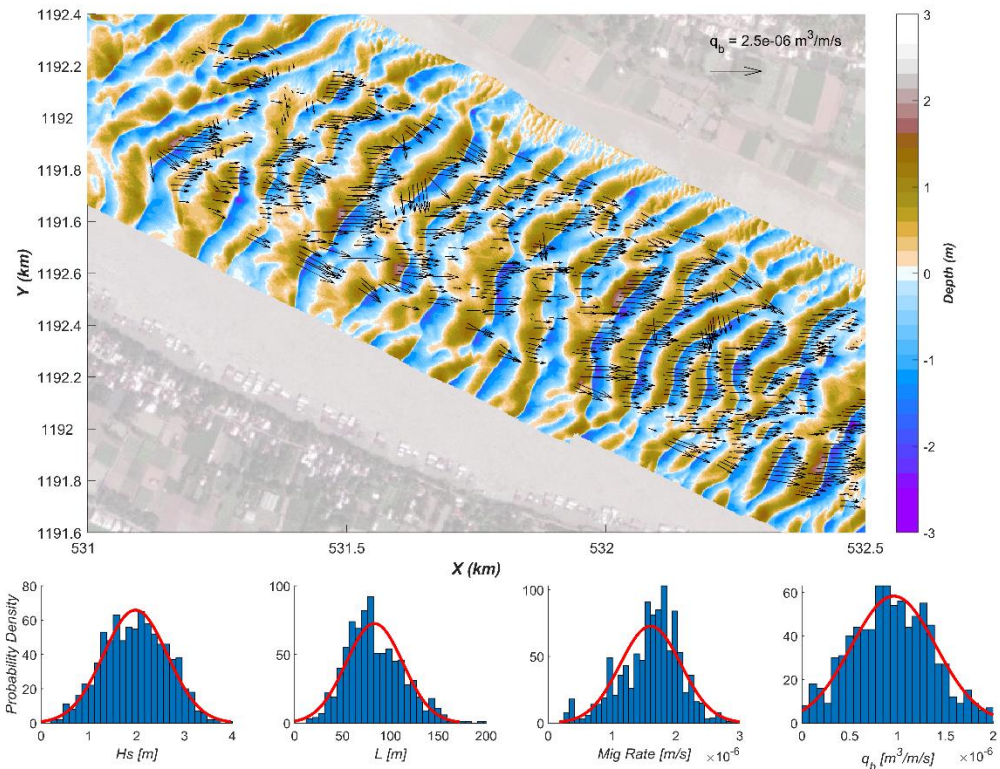


Figure 3-8: Upper panel: Sand wave fields and bed load transport vectors for **Tan Chau** during the **dry season**. Lower panels: Distributions for the sand wave height, sand wavelength, migration rate, and bed load transport.

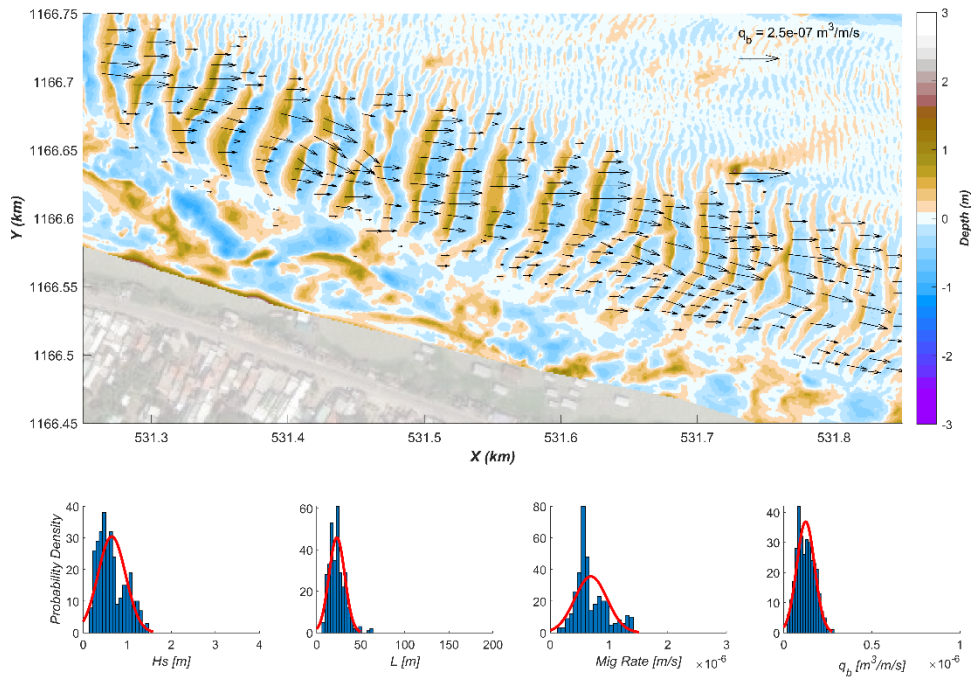


Figure 3-9: Upper panel: Sand wave fields and bed load transport vectors for **Chau Doc, field 1**, during the **dry season**. Lower panels: Distributions for the sand wave height, sand wavelength, migration rate, and bed load transport.

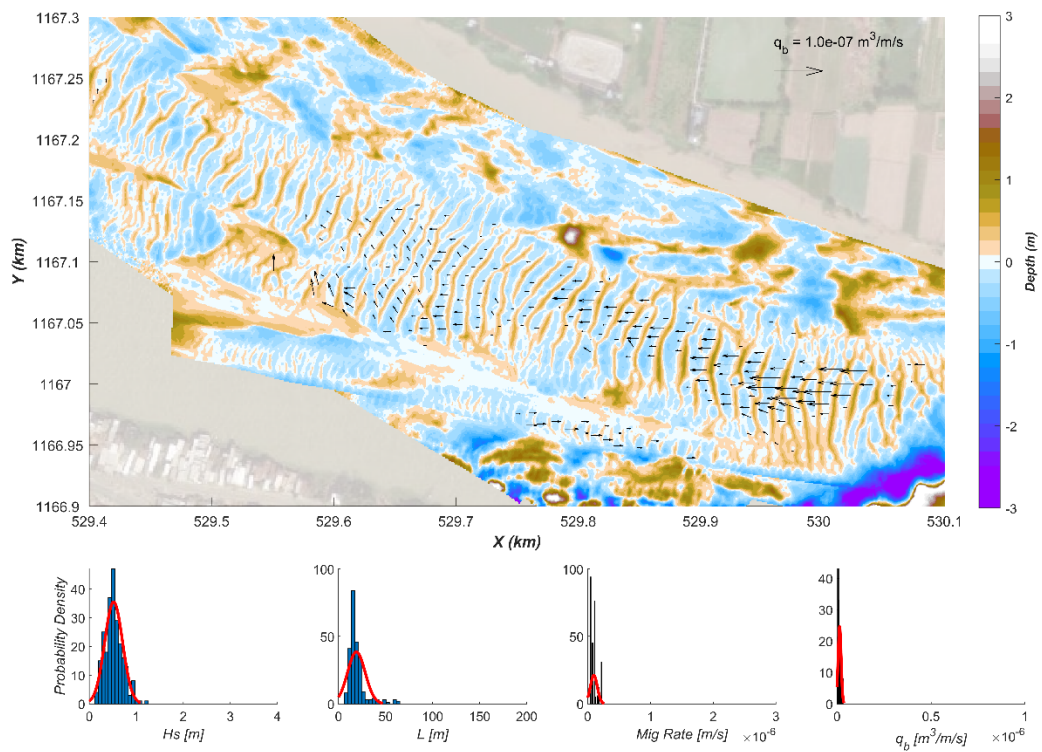


Figure 3-10: Upper panel: Sand wave fields and bed load transport vectors for **Chau Doc, field 2**, during the **dry season**. Lower panels: Distributions for the sand wave height, sand wavelength, migration rate, and bed load transport.

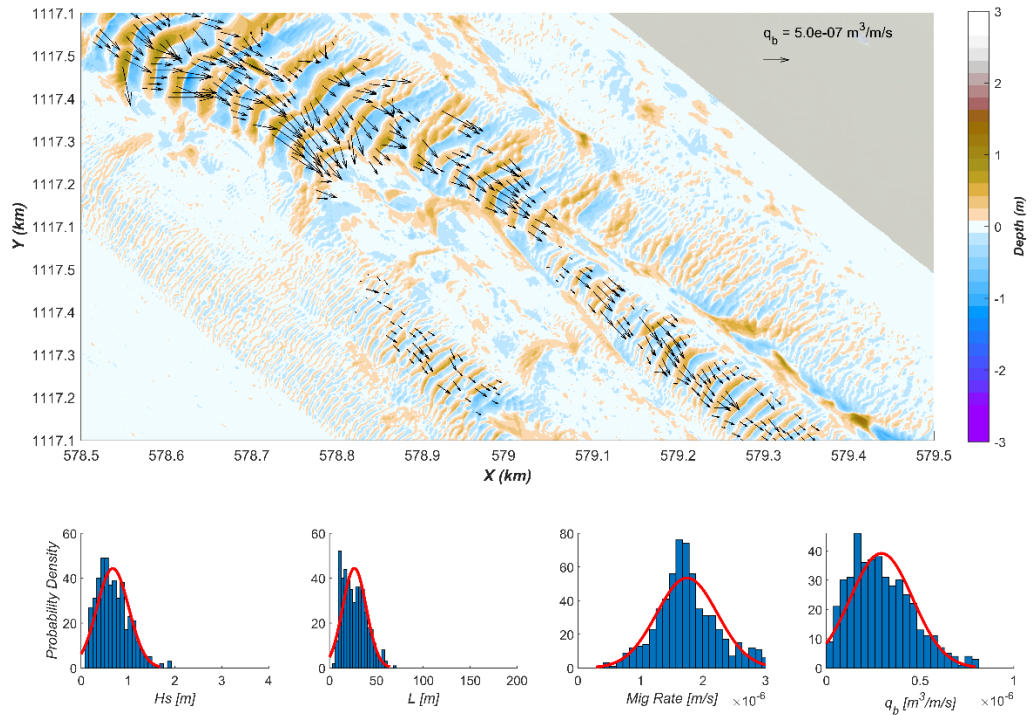


Figure 3-11: Upper panel: Sand wave fields and bed load transport vectors for **Can Tho** during the **dry season**. Lower panels: Distributions for the sand wave height, sand wave length, migration rate, and bed load transport.

3.1.4.2 Wet Season

Results from 2D correlation analysis on successive multibeam surveys for the wet season are summarized in Table 3-5 and Table 3-6 and displayed in Figure 3-12 to Figure 3-18. The results of 2D correlation align well with those from visual examination and manually drawn transects (Table 3-2), providing high confidence in the accuracy of the results. Wet season results are elaborated below.

Table 3-5: Summary of the wet season results from the 2D correlation and Fourier analyses; sand wave field characteristics, migration direction and rates and the resulting bed load for Tan Chau, Chau Doc, and Can Tho. Both mean results and the standard deviation are given.

	Tan Chau		Chau Doc		Can Tho	
	Mean	Std	Mean	Std	Mean	Std
Sand wave height [m]	1.7	0.4	0.8	0.5	0.6	0.3
Sand wavelength [m]	110	31	42	18	49	22
Migration Direction [°]	58	1	90	1	84	45
Migration Distance [m]	66	17	19	3	16	3
Migration Rate [10^{-8} m/s]	6400	1700	1800	300	1500	300
Bed load [10^{-8} m³/m/s]	3300	1200	400	200	300	100

Table 3-6: Summary of the wet season results from the 2D correlation and Fourier analyses; sand wave field characteristics, migration direction and rates and the resulting bed load for Vam Nao, Cho Lach, Long Xuyen, and Cao Lanh. Both mean results and the standard deviation are given.

	Station							
	Vam Nao		Cho Lach		Long Xuyen		Cao Lanh	
	Mean	Std	Mean	Std	Mean	Std	Mean	Std
Sand wave height [m]	0.4	0.2	0.5	0.2	1.6	0.4	1.3	0.4
Sand wavelength [m]	82	43	58	25	62	30	103	58
Migration Direction [°]	16	9	61	7	128	3	83	9
Migration Distance [m]	53	5	20	2	34	4	42	8
Migration Rate [10^{-8} m/s]	5100	500	2000	200	3300	300	4000	800
Bed load [10^{-8} m³/m/s]	500	300	300	100	1700	500	1700	600

Station 1: Tan Chau

Wet season transport patterns at Tan Chau are characterized by strong morphodynamic activity, with large migration distances and sand wave shape transformations over the 12-day surveying interval. Where migration distances were around 2 – 4 m during the dry season, they were as high as 100 m during the wet season. Superimposed on the sand waves, relatively large ripples (0.25 m height) are present.

Because of the significant change in sand wave morphology and large translation distances, the 2D correlation analysis was performed with additional constraints. Firstly, only sand waves that show a consistent shape over the surveying period were included in the analysis. This filtering step removed over 75 % of the sand wave transects. Moreover, the 2D correlation calculation was constricted to only include a translation in downstream direction (100-120° with respect to north). Results (see Figure 3-12) are in line with Table 3-3. Sand wave heights are generally 1 – 2 m and wave lengths 50-150 m. Sand wave heights are lower during the wet season than during the dry season, while sand wave lengths are similar. The migration rate is approximately $6400 \cdot 10^{-8}$ m/s (compared to $160 \cdot 10^{-8}$ m/s for the dry season), resulting in bed load transport of approximately $3300 \cdot 10^{-8}$ m³/m/s ($100 \cdot 10^{-8}$ m³/m/s during the dry season).

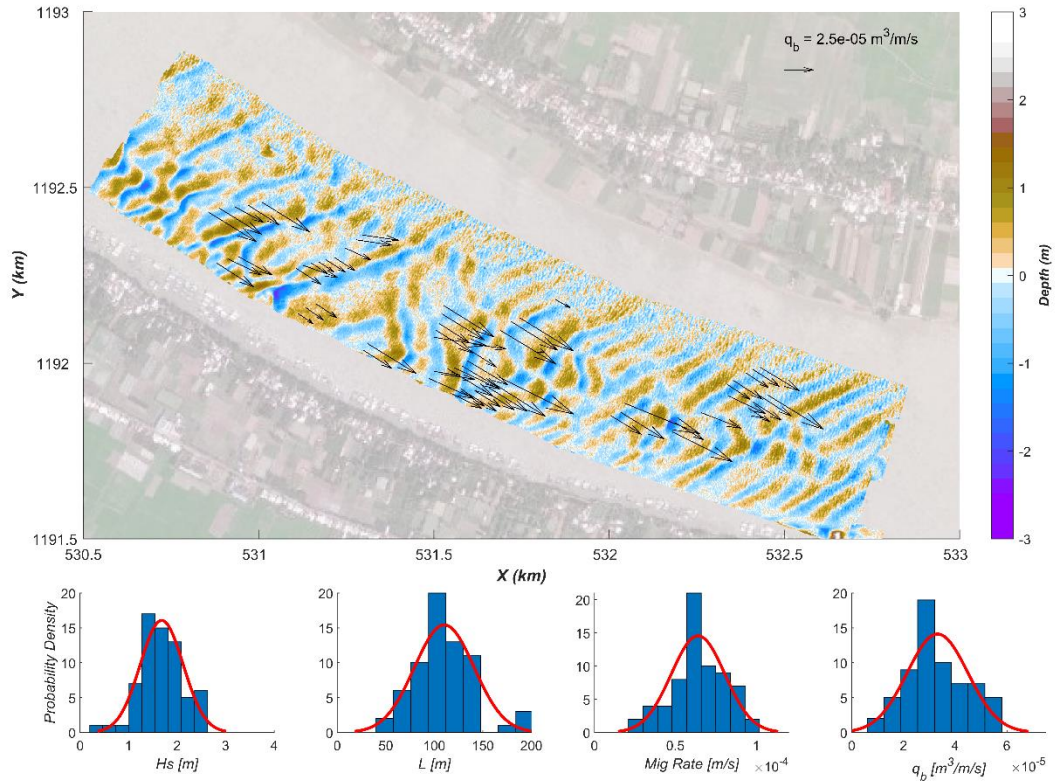


Figure 3-12: Upper panel: Sand wave fields and bed load transport vectors for **Tan Chau** during the **wet season**. Lower panels: Distributions for the sand wave height, sand wavelength, migration rate, and bed load transport.

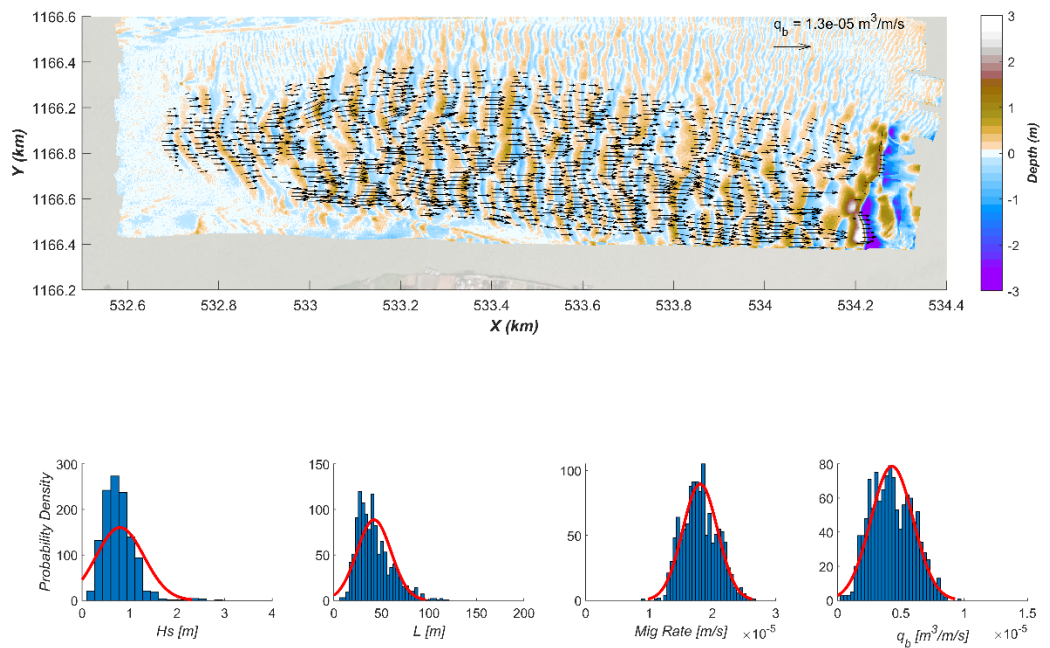


Figure 3-13: Upper panel: Sand wave fields and bed load transport vectors for **Chau Doc** during the **wet season**. Lower panels: Distributions for the sand wave height, sand wavelength, migration rate, and bed load transport.

Station 2: Chau Doc

At Chau Doc, migration distances are lower than at Tan Chau and sand wave shapes are fairly consistent over the surveying period, allowing for an accurate description of the wet season bed load transport. The visual inspection of multibeam results (Table 3-3) shows sand wave lengths of 20-50 m and heights of 0.5-1.5, with very small ripples (5-10 cm) imposed on them. Migration distances are 15 to 20 m in 12 days, compared to approximately 1 m in 18 days for the dry season. The 2D correlation analysis for Chau Doc shows migration rates of approximately 1800×10^{-8} m/s (70×10^{-8} m/s during the dry season), and bed load estimates of $200-600 \times 10^{-8}$ m³/m/s (see Figure 3-13). Most sand waves are 0.5-1 m in height (similar to the dry season) and 30-50 m in length (slightly longer than the dry season). Bed load at Chau Doc is significantly lower than at Tan Chau, but similar to bed loads at Can Tho and Cho Lach 2.

Station 3: My Thuan

During the first survey of the wet season, mainly mega-ripples of 10 m wavelength were observed at My Thuan. For this reason, phase 2 of the survey campaign focused on the area upstream of the phase 1 field. Here, sand waves of 200-300 m wavelength were found outside the area measured during phase 1. There are no waves suitable for 2D correlation analysis.

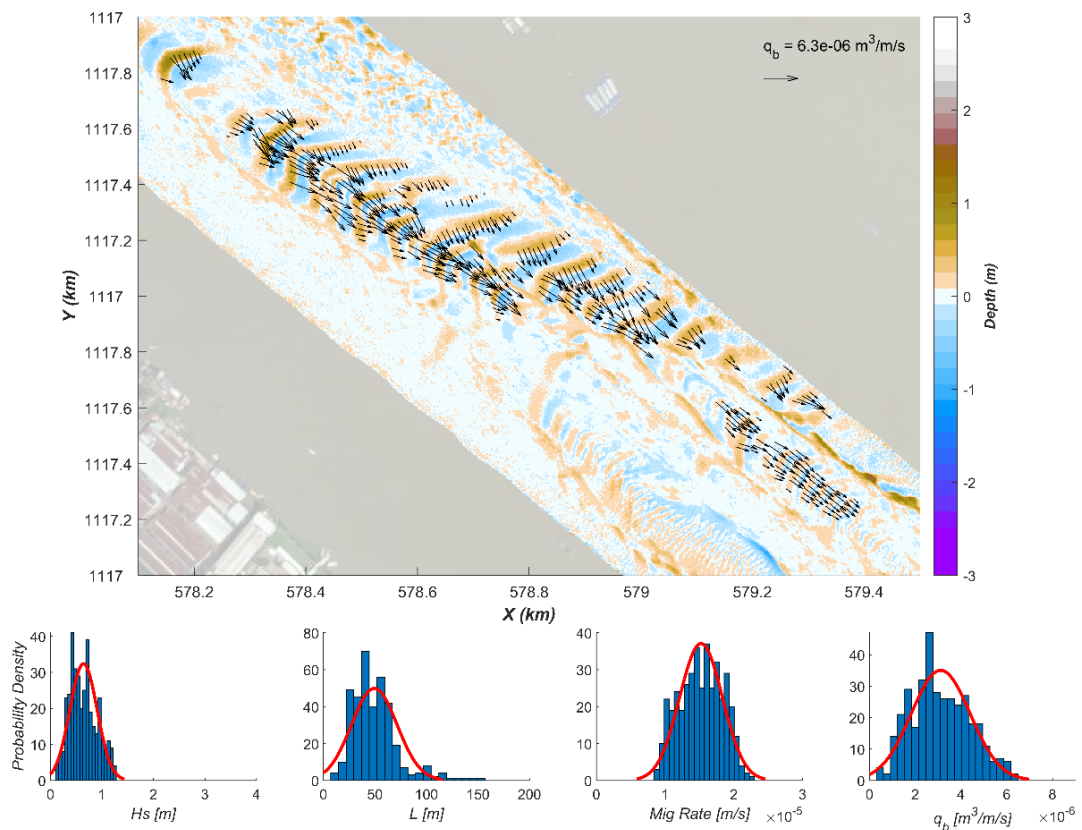


Figure 3-14: Upper panel: Sand wave fields and bed load transport vectors for **Can Tho** during the **wet season**. Lower panels: Distributions for the sand wave height, sand wavelength, migration rate, and bed load transport.

Station 4: Can Tho

Clear sand wave fields were observed near Can Tho. The sand wave amplitude is smaller in the wet season than in the dry season, whereas the sand wavelength has increased. In addition, sand wave lengths are more constant over the river width in the wet season. During the dry season, longer sand waves partitioned into smaller sand waves, which is not observed during the wet season. Migration distances are around 15 – 30 m in 12 days, compared to 2-4 m during the 18-days interval in the dry season. 2D correlation results (Figure 3-14) show that sand waves are 0.25-1 m in height, 25 – 75 m in length, with migration rates of $1500-2000 \times 10^{-8}$ m/s and a bed load of $200-400 \times 10^{-8}$ m³/s/m.

Station 5: Vam Nao

At Vam Nao, a highly dynamic sand wave field was surveyed. Within the 12-day surveying period, large migration distances were observed, as well as significant changes in sand wave morphology. Phase 2 sand waves have a smaller amplitude, but larger mega-ripples imposed on them. Migration distances are of the same order of magnitude as the sand wavelength, for which reason the 2D correlation analysis was constricted to translation in downstream direction only. Migration rates from 2D correlation analysis fit well with visual observations; between 4500 and 6000×10^{-8} m/s. Bed load estimates are $300-800 \times 10^{-8}$ m³/s/m, slightly lower than was estimated based on visual inspection. Bed load at Vam Nao is higher than at Chau Doc and Can Tho, similar to Long Xuyen, but smaller than at Tan Chau and Cao Lanh.

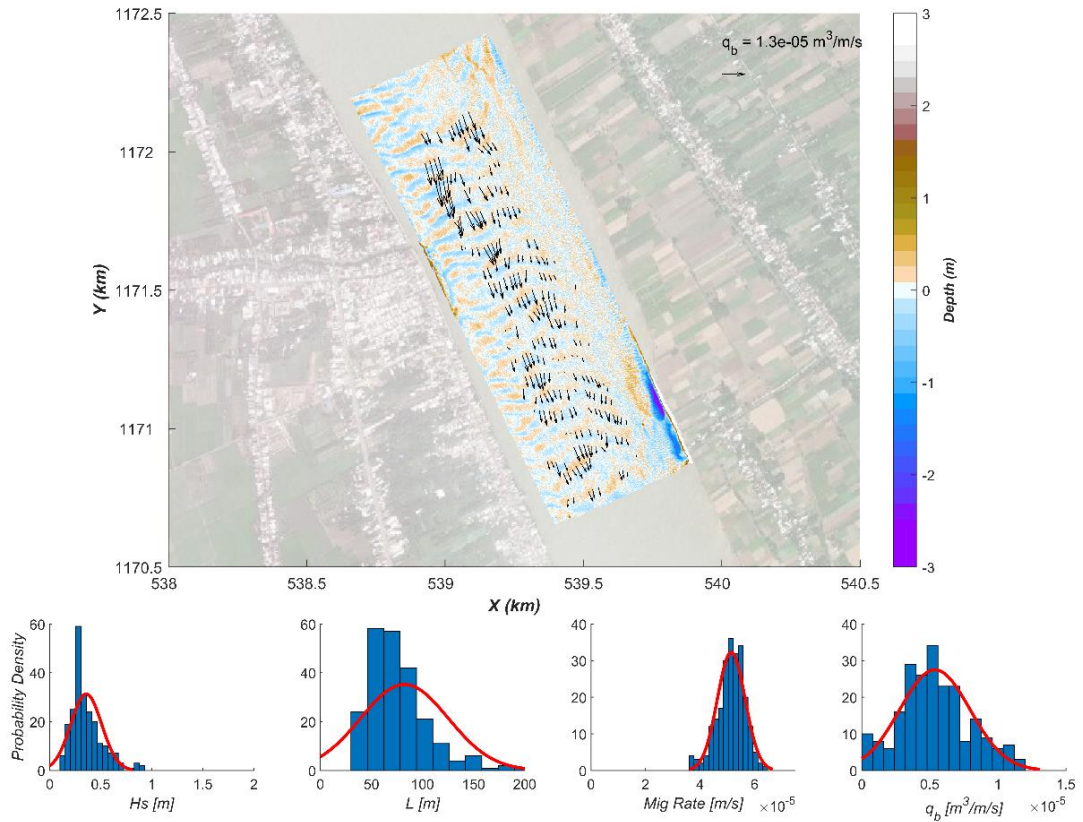


Figure 3-15: Upper panel: Sand wave fields and bed load transport vectors for **Vam Nao** during the **wet season**. Lower panels: Distributions for the sand wave height, sand wavelength, migration rate, and bed load transport.

Station 6: My Tho

At My Tho, no sand waves were observed during both phase 1 and phase 2 measurements.

Station 7: Cho Lach 1 (Ham Luong)

Sand waves are relatively short at Cho Lach station 1, in the Ham Luong branch, and morphological activity high. Within the 12-day period, the sand wave shape has changed significantly, likely accompanied by large migration distances. In addition, the tidal influence is larger close to the mouth, hence the tidal phase could influence the shape of these smaller scale sand waves. For this reason, no clear correlation can be found between successive sand wave measurements.

Station 8: Cho Lach 2 (Co Chien)

A small sand wave field was measured at Cho Lach. The sand wave shape is irregular over the field but relatively consistent over time (see Figure 3-7), enabling an accurate 2D correlation analysis even though migration distances are large compared to the sand wavelength. Sand wave heights at Cho Lach 2 are approximately 0.5 m, sand wave lengths 58 m, migration rates around 2000×10^{-8} m/s, and bed load transport around 300×10^{-8} m³/s/m (Figure 3-16).

These results are in line with results obtained from visual inspection of multibeam measurements (Table 3-3).

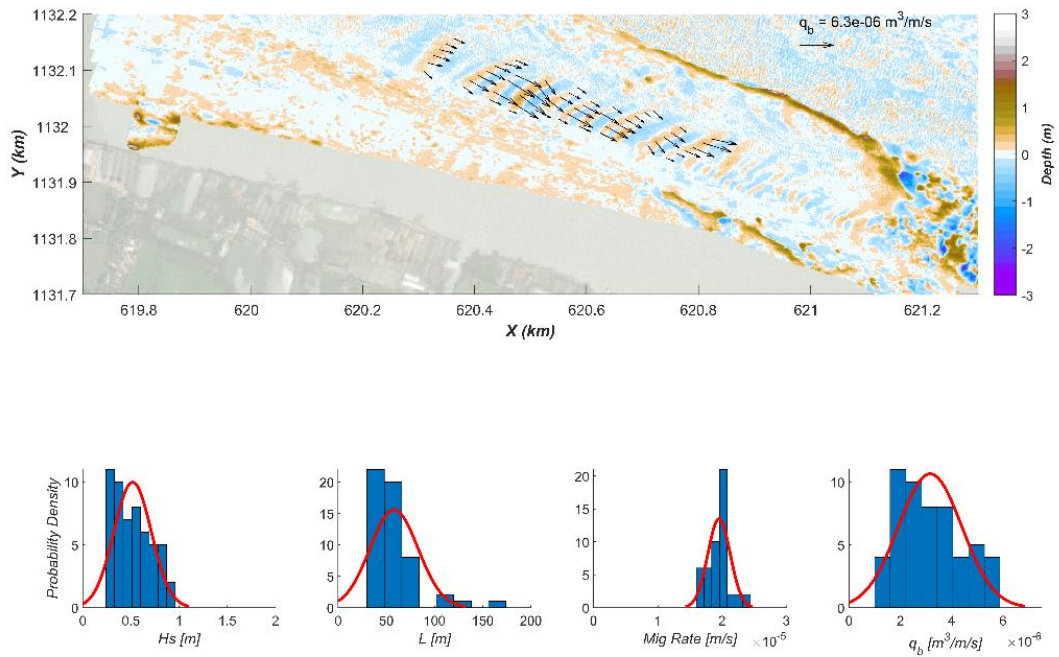


Figure 3-16: Upper panel: Sand wave fields and bed load transport vectors for **Cho Lach 2** during the **wet season**. Lower panels: Distributions for the sand wave height, sand wavelength, migration rate, and bed load transport.

Station 9: Binh Dai

At Binh Dai, no sand waves were observed during both phase 1 and phase 2 measurements.

Station 10: Long Xuyen

At Long Xuyen, a large sand wave field was observed, with significant migration distances but little change in sand wave morphology. This makes sand wave migration clearly traceable. Bed load transport at Long Xuyen is approximately $1700 \times 10^{-8} \text{ m}^3/\text{s/m}$, slightly less than was estimated from the visual inspection (Table 3-3). Compared to other stations; bedload is relatively large. Only at Tan Chau and Cao Lanh, bed load estimates were higher. Sand wave heights are 1 – 2 m and sand wavelength 40-80 m.

Station 11: Dai Ngai

At Dai Ngai, only sand waves of 10 m wavelength were found, which were too small for dune tracking analysis since migration distances are much larger than the wavelength.

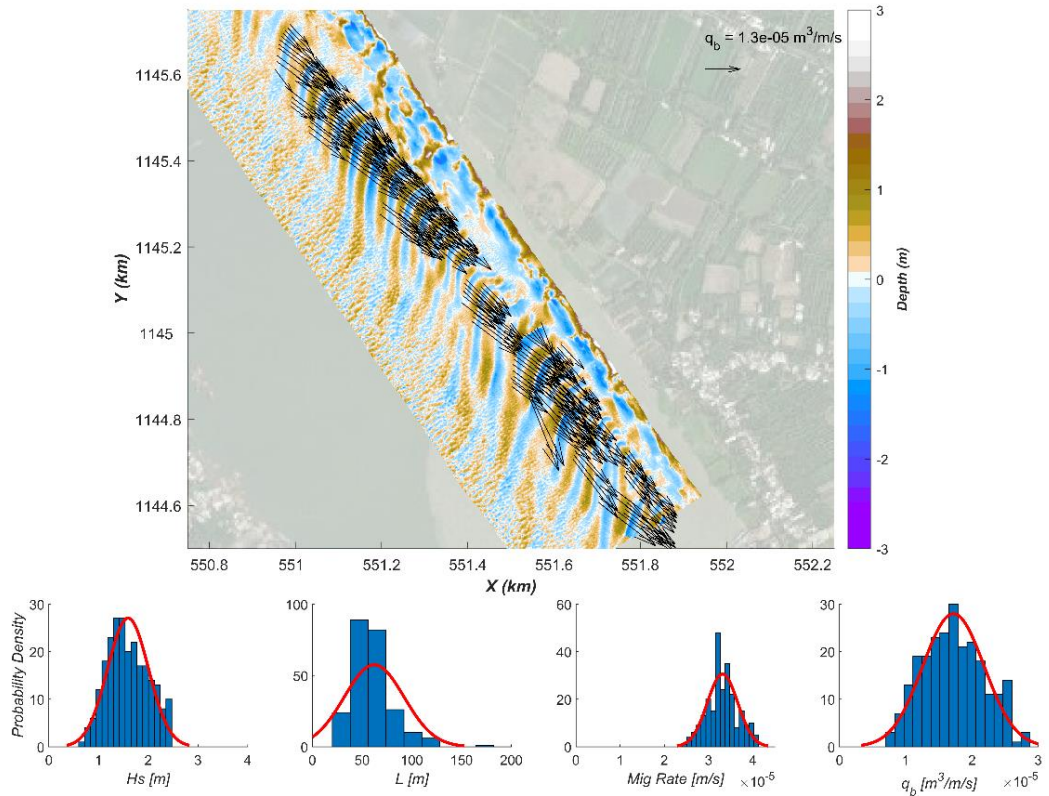


Figure 3-17: Upper panel: Sand wave fields and bed load transport vectors for **Long Xuyen** during the **wet season**. Lower panels: Distributions for the sand wave height, sand wavelength, migration rate, and bed load transport.

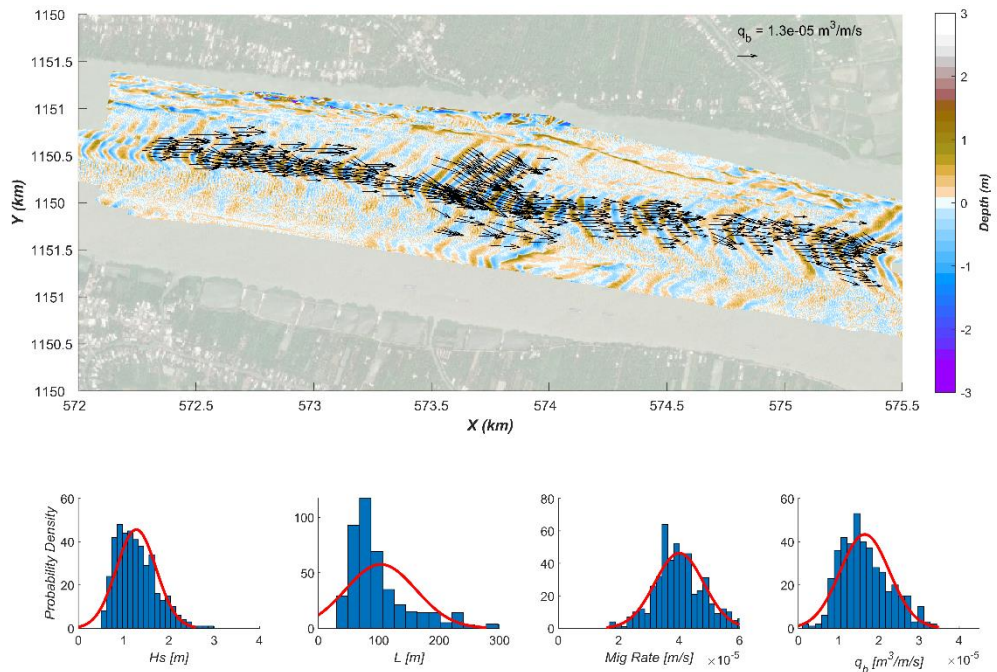


Figure 3-18: Upper panel: Sand wave fields and bed load transport vectors for **Cao Lanh** during the **wet season**. Lower panels: Distributions for the sand wave height, sand wavelength, migration rate, and bed load transport.

Station 12: Cao Lanh

The sand wave field at Cao Lanh is relatively large, with clearly defined sand waves of large wavelength (up to 200 m) and height (up to 2.5 m). Sand waves at Cao Lanh can be accurately tracked over time. The 2D correlation results show that most sand waves migrate at a rate of $3000-5000 \cdot 10^{-8}$ m/s, corresponding to a bed load of $1000-2500 \cdot 10^{-8}$ m³/s/m. This bed load is lower than estimated from visual inspection since average sand wave heights were overestimated.

Conversion of bed load per unit meter to river-wide bed load estimation

Bed load estimates derived from dune tracking were given per unit meter river width. They were extrapolated to total bed load estimates by assuming a distribution of bed load across the river width, referred to as the effective river width. The effective width does not have to be equal to the full width. For instance where parts of the bed consist of erosion-resistant clay or peat without full-capacity sand transport and bed forms, or sections with limited flow velocity such as between groynes.

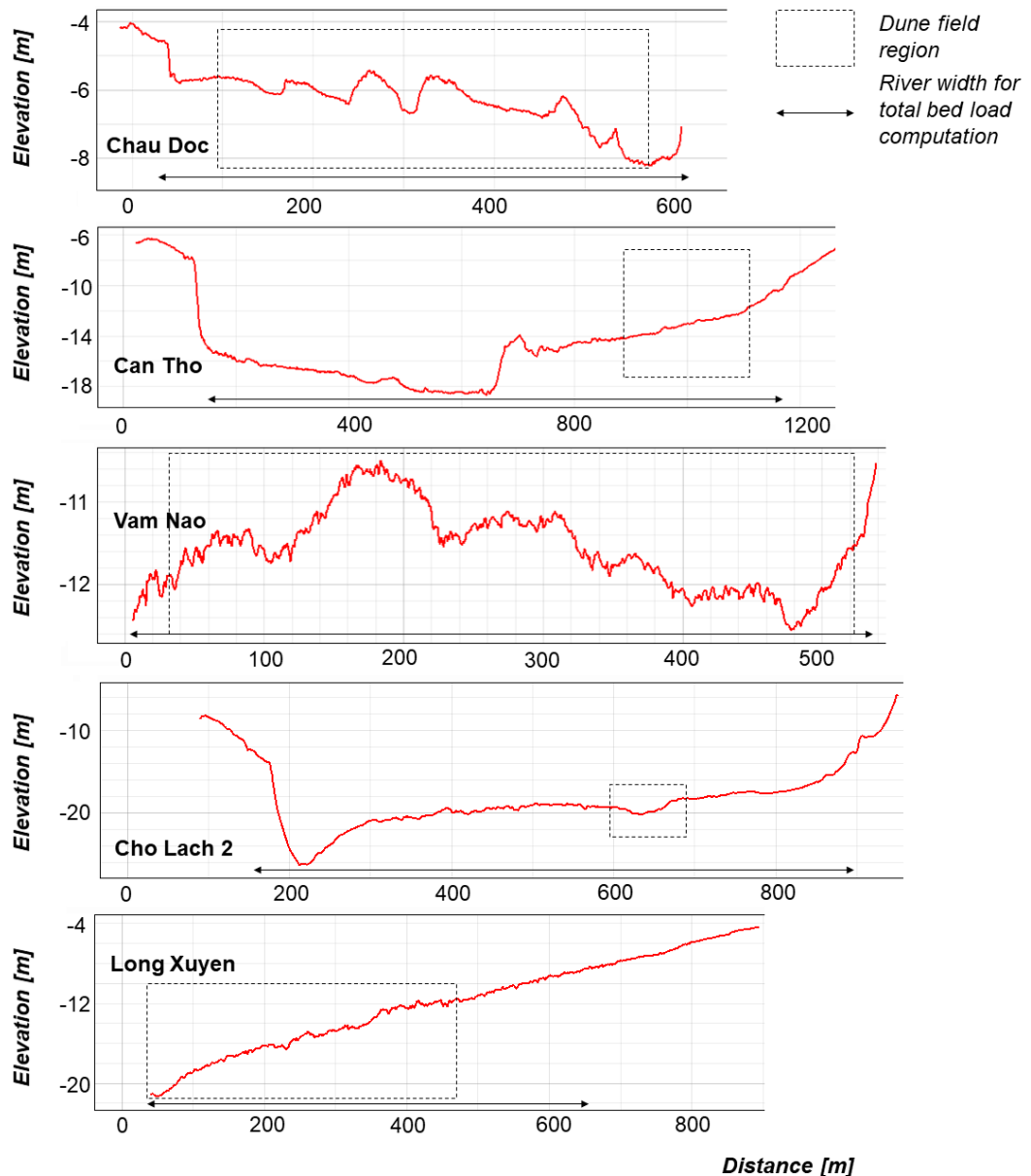


Figure 3-19: Estimation of the effective river width (arrows) for total bed load estimation, showing cross-sections (red lines) and dune field regions (dashed squares) observed in the MBES results, for the five stations where cross-sections were available

As best estimate for the effective river width, we inspected the river cross-sections that were surveyed for the following stations: Chau Doc, Can Tho, Vam Nao, Cho Lach, and Long Xuyen. For these stations, the cross-sectional profiles were investigated to identify the flow area of the river (see Figure 3-19). The effective river width used for the total transport computation is indicated by the arrows in Figure 3-19. For Tan Chau and Cao Lanh, no cross-sections were available, and the bedforms span (almost) the entire width of the multibeam survey. The MBES fields again cover approximately half (Cao Lanh) to two-thirds (Tan Chau) of the river width. Three-quarter of the river width was assumed as best estimate for the effective river width for these two stations. The lower estimate of the effective river width was taken as the width of the observed sand wave field, while the upper estimate was the full river width. The latter may be a conservative estimate, but it takes into account that some sand transport can occur over hard substrate without development of noticeable bed forms. The effective riverbed values, as well as the corresponding total bed load estimations are denoted in Table 3-7 (dry season) and Table 3-8 (wet season).

Table 3-7: Estimation of the total bed load transport in $10^{-8} \text{ m}^3/\text{S}$ during the wet season based on the bed load estimate per unit river width and the estimated effective river width.

Site	Bed load: Mean [Std] [10^{-8} $\text{m}^3/\text{s}/\text{m}$]	Effective river width: (Best estimate [lower, upper]) (m)	Best estimate total bed load: Mean [Std] [$10^{-8} \text{ m}^3/\text{S}$]	Lower limit total bed load: Mean [Std] [$10^{-8} \text{ m}^3/\text{S}$]	Upper limit total bed load: Mean [Std] [$10^{-8} \text{ m}^3/\text{S}$]
1 – Tan Chau	101 [46]	600 [500, 750]	61,000 [28,000]	51,000 [23,000]	76,000 [35,000]
2 – Chau Doc 1	14 [05]	250 [150, 350]	4,000 [1,000]	2,000 [1,000]	5,000 [2,000]
4 – Can Tho	37 [17]	1000 [350, 1500]	37,000 [17,000]	13,000 [6000]	56,000 [26,000]

Table 3-8: Estimation of the total bed load transport in $10^{-8} \text{ m}^3/\text{S}$ during the wet season based on the bed load estimate per unit river width and the estimated effective river width.

Site	Bed load: Mean [Std] (10^{-8} $\text{m}^3/\text{s}/\text{m}$)	Effective river width: (Best estimate [lower, upper]) (m)	Best estimate total bed load: Mean [Std] [$10^{-8} \text{ m}^3/\text{s}$]	Lower limit total bed load: Mean [Std] [$10^{-8} \text{ m}^3/\text{s}$]	Upper limit total bed load: Mean [Std] [$10^{-8} \text{ m}^3/\text{s}$]
1 – Tan Chau	3300 [1200]	600 [500, 750]	1,980,000 [720,000]	1,650,000 [600,000]	2,475,000 [900,000]
2 – Chau Doc	400 [200]	550 [450, 650]	220,000 [110,000]	180,000 [90,000]	260,000 [130,000]
4 – Can Tho	300 [100]	1000 [350, 1500]	300,000 [100,000]	105,000 [35,000]	450,000 [150,000]
5 – Vam Nao	500 [300]	500 [450, 600]	250,000 [150,000]	225,000 [135,000]	300,000 [180,000]
8 – Co Lach 2	300 [100]	750 [100,900]	225,000 [75,000]	30,000 [10,000]	270,000 [90,000]
10 – Long Xuyen	1700 [500]	600 [350, 900]	1,020,000 [300,000]	595,000 [175,000]	1,530,000 [450,000]
12 – Cao Lanh	1700 [600]	700 [450, 900]	1,190,000 [420,000]	765,000 [270,000]	1,530,000 [540,000]

3.1.5 **Bedload transport compared to other studies**

The bed load estimates from this study were compared with those from literature (see Table 3-1). At Can Tho, (Stephens et al., 2017) observed a bed load of approximately $1150 \cdot 10^{-8} \text{ m}^3/\text{s}/\text{m}$ during the wet season, compared to our estimate of $300 \cdot 10^{-8} \text{ m}^3/\text{s}/\text{m}$, giving estimates of the same order of magnitude. The peak instantaneous discharge was significantly higher during the 2014 survey by Stephens et al., (2017) ($30,000 \text{ m}^3/\text{s}$) compared to this study ($22,000 \text{ m}^3/\text{s}$), which may explain that our total bed load transport is lower. Other survey locations described in the literature do not match the survey locations of this study.

3.2 Existing mobile sand stock

This section expands on the approach and the results of the field measurements to quantify, for the first time, existing mobile sand stock of the entire Vietnamese Mekong Delta.

3.2.1 **Sub-bottom profiling as the main approach**

The goal of sub-bottom profiling (see section 2.4, field measurements) analysis is to identify the presence of sandy sediments and to map the thickness of such sand layers to eventually estimate the existing mobile sand stock in a given system.

3.2.2 **Sub-bottom data**

For this campaign, a parametric “*Innomar SES-2000 compact*” system was used. This system produces very high vertical resolution data while still penetrating relatively deeply into the soil below the riverbed. The survey work covered a total of 550 kilometres of sub-bottom profiler lines. For a more detailed description of the SBP as a technique, we refer to the previously submitted inception report.

After the completion of the survey, the acquired data was post-processed. The goal of this was to improve the interpretability of the sub-bottom data for identifying different sediment structures. For positioning of the data, Global Navigation Satellite Systems (GNSS) locations were calculated and added to the meta-data of sub-bottom profiles. The heave experienced by the vessel during surveying was compensated using the onboard motion sensor. The data was exported in an industry-standard full-waveform data format. Post-processing included band-pass filtering to remove unwanted noise from the data. Amplitude recovery was applied to be able to visualise deeper layers. Automatic riverbed detection was performed to gain the profiles of the depth along the survey lines.

From the sub-bottom data, the interfaces between different lithologies can be mapped continuously along the whole profile, but this does not necessarily provide information about the different sediment types directly. The sediment types can partly be interpreted from geological structures identified in the sub-bottom data, but this has to be supplemented with borehole information and with information at the surface of the riverbed using grab samples and additionally the multi-beam data as described in the next sections.

3.2.3 **In-river boreholes and grab samples**

A 195 in-river boreholes were available to aid interpretation and are displayed in Figure 3-21. A borehole provides the information of the sediment type at different depths in one location. Section 3.2.5 outlines how the boreholes are used in interpretation. More borehole data could allow further analysis of deeper layers, potentially revealing buried sand layers. Where no boreholes were available, this was not possible. Therefore, the presented results provide a conservative estimate of the existing mobile sand stock.

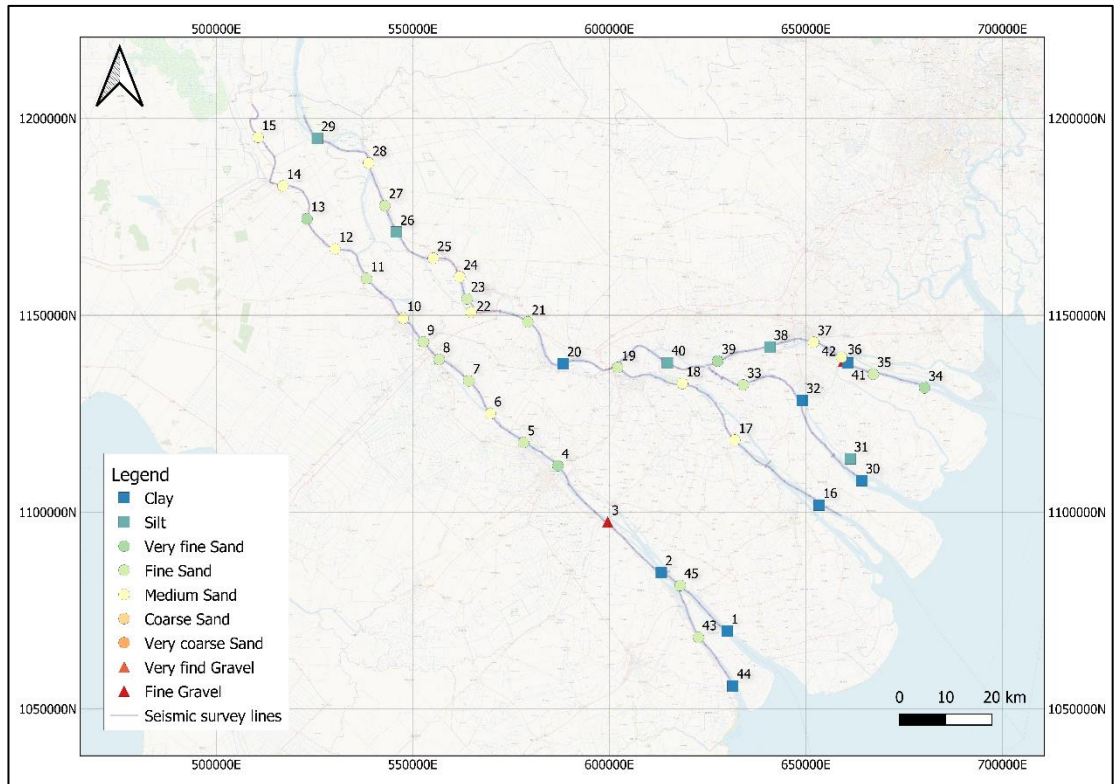


Figure 3-20: Overview of all the SBP coverage (purple line) and the grab samples. The numbers are the sample IDs. The symbol shape represents the different sediment classes, and colours indicate the subclasses based on grain size (D50).

In addition to the available borehole data (Figure 3-21) in three provinces (Hau Giang, Tra Vinh, Vinh Long), during the SBP survey we collected 45 grab samples (roughly every 10 km). The grab sample locations were selected to demonstrate a variety of sediment classes from sand to mud, to potentially correlate the sub-bottom profiler data to different sediment classes. Contrary to the boreholes, the grab samples only provide indications of the sediment types at the riverbed. In areas where no borehole data was available, we verified the presence of sand by identifying sand waves or mega-ripple bedforms visible in the sub-bottom profiler data (e.g., see Figure 3-22). At the scale of this study, it is a reasonable assumption that sections without sand dunes consist of hard substrate or large mud content, e.g., clay and peat beds, that do not have reasonable amounts of sand transport; otherwise, these areas may also show isolated barchan-type of bed forms).

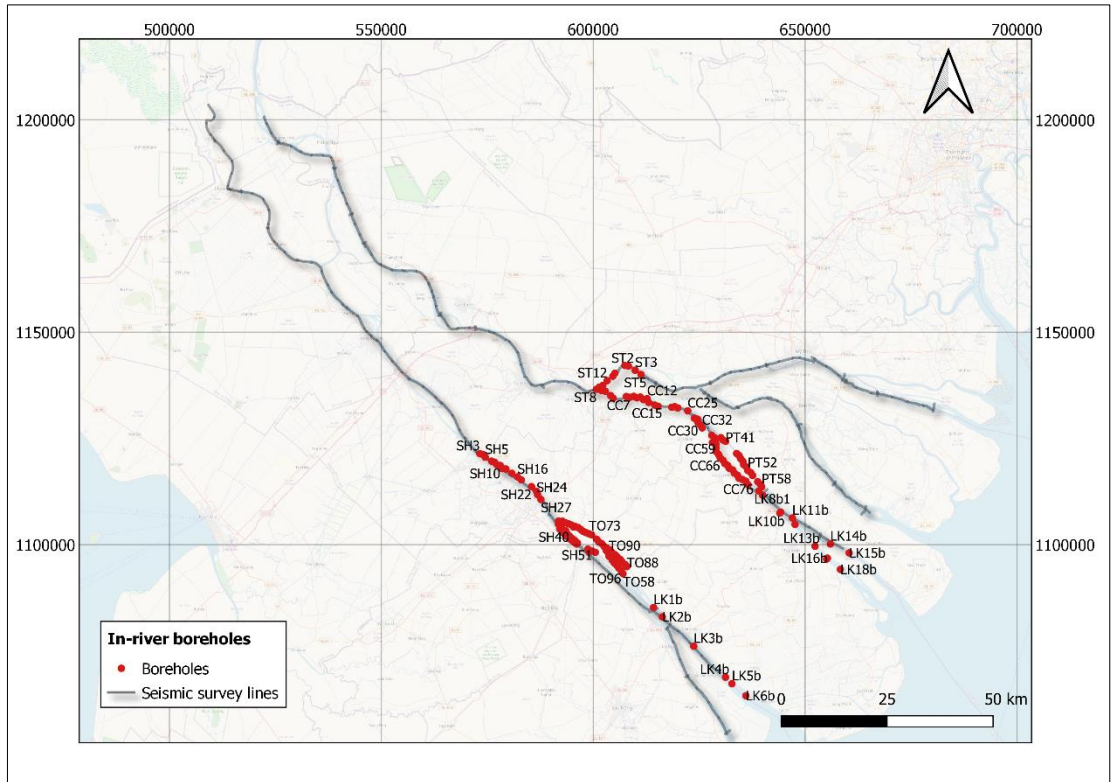


Figure 3-21: In-river boreholes to aid the seismic interpretation available at three provinces (The red points in the map), mostly situated in the lower delta.

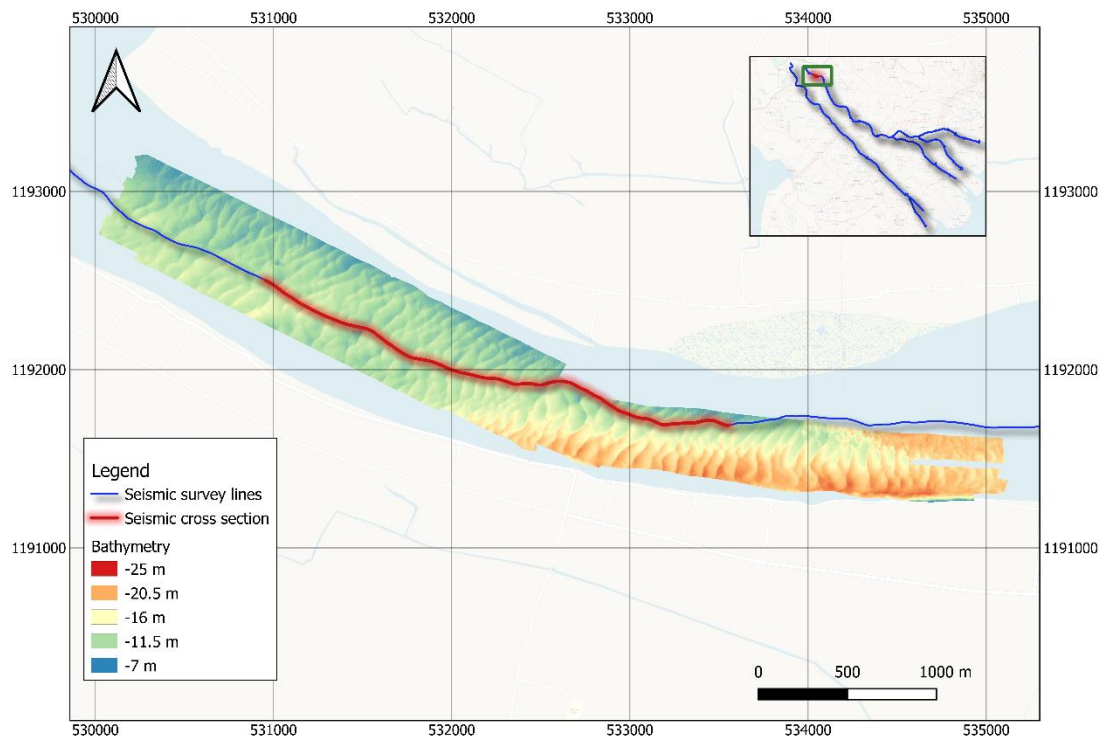


Figure 3-22: A location near Tan Chau where both MBES and SBP data were recorded. From the bathymetric data we can see the extent of the sand waves whereas the sub-bottom data can image the base of the mobile layer and therefore its thickness.

3.2.4 Multi-beam data

Where the thickness of the top sand layer was mapped based on the sub-bottom data, boreholes and grab samples, the lateral extent of the layer still needs to be estimated. The cross-sections of the sub-bottom profiler were not helpful to make this estimate since these lines run perpendicular to the bedforms and in almost all cases the signal at the intersection was very difficult to interpret as in absence of bedforms identifying sand layer was very difficult in the cross sections. However, from MBES survey data that covered the entire river width, we could make good estimates of lateral coverage of sand over the cross-section.

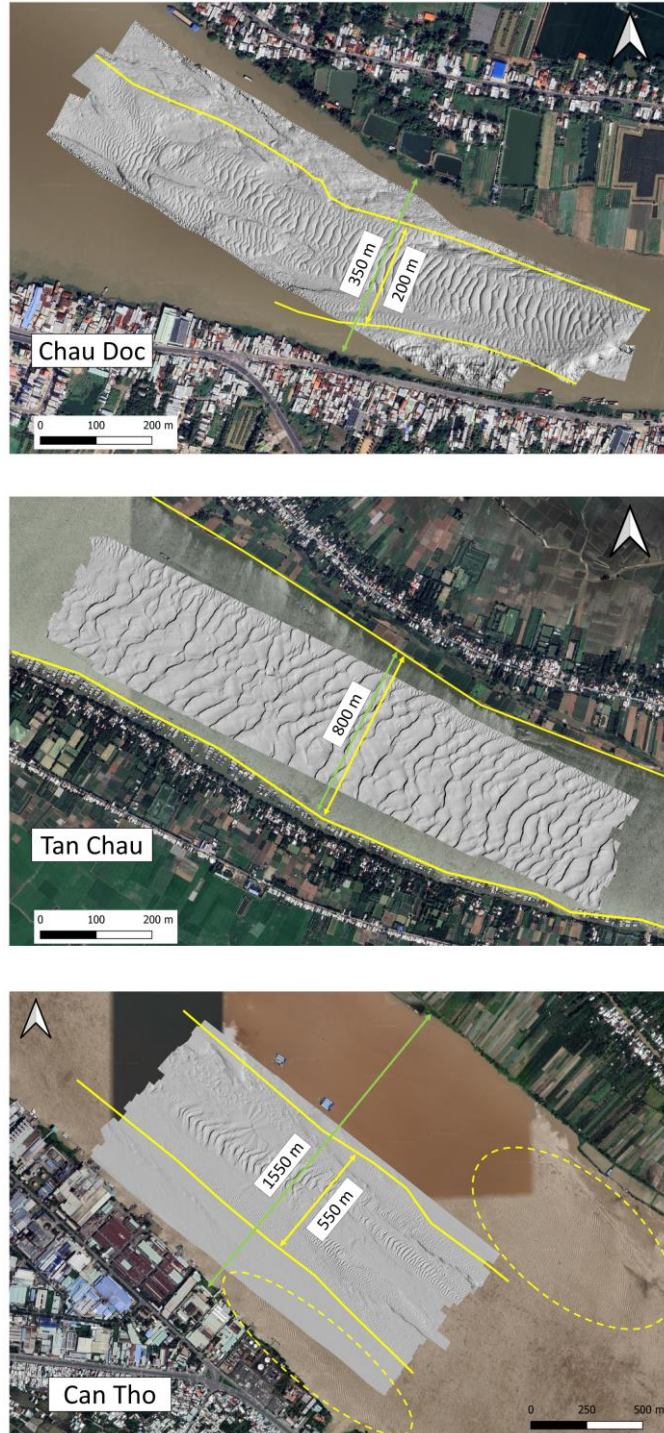


Figure 3-23: Three examples of the width of the section with sand versus the river cross-section.

Figure 3-23 shows examples of the lateral extent of bedforms in three sand rich sections relative to the river width, represented by a strong presence of sand dunes. In Tan Chau this is more than 90% of the river width, in Chau Doc ~75%, and in Can Tho ~35%. Looking at all

the observed cross sections, the 50-75% seems to be a reasonable estimation of river width sand coverage at locations where sand layers were identified.

3.2.5 Interpretation method

After the post-processing of the sub-bottom raw data to improve the signals, the next step was to perform the interpretation itself. This included the following steps:

- Load sub-bottom data into seismic interpretation software 'IXSea'.
- Automated riverbed detection (e.g., blue line in Figure 3-24).
- Load boreholes and grab samples to be displayed in the sub-bottom sections (e.g., see Figure 3-25).
- Perform a manual interpretation of the base of the top sand layer based on the continuation of the reflection at the base of that layer, validated with the sediment type information in the boreholes and grab samples.
- Cross check the interpretation with the cross section where available.

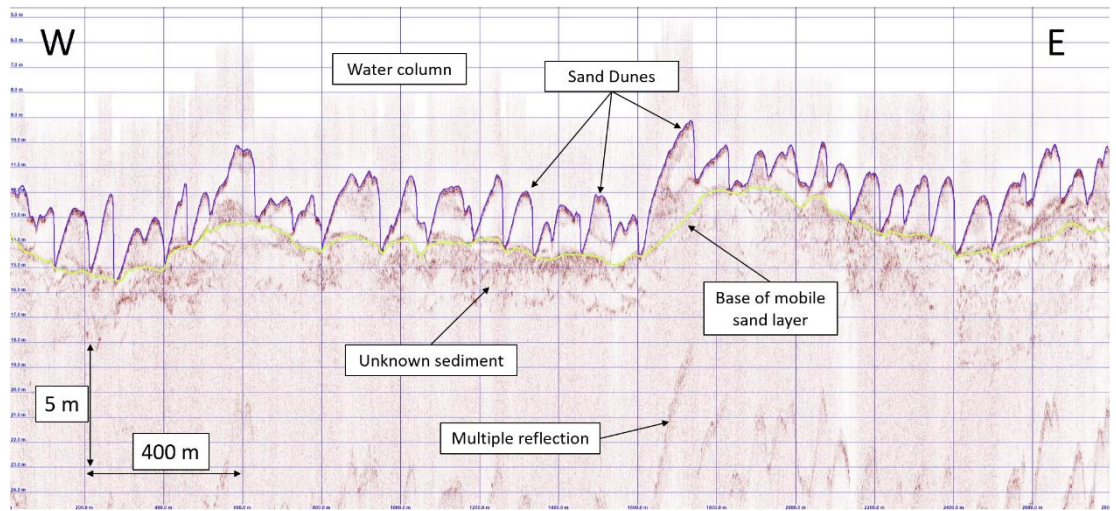


Figure 3-24: SBP section near Tan Chau. The sand dunes are clearly visible, and the base and thickness of the mobile sand layer is mapped. Below the base of the mobile layer there are sedimentary structures visible to which no sediment class can be assigned without any additional ground truthing (e.g., boreholes).

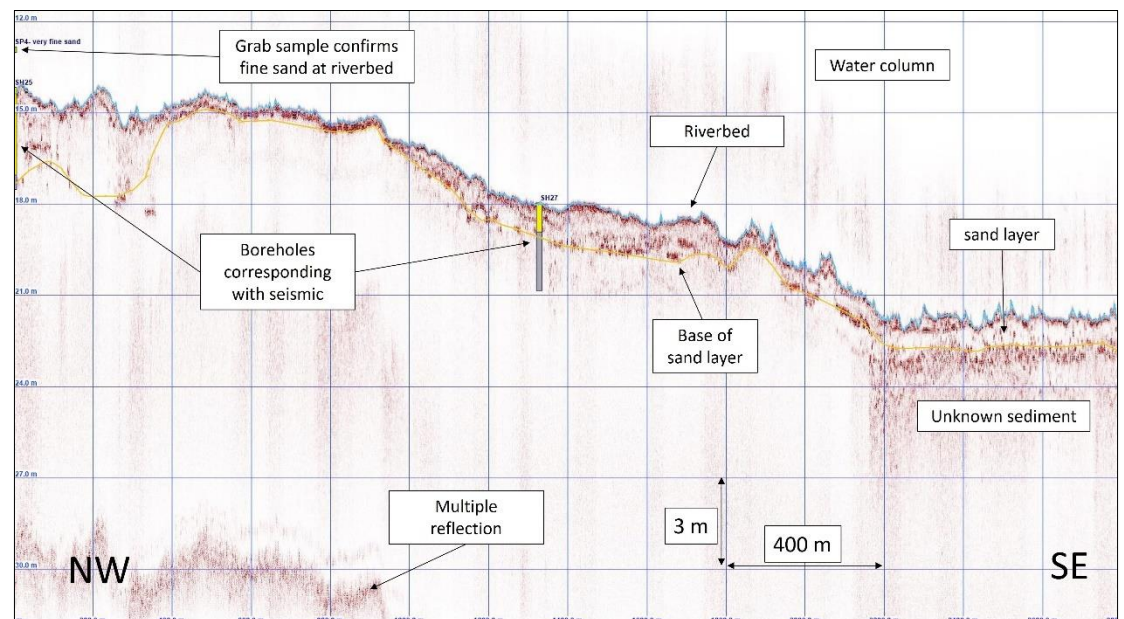


Figure 3-25: Example of a SBP with two boreholes (SH25 and SH27) and one grab sample (indicating fine sand) helping to outline the top sand layer even if there are no clear sand ripples or dunes present.

This interpretation provides the sediment thickness along the sub-bottom profiler lines. When this is combined with the estimates of the lateral extent of the sediment as described in the previous section, the existing mobile sand stock can be calculated.

3.2.6 Existing mobile sand stock calculation method

By multiplying the lateral extent by thickness of a sand layer, we can estimate the sand volume in each section along the river. For the lateral extent we use low and high estimates of 50% and 75% respectively as discussed in 3.2.4 and for the thickness the result of the interpretation method as described in 3.2.5.

Equation 3-1 below shows how the calculation of the sand volume was performed using layer thickness and bank-to-bank river width:

$$V = A * W \quad \text{with} \quad A = \int_0^L D_{base_sand}(x)dx - \int_0^L D_{river_bed}(x)dx \quad (\text{Equation 3-1})$$

where:

V: volume of sand in the analysed section [m³]

W: estimated lateral extent of the sand layer ('width'), taken as 75% of the total river width [m]

A: cross-sectional area of the dunes and or mega ripples along a section [m²]

L: length of the sub-bottom survey line [m]

X: distance along the sub-bottom survey line [m]

D: depth below the sub-bottom sensor, to the base of the sand layer and the riverbed respectively [m]

Here we have also included an example of signal interpretation in comparison to other available survey data. Figure 3-22 shows the surveyed line of the sub-bottom profiler campaign within a measured bathymetry (in this case near Tan Chau). The sub-bottom profiler only images what is vertically under the sensor (Figure 3-24). The bathymetry is indicative of how representative a single profile line is for characterization of the whole width of the river. In this example, most of the bathymetric surface is dominated by sand dunes of 1-3 m in height (Figure 3-22) which is also clearly visible in the SBP of Figure 3-24. The base of the "mobile sand layer" is also clearly visible and mapped to determine the thickness of the mobile sand layer (yellow line). Note that the *mobile sand layer* is the top active layer of sand from the riverbed to as deep as the lithology changes, that is most exposed to both extraction or morphological changes and movement. These data are then used to estimate the mobile sand stock along the stretch and eventually over the entire delta.

3.2.7 Results

The grab sediment samples show a trend of finer material downstream as was previously described by Gugliotta et al. (2017). The observed sand content within the collected samples was mostly categorized as fine to medium sand. Yet, some of the samples comprise of silt or clay, even in the upstream sections. Figure 3-20 gives an overview of the grab samples and their identified sediment classes. Figure 3-20 also shows the surveyed lines of the sub-bottom profiler campaign. Initially, the presence of sand was only validated by the presence of bedforms (sand ripples and dunes) and the grab samples in Figure 3-20. Eventually, the in-river boreholes (secondary data) as depicted in Figure 3-21 were made available to locally validate the presence and thickness of a sand top layer even when no clear bed forms were present. This results in an improved estimate of mobile sand stock in those areas. Figure 3-25 shows an example of how boreholes (and grab samples) were projected onto a sub-bottom profile to validate the interpretation.

The sub-bottom profiler only images what is vertically under the sensor. So, along the survey lines, the thickness (m) of the sand layer can be mapped by subtracting the depth to the base of the sand layer from the depth of the riverbed. This yields the 'raw' interpretation as presented

in Figure 3-26, in which the information from in-river boreholes and grab samples incorporated. Using (Equation 3-1), the mobile sand stock was then calculated per meter of river. The results were summed over 3-kilometre-long sections to give an optimal overview of the distribution of sand along the river. This resulted in the lower estimate (Figure 3-27) and upper estimate (Figure 3-28) images of the mobile sand stock, where the lateral extent of the sand layer spanning 50% and 75% of the river width, were used respectively. At river sections where no mobile sand stock is shown in the map, no sand layer was observed during the interpretation. From the figures, we can observe that the upper Tien and the Co Chien river have the highest existing mobile sand stock, followed by Basac River. Existing mobile sand stocks are significantly lower in the lower Mekong and the Ham Luong River.

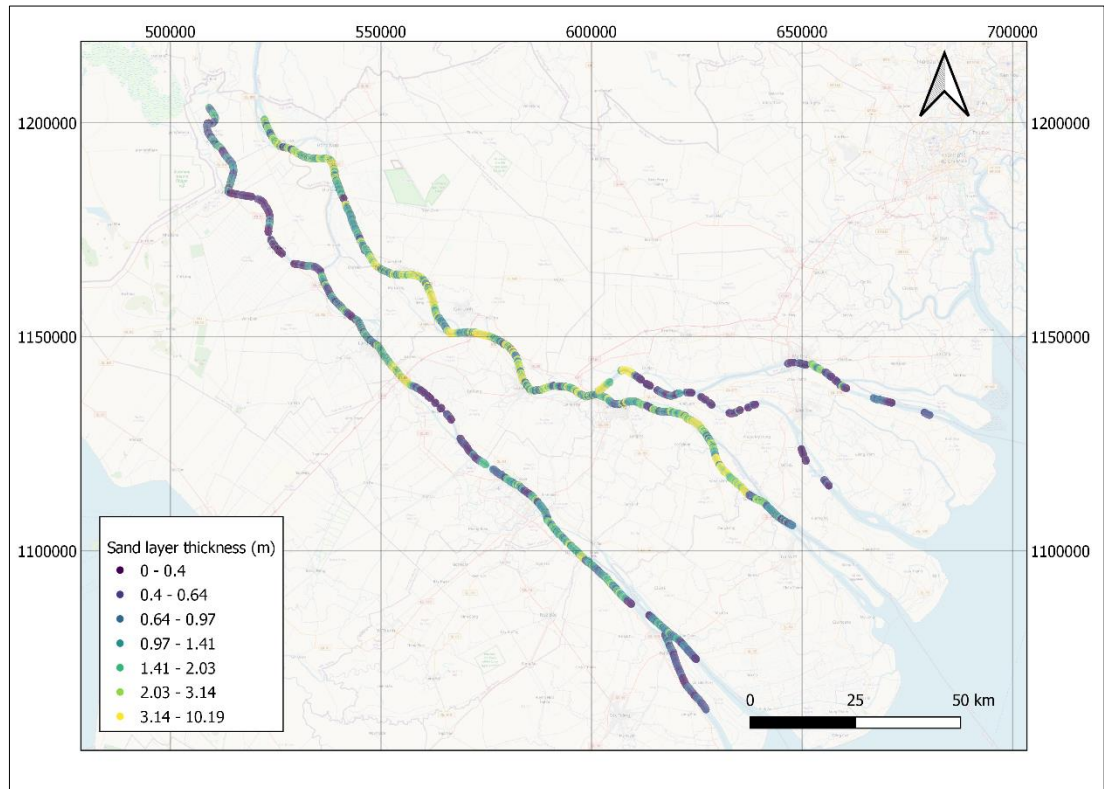


Figure 3-26: Thickness of the top (existing mobile) sand layer along every 1 m of the Mekong River. At river sections where no thickness is shown in the map, no sand layer was observed.

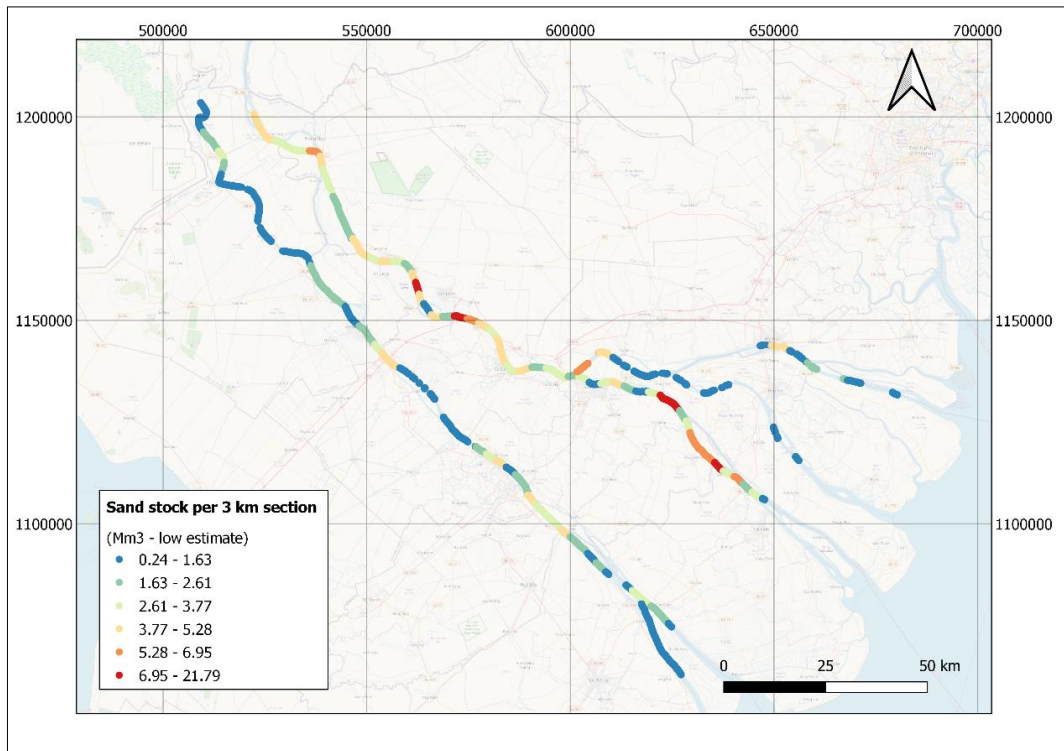


Figure 3-27: Lower estimate of the existing mobile sand stock along sections of 3 kilometres. These are calculated with Equation 3-1, using the sand thickness from and assuming a lateral extent of the sand layer spanning 50% of the river width.

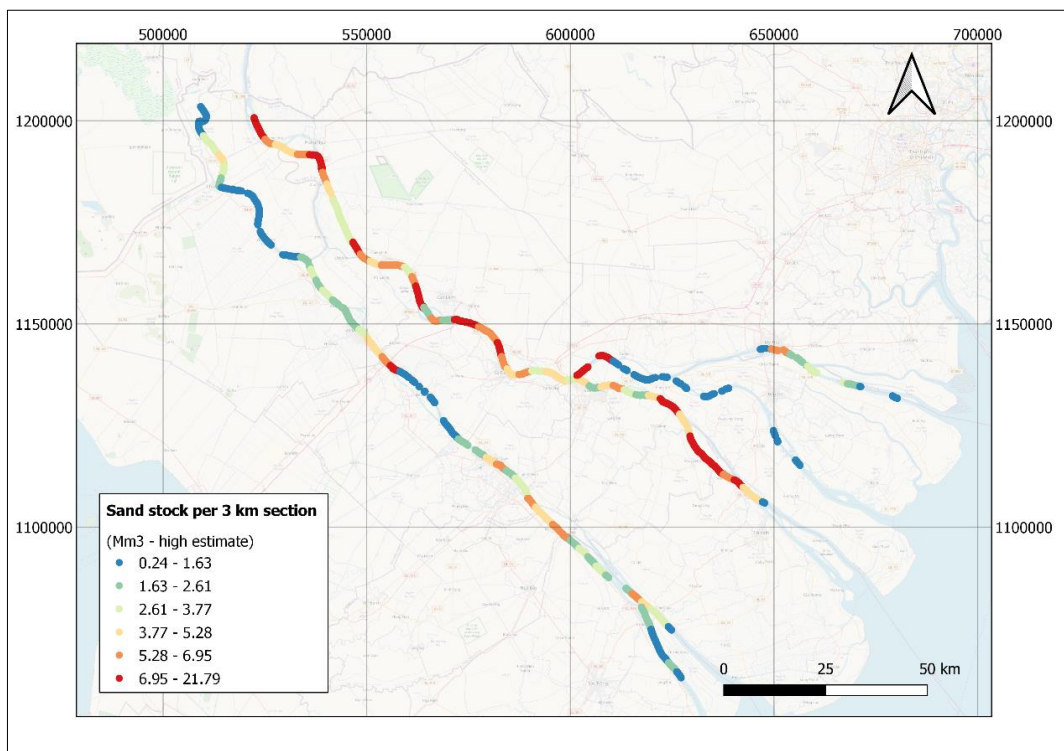


Figure 3-28: Upper estimate of the existing mobile sand stock along sections of 3 kilometres. These are calculated with Equation 3-1, using the sand thickness and assuming a lateral extent of the sand layer spanning 75% of the river width.

3.2.8 Total existing mobile sand stock

In the maps presented in the previous section (Figure 3-27 and Figure 3-28), lower and upper estimates of the existing mobile sand stock, summed over sections of 3 km, were presented to give an overview of the distribution of sand along the Mekong River. Similarly, by summing over the total length of the river, the total existing mobile sand stock in the Mekong River was calculated. Table 3-9 gives the total existing mobile sand stock estimates. For the lower estimate it was assumed that, where sand is interpreted on the sub-bottom profiles, it is laterally present along 50% of the local width of the river. For the upper estimate, 75% of the local width of the river was used. The existing mobile sand stock estimates based on the sub-bottom interpretation are conservative. These estimates could be improved by including more (when available) in-river borehole data in the future. Where no, or sparse borehole data is available, the estimates are less confidently determined. This means that it is possible that underneath the mobile sand layer, there is more sand available. Buried sedimentary structures locally do indicate potential presence of sand in deeper layers, but this cannot be verified in the scope of this study.

Table 3-9: Lower and upper estimates of total existing mobile sand stock for the Mekong River

Description	Total Existing Mobile Sand Stock (Mm ³)
Lower estimate	367.7
Upper estimate	551.5

3.2.9 Discussion

This is the first estimation of the sand budget at the scale of the Mekong Delta. During the stakeholder engagement meetings there have been different impressions of the existing mobile sand stock. Some consider this is an overestimation. However, we believe this estimation is perhaps on the conservative side as it is mainly focused on the mobile sand layer, so likely overlooking lower sand layers especially in the upper delta where there was no borehole data. Furthermore, sand buried in mud does not easily show itself in this data and can only be identified once accurate ground truthing is carried out. Comparison to existing other estimates at the provincial level is very difficult at this stage. Any comparison needs to address questions such as, what the survey coverages are? Or how the data is interpreted? Or was it for the entire province or only for the existing mines? This type of comparison ultimately comes down to experts discussing the analyses in detail to come to a fair comparison.

3.3 Sand extraction estimates

In this section a state-of-the-art method is introduced and applied to estimate the extracted sand volume for the Mekong Delta based on remote sensing data. First, the background provides a brief overview of the available data and literature regarding this subject (Section 3.3.1). Thereafter, the state-of-the-art method applied in this study is described (Section 3.3.2) and the results obtained using this method are presented (Section 3.3.3). Finally, the discussion lists limitations of the current methodology and provides potential further developments (Section 3.3.4).

3.3.1 Background

This section gives a brief overview of the available satellite imagery datasets and the available literature on state-of-the-art methods to estimate extracted sand volumes for the Mekong Delta.

Available satellite imagery datasets

For this study, several satellite imagery datasets with medium-resolution, high spatial and temporal coverage that are readily available are considered. An overview of these satellite imagery datasets is given in Table 3-10. This overview also shows in which studies these datasets have been applied.

Table 3-10: Overview of satellite imagery datasets

Dataset	Type	Spatial resolution & extent	Temporal resolution & extent	Data availability	Applied in study
Sentinel-1	SAR	10 m (Global extent)	12 days (2014 – 2022)	Free access	(Gruel, et al., 2022)
Sentinel-2	Optical	10 m (Global extent)	5 days (2015 – Now)	Free access	This study
Landsat-1	Optical	60 m (Global extent)	18 days (1972 – 1978)	Free access	-
Landsat-2	Optical	60 m (Global extent)	18 days (1975 – 1982)	Free access	-
Landsat-3	Optical	60 m (Global extent)	18 days (1978 – 1983)	Free access	-
Landsat-4	Optical	30 m (Global extent)	16 days (1982 – 1993)	Free access	-
Landsat-5	Optical	30 m (Global extent)	16 days (1984 – 2013)	Free access	-
Landsat-7	Optical	30 m (Global extent)	16 days (1999 – 2022*)	Free access	-
Landsat-8	Optical	30 m (Global extent)	16 days (2013 – Now)	Free access	(Gruel, et al., 2022)
Landsat-9	Optical	30 m (Global extent)	8 days (2021 – Now)	Free access	-
ICEYE	SAR	0.5 m – 3 m (Local extent)	Daily (2018 – Now**)	On-demand	-
PlanetScope	Optical	3 m – 5 m (Global extent)	Sub-daily (2016 – Now)	On-demand	(Hackney, et al., 2021)

* Scan Line corrector (SLC) failure occurred in 2003.
** Full temporal extent is not saved.

The satellite datasets can be classified into two types: optical (multispectral) images and Synthetic-Aperture Radar (SAR) images. Optical (multispectral) detection, which relies on the reflectivity of solar radiation, can be used to provide images during the day and when the sky is clear. Alternatively, SAR detection can be used to obtain images independent of the time of day and weather conditions. SAR can therefore be used during the night and the monsoon season. Moreover, smaller vessels can be detected compared to optical detection. However, due to the limited spectral information, the classification of vessel type is harder, the presence of speckle noise can result in more false positives, and the spread of the backscattering results in a larger uncertainty on the area of the vessels.

Methods to estimate the extracted sand volumes in the Mekong Delta applied in literature.

Hackney et al. (2021) and Gruel et al. (2022) have applied remote sensing methods to estimate the extracted sand volume in the Vietnam Mekong Delta. These methods mainly differ in their approach to converting the number of vessels to an extracted sand volume estimate.

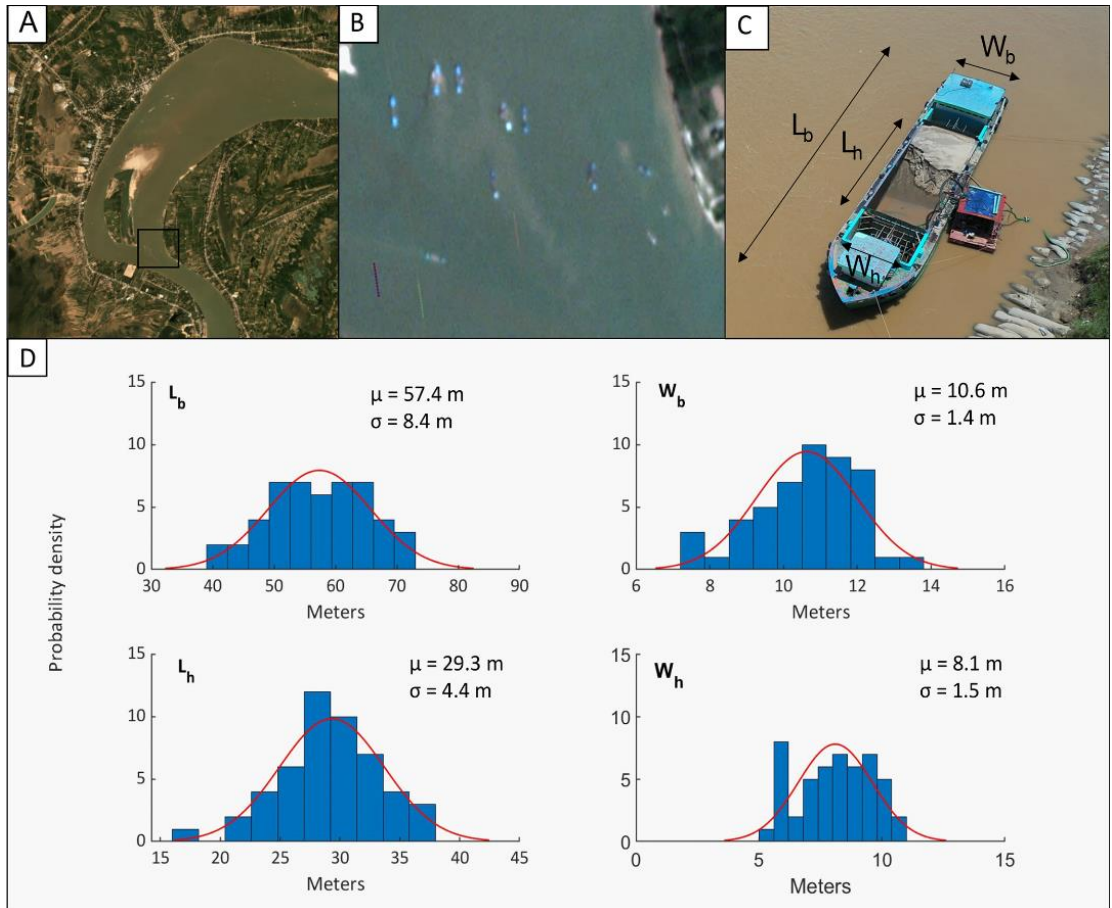


Figure 3-29: A: PlanetScope image of Area of Interest, B: Zoomed in on A, C: definition of vessel dimensions, D: Vessel dimensions as found by Hackney et al., (2021).

The first method is based on the vessel dimensions, following Hackney et al., (2021) as presented in Figure 3-29. The blobs extracted from satellite imagery were filtered to have a width between 6 and 15 m and a length between 30 and 80 m. As all vessels have an elongated shape, a form factor of height larger than 3.5 times width was used to filter the vessels, and all blobs closer than 100 m to the river shore were discarded. This ensures all inactive vessels are filtered away, even when perpendicular to the shore. As the sand is stored in the holds of the vessels, the percentage of vessel area containing sand was calculated to be 39% by dividing the average hold area over the average vessel area derived from the dimensions listed in Figure 3-29. To convert the area into volume the average vessel height of 7 m was used. Every vessel is assumed to be filled with sand once every day. Moreover, the number of vessels for a specific day is assumed to remain constant till the next satellite image is available (Hackney et al., 2021). This method does not account for grouped boats (*i.e.*, boats anchored or fastened close to each other) as these are filtered away because the dimensions of the grouped boats exceed the dimensions used in the filter conditions.

The second method classifies the vessels in 3 groups based on the dimensions in Gruel et al., (2022):

- Barges with cranes: Length: 30-44 m; Area: 352-548 m²
- Barges for transport: Length: 44-50 m; Area: 505-611 m²
- Blue boats: Length: 39-55 m; Area: 288-464 m²

After filtering the vessels in multiple groups, Gruel et al., (2022) calculates the volume of sand estimating that barges with cranes is assumed to be a third of the full area. Employing the postprocessing techniques proposed by Gruel et al. (2022) and Hackney et al. (2021) proved challenging for several reasons. First, the correlation between the quantity of vessels detected and sand extraction might not extrapolate well to other areas due to heterogeneous activities

in different locations, and we currently have insufficient information to verify this hypothesis. Secondly, multi-temporal high resolution optical imagery is not available at the spatial cover and temporal resolution required for the entire VMD during the years of interest. Nevertheless, motivated by these two works, we followed an alternative method based on the re-analysis of Sentinel-2 imagery and the detection of active barges with cranes. In the following section we describe the assumptions and findings related the remote-sensing derived estimation of sand mining activities within the VMD.

3.3.2 Methodology

The methodology applied in this study consists of three steps: 1) the detection of active barges with cranes based on satellite images and 2) the conversion of the number of dredging vessels to an extracted sand volume estimate. These steps have been implemented in the Google Earth Engine framework. Google Earth Engine integrates planetary-scale analysis capabilities with a large collection of geospatial datasets and satellite imagery (Gorelick et al., 2017). The area of interest (VMD) is divided into tiles that cover the main rivers and estuarine distributary channels of the VMD. In this analysis, annual extracted sand volumes are estimated between 2017-01-01 and 2023-01-01. Figure 3-29 conceptualizes the steps taken to estimate sand extraction estimates based on Sentinel-2 satellite images.

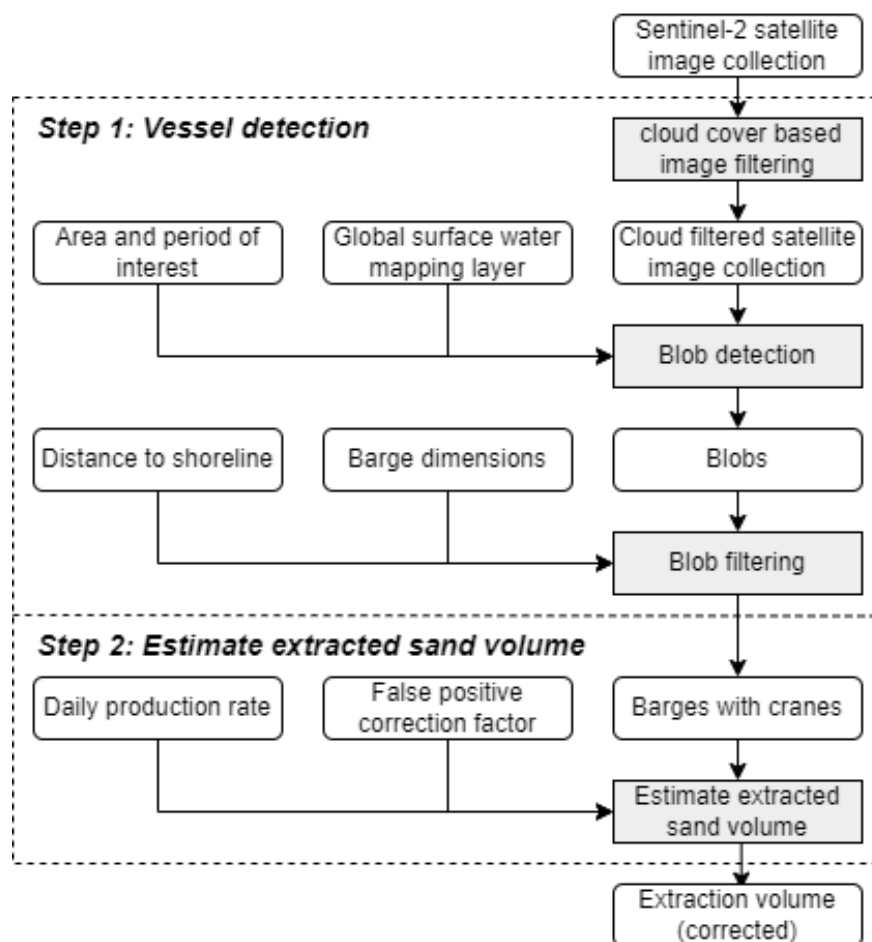


Figure 3-29: Methodology to estimate the sand extraction volume.

Vessel detection: The Sentinel-2 (optical) optical image dataset was selected based on its availability. Ideally, the PlanetScope dataset would have been used in this study, as was done by (Hackney et al., 2021) with higher spatial and temporal resolution. However, this dataset is a private resource, available only after purchasing, which was deemed unfeasible for this project at the required scale. To detect vessels from the Sentinel-2 (optical) images, first the location of the river was determined using the JRC Global Surface Water Mapping Layers (Pekel, Cottam, Gorelick, 2017). The Normalized Difference Water Index (NDWI) is calculated

in the river area, and an adaptative thresholding algorithm is used to segment the water background from non-water elements within the river (similar to Donchyts et al., 2016). These unfiltered blobs contain vessels, patches of land and other false positives (small cloud/shadow elements that pass the thresholding filter).

We focused on the detection of active barges with cranes, to estimate the presence of sand-mining activities. Upon inspection of high-resolution satellite products, we could see that most of the time active barges with cranes have vessels associated in which they are discharging. This results in blobs that are larger than an individual vessel with dimensions ranging 50-80 m long, 20-40 m width and footprint area around 1000-1600 m² (see Figure 3-30)

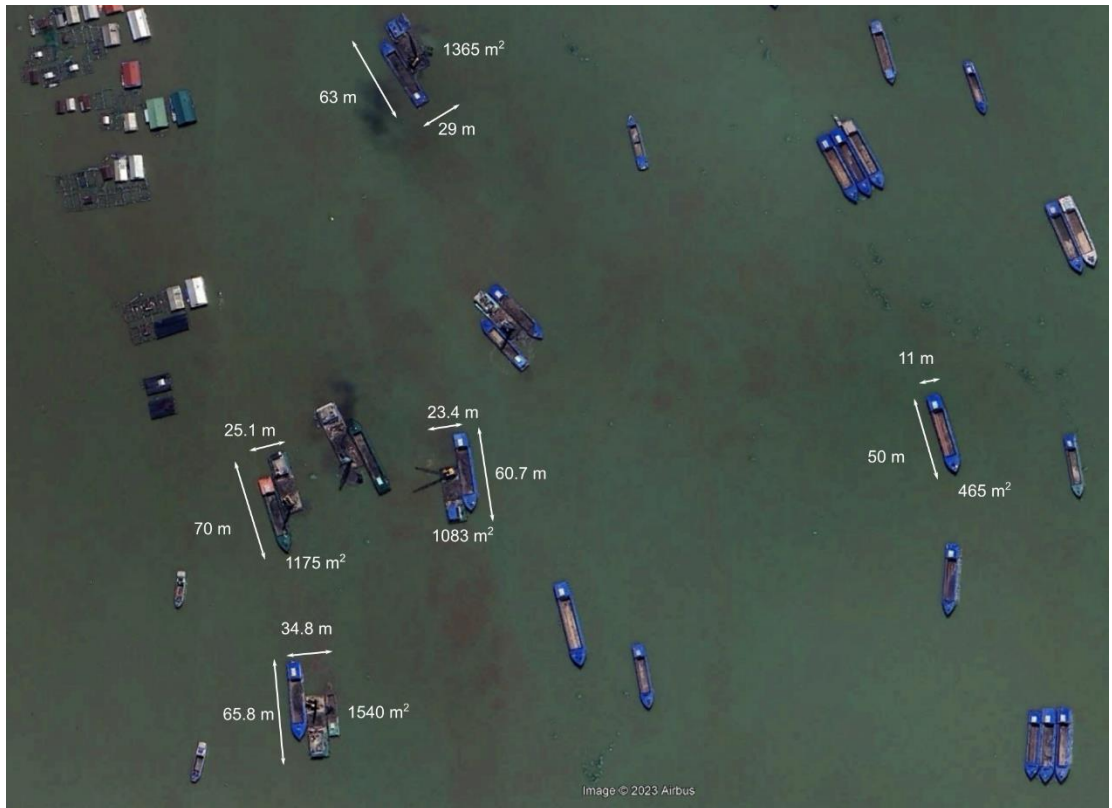


Figure 3-30: Scheme of active dredging barge geometries and sizes from high-resolution imagery (Google earth basemap, Airbus, 2023)

Using these geometrical considerations, we filtered elements that would comply with these dimensions and that are further than 100 m from the shoreline. Following the approach by Hackney et al. (2021), the number of active barges with cranes for a specific day is assumed to remain constant till the next satellite image is available. Figure 3-31 shows the filtered barges with cranes active blobs (in orange) from the yearly detected blobs in a section of the Mekong for 2021 based on the previously described filtering criteria.



Figure 3-31: Blobs detected as potential vessels (brown blobs) and filtered barges with cranes (orange blobs) for a section of the Mekong during 2021.

Estimate extracted sand volume: After classifying the dredging barges, estimate of sand extraction volumes is done by assuming active days (a dredger is assumed to be active in the detected location until the next available image). Then, by assigning an extraction rate (production rate) to one single vessel (see next paragraph), the extraction rate for the total number of vessels per day is estimated. Note that in our estimates, we assumed zero production during the Vietnam lunar new year holidays (Tet).

Estimating the production rate: To estimate the production rate for the typical grab dredgers (barges with crane) active in the VMD, we used the production charts of Central Dredging Association (2023). This chart incorporates the grab volume (typically 2.5-3 m³ in VMD) and hoisting time (30-45 seconds based on observations) to arrive at an hourly production estimate. Note that the chart is based on 10 m³ grab volume. This means the hourly estimate needs to be adjusted linearly for the smaller grab sizes of 2.5-3 m³ in VMD. This results in a production range of 967 to 1530 m³/day. The assumptions on hoisting time and grab volume are based on the secondary information from the provincial authorities and in-field observations.

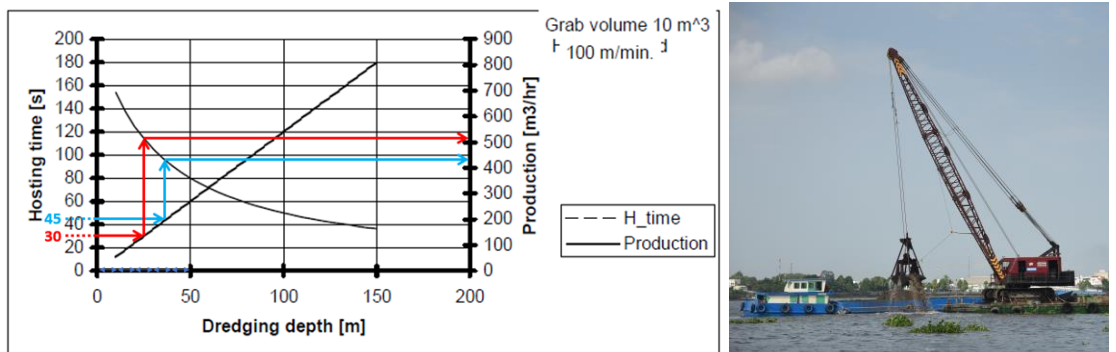


Figure 3-32: Production chart of a 10 m³ grab dredgers based on hoisting time and dredging depth (Central Dredging Association, 2023).

Correction for cloud coverage: A cloud filtering routine (described in Donchyts et al. 2022) was applied to filter the sentinel 2 imagery. This method filters images with clouds based on local statistics of cloud cover and on the distribution of brightness across time in the image. This ensures that tiled images contain mostly cloudless conditions. Vessels are detected within these images, and following Hackney et al. (2021), the number of daily active sand mining vessels is assumed constant until a new image is available.

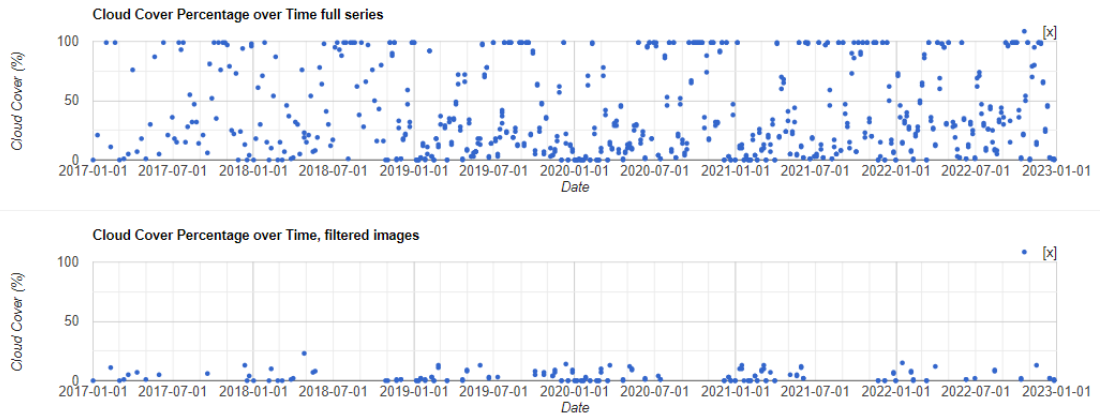


Figure 3-33: Percentage of cloud cover in a tile area next to Vinh Long (2017-2022), for (above) the full Sentinel 2 series, and (below) the filtered cloudless conditions.

Finally, Table 3-11 provides an overview of the differences between the methodology applied in this study, versus Hackney et al. (2021) and Gruel et al. (2022).

Table 3-11: Overview of the difference between the methodology applied in this study, Hackney et al. (2021) and Gruel et al. (2022).

Steps of methodology	This study	Hackney et al. (2021)	Gruel et al. (2022)
Detection of vessels based on satellite images	Detection based on Sentinel-2 (Optical) and dimensions of barges with cranes.	Detection based on PlanetScope (Optical) and dimensions of sand mining vessels.	Detection based on Sentinel-1 (SAR) & Landsat-8 (Optical) and dimensions of 3 types of barges.
Conversion of the number of vessels to an extracted sand volume estimate	Conversion based on extraction rate of barges with cranes.	Conversions based on volume (carrying capacity) of sand mining vessels.	Conversions based on volume of barges for transport and blue boats.

3.3.3 Results

This section contains the results obtained using the methodology described in the previous section. The annual sand extraction volumes between 2017-01-01 and 2023-01-01. Figure 3-34 shows filtered blobs (as dark polygons) in 2022 for a section of the Mekong River. The figure showcases the local distribution of potentially active barges during the full year.

Figure 3-35 shows the annual number of active barges with cranes (*i.e.*, after filtering) detected between 2017-01-01 and 2023-01-01 in the VMD. The number of detected vessels decreases annually between April and September, reaching a minimum around September. This annual decrease is most likely related to the increased cloud coverage or decrease of activity due to high-river discharge, hence less workability. The heatmaps of the detected barges with cranes for looking at the spatial resolution of the vessels is presented in Appendix-B.

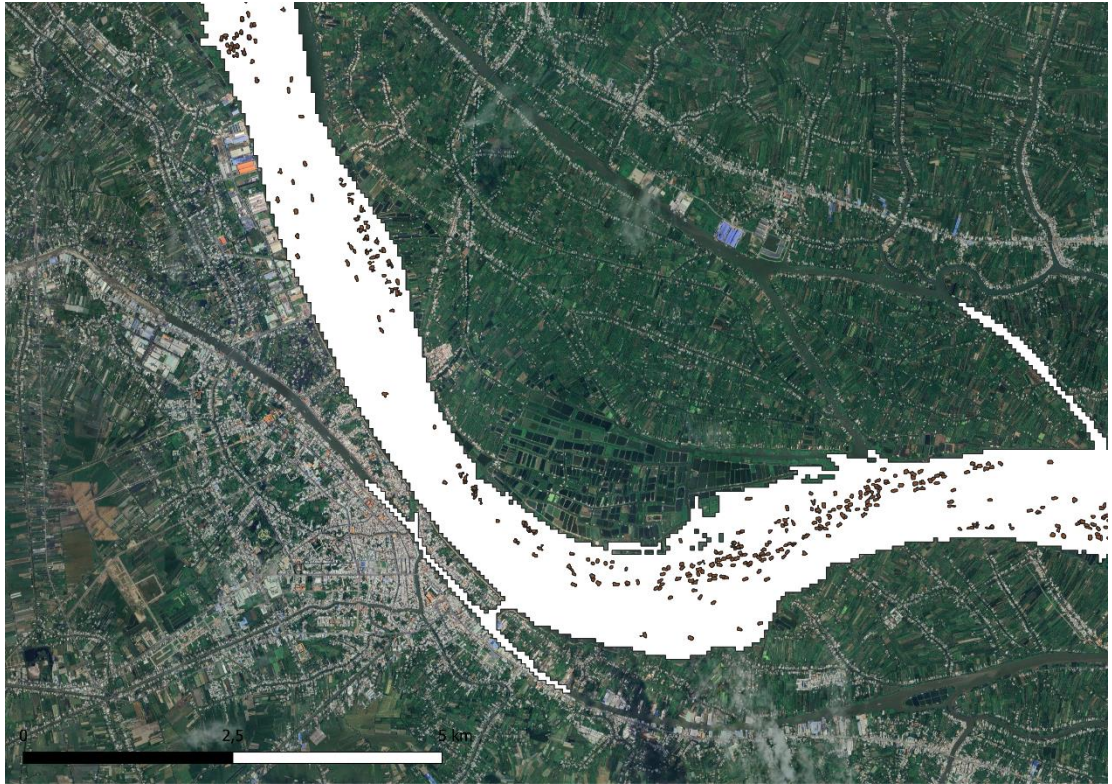


Figure 3-34: Filtered barges with vessels (blobs) detected between 2022-01-01 and 2022-12-31 for a section of the Mekong River.

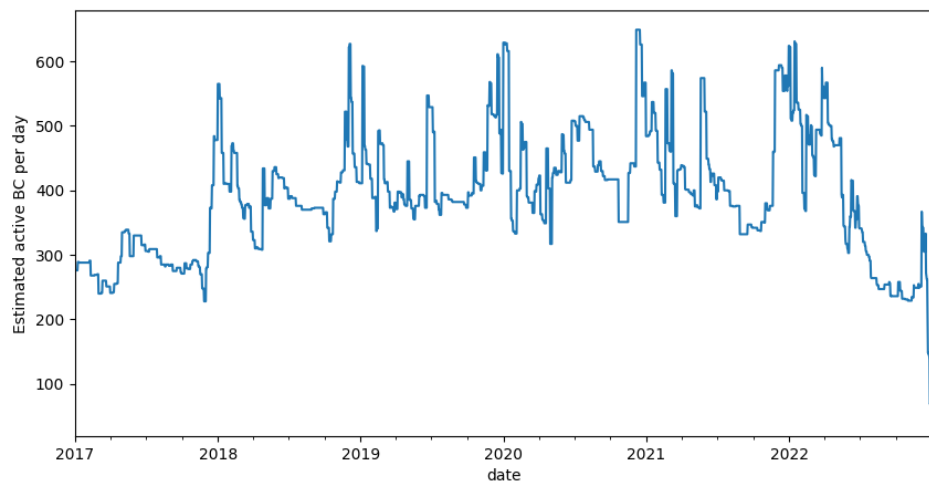


Figure 3-35: Number of active barges with cranes (BC) detected between 2017-01-01 and 2023-01-01 in the Vietnam Mekong Delta (daily sum of all tiles)..



Figure 3-36, Manually classified active barges with cranes vs. double moored transport vessels (which show the same geometrical characteristics in S2 imagery), zone-example.

Additionally, the detection of active dredgers relies on geometrical aspects. Given the limited resolution of Sentinel-2 imagery (10 m), it is challenging to differentiate between barges and cranes with loading vessels attached and multiple vessels moored together. Thus, the filtered active vessels are likely containing false positives, which can't be ascertained from Sentinel 2 imagery alone. Based on the observed vessels, documented during the SBP campaign over 550 km, we estimated a correction factor of 26%. By manual comparison of the satellite images in early April of 2022 by those observed vessels, we identified various sources of false positive such as, fish farms, areas with high vessel density, and shadows of the clouds in the images (e.g., see an example in Figure 3-36). A correction factor of daily active dredging vessels of 0.26 was therefore applied to mitigate the number of misclassifications.

Estimate extracted sand volume

Figure 3-36 shows the annual extracted sand volumes estimated between 2017 and 2022 within the VMD. Due to uncertainties and limitations in the available data and analyses, we introduce an annual extraction rate based on the potential production rate of the dredging barges (967 to 1500 m³/day). This figures, for 2017 to 2022 are in the same range of estimated volumes by Gruel et al. (2022). The sand volumes determined in this study seem to comply with those determined by Gruel. The annual volumes seem to change over time. However, due to the uncertainty it is not possible to distinguish a trend based on these results.

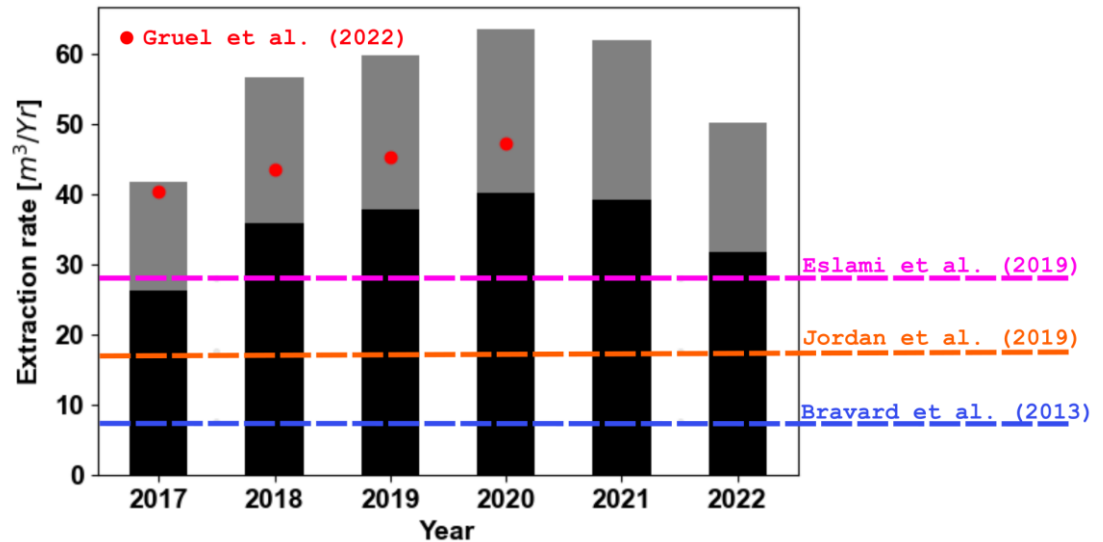


Figure 3-37: Annual extracted sand volume estimated in this study between 2017 and 2023-01-01 in black (min) and grey (max) bar charts compared to those determined by other studies previously.

3.3.4 Discussions

The estimated annual sand extraction volumes between 2017 and 2021 were in the range of 35 to 55 M m³/year, which agrees with findings of Gruel et al. (2022) who estimated the extraction to be around 40-45 M m³/yr. This exceeds Eslami et al., (2019b) of 28 M m³/yr based on the sand mining licenses. Estimating sand extraction volumes from satellite imagery is NOT without limitations. The low spatial resolution (10 m) of open-access Sentinel-2 satellite images, makes it difficult to detect boats with lengths in the order of several pixels (e.g., 30 to 44 m) and to differentiate between vessel types. For example, this makes it difficult to detect small boats with a dredging pump. This is one source of error in vessel detection that will surely affect this estimate. Moreover, in the scope of this study, we need to rely on simplified filter methods for vessel classification. More advanced methods that consider spectral indices or trained pattern recognition algorithms (deep learning-based object detection) could enhance vessel classification, although it is arguable that the relatively low-resolution of Sentinel 2 will still pose a significant challenge to supervised classification algorithms.

In a follow up of this early step forward, improving the estimates of sand mining activities will likely require higher resolution data sources (e.g., ICEYE, Planet, Pleiades or Maxar), although acquisition of these products at the required scale (the entire VMD for multi-year timeframes) is still a challenge both in terms of completeness of historical records and cost of purchase of the imagery. On the other hand, it would be interesting to explore SAR images (e.g., ICEYE / Sentinel 1) to detect vessels, as suggested by Gruel et al. (2022). The advantage of using SAR is that it can be used during night and the monsoon season (cloudy or overcast). Nevertheless, the Sentinel 1 resolution (10 m, SAR reflectivity) is insufficient to discriminate between type of vessels, whereas ICEYE might be capable to do it due to a higher resolution (0.5 – 3 m), yet this remains to be explored in the follow up studies.

4 Sand transport modelling (WP2)

4.1 Introduction

4.1.1 Area description and flow dynamics

The Vietnamese Mekong Delta (VMD) is vital to the livelihoods and food security of local people. The region has about 17 million inhabitants (Van et al., 2012). In particular, the Mekong VMD is considered as the “rice bowl” of Southeast Asia. The VMD covers an area of 39,700 km², and 60% of which is dedicated to agriculture (Van et al., 2012). Abundant supply of water and the rich soil of the delta (similar to other delta’s worldwide) feeds agriculture in the large scale. The Mekong River supplies 340-450 km³ of water annually (Eslami et al., 2021a) and supplied 40-80 Mt sediments to its delta (MRC, 2005; Koehnken, 2014; Thanh et al., 2020). Recent studies (Kummu and Varis, 2007; Manh et al., 2014; Lu et al., 2014; Darby et al., 2016) have shown that fluvial sediment to the delta has significantly declined over the past two decades. This has largely to do with the development of mainstream hydropower dams upstream, and its impact on the fine sediment supply (silt and clay) to the delta. The dams not only trap sediment, but also impact the hydrology of the Mekong River. (Lauri et al., 2012) showed that these reservoirs can increase Kratie flows by 25-160% during low-flow seasons and reduce flows by 24 % during high-flow seasons. Annual flooding is the main source of freshwater for the VMD, while sediments supplied serve as natural and valuable sources of fertilizers for agricultural production (Chapman and Darby, 2016). However, due to climate change, and significant human intervention, VMD faces challenges relating to both freshwater and fluvial sediment supply, hence its overall livelihood. This chapter addresses the movement of sand (as a portion of sediment) incoming to the delta, distributing within the delta and leaving the delta as part of the comprehensive sand budget of the VMD.

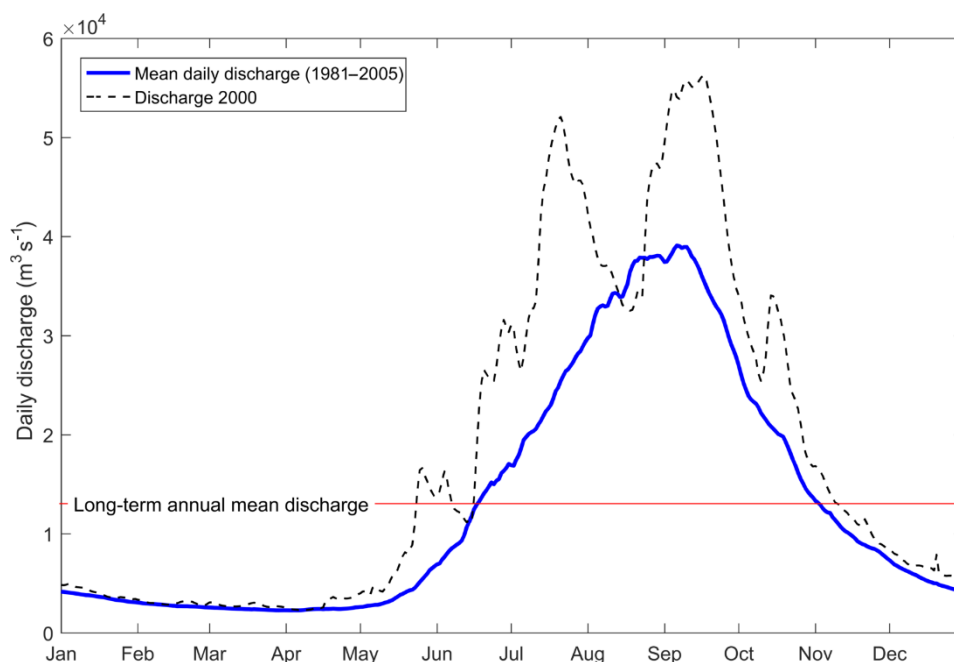


Figure 4-1: Temporal variation of daily water discharge at Kratie (data from Darby et al., 2016).

The Mekong Delta may be spatially separated into inner and outer sections. The former is dominated by fluvial processes, whereas the latter is dominated by marine processes, including tides, waves and surges (Ta et al., 2002; Eslami et al., 2019a). The VMD is characterized by its monsoon-driven seasonality. Figure 4-1 shows that water discharge varies from 1700 to 40 000 m³ s⁻¹ between the low-flow and high-flow seasons (Frappart et al., 2006; Le et al., 2007; MRC, 2009; Wolanski et al., 1996). During the high-flow season, high discharge and

river stage floods the floodplains of Cambodia and Vietnam and carries large amount of sediment and debris. During the low flow season, tidal dynamics dominate the delta, estuarine channels are impacted by larger amounts of mud and salinity intrudes up estuaries as much as ~50 km (Eslami et al., 2019a, 2021a). Figure 4-1 and Figure 4-2 show the yearly discharge variation and discharge variations over the years at Kratie, Cambodia.

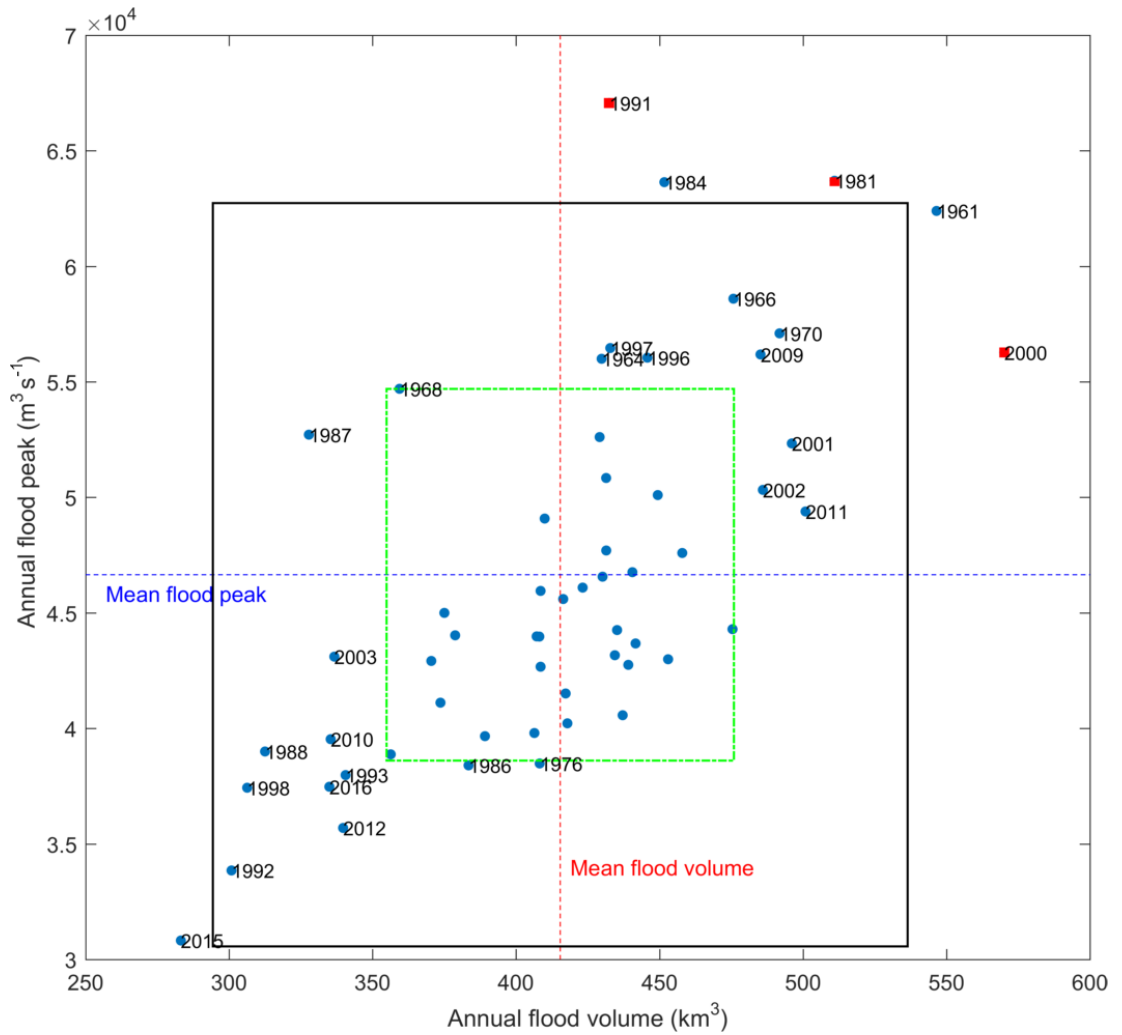


Figure 4-2: The annual flood peaks and volumes at Kratie from 1961 to 2022. The green and black boxes indicate significant ($\text{mean} \pm \text{SD}$) and extreme ($\text{mean} \pm 2 \text{SD}$) drought or flood years respectively (SD refers to standard deviation).

4.1.2 Hydrodynamic modelling

A number of modelling studies has been carried out in order to understand hydrodynamics and sediment transport in the Mekong Delta. For modelling at the scale of the whole delta, Wassmann et al., (2004) conducted a study to assess impacts of sea level rise on rice production by using a 1D numerical model (VRSAP). Results show that inundation in the VMD would shift significantly landward due to projected sea level rise. It can be concluded that the tide plays a significant role in the flood drainage in the VMD. A similar inundation pattern was found by (Van et al., 2012). They also applied a 1D hydrodynamic model (ISIS) which was used by the MRC (Mekong River Commission) to study changes of flood characteristics under upstream development and sea level rise. As a result, flooding caused by tides would be stronger under sea level rise and may lead to changes in sediment convergence near the river mouths. (Eslami et al., 2019a) studied the role of tidal dynamics on flow division in the estuarine channels and quantified the importance of the secondary channels to the tidal dynamics of the delta. That study concluded that although the network of primary and secondary channels contributes to not more than 1-2% of the total tidal prism, it has a nearly 10% effect on the tidal amplitudes, *i.e.*, without them, it is very difficult to capture both vertical (water level) and horizontal (discharge) tidal dynamics. (Manh et al., 2014) estimated the spatial sediment

distribution in the Mekong Delta by using a MIKE11 model to simulate rivers (1D) and floodplains (quasi-2D). The study indicated that more than half (53%) of the sediment is transported to the VMD's coastal areas (via the Can Tho and My Thuan). Xing et al., (2017) investigated sand dynamics of the Song Hau branch and morphological changes. Their model suggests that the ratio between seaward and landward velocity will increase, and morphology would be highly affected in the context of relative sea level rise and delta plain subsidence. (Thanh, 2021) was able to derive a sediment budget of the Vietnamese Mekong Delta based on fine cohesive, sediments using a Delft3D FM model in 2DH mode validated against measured water levels, flow discharges and suspended sediment concentrations. Fine sediments cover the majority of sediment delivered yearly by the Mekong River. The current project applies the model by (Thanh, 2021) and adds the transport of coarser sand fractions.

4.1.3 Observation based sediment properties.

Figure 4-3 and Figure 4-4 present rare measurements of sediment size distribution in suspended sediments and bed load available along the Mekong River for 2018 and 2019 at Kratie, Prek Kdam, Chau Doc and Tan Chau (MRCS, personal communication). For the sediment classification the Wentworth scale is used, see Table 4-1. This shows that:

- Bedload at Kratie (2019) consists mainly of medium to fine sand.
- Suspended load at Kratie and Prek Kdam (2019) is mainly coarse silt (~80%) with limited fine sand (~10%).
- Suspension load at Tan Chau and Chau Doc (2018-2019) is mainly fine/coarse silt (~90%) while fine sand SSC is a little bit higher (up to 10%) in 2018.

The current study focusses on sand transport. These data suggest that sand transport remains small compared to the transport of fines (silt and clay), and that fine sand dominates both bed load and suspended load.

Table 4-1: Sediment classification (Wentworth scale)

Gravel	Pebbels	>5mm
	Fine Pebbles	5-2mm
sand	V. Coarse	2-1mm
	Coarse	1-0.5mm
	Medium	0.5-0.25mm
	Fine	0.25-0.125mm
	V. Fine	0.125-0.063mm
Silt	Coarse/Med	0.063-0.020mm
	Fine/ V. Fine	0.020-0.002mm
Clay		<0.002mm

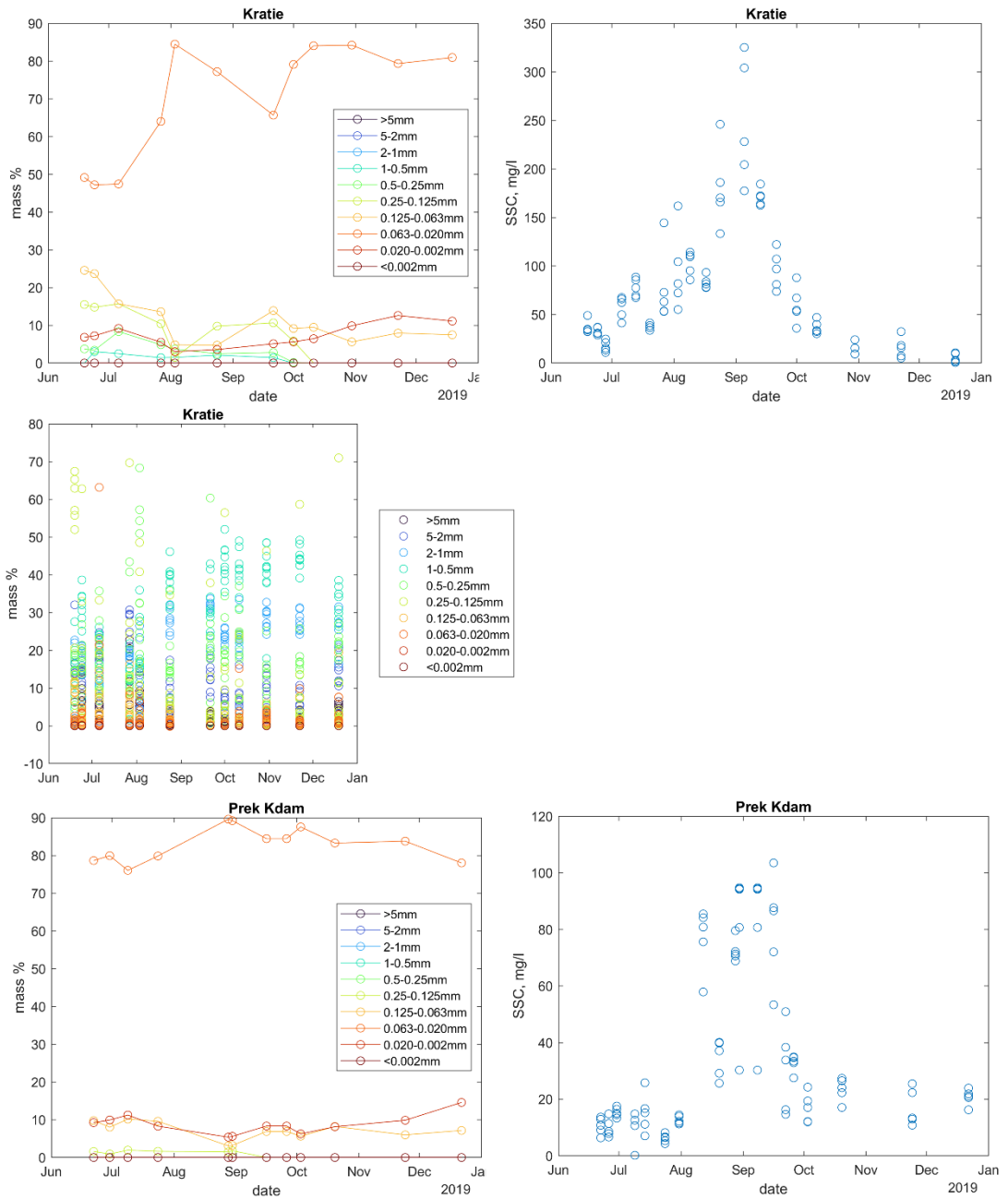


Figure 4-3: Kratie mass percentage of sediment fractions in suspended load 2019 and SSC at 4 vertical positions in water column (upper panels) and bed load (middle panel, mind that up to 10 samples are presented per date); Prek Kdam mass percentage of sediment fractions in suspended load 2019 and SSC at 4 vertical positions in water column.

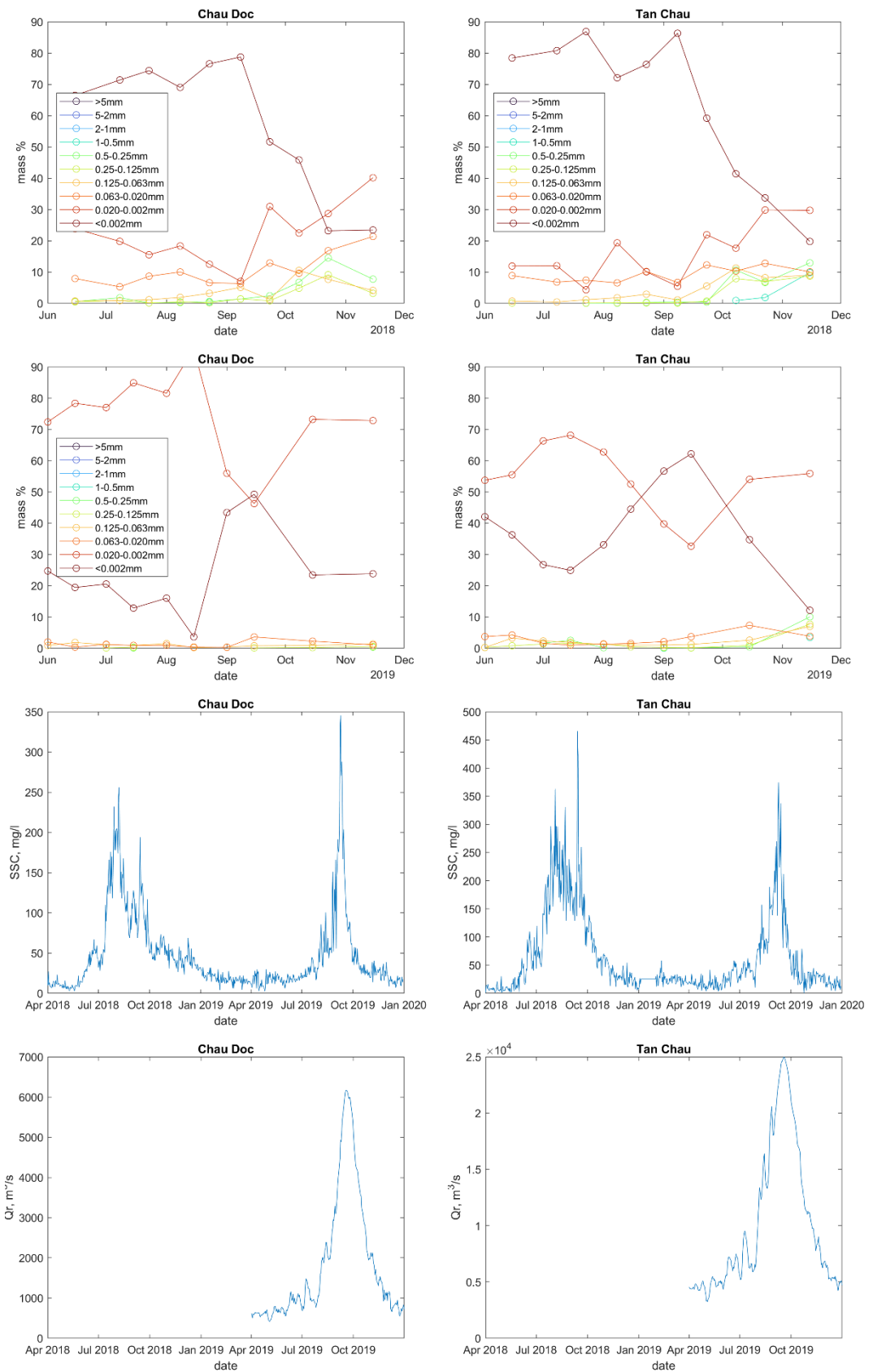


Figure 4-4: Mass percentage of sediment fractions in sediment suspension 2018 and 2019 (1st and 2nd rows), suspended sediment concentration (3rd row) and river discharge (4th row) for Chau Doc (left panels) and Tan Chau (right panels).

Bed surface sediment samples taken during the project by sediment grabs (Figure 4-5) resemble observations by Gugliotta et al., (2017) with sandy bed material throughout the VMD and finer, muddier sediment in the mouth area. The majority of most of the bed samples consist of fine (125-250 μm) to medium (250-500 μm) sand. The samples give a first indication of presence and distribution of sediment classes over the domain. Still, application of the sediment class distribution in modelling should be done with care, since the samples involve only point measurements. Bed composition may vary considerably over river cross-sections as well as over time.

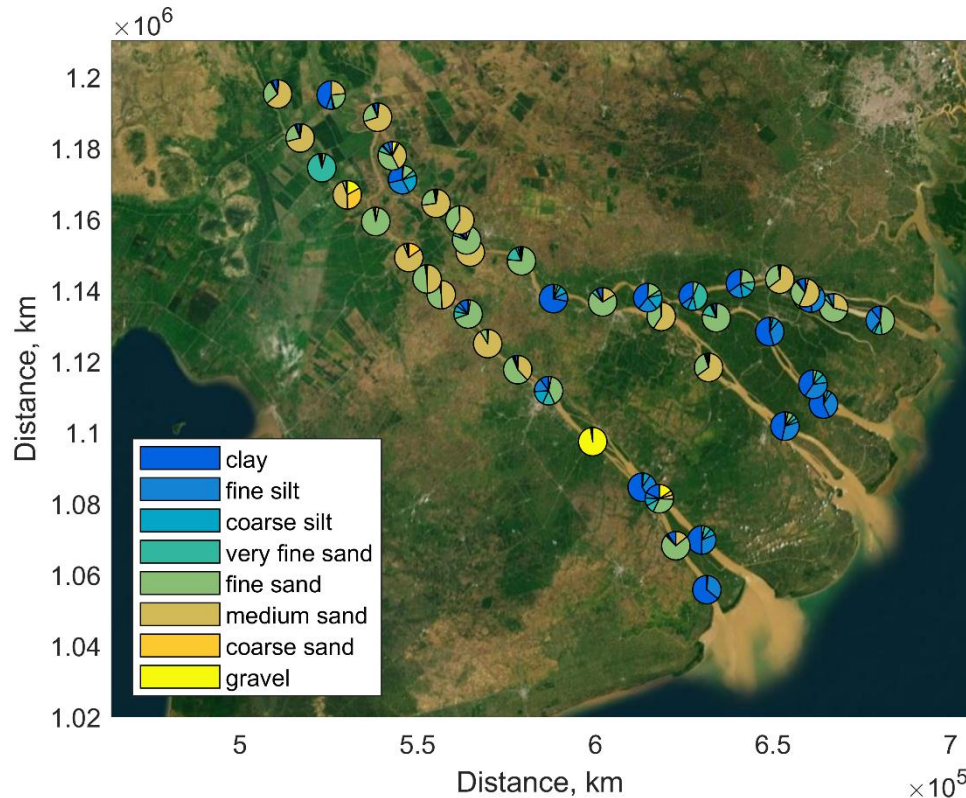


Figure 4-5: Bed sediment composition distribution over VMD based on grab samples.

4.2 Model setup

4.2.1 Software requirements

Assessing sand dynamics in the VMD requires modelling software that is able to predict the flow and sand transport at high spatial resolution ($\sim 100\text{m}$) throughout the VMD accounting for the topography and bathymetry of wide river branches and the drainage/irrigation channel network. Also, the model would need enough flexibility to describe forcing conditions by both seasonally varying river flow and tidal motion and a time resolution that is detailed enough to cover expected time variations in flow processes (\sim minutes). Finally, the model needs to be able to account for spatially varying mobile sand stock and roughness.

4.2.2 Software description

For this work package, DFM suite is used to model the hydrodynamic and sand transport within the Mekong Delta. The modelling framework is used to integrate various components of sand transport in sand import from upstream and export to the ocean and distribution in different channels to support interpreting the final sand budget. DFM carries out computation on both curvilinear and unstructured grids as well as combination of 1D and 2D meshes. This makes the software particularly suitable for regions with complex geometry like the Mekong Delta including its variable river widths, flood plains, network of primary and secondary channels and hydraulic structures.

The hydrodynamics and sediment transport are modelled by a flow and sediment transport module combined with the Delft3D-Flexible Mesh modelling software developed by Deltares

(Deltares, 2020a, hereafter; DFM). DFM is the successor to Delft3D4 and is widely used in hydrodynamic modelling of the sea, rivers, and flood plains. DFM has greatly improved by using unstructured networks and simultaneous multidimensional modelling, including 1D, 2D, and 3D domains. The current study applies DFM 2D which solves the two-dimensional shallow-water equations based on the finite volume numerical method (Kernkamp et al., 2011). The hydrodynamic module describes water levels and velocities at every grid cell and every point in time. Based on these time varying water level and velocity fields, the sediment module derives a time varying sand transport field.

This implies that flow dynamics and sand transport are solved at high time resolution (~minutes) on a spatially high-resolution grid (~100m) describing the river branches and channel network in the VMD. Achete et al., (2016); Martyr-koller et al., (2017); Thanh et al., (2020); Eslami et al., (2019a), (2021a) provide examples of successful 1D, 2D and 3D applications of DFM in estuarine environments around the world.

4.2.3 Hydrodynamic model setup

The large-scale hydrodynamic model of the Mekong Delta, the basis of this study, was well calibrated against hydrodynamics data (water level and discharge) during the large floods in 2000 and 2001 (Thanh et al., 2020). The current study builds on this model development with a focus on hydrodynamic calibration and validation (2021/2022) and 2022 validation of the transport of non-cohesive sediments (sand) against recent datasets partly obtained within the framework of this project. The differences between model by Thanh et al., (2020) and the current study are the bathymetry, hence, roughness field, the boundary conditions, the sediment transport formulations, and sediment properties. These adjustments are elaborated in upcoming sections.

The model is forced by river flow at Kratie and tidal constituents at the seaward boundary. The model is 2D, does not include wind waves or wind but includes sand and mud transport. The 2D model also does not include salinity gradients which would be inducing 3D gravitational circulation flow near the mouth sections of the estuaries. Note that ocean wind-driven waves are not relevant to sand transport within the VMD and the effect of wind on yearly sand transport is negligible as it only partially impacts water levels and water depth within the VMD (occasionally and in the order of 15-20cm, see Eslami et al., (2021a)).

4.2.4 Grid generation and improvement

The unstructured model applies a multi-scale modelling approach. Specifically, it consists of a combination of 1-D (canals) and 2-D (the main branches of the Mekong River, its floodplains and shelf) parts (Figure 4-6). The approach shows efficiency in the case of complex geometry such as the entire Mekong Delta. To capture the hydrodynamics of the main branches and estuaries of the delta, the main channels are represented in enough horizontal detail to resolve the flow patterns over channels and shoals and at the main bifurcations and confluences. The 1D canal structure and flood plains are essential to be able to capture the propagation and damping of tidal waves and river flood waves through the delta. Regarding the shelf, the model extended to approximately 80 km from the coastline of the delta to fully contain the river plume and include the interaction between the estuary and the coastal sea (Figure 4-7).

The grid includes the river system of the Mekong River from Kratie to the East Sea and part of its continental shelf. The mainstream of the Mekong River, the subaqueous delta and floodplains are represented by 2-D cells, whereas the primary and secondary canals are modelled as 1-D networks. The 2-D cells are a combination of curvilinear (in the main channels) and triangular grid cells. The grid creation was introduced and recommended by Kernkamp et al., (2011) and Bomers et al., (2019). The grid/element sizes vary from about 0.1 km in rivers to 2 km over the delta shelf. The length of the grids varies depending on the river geometry. The uniform length of 1-D segments is 400 m while the 2D cells have a different resolution depending on the spatial scale of the locally dominant morpho- and hydrodynamic processes. Specifically, the 2D cell sizes for the Mekong River mainstreams are approximately 0.7 km in general and decrease to about 0.2 km at river bifurcations and confluences.

The 2D cells are coarser for floodplains and sea areas, increasing up to around 2 km in size. The grid totally contains 73,504 cells (Thanh 2021). The grid quality is critical for accurate simulations; therefore, the grid has been made orthogonal, smooth, and sufficiently dense.

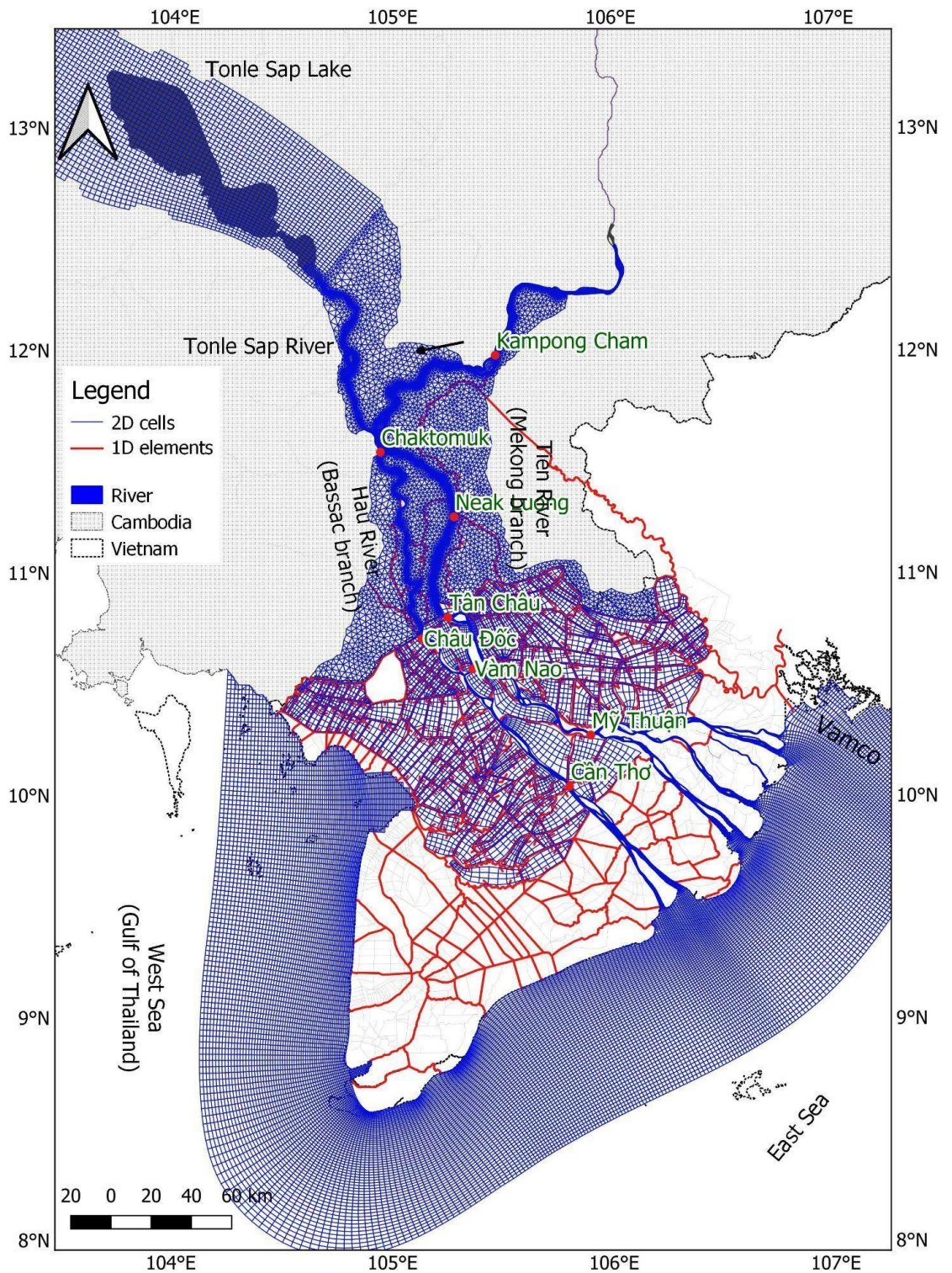


Figure 4-6: Numerical grid consisting of 1D elements and 2D cells.

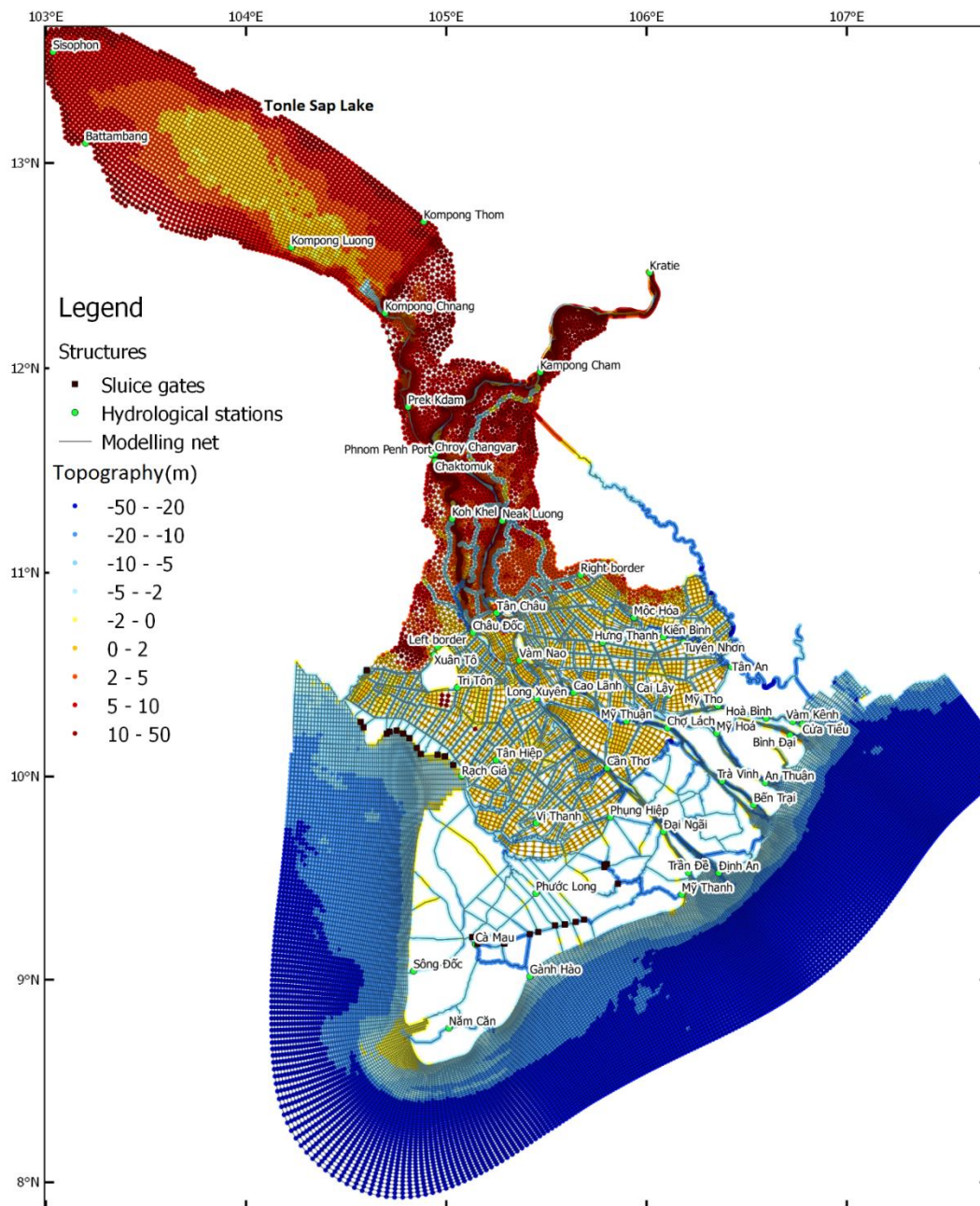


Figure 4-7: Numerical grid and river topography and shelf topography of the VMD.

4.2.5 Bathymetry

Detailed bathymetries of the Mekong Delta are sparse and limited in extent. Therefore, the bathymetry has been composed from different sources and time periods. The current study uses the 2018 bathymetry of Vasilopoulos et al., (2021b) the main river/estuarine channels, interpolated and incorporated in Eslami et al., (2021a). In addition, several areas of the Mekong River in Vietnam were updated by the bathymetry which was collected in 2022 by WWF (Figure 4-7). The network of primary and secondary channels was extracted from the 1D-ISIS model of the MRC (1998, updated in 2015, following Thanh, 2020). The bathymetry of the river mouths was updated following Eslami et al., (2021a). For further offshore, bathymetry is derived from ETOPO of ~1 km resolution. The floodplain topography is obtained from the digital elevation model, with a resolution of 250 m provided by the MRC.

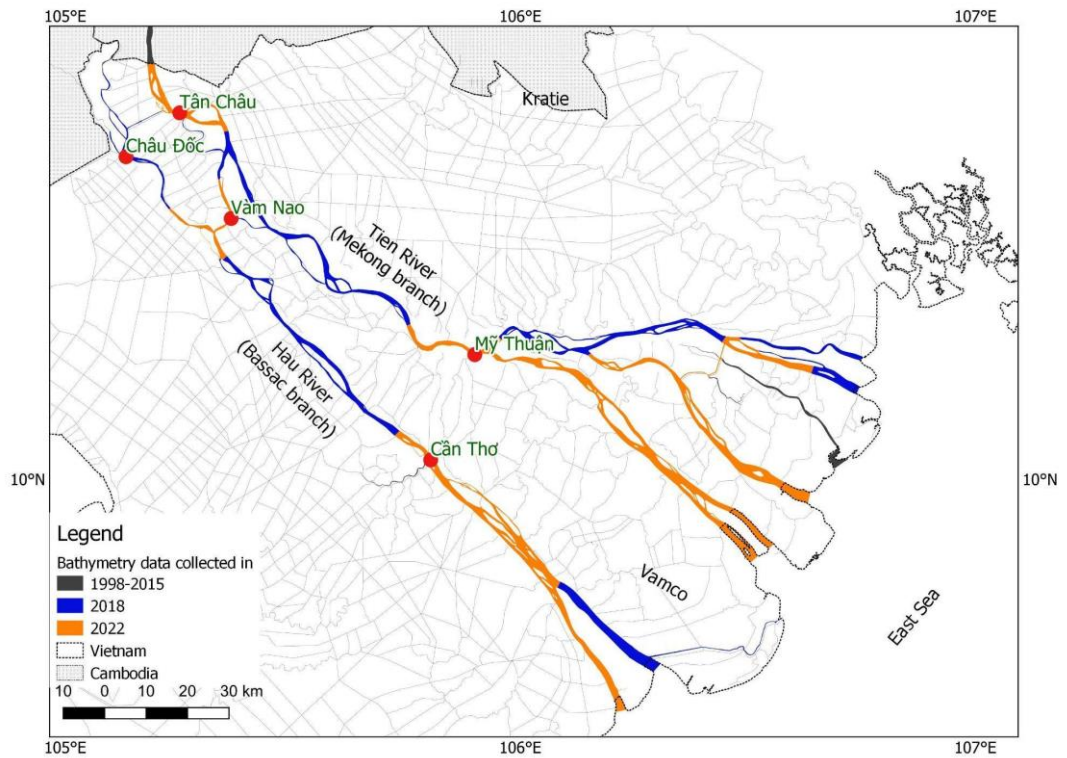


Figure 4-8: Bathymetry collected in the Mekong Delta

4.2.6 Boundary conditions

Open boundaries are defined as water discharge (at Kratie) and water levels (the sea). The measured water discharges were used for the upstream boundary at Kratie and were collected from the Mekong River Commission. The latter were defined as astronomical tidal constituents and extracted from a global tidal model (TPXO 8.2; Egbert and Erofeeva, 2002). Furthermore, to allow for alongshore transport, the northern cross-shore boundary is defined as a Neumann boundary which is driven by the alongshore water level gradient (Tu et al., 2019).

4.2.7 Initial conditions

The hydrodynamics of the VMD are strongly influenced by the annual floods. Furthermore, Lake Tonle Sap plays an essential role in the regulation of the river flows to the VMD. The water level of Tonle Sap Lake varies greatly depending on the season, which is why the parameters of the appropriate conditions reduce the spin-up cycle of the model. We assume that the previous flooding had filled Tonle Sap Lake, so the model spun off during the 2020 flooding. To minimize this effect, the simulation should start in the low flow season when the water levels are low. We used the water level at the end of Apr 2021 as the initial conditions for the simulation from May 2021. The simulation was defined for a period of May 2021 - October 2022. This period was selected since it covers over a year to capture inter-/annual hydrological regime.

4.2.8 Sediment transport model setup

In our approach we applied the Van Rijn (1993) sediment transport formulations which distinguishes between a bed-load predictor and a suspended-load predictor (see also Delft3D FM manual (<https://oss.deltares.nl/web/delft3dfm/manuals>)). This implies that at every timestep and for every cell both equilibrium suspended load and bed load transports are calculated based on local velocities. The bed load transport is then determined by the equilibrium bed load transport. The suspended-load transport (being generally more diffusive than bed load transport) is simulated using an advection-diffusion solver. The sediment concentration in a cell depends on the advection and diffusion from neighbouring cells and local erosion and deposition fluxes (bed exchange) based on the between the actual sediment concentration in

a cell and its equilibrium sediment concentration. Applying this methodology with its default and validated settings requires only bed roughness and sand diameter as input parameters. The actual separation of bedload and suspended load in Van Rijn's model is partially theoretical and therefore not necessarily equal to separation of 'bedload' from dune tracking and from concentrations samples. The model applied in the current study is simulated without bed updating, which means it does not allow for bed level changes, but it allows for changes in sediment stock and composition (the latter in case mud fractions were included).

Following observed SSC levels in 2018/2019 at Kratie, the model was forced with a 0.01 mg/l sand concentration at the Kratie boundary of which about 90% is in suspension and 10% is bed load. This assumes that sand covers about 10% of the SSC at Kratie. For 2022 the upstream Kratie boundary results in a yearly load of 5 Mt (suspension) and 0.1 Mt (bedload). This corresponds with observations in the lower, Cambodian portion of the Mekong River by Hackney et al. 2020 who found a bedload of 0.18 ± 0.07 Mt/yr and a suspended sand load of 6 ± 2 Mt/yr for the 2013-2014 period. A 2011 point based measurement of bed load transport at Kratie estimated a bed load of about 1.5% of the suspended load which compares to the model results in the current study (Koehnken, 2012a & b & 2014; Kondolf et al., 2014).

Table 4-2: Describes how data were used for model validation and calibration.

Data	Source	Use
Water levels at Kratie	MRC	Boundary conditions
Water levels at 16 stations throughout the Mekong delta (5-Cambodja and 11-Vietnam)	MRC and current project	Validation/calibration data
Discharge at 10 stations throughout the Mekong delta (5-Cambodja and 5-Vietnam)	MRC and current project	Validation/calibration data
Bed Sediment data by grabs	Current project	Initial bed composition conditions
Suspended sediment data at 9 VMD stations	Current project	Validation of mud sediment transport model
Dune tracking at 7 VMD stations	Current project	Validation/calibration of sand bed load transport model
Historic bed and suspended sediment composition data at 4 stations along Mekong River	MRC	Assessment and validation/calibration of sediment composition transport

The model results show that total sand transport is about 5% of the total sediment transport which compares well with the 7% reported by Hackney et al. 2020. Also, preliminary model runs show that increasing this concentration to equilibrium sand concentration at Kratie does not impact cumulative sand transports in cross-sections much further downstream of Kratie. This suggests that sand transports are merely a function of local velocities and local suspension and deposition processes. This is in contrast to finer sediment fractions that may be carried in suspension over much longer distances. At the seaward boundary we applied an equilibrium concentration, i.e. a time varying equilibrium sand concentration belonging to the velocity at the boundary. Since velocities at the ocean boundary typically remain low due to the large depth, sand transports across the boundary remain low as well.

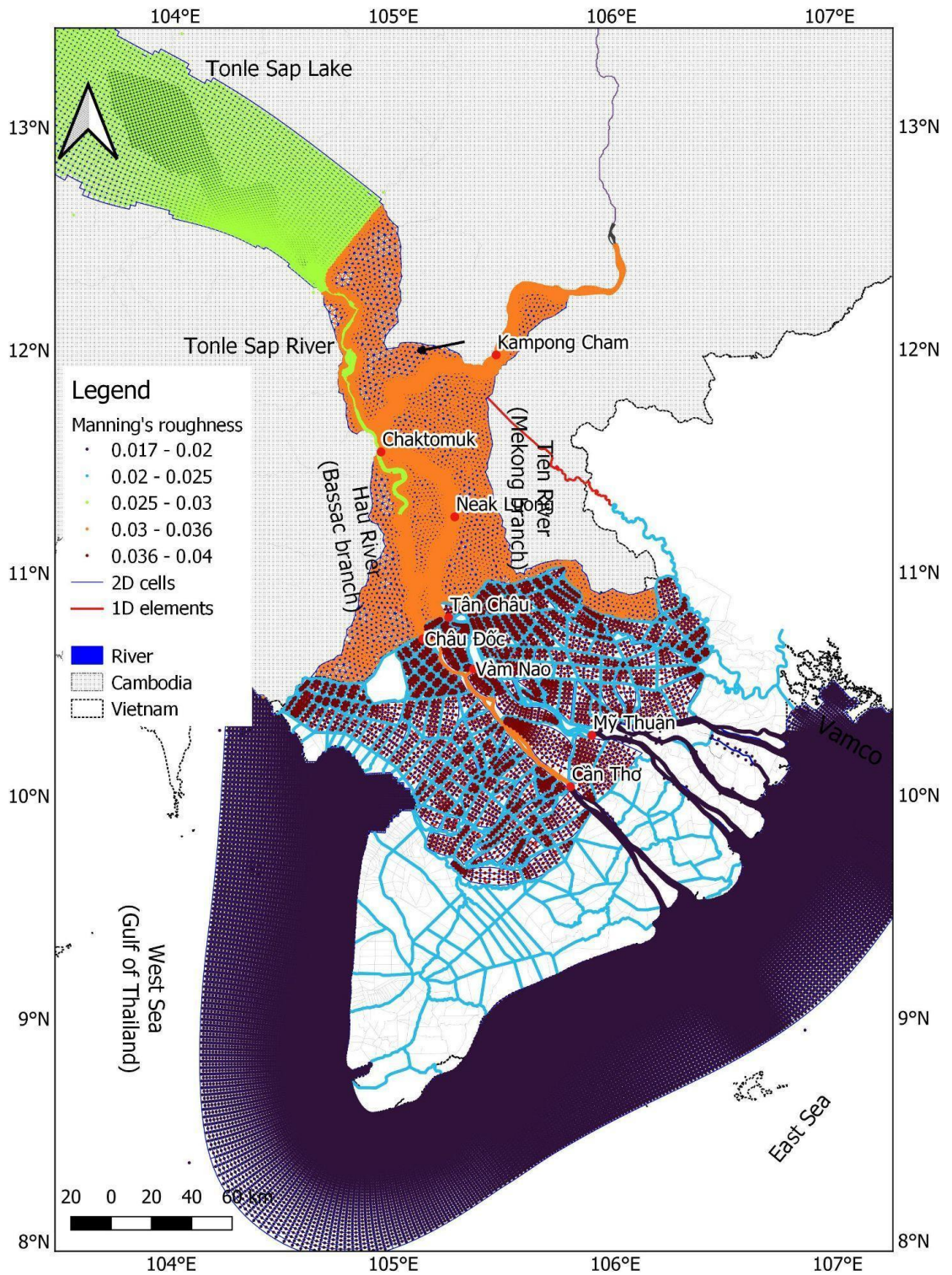


Figure 4-9: Calibrated manning's roughness.

4.3 Hydrodynamic model validation

Here we present a validation of the model against 2022 discharge and water level data with a 2018 bathymetry in which parts of the model bed are replaced by bathymetric measurements taken in 2022, after careful quality control. In this study, the initial roughness was extracted from (Thanh et al., 2020; Eslami et al., 2021a). The hydrodynamic model was recalibrated by adjusting spatially varying roughness coefficients following an iterative method leading to the roughness definition in Figure 4-9. 16 Stations in Cambodia and Vietnam were used to assess

the model's performance in reproducing water levels and discharge. The model calibration was finalised when the indexes at all stations were greater than the satisfactory level.

The objective function of the Nash-Sutcliffe efficiency (Nash and Sutcliffe, 1970) was used to evaluate the model performance against observed data (NSE). NSE is a normalized statistical indicator that employs a comparison between residual variance and measured data variance, and it reads as Equation 3-1 below.

$$NSE = - \frac{\sum^{t=1T} (Q_m^t - \bar{Q}_0)^2}{\sum^{t=1T} (Q_0^t - \bar{Q}_0)^2} \quad (\text{Eq. 3-2})$$

where \bar{Q}_0 is the mean of the observed discharges, Q_m^t is the simulated discharges and Q_0^t is the observed discharge at time t.

Figure 4-7 and Figure 4-8 show the model performance for water levels at stations in Cambodia and Vietnam respectively at, in total, 16 stations. According to Moriasi et al., (2007) categorization, all stations have NSE values higher than the acceptable level of 0.5. VMD stations Can Tho and My Thuan perform worst in terms of water level, but they are still satisfactory, with NSE values higher than 0.5.

Table 4-3: Location of stations.

Name	Name in model (figures)	Latitude (degree N)	Longitude (degree E)
Stations in Cambodia			
Kratie	kratie	12.46703	106.01557
Prek Kdam	prekkdam	11.81217	104.80931
OSP MRC	bassacchaktomuk	11.54654	104.94454
Koh Khel	kohkhel	11.26781	105.02946
Neak Luong	neakluong	11.26435	105.28054
Phnom Penh Port	phnompenhport	11.57828	104.92795
Chroy Changvar	chroychangvar	11.58193	104.94366
Kaoh Norea	mk_chaktomuk	11.55151	104.95692
Stations in Vietnam			
Can Tho	cantho	10.04219	105.8033
My Thuan	mythuan	10.27305	105.90002
Binh Dai	binhdai	106.71812	106.71812
An Thuan	anthuan	9.86067	106.54004
My Tho	mytho	10.34789	106.36095
Cho Lach	cholach	10.28262	106.12698
Chau Doc	chaudoc	10.70702	105.13378
Tan Chau	tanchau	10.80329	105.2518
Kampong Cham	vamnao	11.98164	105.46922
Đai Ngai	daingai	9.73009	106.08505
Tra Vinh	travinh	9.98546	106.36851

Calibration of the water discharge is performed at 5 stations in Cambodia at 5 stations in the VMD- (Figure 4-10 & Figure 4-11). The NSE is smallest at Chau Doc, with a value of 0.53. This is caused by overestimation of the tidal discharge although we found that the 2022 updated bathymetry improved the modelled results.

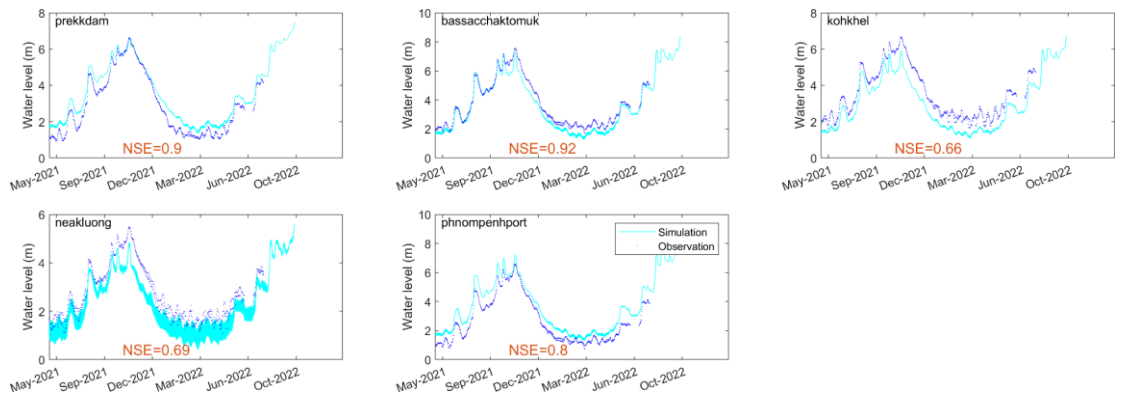


Figure 4-10: Model performance of water levels at Cambodia stations in 2021-2022.

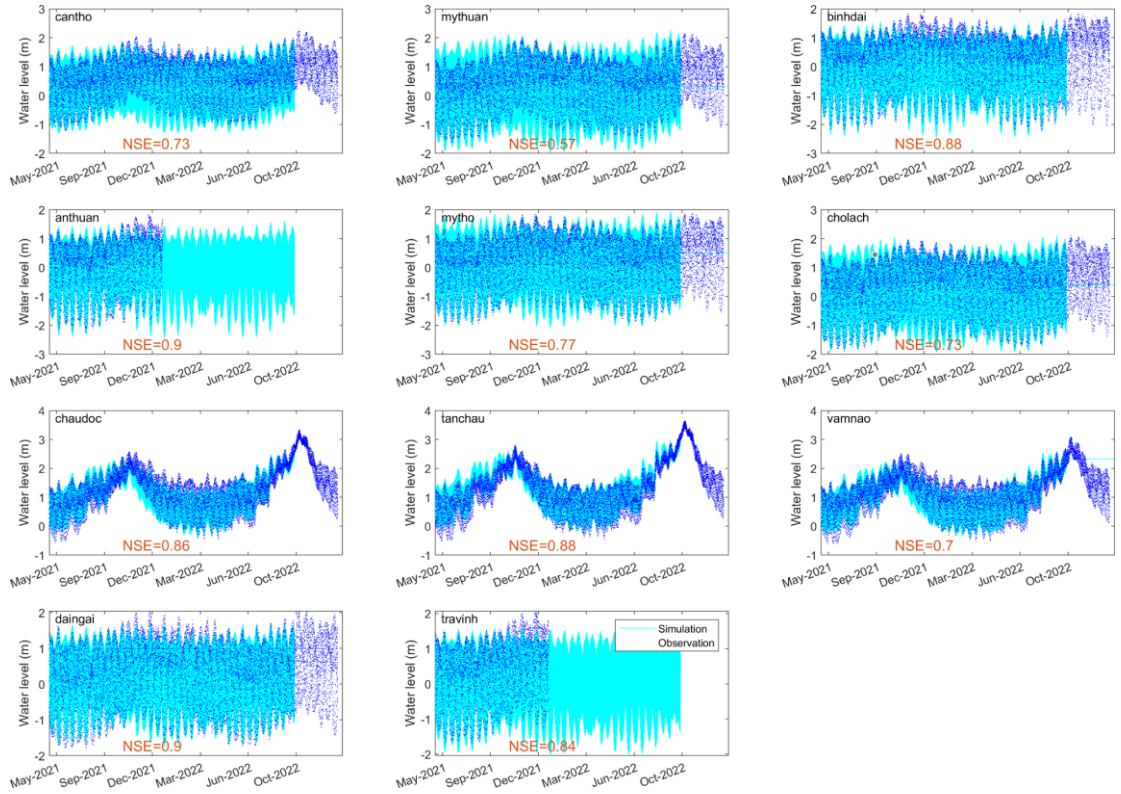


Figure 4-11: Model performance of water levels at Vietnamese stations in 2021-2022.

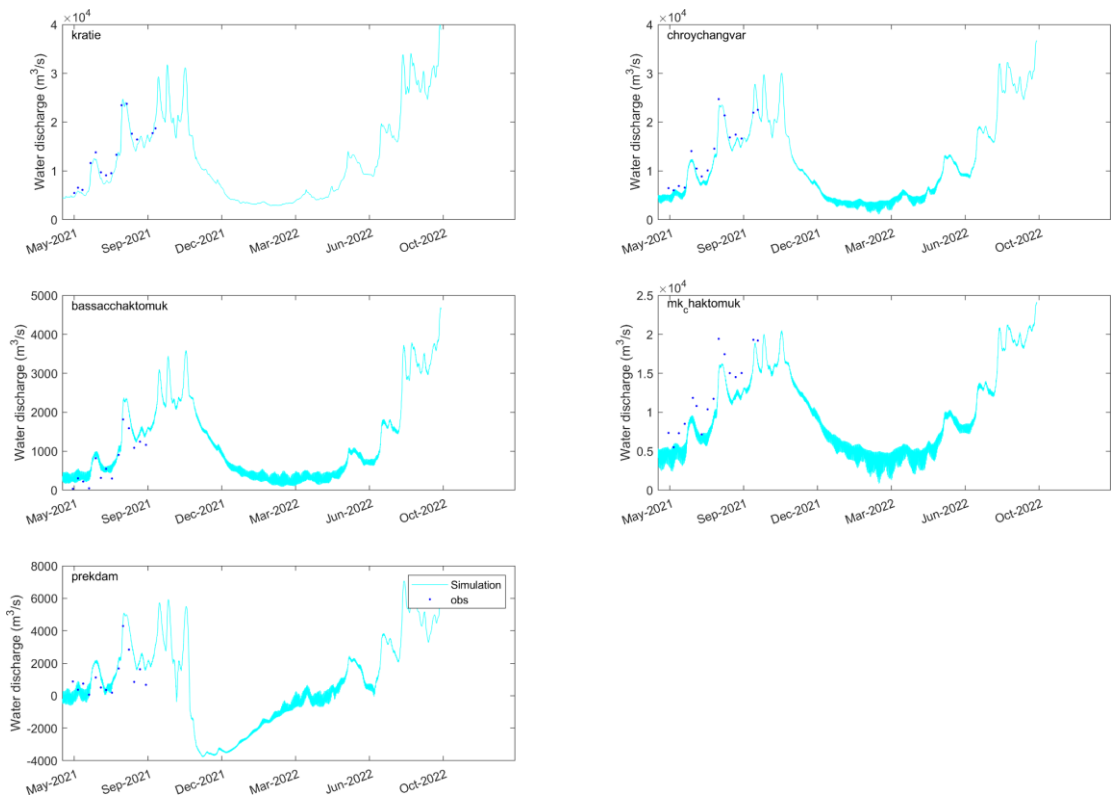


Figure 4-12: Model performance of discharges at Cambodian stations.

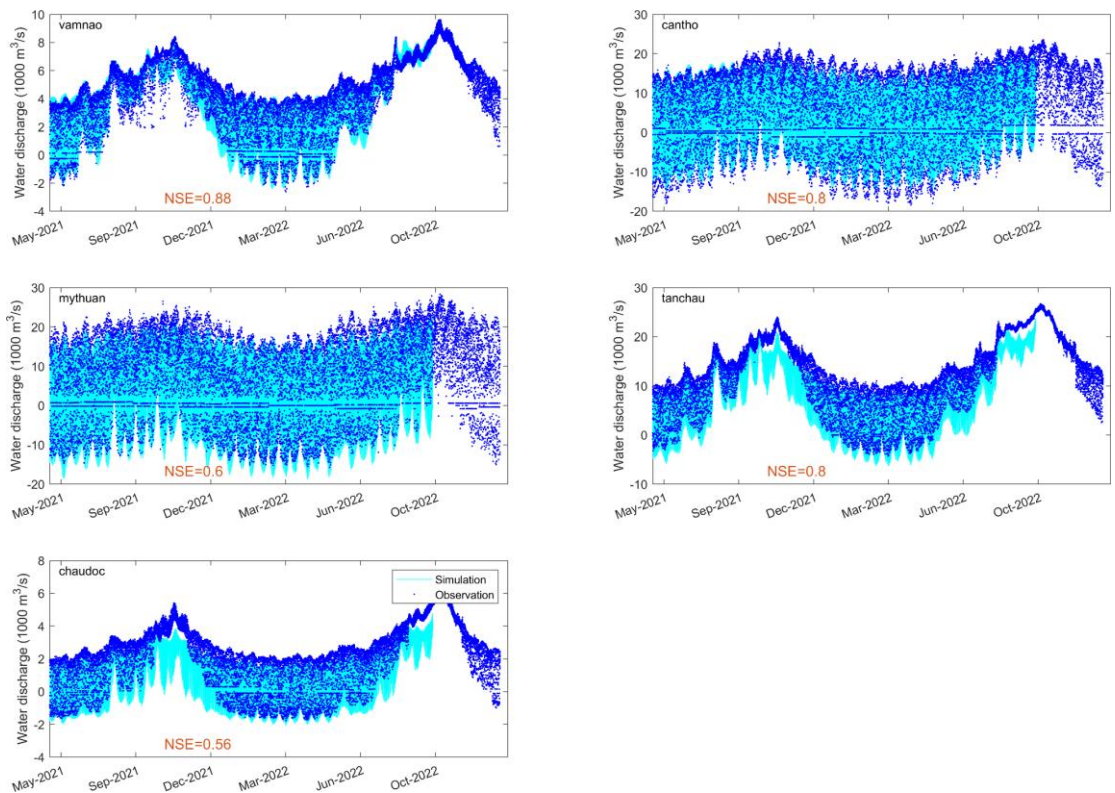


Figure 4-13: Discharge validation for Vietnamese stations.

In general, the calibrated model performed well in terms of water levels and discharges since the NSE values are greater than the satisfactory level. The model is able to capture interannual variability in the measured data which is an important index of its performance. Model performance improved by more accurate bathymetric data.

4.4 Sediment transport scenario simulations

To start as simple as possible, preliminary runs apply a 50m sand layer thickness with a sediment diameter of 200 μ m (fine sand) in the entire model domain (runfs). The 50 m thickness was applied to assure abundance of sand everywhere during the entire year. Runfs acts as a basis for more advanced model settings, sensitivity analysis and model refinement.

Sensitivity analysis systematically explores the impact of bed sediment availability (with no sand near the mouth in line with observations), sand properties (*i.e.*, median diameter, $D_{50} = 100 \mu\text{m}$ and $D_{50} = 300 \mu\text{m}$) and inclusion of finer, muddy sediment fractions, where we applied mud settings as suggested by (Thanh et al., 2019). Table 4-4 shows specification of the runs conducted. In addition, we compare the model results against SSC from the field observations and MBES derived bed load transport. All runs were run for two consecutive years with equal forcing conditions. This was done as a spin-up for hydrodynamics (*e.g.*, considering hydrodynamic processes of filling and emptying by Ton Le Sap Lake) and morphodynamics when two sediment fractions and/or spatially varying sediment availability were used. The latter “morphodynamic” spin-up only considered updating sand availability and bed composition (in case of mud presence), not bed levels itself.

Table 4-4: Definitions of various simulation ID's (run-names).

Run-name	
Fs	Sand D=200 μ m, uniform
fsD100	Sand D=100 μ m, uniform
fsD300	Sand D=300 μ m, uniform
Fssdb	Sand D=200 μ m, sand availability based on data
Fsm	Sand/mud D=200 μ m, sand availability based on data only mud near mouth, $w_{\text{mud}}=0.1\text{mm/s}$
Fsmc	Sand/mud D=200 μ m, sand availability based on data only mud near mouth, $w_{\text{mud}}=0.5\text{mm/s}$
Fsmf	Sand/mud D=200 μ m, sand availability based on data only mud near mouth, $w_{\text{mud}}=0.05\text{mm/s}$

4.5 Sand transport calibration

4.5.1 Bed load

Figure 4-14 and Figure 4-15 compare 2022 modelled bed load transport against 2022 MBES derived bedload estimates including uncertainty ranges. The modelled bed load transports show a strong tidal signal whereas the MBES based data are based on the residual bed load averaged over 18 and 12 days for the dry and wet season respectively. The MBES derived bed load should thus be considered as an average, or better “residual” value. Furthermore, it should be remarked that bedload calculated by (van Rijn et al., 1993) does not include the suspended-load component of sand that contributes to the dune migration and is included in the ‘bed-load’ values obtained from the dune-tracking method. The modelled bedloads are generally of the same order of magnitude as the MBES derived transports. No further calibration of Van Rijn’s predictor seems therefore required. Remarkably, Vam Nao shows less tidal variations which is attributed to the fact that the water level *difference* at the Vam Nao River stretch is less subject to tidal variations. In the wet season MBES-based data at Tan Chau, Chau Doc, Long Xuyen and Cao Lanh tends to be higher than modelled values in three stations. Sensitivity analysis applying different sediment diameters ($D=100,200$ and $300\mu\text{m}$, uniformly applied) shows that the dynamics remains similar, but the magnitudes vary. Mind that a larger sediment diameter does not necessarily lead to less bed load. Given equal flow regimes the total sediment transport (*i.e.*, suspension and bed load) will be smaller for larger diameters while the bed load itself (generally a small portion of the total load) may be larger.

Figure 4-16 and Figure 4-17 present the cumulative bed load transports during the dry season and wet season. MBES derived and modelled cumulative bed loads are in the same direction and, again, generally of the same order of magnitude. MBES derived transports generally overestimate modelled bed loads, except for Tan Chau during the dry season and Vam Nao and Co Lach during the wet season. The uncertainty of the MBES derived transports is generally large compared to the uncertainty related to the sediment diameter.

The resemblance between MBES derived transports and the model results is promising especially given the data uncertainty and width-extrapolation associated with the MBES based analysis and given the uncertainty associated with sediment properties applied in the model. We expect bed forms to be most likely present at locations of largest flow velocities (and bed load transports) in the cross-section. Extrapolating the MBES derived bed loads over the entire width would thus lead to overestimation which is apparent from the figures. It is likely that the MBES derived bed loads are more realistic for lower transport rates which are indeed closer to the modelled values.

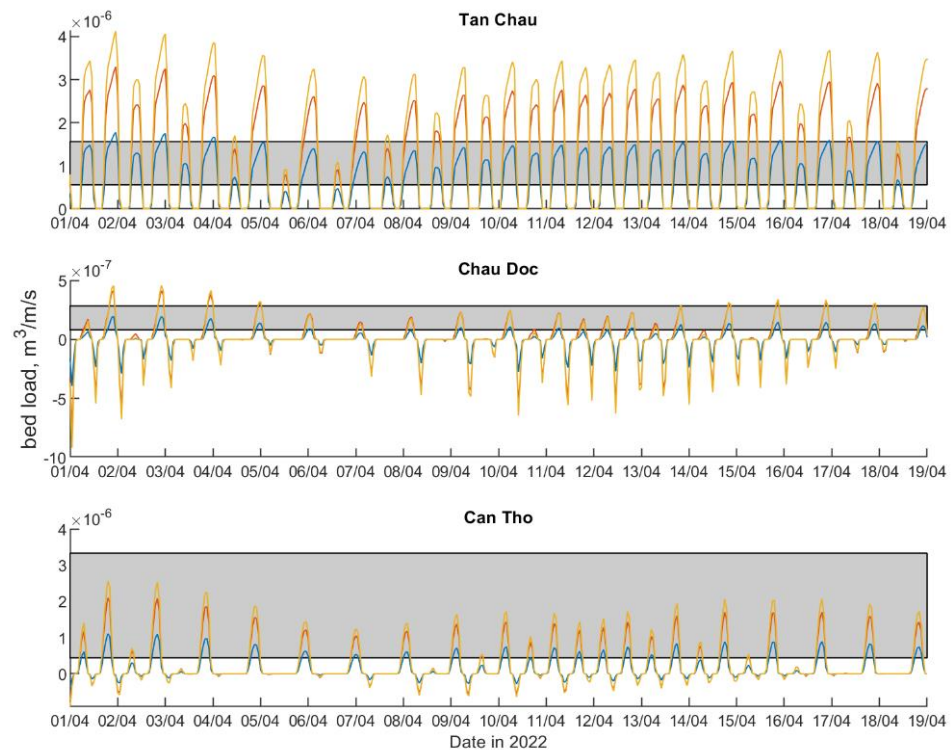


Figure 4-14: Dry season bed load transport at Tan Chau (upper panel), Chau Doc (middle panel) and Can Tho (lower panel). Model results are given in red lines ($D=100\mu\text{m}$, runfsD100), blue lines ($D=200\mu\text{m}$, runfs) and yellow lines ($D=300\mu\text{m}$, runfsD300). Grey area reflects bed load estimate ranges (mean \pm standard deviation including flow width uncertainty) averaged over 18 days based on MBES analysis.

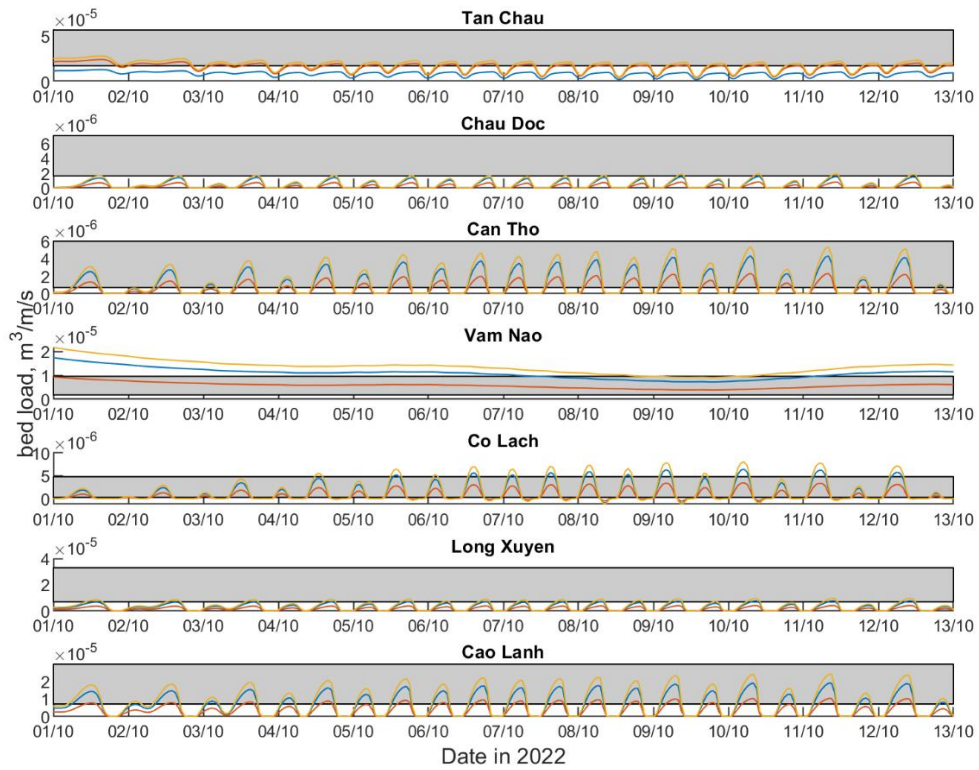


Figure 4-15: Wet season bed load transport at, from top to down, Tan Chau, Chau Doc, Can Tho, Vam Nao, Co Lach, Long Xuyen, Cao Lanh. Model results are given in red lines ($D=100\mu\text{m}$, runfsD100), blue lines ($D=200\mu\text{m}$, runfs) and yellow lines ($D=300\mu\text{m}$, runfsD300). Grey area reflects bed load estimate ranges (mean \pm standard deviation including flow width uncertainty) averaged over 12 days based on MBES analysis.

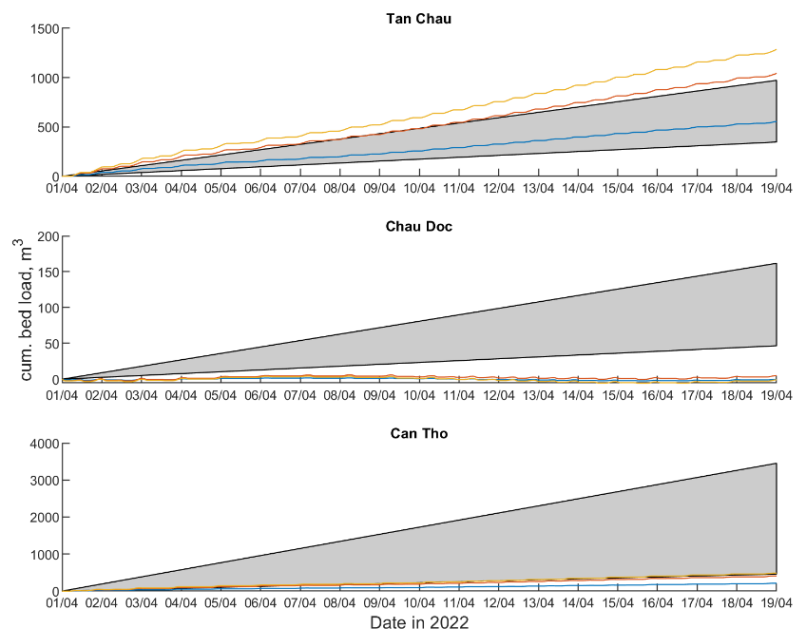


Figure 4-16: Dry season cumulative bed load transport through Tan Chau (upper panel), Chau Doc (middle panel) and Can Tho (lower panel) cross sections. Model results are given in red lines ($D=100\mu\text{m}$, runfsD100), blue lines ($D=200\mu\text{m}$, runfs) and yellow lines ($D=300\mu\text{m}$, runfsD300). Grey area reflects bed load estimate ranges (mean \pm standard deviation including flow width uncertainty) averaged over 18 days based on MBES analysis and extrapolated over cross-section.

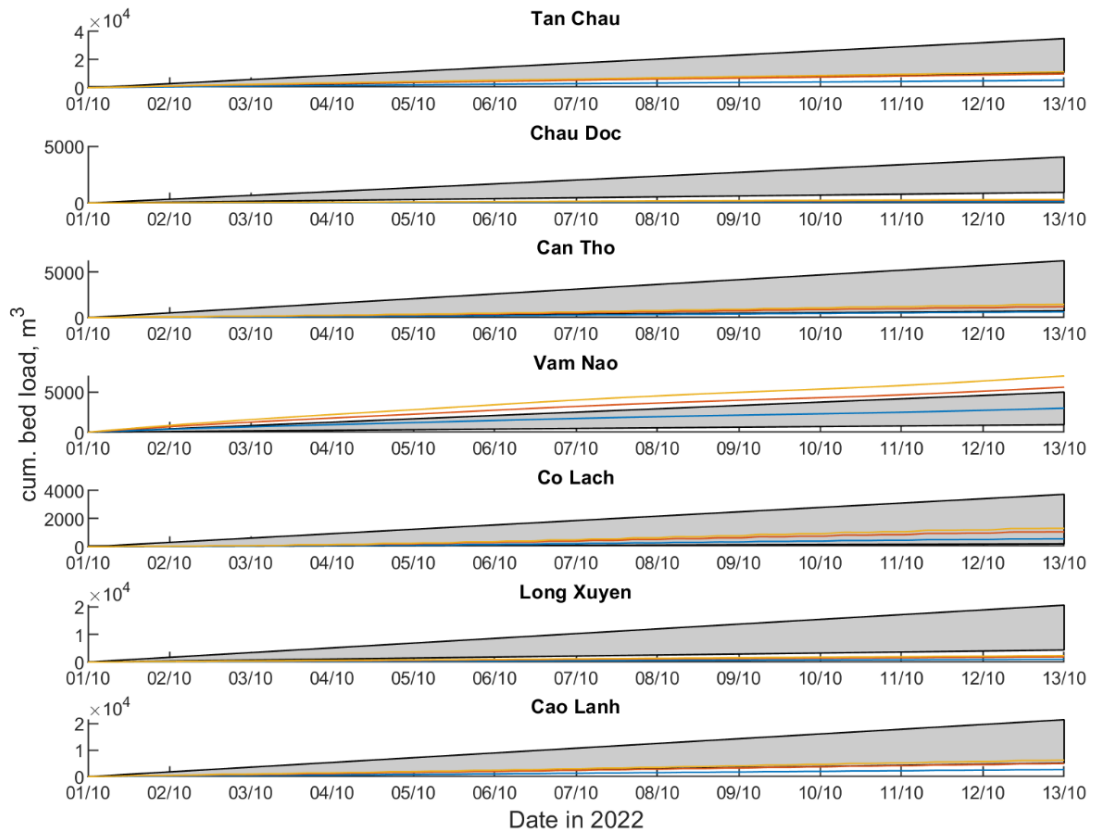


Figure 4-17: Wet season cumulative bed load transport through (from top to down) Tan Chau, Chau Doc, Can Tho, Vam Nao, Co Lach, Long Xuyen, Cao Lanh cross-sections. Model results are given in red lines ($D=100\mu\text{m}$, runfsD100), blue lines ($D=200\mu\text{m}$, runfs) and yellow lines ($D=300\mu\text{m}$, runfsD300). Grey area reflects bed load estimate ranges (mean \pm standard deviation including flow width uncertainty) averaged over 12 days based on MBES analysis and extrapolated over cross-section.

4.5.2 Suspended load

Since SSC levels are governed by fine sediment fraction (silt/clay), we used the sand-mud model to validate modelled SSC against observed SSC during the project. Figure 5-16 shows that modelled mud SSC levels are similar to observed SSC levels in all stations except for Chau Doc where observed SSC levels are 2-3 times larger. An important finding is that suspended sand concentrations remain at least an order of magnitude smaller than the modelled mud concentrations. This is in line with measurements at locations more upstream (see Figure 4-4 and Figure 4-5). Further fine tuning and calibration could lead to better resemblance between observed and modelled SSC levels but is not considered to be part of the current study.

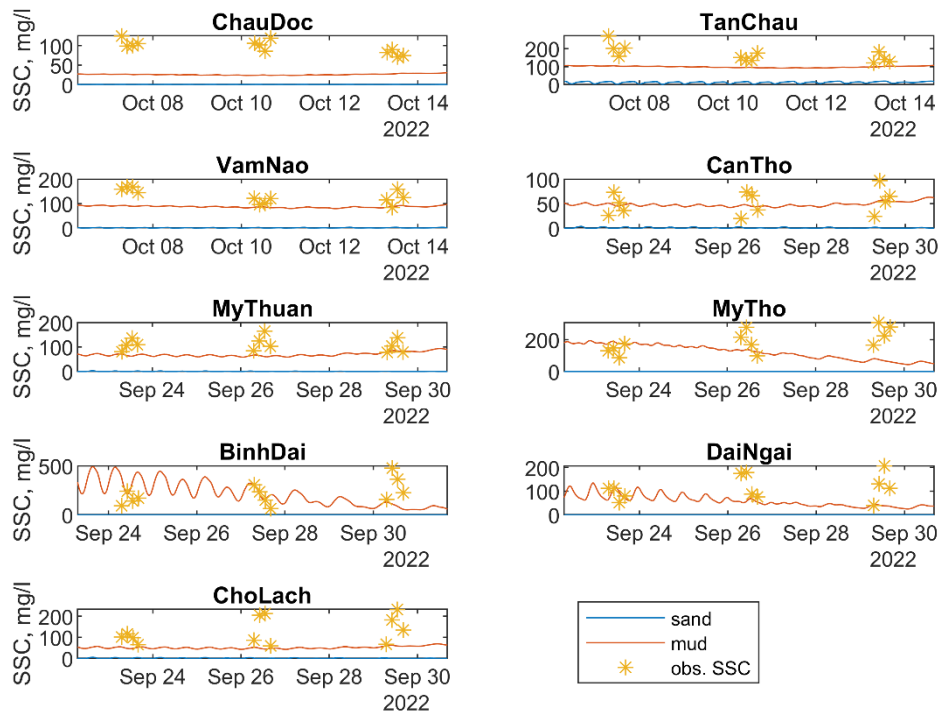


Figure 4-18: Comparison of modelled (sand and mud, runfsm) and observed SSC levels.

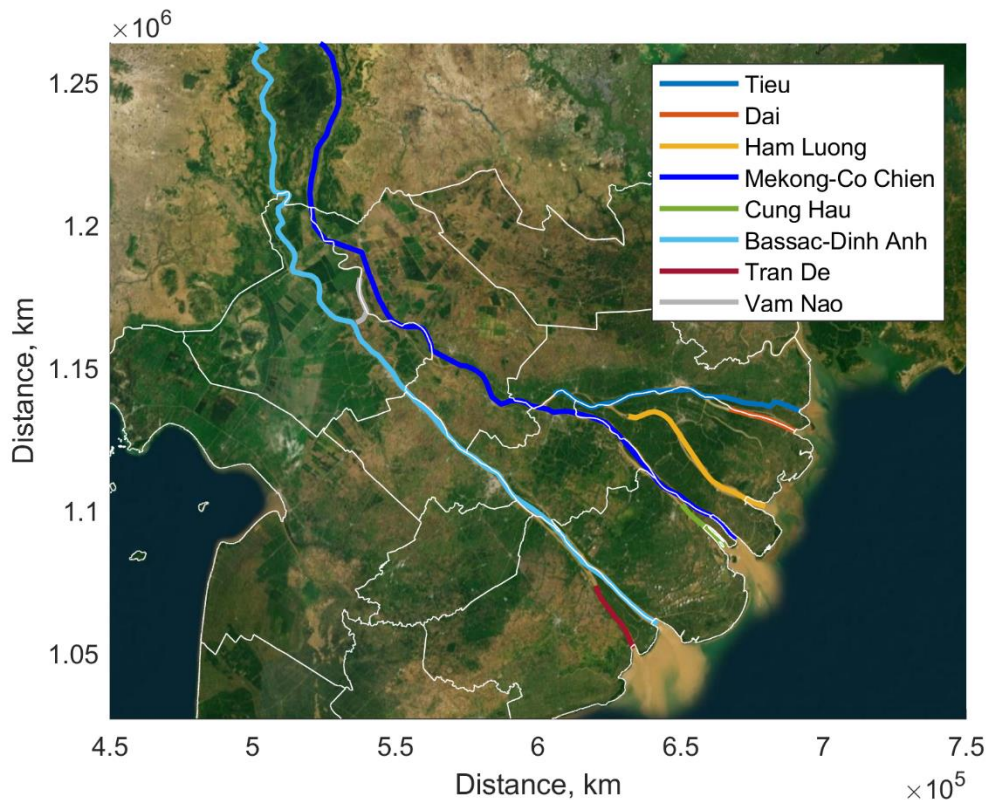


Figure 4-19: Colour definition of VMD river branches. Provincial borders in white lines.

This section presents the 2022 flow and sediment distribution over the different branches in the VMD. Figure 4-19 defines the colour scheme applied for the different VMD river branches. First of all, Figure 4-20 shows the distribution of 2022 river flow. Largest flow enters the VMD at Tan Chau via the Mekong-Co Chien branch while about 5% of the flow enters the VMD at Chau Doc via the Bassac River. The Vam Nao River stretch distributes these amounts to almost similar volumes around 175 km from the mouth. At 100 km from the mouth the Bassac and Co

Chien branches further divide into 7 sub-branches of which the Bassac carries the largest water volume. Figure 4-21 shows the cumulative total (bed load and suspended load) sand transport through cross-sections at locations where MBES data were derived. Largest transports (steepest curves in Figure 4-21) occur during the wet season for all stations although the magnitude differs per station. The wet season signal is weaker for the stations of Chau Doc, Long Xuyen and Can Tho (along the Hau River) and Co Lach. Following the Co Chien river branch stations Tan Chau, Vam Nao and Cao Lanh show largest transports. As these results follow from the simulation with an excess of sand in the system (run with 50 m initial sand thickness), they overestimate the actual transport rates.

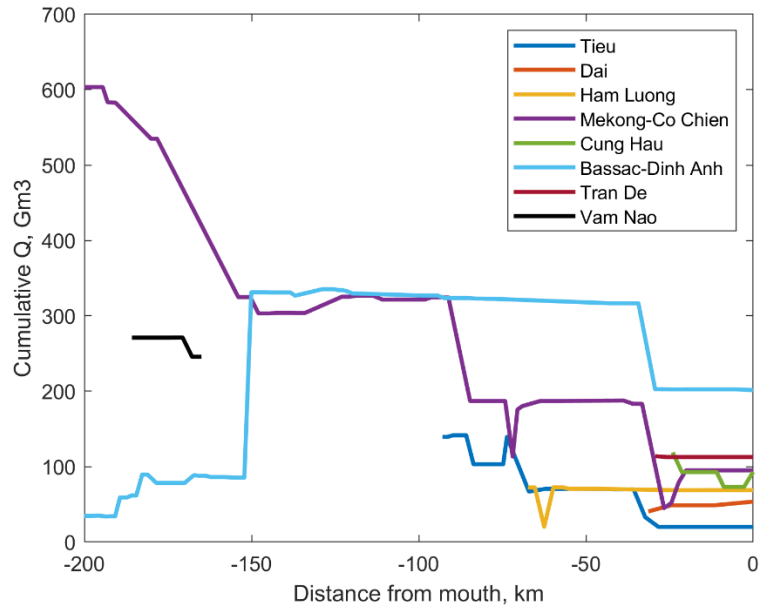


Figure 4-20: 2022 Cumulative river flow distribution over VMD river branches

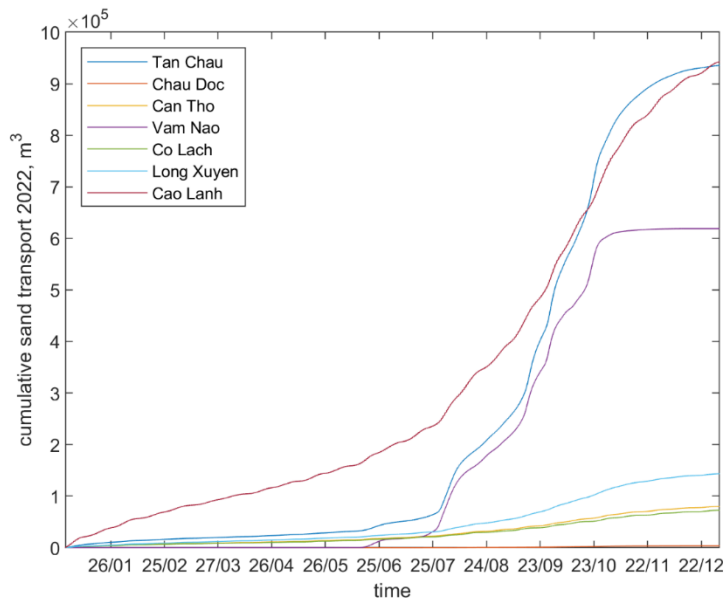


Figure 4-21: Runfs cumulative sand transport over year 2022 for various stations spread over the VMD that have MBES data.

At approximately 10 km intervals Figure 4-22 shows the 2022 cumulative bedload and suspended load transport along the VMD branches. Bedload is typically an order of magnitude smaller than the suspended load. Largest suspended load occurs between km 200 and km 90, that is, in the Mekong-Co Chien branch between the Cambodian border and the bifurcation into the Tieu River. Still, maximum 2022 sand transport volumes hardly exceed 8 Mt/yr, which is much smaller than the estimated sand mining volumes estimated in Chapter 3.

Both bedload and suspended load transports reduce considerably in the Mekong-Co Chien branch after bifurcation of the Tieu branch. A possible reason is that the bifurcations cause distribution of flow and lower velocities with lower corresponding sand transport capacity. Other explanations are that the bifurcations are located in an environment where the fluvial regime turns into a tidal regime where tide residual sand transports reduce due larger cross-sections. A third reason may be that historic mining led to deeper cross-sections reducing flow and sand transports. Sand deposition will be most likely in area of largest spatial sand transport gradients.

Both the calculated bed load and suspended load volumes show “spiky” behaviour along the river branches. This is attributed to spatial variations in velocity magnitude. Sand transport, and especially bedload transport, is governed by local velocities. These velocities may vary considerably along the Mekong River due to variations in cross-sectional area. The variations may be real (wider, shallower versus deeper and narrower cross-sections as the result of embankments or hard substrate) but may also result from the model setup. The grid resolution may be occasionally too coarse missing deeper channel sections. Another cause is that the limited amount of cross-sectional data in some of the river stretches requires longitudinal interpolation of data leading to best possible but still too rough 2D bathymetry interpolation in parts of the model domain.

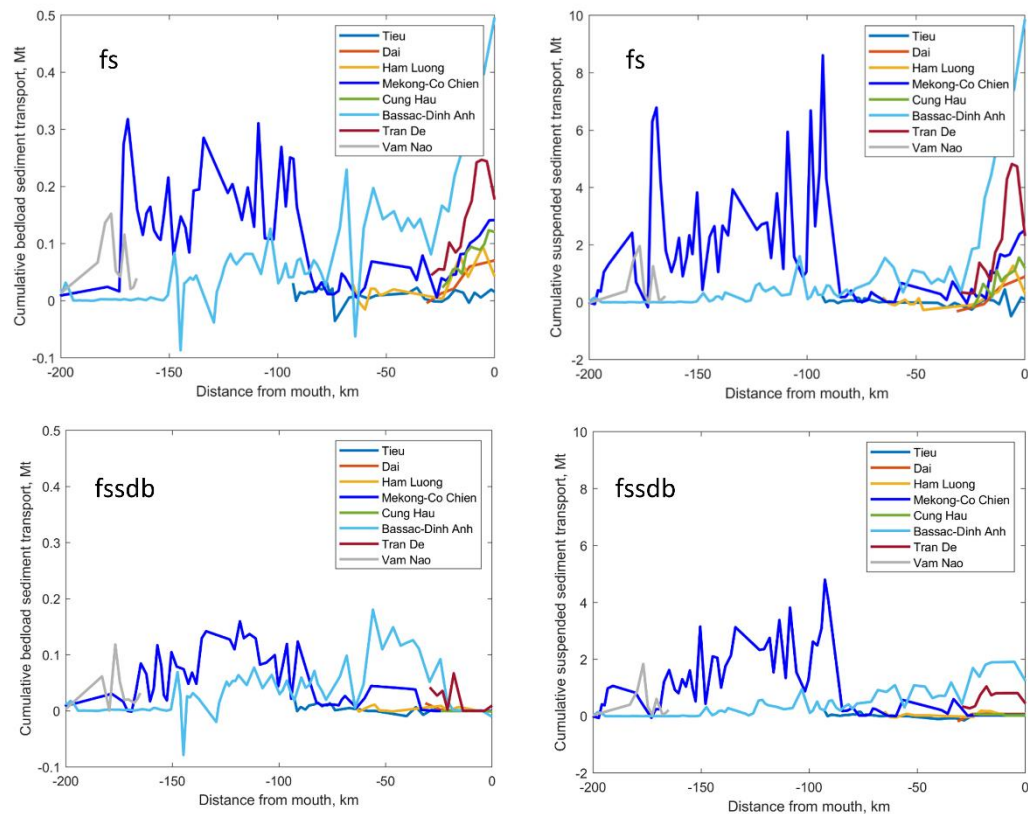


Figure 4-22: 2022 cumulative bed load (left column) and suspended load (right column) sand transport for runs *fs* (upper row) and *runfssdb* (lower row)

Preliminary model runs show that the “spiky” behaviour decreases when the model allows for morphodynamical adaptation, which can be a useful spin-up approach. Typically, the largest spikes would reduce 30% over a 3-year morphodynamic run. The spatial gradients in sand transport thus lead to morphodynamical change that smoothens the bathymetry and reduces the spatial transport gradients. Yet, assuming that a large part of these irregularities is caused by the limited resolution of the bathymetry, it can be concluded that the calculated

morphodynamics do not have a close relation to the real morphodynamic changes. Morphodynamic runs are not further considered in this study.

At some locations the bed load transport shows negative (i.e., landward) transport. These locations are associated with confluences of branches or locations downstream of islands in a branch. They are more or less artificial and likely related to simplifications in the schematisations and should therefore be ignored.

Figure 4-23 shows the sensitivity analysis with respect to the sand diameter. A larger diameter indeed leads to a reduced overall load, but a proportionally larger bed load transport and a proportionally lower suspended sediment transport. Applying a 100 μm sand diameter leads to largest transports albeit that the maximum sand transports ($\sim 12 \text{ Mt/yr}$) remain small compared to the mining volumes ($\sim 50 \text{ Mt/yr}$).

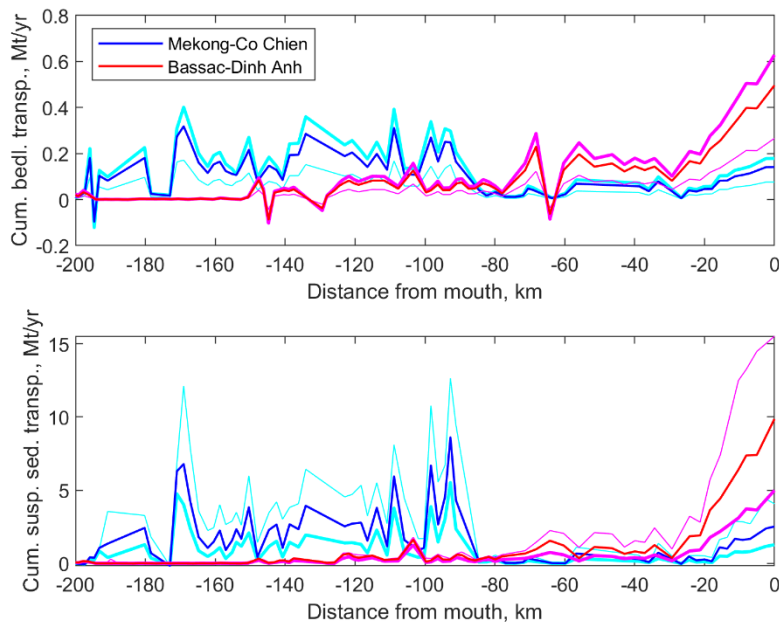


Figure 4-23: 2022 cumulative sand transport along Co Chien and Bassac branches. Solid line reflects runfs whereas thin lines reflect runfsD100 and thick lines runfsD300.

Remarkably, cumulative sand transports increase considerably towards many of the mouths of the branches. At the same time, Gugliotta et al (2017) and Figure 4-5 show that these areas are mud-covered in reality, with very limited amounts of sand being present. The larger sand transports in the mouth must thus be considered as a model deficit.

Figure 4-22 also shows the results of runfssdb with an adapted sand availability in the bed describing limited sand availability the first 25 km from the mouth and limited amounts in the VMD based on the sand availability analysis described in Chapter 3. In that case the transported sand volumes are reduced throughout the domain but especially in the mouth areas.

Figure 4-24 and Figure 4-25 show the yearly mud and sand volumes for runfsm including both sand and mud. Mud volumes are typically an order of magnitude larger than the sand volumes. Also, spatial spikiness is much less. This is because the fine sediment remains in suspension more easily than sand so that it is less subject to local velocity variations. The fine sediment transport is thus governed by advection-diffusion processes rather than suspension-deposition processes in case of sand. Areas with no sand availability prohibit local sand transports. Also, general sand transport volumes reduce by 10-20% due to the presence of mud in the bed hindering the suspension and transport of sand.

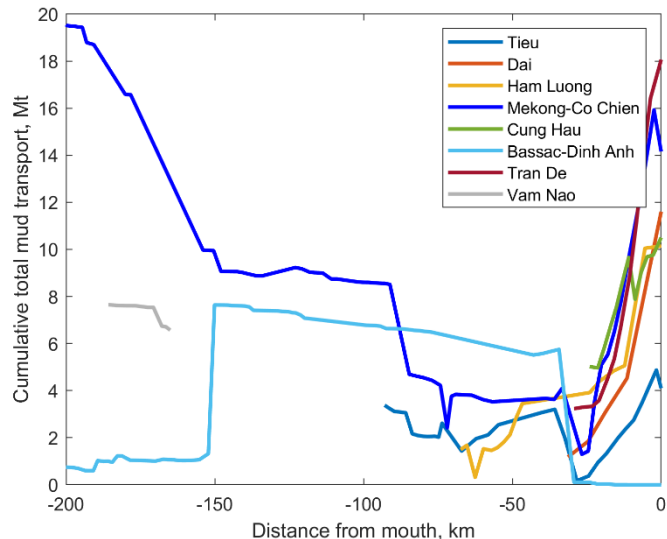


Figure 4-24: 2022 cumulative mud transport for runfsm

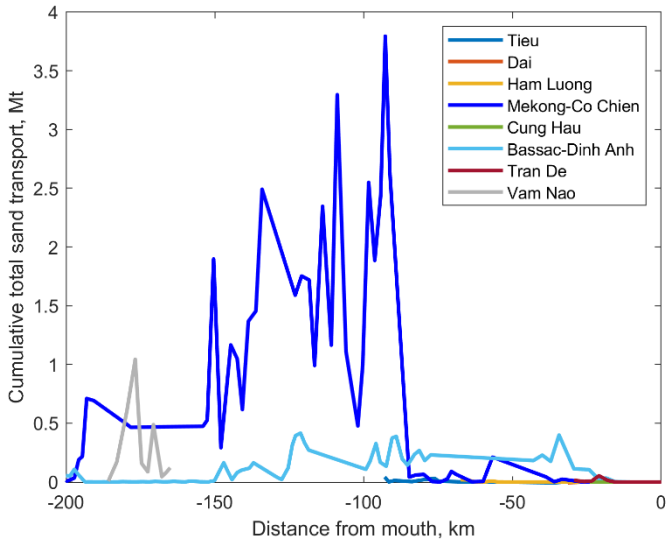


Figure 4-25: 2022 cumulative total (bed load + suspended load) sand transport for runfsm.

4.6 Comparison to fine sediment transport modelling

Thanh et al. (2021) calibrated their model of fine cohesive sediment transport against estimated sediment loads from measurements. Table 5-3 compares the cumulative fine sediment transport magnitude by Thanh et al (2021) with cumulative sand transport magnitude (suspended load and bed load) in this study (runfsm). Clearly, the fine sediment transport is much larger than suspended sand transport, while bed load is much smaller than the suspended sand transport. The transported fine sediment remains low, at about 30% of the fine sediment load in Thanh et al (2021). This is perhaps due to the higher river flow during year 2018 for which Thanh et al. (2021) derived the budget. Sand transport at the mouths of the different branches is hardly present in this study (at least in most realistic runfsm) due to the limited sand availability in that area. Thanh et al (2021) applied a solid riverbed, therefore,

mud volumes in the mouth in the current study (having an initial mud stock in the mouth bed) are much larger.

The modelled estimates of bedload and suspended load sand transport entering the VMD at Tan Chau (3.1 Mt/yr) are lower than estimated volumes, 6.18 ± 2.01 Mt/yr for the 2013-2014 period, by Hackney et al. 2020.

Table 4-5: Sediment load through cross-sections. * Indicates mouth cross-section.

Station	Fine sediment (Thanh et al 2021.) for 2011 [Mt]	Fine sediment (this study runfsm) for 2022 [Mt]	Suspended load sand (this study runfsm) for 2022 [Mt]	Bedload sand (this study runfsm) for 2022 [Mt]
Kratie	99.6	36.5	3	0.3
Chroy Changvar	93.6	33.6	10	0.6
OSP MRC	11.3	5.6	0.0	0.00
Koh Norea	72.4	29.9	2.8	0.3
Chau Doc	4.5	3.1	0.0	0.0
Tan Chau	73.9	21.8	3.0	0.14
Vam Nao	25.8	7.6	0.9	0.07
Can Tho	21	6.7	0.11	0.05
My Thuan	30.7	8.6	0.16	0.05
Tran De*	3.3	18.6	0.04	0.0
Dinh An*	8.8	0.0	0.04	0.0
Cung Hau*	3.3	10.3	0.0	0.0
Co Chien*	2.8	14.1	0.0	0.0
Ham Luong*	1.3	10.1	0.0	0.0
Dai*	1.9	11.6	0.0	0.0
Tieu*	1.4	4	0.0	0.0

4.7 Sand transport modelling discussion

Validation of the model results against measured sand concentrations remains a challenge, especially regarding the suspended sand load. The unique, MBES derived bed load estimates from this study are typically larger but of the same order of magnitude as the modelled bed load. Although suspended sand transport forms the largest contribution to the total sand transport, no measurements are available on suspended sand concentration. Model results and scarce data from locations upstream in Cambodia and at the Cambodian border suggest that suspended sand transport is an order of magnitude larger than bed load, whereas the transport of fines (silt/mud) is an order of magnitude larger than suspended sand transport. This is confirmed by model results.

Model results show that total 2022 sand transport volumes remain small compared to yearly estimated sand mining volumes of ~50 Mt/yr for a variety of model parameter settings. Maximum sand transport volumes hardly exceed 7Mt/yr and are often, and for large parts of the VMD, much less. As expected, modelled bed load transports are typically an order of magnitude smaller than suspended load transports. Model input is subject to data scarcity and validation data remains spatially scarce and of limited quality. This leads to an uncertainty range in model output and its interpretation. Sensitivity analysis shows that sand transports are a function of sediment diameter, sediment availability and the presence of mud. However, Figure 4-26 shows that sand transports remain low compared to estimated mining volumes for a range of best estimate model input parameter variations. Applying an unrealistic 50% decrease in diameter somewhat (~30%) increases maximum sand transport volumes at some locations. Applying more realistic sand availability distribution and mud presence reduces sand

transport volumes by 20-30%. Runfsm may be considered as the most realistic run. The impact of mud property variation (runfsmc and runsmf) remains limited.

Our modelling approach was suitable to assess the system scale sand transport behaviour, like the seasonal fluctuations and the decline in sand transport trends in the VMD. Interpreting and translating the model results towards smaller scales raises more questions. This holds, for example, when provincial sand budgets need to be derived. The primary reason for the concern is that sand transport through a certain cross-section highly depends on the quality of the bathymetry in that cross-section. As a result, the modelled sand transport through cross-sections some km's upstream or downstream could easily differ a factor 2-5. The model results are based on the sand transport capacity. In reality, sand transport would also depend on varying sand availability in the bed, detailed turbulence patterns and lag effects. Model results would be more reliable when these detailed data are available at provincial boundaries to calibrate a higher resolution of the model on local conditions. Finally, some of the provincial boundaries are located along the thalweg of Mekong River branches. This implies that lateral distribution of sand becomes an important factor. Model results on the cross-sectional distribution of sand erosion and deposition volumes could not be validated and could easily differ by a factor 2-3 from [missing] observed volumes.

We stress that the modelled sand transports and budgets presented in this report should be interpreted with care. Especially the sand transport towards the sea at the estuarine mouth of the different branches are considered not representative due to the 2D approach not covering 3D salt-fresh water dynamics. Still, model results suggest that the sand supply towards the mouth area remains rather small compared to sand supply volumes into the VMD.

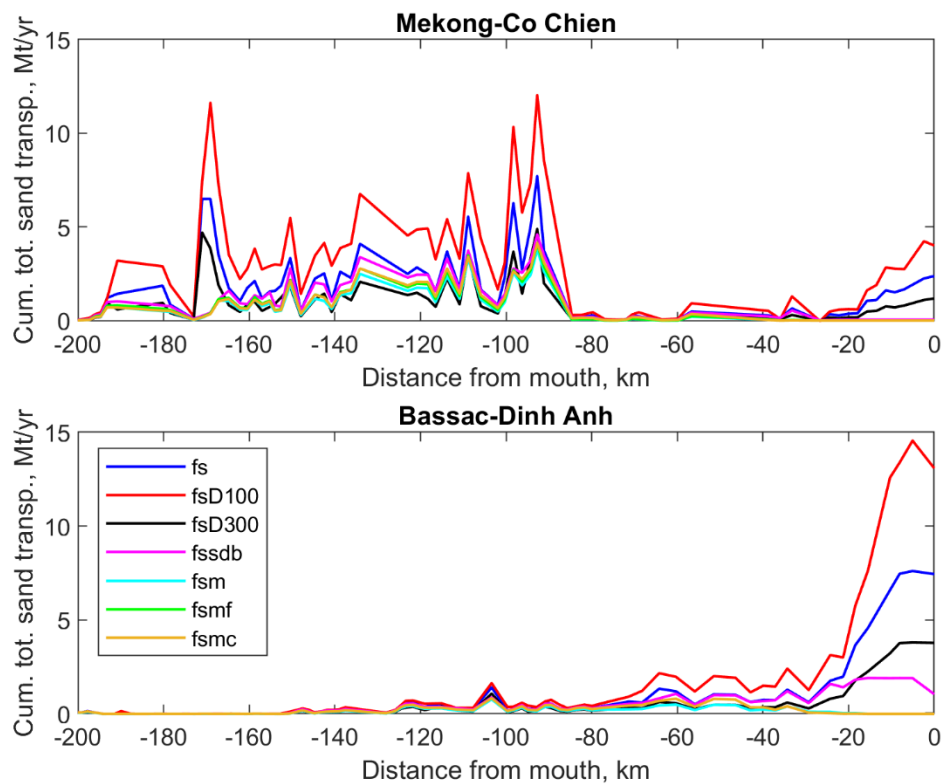


Figure 4-26: 2022 cumulative sand transport along two main Mekong branches for different model runs, where runfsm may be considered as the most adequate.

5 Stakeholder engagement

5.1 Consultations

Consultation meetings were carried out at regional level with Vietnam Mekong River Committee, national level with 4 ministries (MONRE, MARD, MOC, MPI) and provincial level with 13 provinces (DONRE & DARD). The list of consultant meetings is provided in Table 5-1 while more details can be found in Appendix B. Other consultants had been sent related documents and information via email. Some key findings from consultation are also summarized in the following paragraph for attention.

Table 5-1: List of Consultation Meetings

#	Name of Organization	Time for Consultation	Type of Communication	Contact Person
1	Department of National Remote Sensing	25/02/2022	Direct meeting	Ms Loan, Clerical Assistant 097 7036268 Mr Lê Quốc Hưng, 0914486663 Mr Đạt, 0983156866
2	Department of building materials - Ministry of Construction	21/02/2022	Email	Mr Hùng: 0983197966 Email: luongvanhungbxd@gmail.com
3	Department of Planning Management - Ministry of Planning and Investment	01/03/2022	Online meeting	Clerical Assistant, Mr Sơn: 0898579189 In charge: Ms Nguyễn Thị Thu Phương 0902186816 - Specialist Ms. Đinh Tam Hien- Department of Planning Management
4	Can Tho University	01/03/2022	Online meeting	Climate Change Research Institute Email: vbdkh@ctu.edu.vn Mr Tuấn 0908909063
5	General Department of Geology and Minerals of Vietnam;	01/03/2022	Email	Mr. Lưu Thế Long 0918840648 Email: long.luu2003lddb@gmail.com
6	Department of Agriculture and Rural Development; Departments of Natural Resources and Environment of Tien Giang, Ben Tre, Tra Vinh, Soc Trang, Vinh Long, Can Tho, Hau Giang, An Giang, Dong Thap provinces	21-25/02/2022	Direct meeting	

Some key points were discussed in these meetings and are summarised as follows:

- Key comments / feedbacks:
 - ✓ The project results can be integrated into local provincial planning;
 - ✓ It is necessary to review existing regulations, clarify the main objectives of sand mining plan and identify the key authority who is responsible for sand mining management and planning;
 - ✓ Project results are expected to be shared to integrate into the provincial planning;
 - ✓ Most agencies showed their willingness to support and share relevant data /information but the data sharing mechanism as well as relevant costs (in compliance with legal regulations) would be discussed and accepted by higher managers;
 - ✓ Two models are proposed to use for VMD hydrodynamic and sediment simulation in this project (Delft3D-FM and TELEMAC) so the integration of these models is important.

Secondary data collection: Most relevant data / information has been gathered. Data includes reports, documents, previous and /or existing studies / projects that were available. After the first progress report conference took place on July 14, 2022, in Ho Chi Minh City, the Deltares Research Institute (Netherlands) consulting unit, in collaboration with the Center for Environmental Hydrodynamics (CEFD - Vietnam), implemented a plan to collect geological borehole data in the Mekong Delta. With the active support of the General Department of Geology and Minerals and the Departments of Natural Resources and Environment of the provinces in the study area, the consulting unit has collected over 20 documents, mainly reports on the regulation of natural resources, planning for exploration, exploitation, and use of minerals, and levelling sand and river sand as common building materials. The above documents provide borehole coordinates, depth, depth of each layer/geological section, depth of soil surface, grain-size analysis of soil samples taken from boreholes, and sand dune information such as length, width, coordinates, estimated total sand reserves, sand quality, etc., which meet the needs of calculating reserves and distribution of sand resources in the Mekong Delta and the provinces in the study area.

5.2 Workshops

Workshops are one of the key activities for stakeholder engagement, aiming to keep relevant stakeholders informed and involved in project activities and its progress throughout the project. During the first 6 months of the project, two workshops were held, 1) the inception workshop on 3rd March 2022, 2) the 1st progress workshop on 14th July 2022, and 3) the 2nd progress workshop on 18th May 2023. The workshops were organized in hybrid mode (online and offline) by WWF Vietnam, in coordination with the Vietnam Disaster Management Authority (VNDMA) as the main counterpart. Most key stakeholders as indicated in the inception phase participated. Presentations and other supporting materials (such as leaflet, questionnaire) were prepared by the Consultant and reviewed by WWF – Vietnam before the workshop. A Q&A section was held right after the consultant's presentations for an open and fruitful interaction with stakeholders. Besides the Q&A section, a questionnaire was distributed to all participants for written responses to the Consultant's works.

5.2.1 Inception workshop

The inception workshop (3rd of March 2022) was intended to introduce the team members to the stakeholders and collect feedback on the proposed approach of the project as well as the details of the two work packages of field observation and modelling. The following summarizes the main takeaways:

- Locations of monitoring stations: the initial locations for survey was proposed by the Consultant and consulted with WWF – Vietnam, VNDMA and all participants. Most key stakeholders agreed with the selected locations and survey schedule.
- The accuracy of monitoring methods: Methods of monitoring have proven to be applicable worldwide up to international or national standards or guidelines.
- Data collection for model calibration and validation: Most historical and near real-time hydrodynamic and sediment observation data up to 2022 will be provided by SRHMC, the sub-consultant of the Deltares JV. Other data have been obtained from previous studies. Data will be checked and verified before being used for modelling works.
- Training needs: the consortium team will provide training for technical officers at both national and provincial levels.



Figure 5-1: Inception workshop in Can Tho

5.2.2 1st Progress workshop

The 1st progress workshop (12th of May 2022) was intended to collect feedback on the first measurement campaign and the early results of different work streams, especially as a preparation for the wet season field campaign. The following points were the main takeaways from the 1st progress workshop:

- Existing mobile sand stock will be estimated based on SBP measurements according to presented methodology in the inception report.
- Determination of eroded and deposited bank locations: the factors involved in the erosion and sedimentation processes will be analysed.
- Estimates of sand mining using satellite imagery: Google Earth Engine and classification algorithms will be applied to distinguish different types of ships for estimating the sand extraction volumes. However, it is essential to collect more information from local authorities to calibrate and validate the analysis.
- Moving a station between My Thuan and Tan Chau: In principle the locations are previously agreed upon. However, there was a discussion to consider moving one of the stations from downstream (near the sea) upstream (between Tan Chau and My Thuan) to have additional information for that stretch of the rivers. The counter arguments were that a) the additional station may not increase our system understanding as it is only one point of reference with

relatively similar conditions to its upstream and downstream stations compared to a station that is near the sea and influenced by salinity, and b) lack of reliable water level data nearby can potentially compromise the accuracy of those MBES observations.

- Data sharing and exchange: Data sharing with the local authorities should follow governmental regulations. Data exchange with MRC is needed and requires some further coordination between the consortium and WWF – Vietnam.

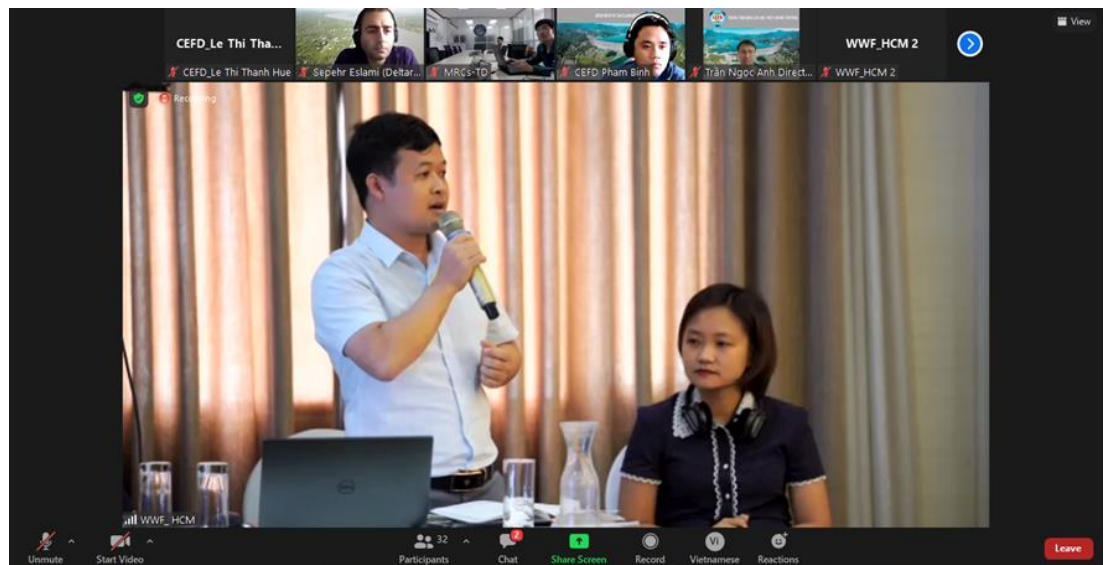


Figure 5-2: Consortium team members answered participant's questions during 1st Progress workshop.

5.2.3 2nd Progress workshop (Validation Workshop)

The 2nd progress workshop (18th of May 2023) was to reflect on the completed field campaigns and especially collect feedback on the draft sand budget of the Mekong Delta. A summary of the main takeaways is presented in below bullet-wise:

- Results of the following activities were presented at the workshop: field campaign, bedload transport, satellite image estimation of sand mining, existing mobile sand stock estimation, sand budget modelling.
- Responses from provinces' officials show that the results are overall in line with the data from localities.
- However, there are some needs to be further detailed and visualized the sand stock results for each province so they could integrate them into the Provincial Planning.



Figure 5-3: Consortium team members presenting draft sand budget results in the 2nd progress workshop.

5.3 Trainings

5.3.1 Training on monitoring

In order to exchange the knowledge of essential measurements and survey required for the sand budget study, a two-day training workshop was organized on March 28 and 29, 2022 in Vinh Long City. A total of 35 participants joined the training, mostly technical staffs from MONRE, MARD, DONREs and DARDs. The training focused on two main topics: (i) methods and plan for hydrodynamic and suspended sediment monitoring including data post-processing and (ii) methods and plan for sand dune tracking and sub-bottom profiling. A theoretical training was given on the 1st day and then followed by a field training at My Thuan hydrological station for practical demonstrations on the 2nd day. Q&A session were intensively integrated during training, which was facilitated by proactive interactions between trainees and trainers. The training materials were also distributed to the participants in Vietnamese for easy understanding and later references. During the training, several questions were raised about methods and their accuracy. Experts of the consortium team expanded on the methods to thoroughly address the concerns of the audience.



Figure 5-4: Demonstration / testing EdgeTech 6205s (Multi-beam Echo Sounder, MBES) components

5.3.2 Training on modelling

In pursuit of the primary goal of introducing fundamental functionalities and offering comprehensive guidance on mesh generation, bathymetry interpolation, hydrodynamic model setup, model execution, and post-processing results utilising Delft 3D-FM and the sediment model for the Mekong Delta, a two-day training workshop was convened on July 06 and 07, 2023, in Can Tho City.

The workshop participants included representatives of various agencies and organisations, including the Vietnam Disaster and Dyke Management Authority, the Vietnam Mekong River Commission Office in Ho Chi Minh City, the Vietnam Geological Department, and the Vietnam Minerals Authority. Also present were representatives from the Departments of Agriculture and Rural Development and the Departments of Natural Resources and Environment of An Giang, Dong Thap, Can Tho, Hau Giang, Vinh Long, Ben Tre, Tra Vinh, Soc Trang, and Tien Giang. Additionally, representatives from WWF Vietnam and various research institutions, universities, and research units participated in the event.

As part of the preparatory phase for the training course, a comprehensive survey was conducted to gauge the participants' familiarity with sediment transport models. Out of the 20 survey forms collected from the trainees, it was observed that a mere two individuals (10% of the respondents) had prior experience or practical exposure to sediment transport models in their professional endeavours. This indicated that most of the trainees, comprising 18 individuals (90% of the respondents), had yet to experience such models. The survey also provided valuable insights into the trainees' expectations and aspirations regarding the training course. Among the respondents who had not previously encountered or used sediment transport models, a unanimous and unwavering desire was expressed to augment their knowledge, understanding, and proficiency in effectively utilising the sediment transport model for their work-related tasks. The trainees perceived the training course as an exceptional opportunity to bridge their knowledge gap and acquire practical skills, significantly enhancing their professional capabilities.

Table 5-2: Survey statistics of participants before the training course on using the model.

Category	Evaluation				
	Excellent	Good	Fair	Average	Limited
Creating mesh			1	1	
Bathymetry Interpolation			2	1	
Preparing boundary conditions		1	2	1	
Setting parameters of model		1	2		
Post-processing results			1	1	
Establishing sediment transport model					

The training course was meticulously designed to impart essential knowledge and practical skills required for effectively utilising the sediment transport model in the project. Participants were introduced to the model's core functionalities and were systematically guided through a comprehensive set of steps for its successful implementation. The course covered crucial aspects such as mesh creation, bathymetry interpolation, boundary condition preparation, model parameter setting, result processing, and sediment transport model establishment.

Upon the conclusion of the training, the participants conducted a post-training assessment to evaluate the effectiveness of the course and its impact on their learning outcomes. The evaluation involved surveying the participating members to gauge their level of proficiency in using the sand budget model, which constitutes a vital component of the sediment transport model. Notably, the results obtained from the post-training survey indicated that the participants demonstrated commendable proficiency, achieving positive outcomes in their utilisation of the sand budget model (see Table 5-3 for detailed results).

In addition to the technical assessment, the training course received feedback from the participating members through evaluation forms. The responses were overwhelmingly positive, with participants expressing satisfaction with the training course's quality, content, and delivery. The participant feedback reflected a high level of appreciation for the valuable insights gained and the practical applicability of the acquired knowledge. Detailed feedback and participant evaluations can be found in Table 5-4.

Table 5-3: Survey statistics of participants after the training course on using the model.

Category	Evaluation				
	Excellent	Good	Fair	Average	Limited
Creating mesh	6	9	5	1	
Bathymetric Interpolation	6	7	8		
Preparing boundary conditions	5	11	5		
Setting parameters of model	4	11	6		
Post-processing results	5	8	7	1	
Establishing sediment transport model	7	5	8		1

Table 5-4: Evaluation of the quality of the training course.

Category	Evaluation				
	Excellent	Good	Fair	Average	Limited
1. Training content	8	13			
2. Training materials	8	12	1		
3. Quality of instructors/lecturers	10	11			
4. Level of student absorption/comprehension	5	12	3		

The training course proved to be a resounding success, fulfilling its objective of equipping the participants with the necessary expertise to employ the sediment transport model proficiently. The positive post-training assessment results and participant feedback underscore the effectiveness of the training in enhancing the participants' understanding and skill set, ensuring their ability to apply the model effectively in the project's context. The knowledge gained from the training course will undoubtedly contribute to the project's overall success in addressing sediment transport challenges and environmental management.



Figure 5-5: Modelling training in Can Tho.



Figure 5-6: Training to use sand budget model.

6 Sand Budget Mekong Delta (WP2)

To establish a sand budget for the VMD, five factors needed to be determined: **1)** the sand entering the Mekong Delta, **2)** sand movement within the delta, **3)** existing mobile sand stock of the VMD, **4)** sand extraction from the delta, and **5)** sand leaving the delta. Figure 6-1 provides an overview of how different components of the current study contribute to the delta-wide sand budget. Sand input from upstream is obtained from numerical modelling results, calibrated with MRC upstream data and collected field measurements (MBES). Sand extraction in different river sections is estimated from satellite imagery. Sand movement in the delta, as well as sediment leaving the delta is captured by the numerical model and supported by MBES measurements. Finally, the existing mobile sand stock within the delta is derived from a ~550 km of sub-bottom profiling measurement.

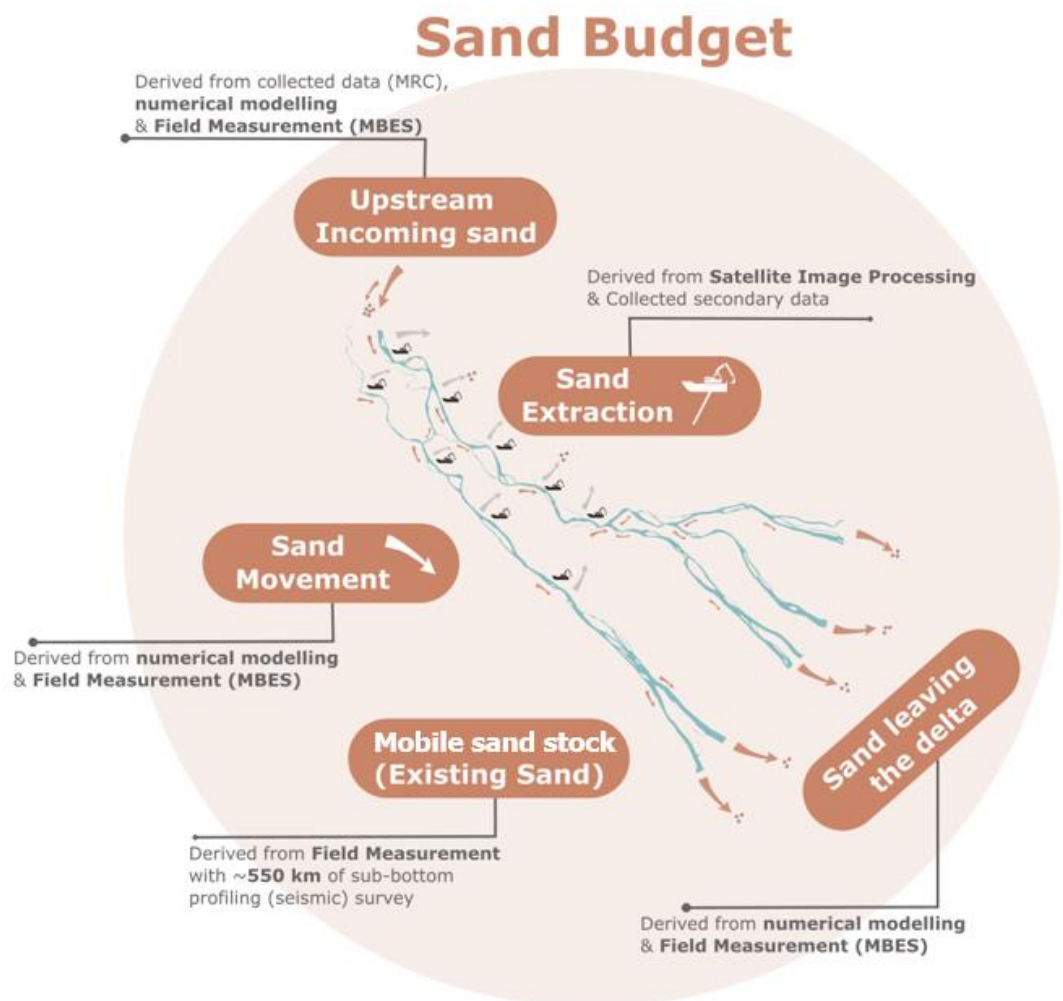


Figure 6-1: An overview of contribution from different activities leading to the VMD sand budget.

Various components of the sand budget have been finalized in different sections of the report. From the analysis we have identified that the sediment entering the data is in the order of 2-4 M m³/yr while the exchange with the ocean is expected to be nearly negligible (0-0.6 M m³/yr). The estimation of existing mobile sand stock (*mostly mobile sand*) amounts to a nearly 367-550 M m³ of sand within the delta, while sand extraction is in the order of 35-55 M m³/yr. Figure 6-2 summarizes the sand budget of the Mekong Delta in a simple form as incoming, outgoing and extraction against the existing stock.

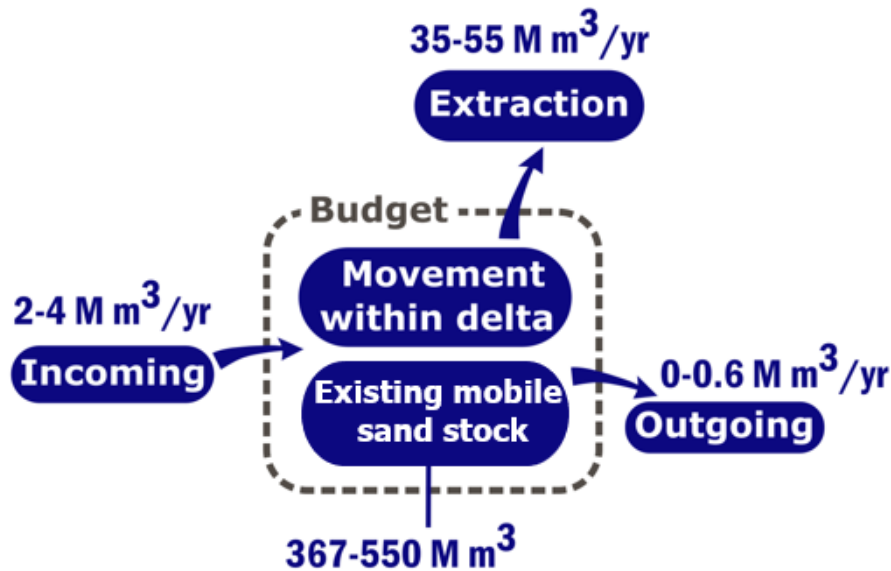


Figure 6-2: Estimates of various components of the sand budget.

The results of this study have significant implication for managing resources of the Mekong Delta. At current extraction rates, despite the marginal volumes of sand leaving the delta, given the limited upstream supply, we expect that current existing mobile sand stock can only last as far as a decade. Figure 6-3 shows the upper and lower estimates of the existing mobile sand stock decline under three different scenarios of extraction: a) 5% increase in current extraction rates, b) business as usual, and c) gradual reduction of extraction rates at a 5% rate. Under a mitigating regime of controlled reduction to river sand dependency, the existing mobile sand stock may last until 2040. However, this project does not study the morphological and environmental impacts of total extraction of the existing sand. While this will likely lead to further river bank instability (bank erosion) as well as coastal erosion, based on the projections of salinity by Eslami et al., (2021c), a loss of half a Billion m³ of sediment (in this case in form of sand) from the VMD riverine system can lead to an additional 10-15% increase in areas affected by salt intrusion within the VMD. Note that the existing sand budget is a snapshot in 2022. For example, the sand supply from upstream can decline because of further extraction in Cambodia, but as the supply is a small portion compared to the stock and extraction, this will have limited impact on the future projections. Furthermore, the erosion from sand mining upstream can also travel downstream. Therefore, it is advised to consider the transboundary nature of sediment management beyond the VMD in multi-lateral cooperations.

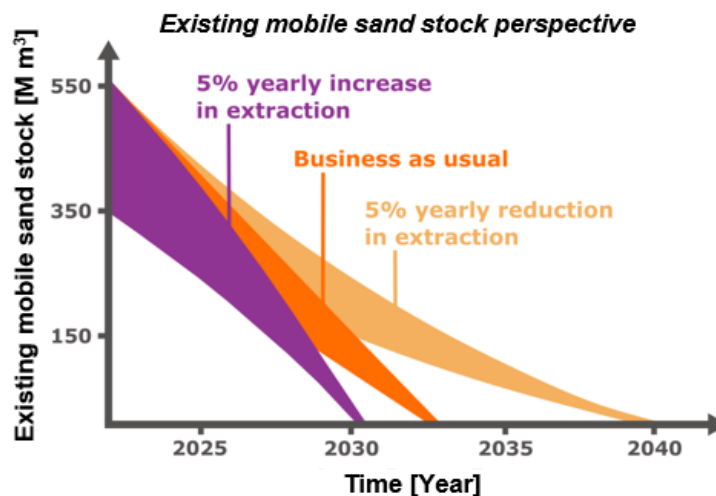


Figure 6-3: An outlook towards mid-century given the upper and lower estimates of incoming, outgoing, extraction and existing mobile sand stock.

7 References

- Achete, F. M., van der Wegen, M., Roelvink, D., and Jaffe, B.: Suspended sediment dynamics in a tidal channel network under peak river flow, *Ocean Dyn.*, 66, 703–718, <https://doi.org/10.1007/s10236-016-0944-0>, 2016.
- Allison, M. A., Weathers, D. H., and Meselhe, E. A.: Bottom morphology in the Song Hau distributary channel, Mekong River Delta, Vietnam, *Cont. Shelf Res.*, 147, 51–61, <https://doi.org/10.1016/j.csr.2017.05.010>, 2017.
- Anthony, E. J.: Deltas, <https://doi.org/https://doi.org/10.1002/9781119117261.ch13>, 9 March 2015.
- Ashley, G. M.: Classification of large-scale subaqueous bedforms; a new look at an old problem, *J. Sediment. Res.*, 60, 160–172, <https://doi.org/10.2110/jsr.60.160>, 1990.
- Bernard, L. and Stéphane, M.: Evolution of Ripple Field Architecture during Sediment Transport, as Measured by CT Scanning, in: *Sediment Transport*, IntechOpen, 2011.
- Bomers, A., Schielen, R. M. J., and Hulscher, S. J. M. H.: The influence of grid shape and grid size on hydraulic river modelling performance, *Environ. Fluid Mech.*, 19, 1273–1294, <https://doi.org/10.1007/s10652-019-09670-4>, 2019.
- Bravard, J.-P., Goichot, M., and Gaillot, S.: Geography of Sand and Gravel Mining in the Lower Mekong River, 26, <https://doi.org/10.4000/echogeo.13659>, 2013.
- Brunier, G., Anthony, E. J., Goichot, M., Provansal, M., and Dussouillez, P.: Recent morphological changes in the Mekong and Bassac river channels , *Mekong delta : The marked impact of river-bed mining and implications for delta destabilisation*, 224, 177–191, <https://doi.org/10.1016/j.geomorph.2014.07.009>, 2014.
- C., V. R. L., C., N. M. W., Theo, van der K., Eelco, N., and Arnold, van K.: Transport of Fine Sands by Currents and Waves, *J. Waterw. Port, Coastal, Ocean Eng.*, 119, 123–143, [https://doi.org/10.1061/\(ASCE\)0733-950X\(1993\)119:2\(123\)](https://doi.org/10.1061/(ASCE)0733-950X(1993)119:2(123)), 1993.
- Central Dredging Association: Clumshell or grab dredgers, in: *Lecture notes introduction to dredging equipments*, Delft university of Technology, Delft, 2023.
- Chapman, A. and Darby, S.: Evaluating sustainable adaptation strategies for vulnerable mega-deltas using system dynamics modelling: Rice agriculture in the Mekong Delta's An Giang Province, Vietnam, *Sci. Total Environ.*, 559, 326–338, <https://doi.org/https://doi.org/10.1016/j.scitotenv.2016.02.162>, 2016.
- Darby, S. E., Hackney, C. R., Leyland, J., Kumm, M., Lauri, H., Parsons, D. R., Best, J. L., Nicholas, A. P., and Aalto, R.: Fluvial sediment supply to a mega-delta reduced by shifting tropical-cyclone activity, *Nature*, 539, 276–279, <https://doi.org/10.1038/nature19809>, 2016.
- Donchyts, G., Baart, F., Winsemius, H., Gorelick, N., Kwadijk, J., and van de Giesen, N.: Earth's surface water change over the past 30 years, *Nat. Clim. Chang.*, 6, 810–813, <https://doi.org/10.1038/nclimate3111>, 2016.
- Dunn, F. E., Darby, S. E., Nicholls, R. J., Cohen, S., Zarfl, C., and Fekete, B. M.: Projections of declining fluvial sediment delivery to major deltas worldwide in response to climate change and anthropogenic stress, *Environ. Res. Lett.*, 14, 84034, <https://doi.org/10.1088/1748-9326/ab304e>, 2019.

- Eslami, S.: Environmental change in a mega-delta, dynamics of salt intrusion in the Vietnamese Mekong Delta, Utrecht University, <https://doi.org/10.33540/1367>, 2022.
- Eslami, S., Hoekstra, P., Kernkamp, H., Trung, N. N., Duc, D. Do, Quang, T. T., Februarianto, M., Dam, A. Van, and Vegt, M. van der: Flow Division Dynamics in the Mekong Delta: Application of a 1D-2D Coupled Model, <https://doi.org/10.3390/w11040837>, 2019a.
- Eslami, S., Hoekstra, P., Nguyen Trung, N., Ahmed Kantoush, S., Van Binh, D., Duc Dung, D., Tran Quang, T., and van der Vegt, M.: Tidal amplification and salt intrusion in the Mekong Delta driven by anthropogenic sediment starvation, *Sci. Rep.*, 9, 18746, <https://doi.org/10.1038/s41598-019-55018-9>, 2019b.
- Eslami, S., Hoekstra, P., Kernkamp, H. W. J., Nguyen Trung, N., Do Duc, D., Nguyen Nghia, H., Tran Quang, T., van Dam, A., Darby, S. E., Parsons, D. R., Vasilopoulos, G., Braat, L., and van der Vegt, M.: Dynamics of salt intrusion in the Mekong Delta: results of field observations and integrated coastal-inland modelling, *Earth Surf. Dyn.*, 9, 953–976, <https://doi.org/10.5194/esurf-9-953-2021>, 2021a.
- Eslami, S., Hoekstra, P., Minderhoud, P. S. J. ., Trung, N. N., Hoch, J. M. ., H.Sutanudjaja, E., Dung, D. D., TranQuang, T., Voepel, H. E. ., Woillez, M.-N., and Vegt, M. van der; Projections of salt intrusion in a mega-delta under climatic and anthropogenic stressors, *Nat. Commun. Earth Environ.* (accepted Publ., <https://doi.org/10.1038/s43247-021-00208-5>, 2021b.
- Eslami, S., Hoekstra, P., Minderhoud, P. S. J., Trung, N. N., Hoch, J. M., Sutanudjaja, E. H., Dung, D. D., Tho, T. Q., Voepel, H. E., Woillez, M.-N., and van der Vegt, M.: The projection data of saline water intrusion in the Mekong Delta under climatic and anthropogenic drivers, <https://doi.org/10.5281/zenodo.4772967>, May 2021c.
- Frappart, F., Do Minh, K., L’Hermitte, J., Cazenave, a., Ramillien, G., Le Toan, T., and Mognard-Campbell, N.: Water volume change in the lower Mekong from satellite altimetry and imagery data, *Geophys. J. Int.*, 167, 570–584, <https://doi.org/10.1111/j.1365-246X.2006.03184.x>, 2006.
- Gorelick, N., Hancher, M., Dixon, M., Ilyushchenko, S., Thau, D., and Moore, R.: Google Earth Engine: Planetary-scale geospatial analysis for everyone, *Remote Sens. Environ.*, 202, 18–27, <https://doi.org/https://doi.org/10.1016/j.rse.2017.06.031>, 2017.
- Gruel, C.-R., Park, E., Switzer, A. D., Kumar, S., Loc Ho, H., Kantoush, S., Van Binh, D., and Feng, L.: New systematically measured sand mining budget for the Mekong Delta reveals rising trends and significant volume underestimations, *Int. J. Appl. Earth Obs. Geoinf.*, 108, 102736, <https://doi.org/https://doi.org/10.1016/j.jag.2022.102736>, 2022.
- Gugliotta, M., Saito, Y., Nguyen, V. L., Ta, T. K. O., Nakashima, R., Tamura, T., Uehara, K., Katsuki, K., and Yamamoto, S.: Process regime, salinity, morphological, and sedimentary trends along the fluvial to marine transition zone of the mixed-energy Mekong River delta, Vietnam, *Cont. Shelf Res.*, 147, 7–26, <https://doi.org/10.1016/j.csr.2017.03.001>, 2017.
- Hackney, C. R., Darby, S. E., Parsons, D. R., Leyland, J., Best, J. L., Aalto, R., Nicholas, A. P., and Houseago, R. C.: River bank instability from unsustainable sand mining in the lower Mekong River, *Nat. Sustain.*, <https://doi.org/10.1038/s41893-019-0455-3>, 2020.
- Hackney, C. R., Vasilopoulos, G., Heng, S., Darbari, V., Walker, S., and Parsons, D. R.: Sand mining far outpaces natural supply in a large alluvial river, *Earth Surf. Dyn.*, 9, 1323–1334, <https://doi.org/10.5194/esurf-9-1323-2021>, 2021.
- Jean-Francois Pekel, Andrew Cottam, Noel Gorelick, A. S. B.: Global Surface Water Explorer dataset, <http://data.europa.eu/89h/jrc-gswe-global-surface-water-explorer-v1>, 2017.

- Jordan, C., Tiede, J., Lojek, O., Visscher, J., Apel, H., Nguyen, H. Q., Quang, C. N. X., and Schlurmann, T.: Sand mining in the Mekong Delta revisited - current scales of local sediment deficits, *Sci. Rep.*, 9, 17823, <https://doi.org/10.1038/s41598-019-53804-z>, 2019.
- Kernkamp, H. W. J., Van Dam, A., Stelling, G. S., and De Goede, E. D.: Efficient scheme for the shallow water equations on unstructured grids with application to the Continental Shelf, *Ocean Dyn.*, 61, 1175–1188, <https://doi.org/10.1007/s10236-011-0423-6>, 2011.
- Koehnken, L.: Discharge Sediment Monitoring Project (DSMP) 2009 - 2013: Summary & Analysis of Results Final Report, Mekong River Commission, Vientiane, Lao PDR, 2014.
- Kondolf, G. M., Rubin, Z. K., and Minear, J. T.: Dams on the Mekong: Cumulative sediment starvation, *Water Resour. Res.*, <https://doi.org/10.1002/2013WR014651>, 2014.
- Kummu, M. and Varis, O.: Sediment-related impacts due to upstream reservoir trapping, the Lower Mekong River, 85, 275–293, <https://doi.org/10.1016/j.geomorph.2006.03.024>, 2007.
- Lauri, H., De Moel, H., Ward, P. J., Räsänen, T. A., Keskinen, M., and Kummu, M.: Future changes in Mekong River hydrology: Impact of climate change and reservoir operation on discharge, *Hydrol. Earth Syst. Sci.*, 16, 4603–4619, <https://doi.org/10.5194/hess-16-4603-2012>, 2012.
- Le, T. V. H., Nguyen, H. N., Wolanski, E., Tran, T. C., and Haruyama, S.: The combined impact on the flooding in Vietnam's Mekong River delta of local man-made structures, sea level rise, and dams upstream in the river catchment, *Estuar. Coast. Shelf Sci.*, 71, 110–116, <https://doi.org/10.1016/j.ecss.2006.08.021>, 2007.
- Leary, K. C. P. and Buscombe, D.: Estimating sand bed load in rivers by tracking dunes: a comparison of methods based on bed elevation time series, *Earth Surf. Dyn.*, 8, 161–172, <https://doi.org/10.5194/esurf-8-161-2020>, 2020.
- Lu, X., Kummu, M., and Oeurng, C.: Reappraisal of sediment dynamics in the Lower Mekong River, Cambodia, *Earth Surf. Process. Landforms*, 39, 1855–1865, <https://doi.org/10.1002/esp.3573>, 2014.
- Manh, N. V., Dung, N. V., Hung, N. N., Merz, B., and Apel, H.: Large-scale suspended sediment transport and sediment deposition in the Mekong Delta, *Hydrol. Earth Syst. Sci.*, 18, 3033–3053, <https://doi.org/10.5194/hess-18-3033-2014>, 2014.
- Manh, N. Van, Dung, N. V., Hung, N. N., Kummu, M., Merz, B., and Apel, H.: Future sediment dynamics in the Mekong Delta floodplains: Impacts of hydropower development, climate change and sea level rise, *Glob. Planet. Change*, 127, 22–33, <https://doi.org/10.1016/j.gloplacha.2015.01.001>, 2015.
- Martyr-koller, R. C., Kernkamp, H. W. J., Dam, A. Van, and Wegen, M. Van Der: Application of an unstructured 3D finite volume numerical model to flows and salinity dynamics in the San Francisco Bay-Delta, *Estuar. Coast. Shelf Sci.*, 192, 86–107, <https://doi.org/10.1016/j.ecss.2017.04.024>, 2017.
- Milliman, J. D. and Fransworth, K. L.: *River Discharge to the Coastal Ocean: A Global Synthesis*, Cambridge University Press, Cambridge, 392 pp., 2011.
- Minderhoud, P. S. J., Middelkoop, H., Erkens, G., and Stouthamer, E.: Groundwater extraction may drown mega-delta: projections of extraction-induced subsidence and elevation of the Mekong delta for the 21st century, *Environ. Res. Commun.*, 2, 11005, <https://doi.org/10.1088/2515-7620/ab5e21>, 2020.
- MRC: *Overview of the Hydrology of the Mekong Basin*, Mekong River Commission, Vientiane, 2005.
- MRC: *The Flow of the Mekong*, Mekong River Comm., 1–12, 2009.

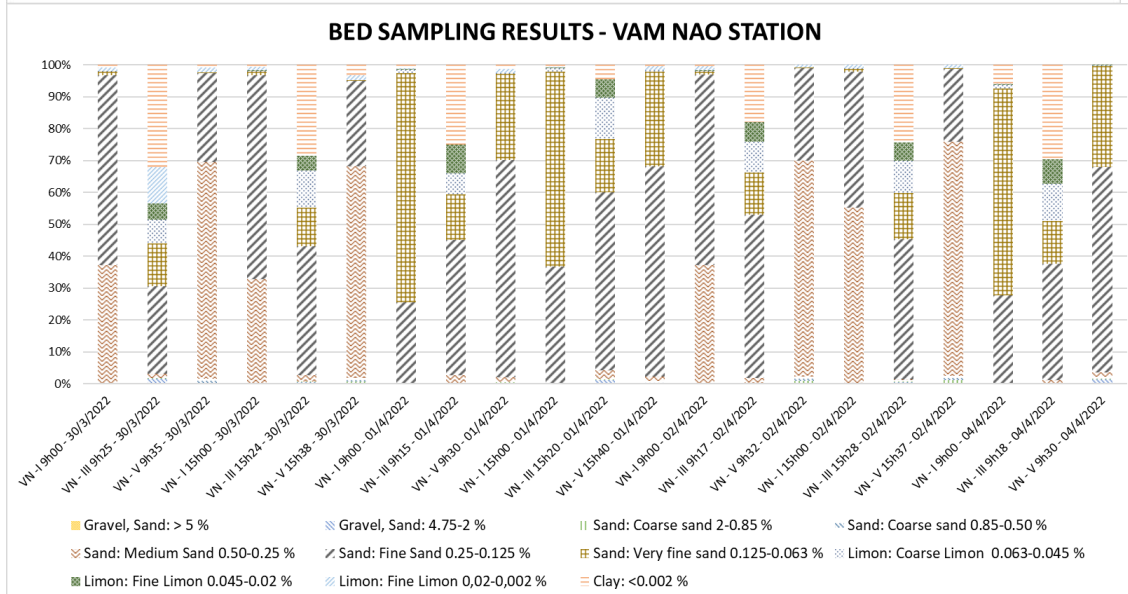
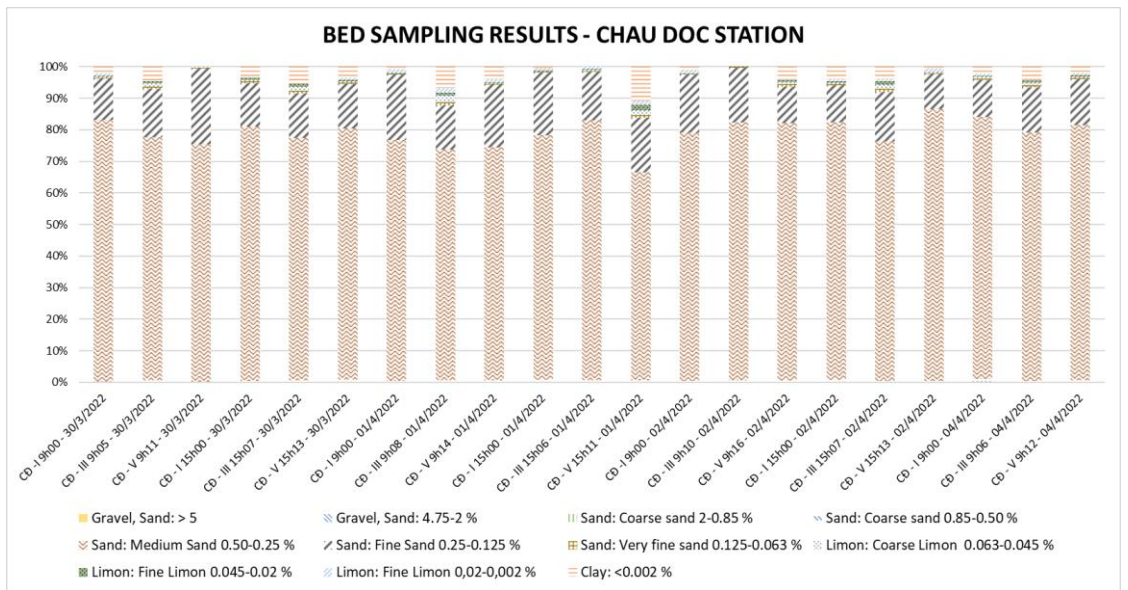
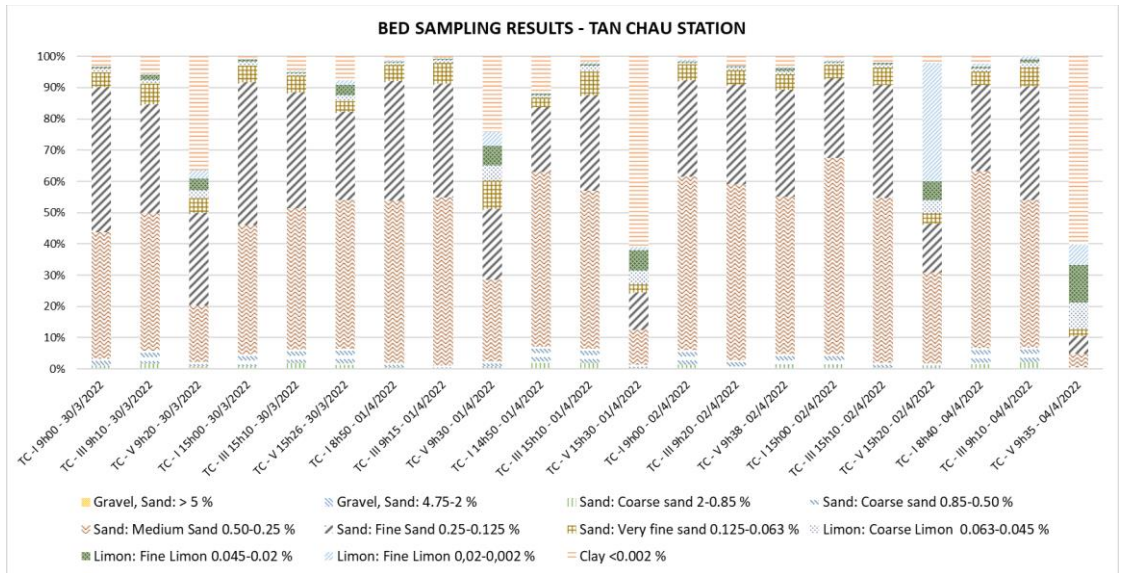
- N. Moriasi, D., G. Arnold, J., W. Van Liew, M., L. Bingner, R., D. Harmel, R., and L. Veith, T.: Model Evaluation Guidelines for Systematic Quantification of Accuracy in Watershed Simulations, *Trans. ASABE*, 50, 885–900, <https://doi.org/https://doi.org/10.13031/2013.23153>, 2007.
- Nash, J. E. and Sutcliffe, J. V.: River Flow Forecasting Through Conceptual Models Part I-a Discussion of Principles*, *J. Hydrol.*, 10, 282–290, [https://doi.org/10.1016/0022-1694\(70\)90255-6](https://doi.org/10.1016/0022-1694(70)90255-6), 1970.
- Simons, D. B., Richardson, E. V., and Nordin Jr., C. F.: Bedload equation for ripples and dunes, Professional Paper, <https://doi.org/10.3133/pp462H>, 1965.
- SIWRP: Report on existing sand exploitation and sand demand forecast up to 2020 and 2040 in lower mekong Delta, Ho Chi Minh City, Vietnam, 2015.
- Stephens, J. D., Allison, M. A., Di Leonardo, D. R., Weathers, H. D., Ogston, A. S., McLachlan, R. L., Xing, F., and Meselhe, E. A.: Sand dynamics in the Mekong River channel and export to the coastal ocean, *Cont. Shelf Res.*, 147, 38–50, <https://doi.org/10.1016/j.csr.2017.08.004>, 2017.
- Ta, T. K. O., Nguyen, V. L., Tateishi, M., Kobayashi, I., Saito, Y., and Nakamura, T.: Sediment facies and Late Holocene progradation of the Mekong River Delta in Bentre Province, southern Vietnam: An example of evolution from a tide-dominated to a tide- and wave-dominated delta, *Sediment. Geol.*, 152, 313–325, [https://doi.org/10.1016/S0037-0738\(02\)00098-2](https://doi.org/10.1016/S0037-0738(02)00098-2), 2002.
- Thanh, V. Q.: Modeling of hydrodynamics and sediment transport in the Mekong Delta, IHE-Delft, <https://doi.org/https://doi.org/10.4233/uuid:8f42f588-17a1-4e1e-af12-dcc52e7a26b2>, 2021.
- Thanh, V. Q., Reyns, J., Wackerman, C., Eidam, E. F., and Roelvink, D.: Modelling suspended sediment dynamics on the subaqueous delta of the Mekong River, *Cont. Shelf Res.*, 0–1, <https://doi.org/10.1016/j.csr.2017.07.013>, 2017.
- Thanh, V. Q., Roelvink, D., van der Wegen, M., Reyns, J., Kernkamp, H., Van Vinh, G., and Thi Phuong Linh, V.: Flooding in the Mekong Delta: Impact of dyke systems on downstream hydrodynamics, *Hydrol. Earth Syst. Sci. Discuss.*, 2019, 1–34, <https://doi.org/10.5194/hess-2019-64>, 2019.
- Thanh, V. Q., Roelvink, D., van Der Wegen, M., Reyns, J., Kernkamp, H., Vinh, G. Van, and Linh, V. T. P.: Flooding in the Mekong Delta: the impact of dyke systems on downstream hydrodynamics, *Hydrol. Earth Syst. Sci.*, 24, 189–212, 2020.
- Thi Ha, D., Ouillon, S., and Van Vinh, G.: Water and Suspended Sediment Budgets in the Lower Mekong from High-Frequency Measurements (2009–2016), <https://doi.org/10.3390/w10070846>, 2018.
- Tu, L. X., Thanh, V. Q., Reyns, J., Van, S. P., Anh, D. T., Dang, T. D., and Roelvink, D.: Sediment transport and morphodynamical modeling on the estuaries and coastal zone of the Vietnamese Mekong Delta, *Cont. Shelf Res.*, 186, 64–76, <https://doi.org/10.1016/j.csr.2019.07.015>, 2019.
- Van, P. D. T., Popescu, I., Van Griensven, a., Solomatine, D. P., Trung, N. H., and Green, a.: A study of the climate change impacts on fluvial flood propagation in the Vietnamese Mekong Delta, *Hydrol. Earth Syst. Sci.*, 16, 4637–4649, <https://doi.org/10.5194/hess-16-4637-2012>, 2012.
- Vasilopoulos, G., Quan, Q. L., Parsons, D. R., Darby, S. E., Tri, V. P. D., Hung, N. N., Haigh, I. D., Voepel, H. E., Nicholas, A. P., and Aalto, R.: Establishing sustainable sediment budgets is critical for climate-resilient mega-deltas, *Environ. Res. Lett.*, 16, 64089, <https://doi.org/10.1088/1748-9326/ac06fc>, 2021a.
- Vasilopoulos, G., Quan, Q. L., Parsons, D. R., Darby, S. E., Tri, V. P. D., Hung, N. N., Haigh, I. D., Voepel, H. E., Nicholas, A. P., and Aalto, R.: Establishing sustainable sediment budgets is critical for climate-resilient mega-deltas, *Environ. Res. Lett.*, 16, 064089, <https://doi.org/10.1088/1748-9326/ac06fc>, 2021b.

- Wassmann, R., Hien, N. X., Hoanh, C. T., and Tuong, T. P.: Sea level rise affecting the Vietnamese Mekong Delta: water elevation in the flood season and implications for rice production, *Clim. Change*, 66, 89–107, <https://doi.org/10.1023/B:CLIM.0000043144.69736.b7>, 2004.
- Wolanski, E., Huan, N. N., Dao, L. T., Nhan, N. H., and Thuy, N. N.: Fine-sediment dynamics in the Mekong River estuary, Viet Nam, *Estuar. Coast. Shelf Sci.*, 43, 565–582, 1996.
- Xing, F., Meselhe, E. A., Allison, M. A., and Weathers, H. D.: Analysis and numerical modeling of the flow and sand dynamics in the lower Song Hau channel, Mekong Delta, *Cont. Shelf Res.*, 147, 62–77, <https://doi.org/10.1016/j.csr.2017.08.003>, 2017.

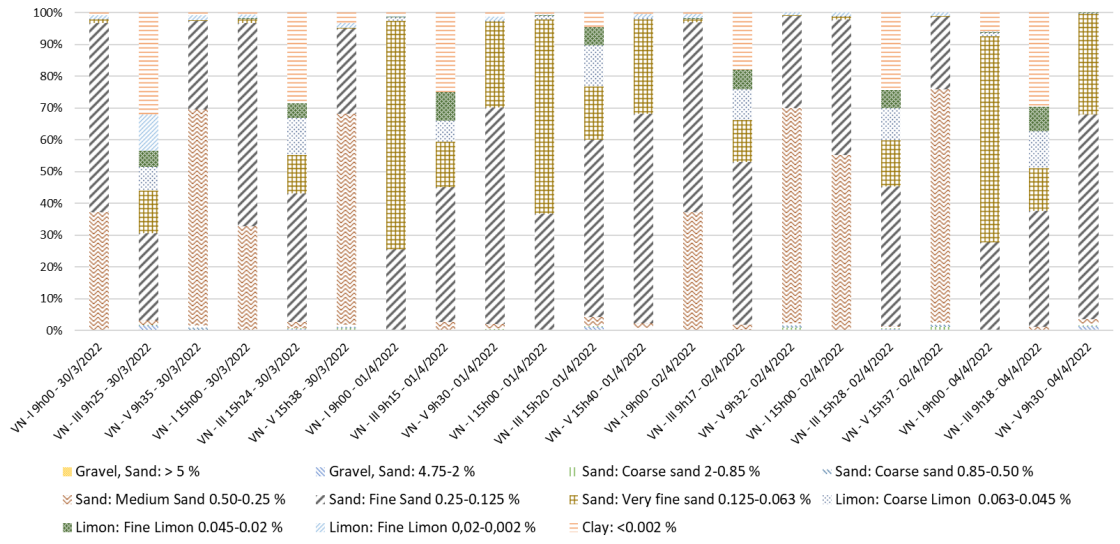
A Appendix-A

The detailed results of collected riverbed samples in both dry and wet seasons.

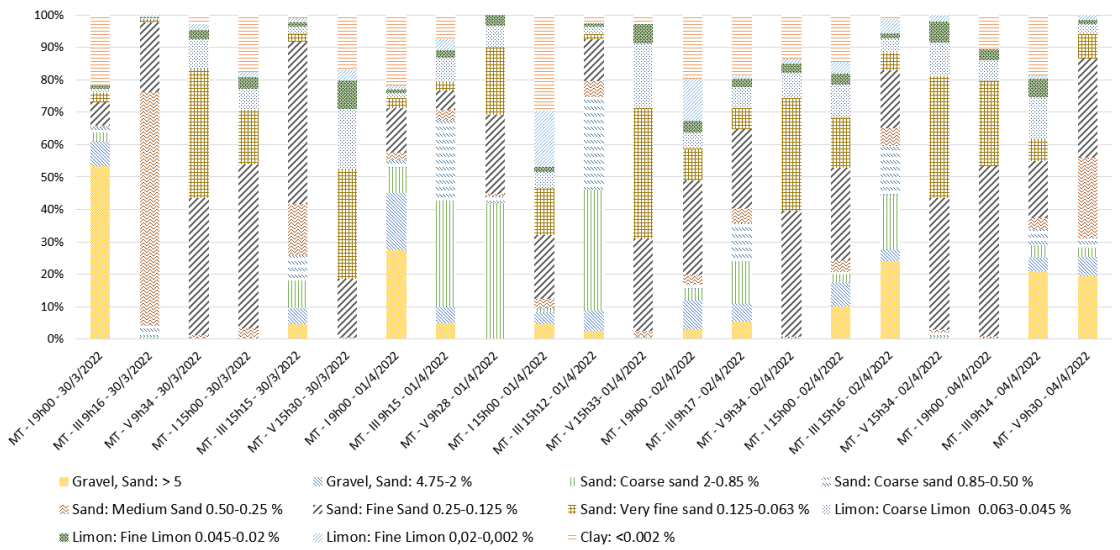
A.1 Dry season riverbed sampling results



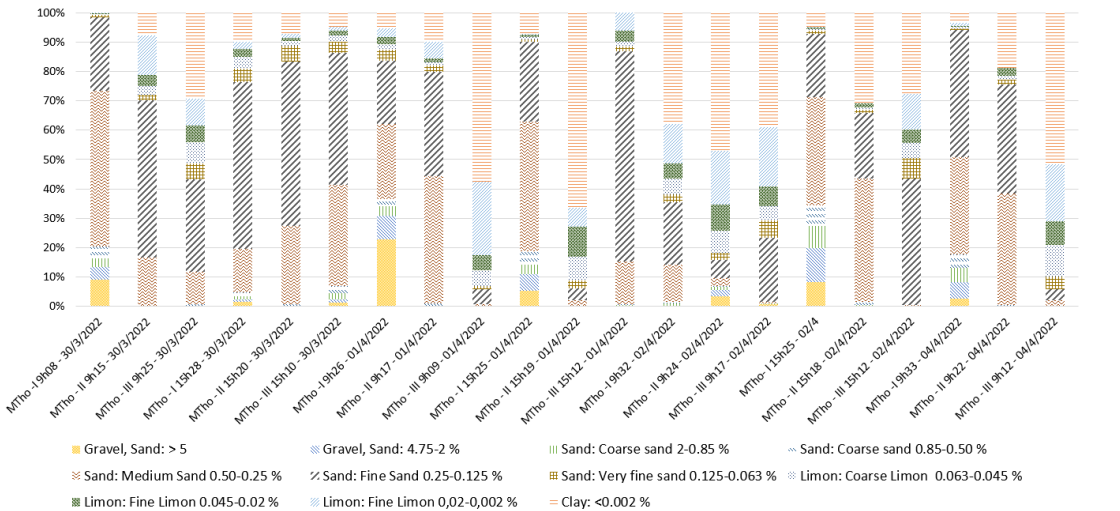
BED SAMPLING RESULTS - VAM NAO STATION



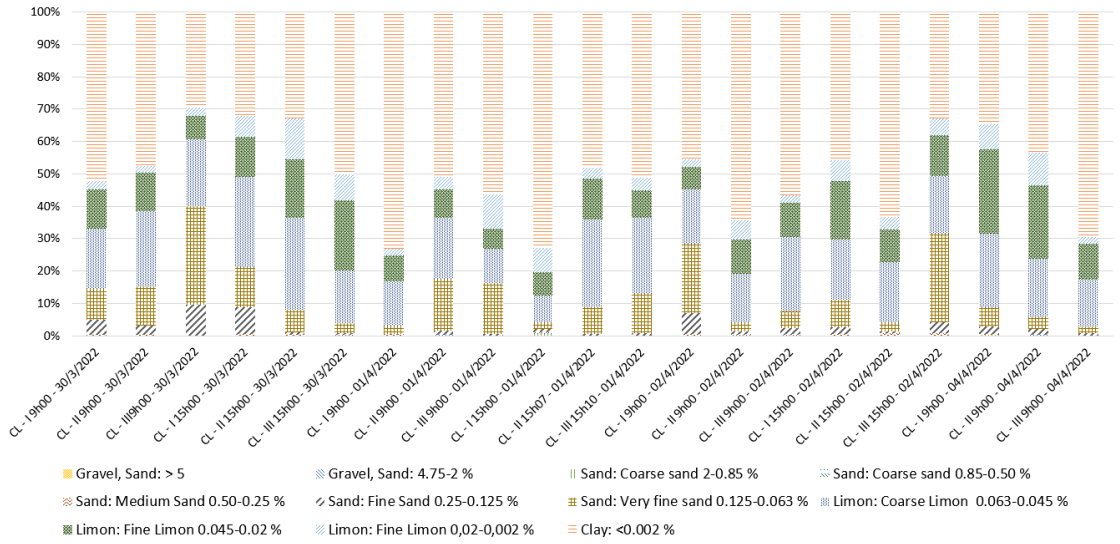
BED SAMPLING RESULTS - MY THUAN STATION



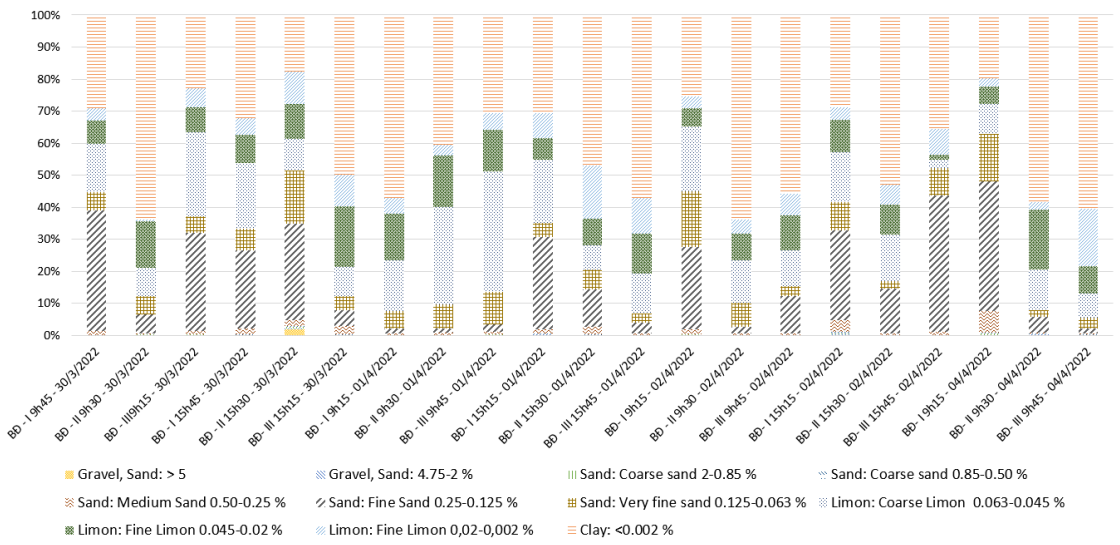
BED SAMPLING RESULTS - MY THO STATION



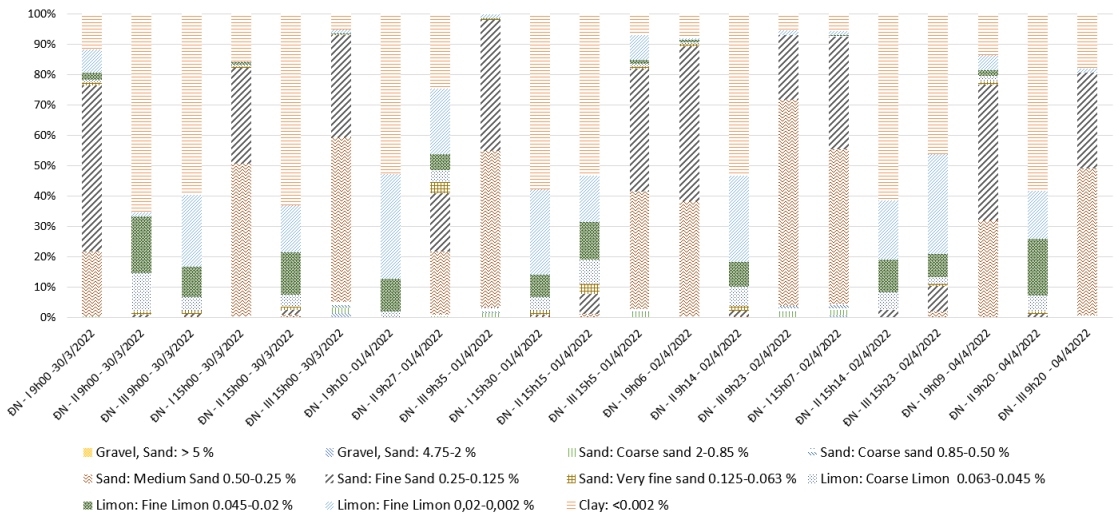
BED SAMPLING RESULTS - CHO LACH STATION



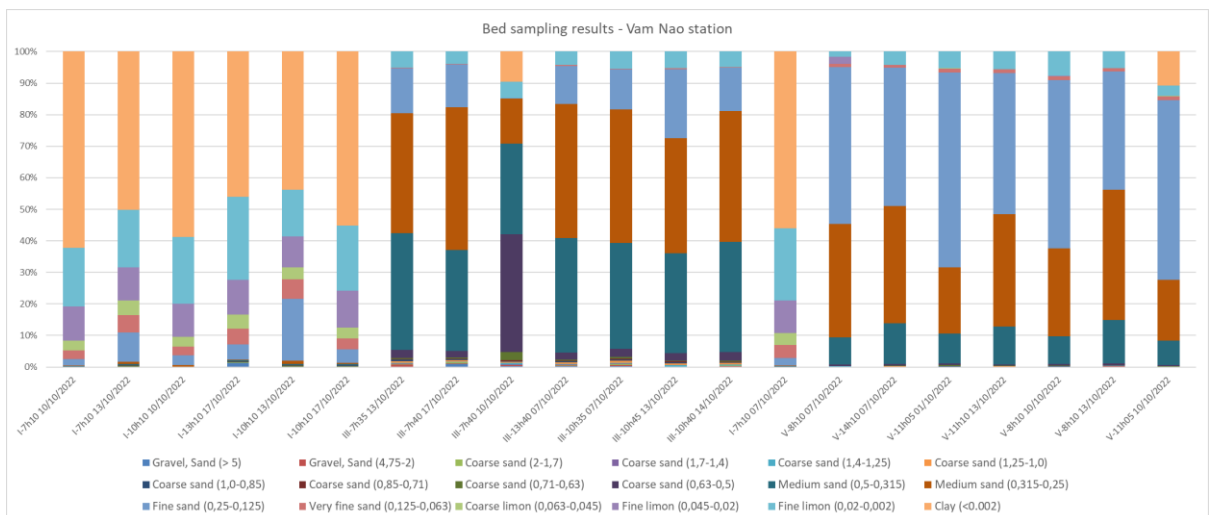
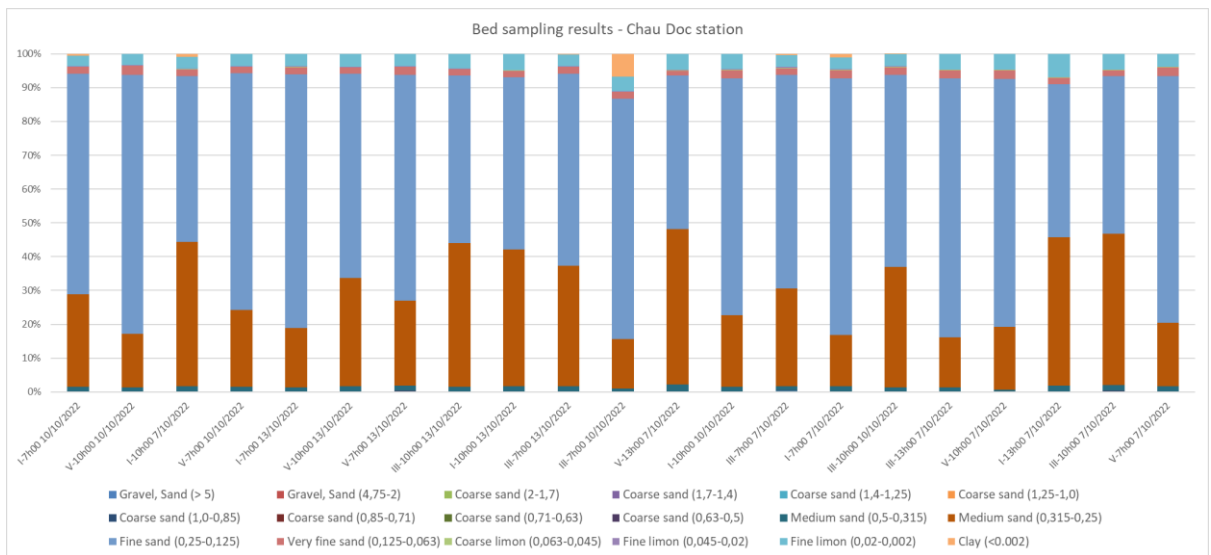
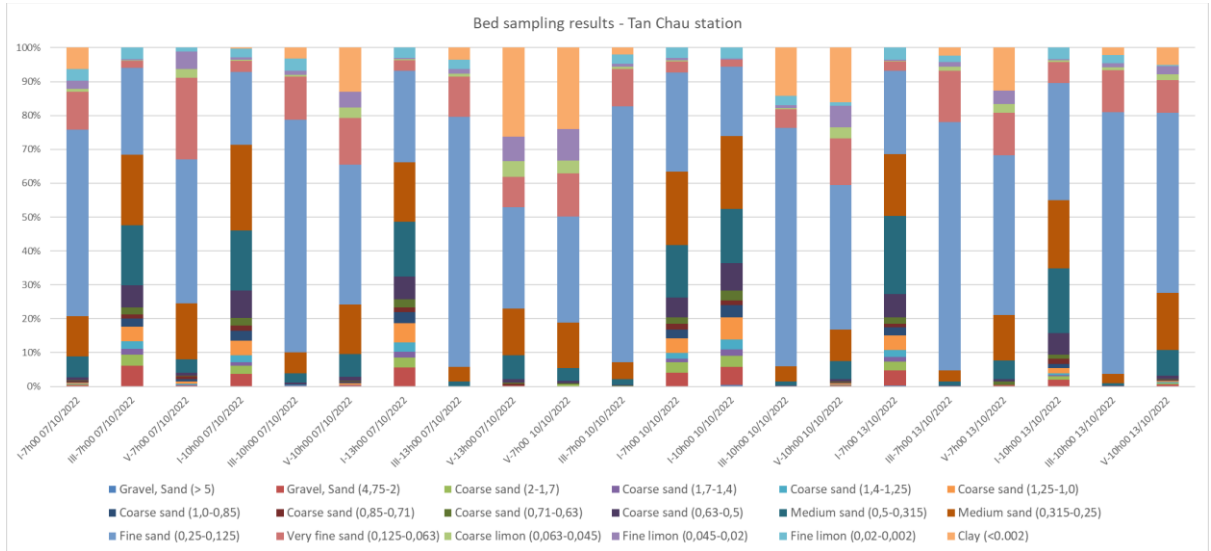
BED SAMPLING RESULTS - BINH DAI STATION

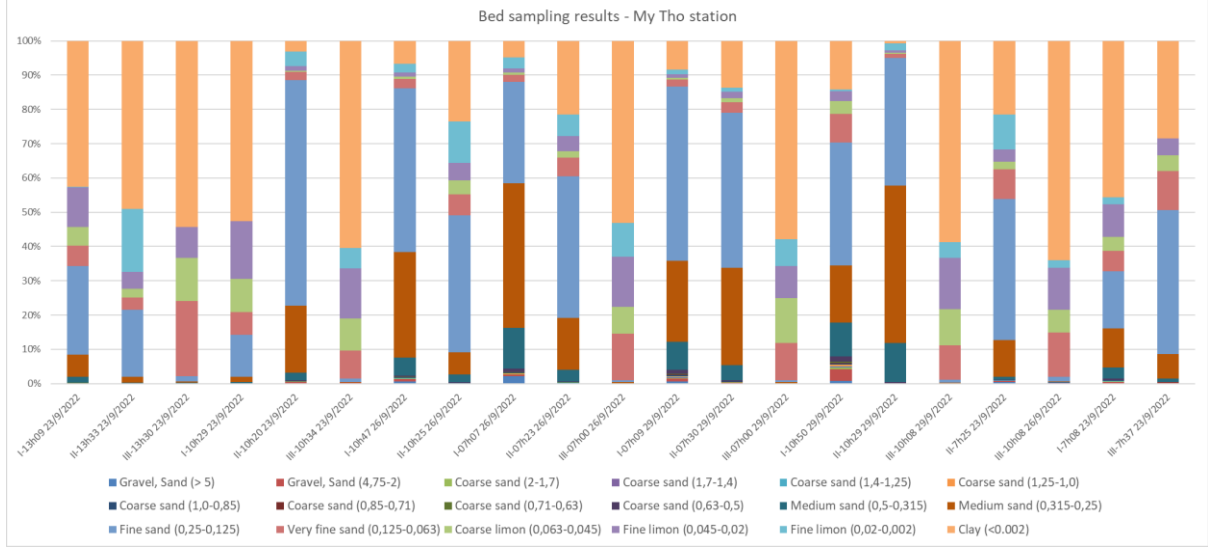
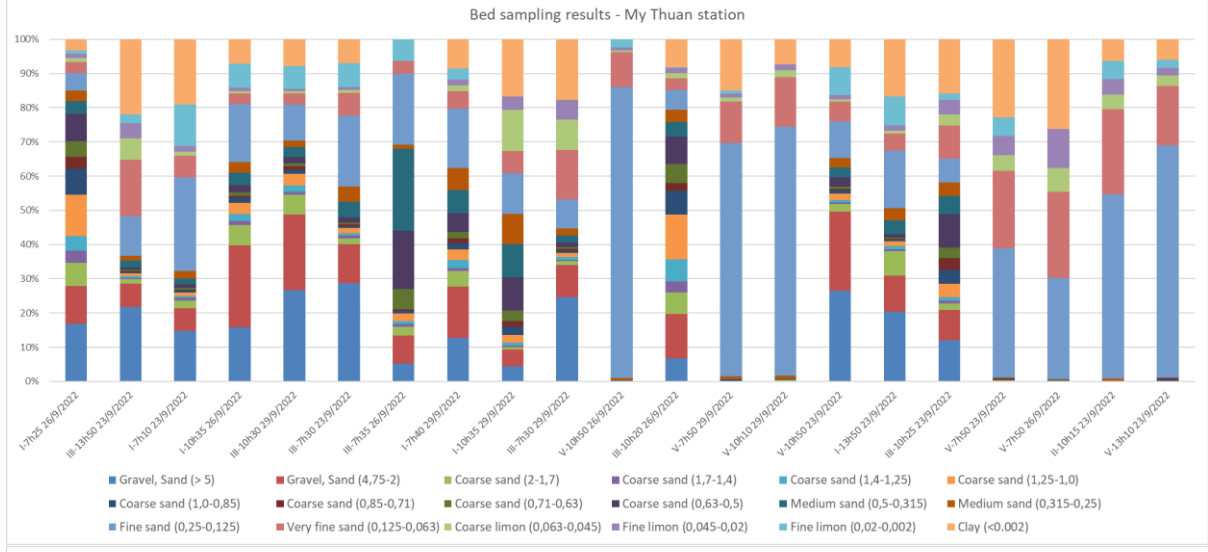
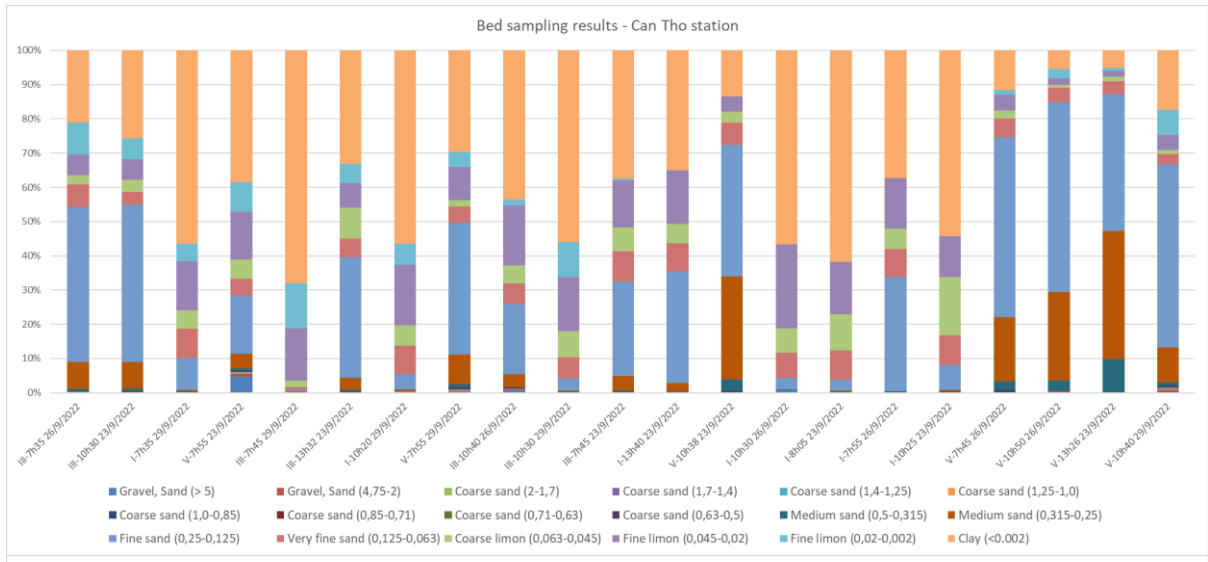


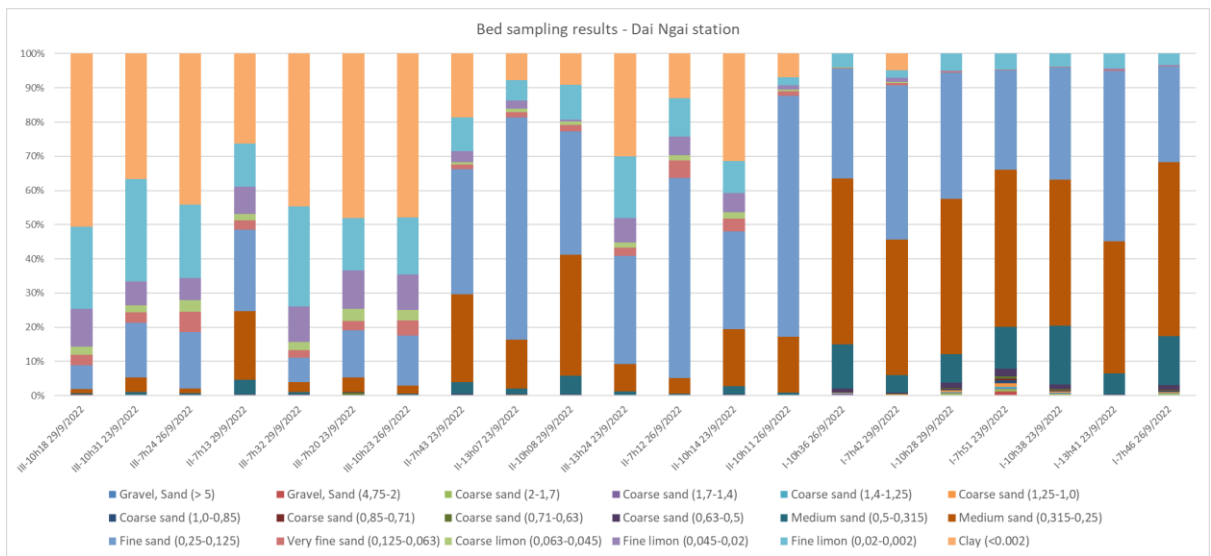
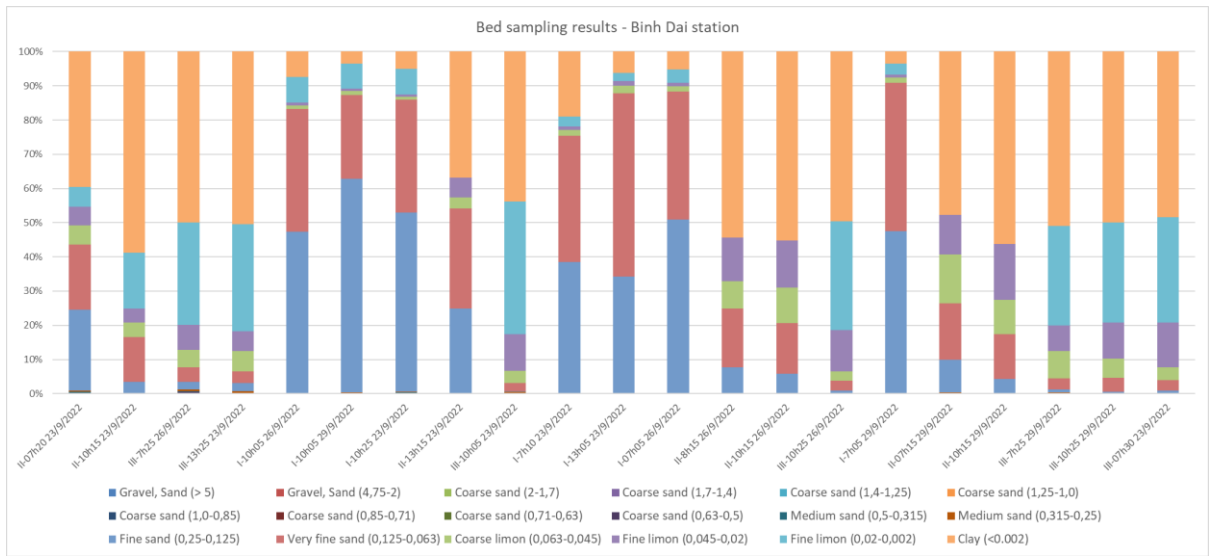
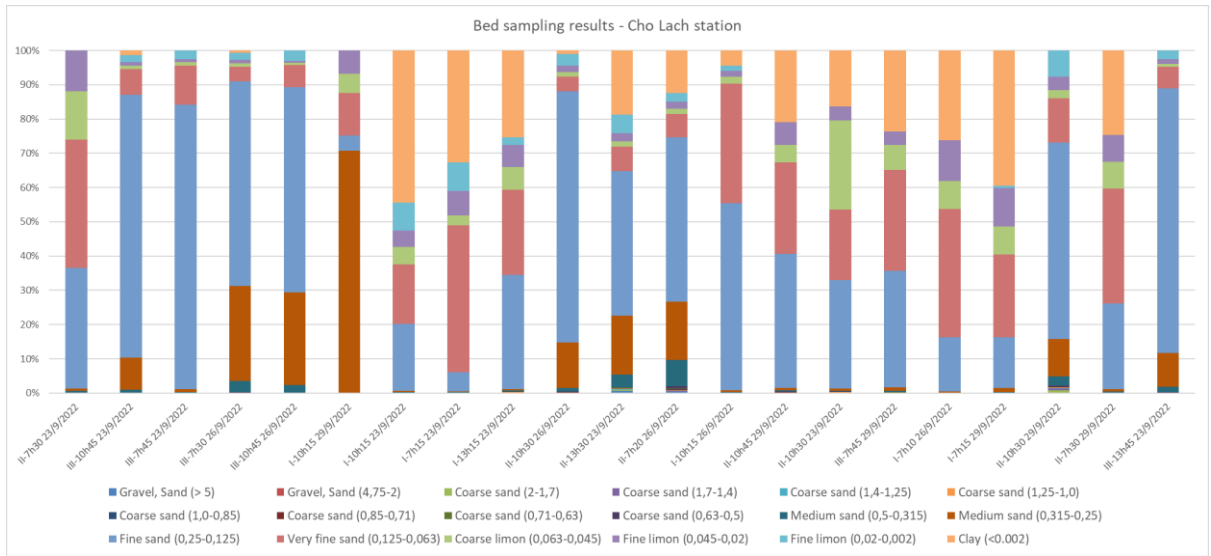
BED SAMPLING RESULTS - DAI NGAI STATION



A.2 Wet season riverbed sampling results

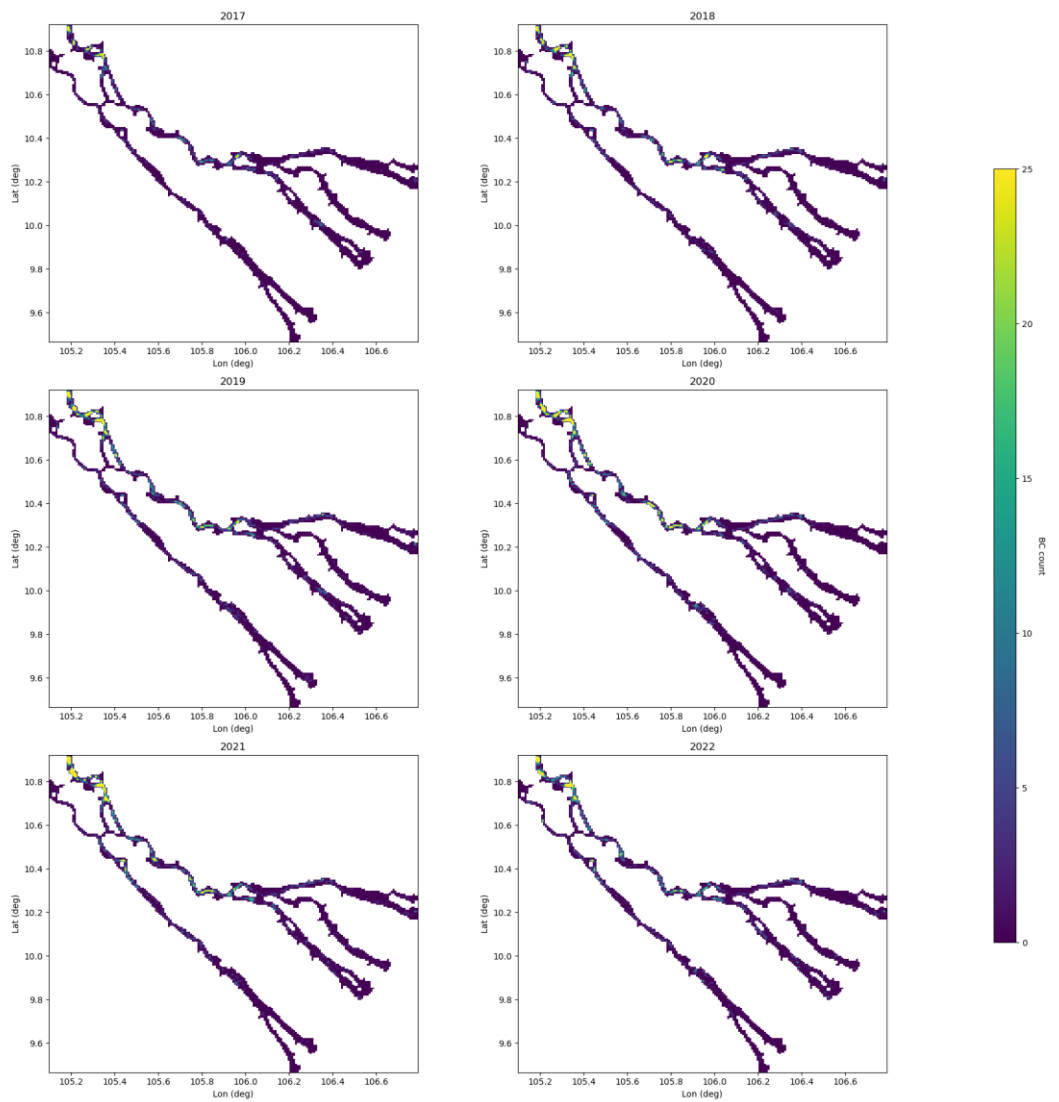






B Appendix B

The spatial heat maps of the detected dredging vessels across the Mekong Delta.



Deltares is an independent institute for applied research in the field of water and subsurface. Throughout the world, we work on smart solutions for people, environment and society.

Deltares

www.deltares.nl